23 November 2007 | $10

Science

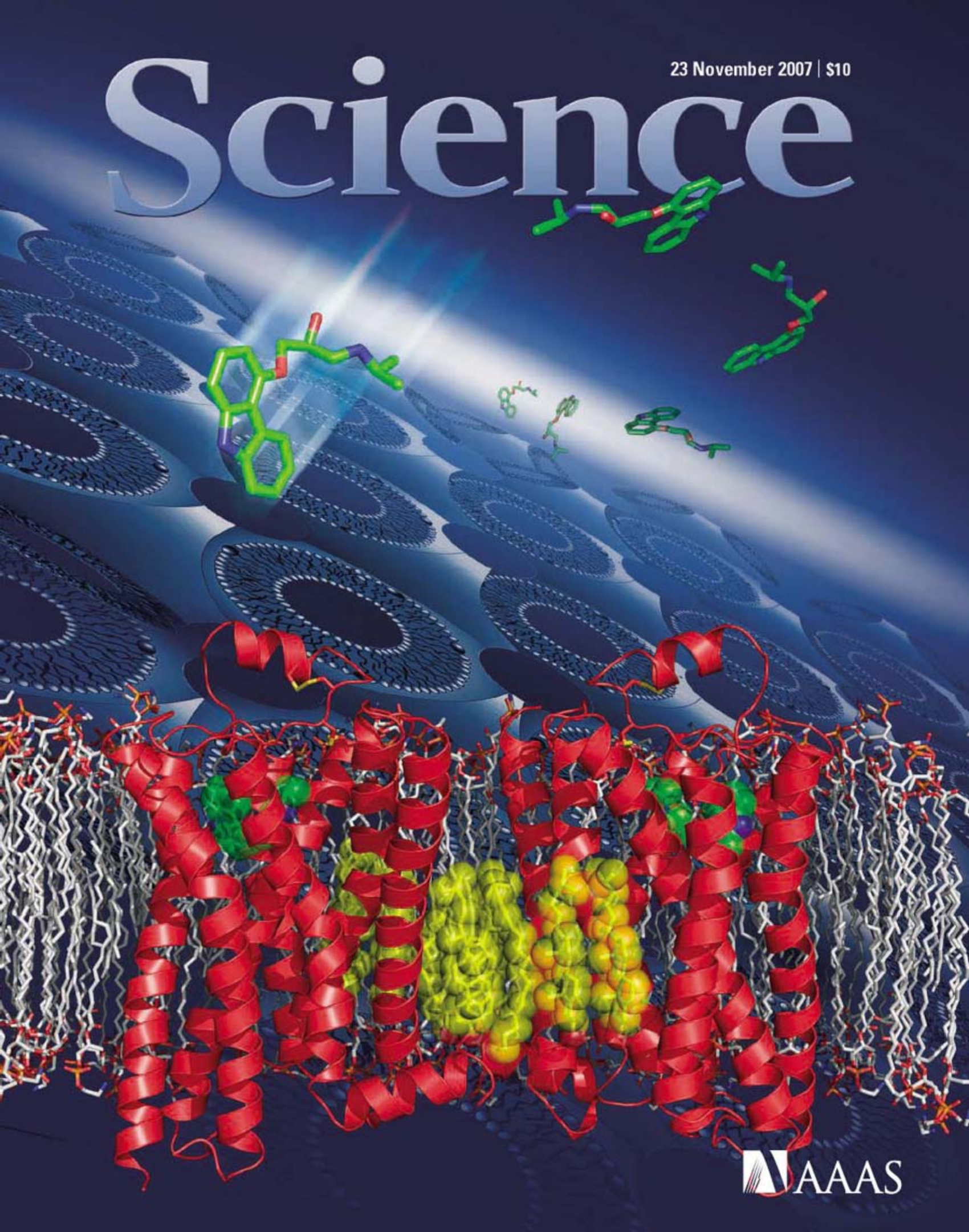

AAAS

Volume 318, Issue 5854

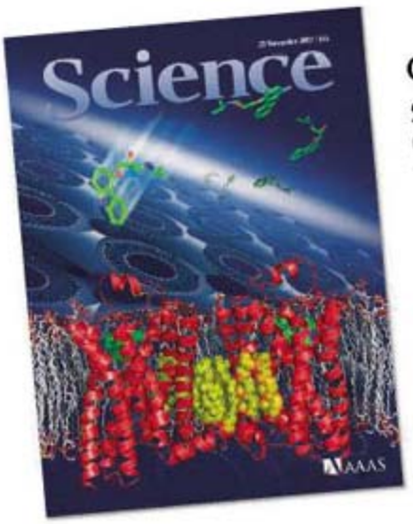

COVER

Structure of the human β_2-adrenergic receptor (red) embedded in a lipid membrane and bound to a diffusible ligand (green), with cholesterol (yellow) between the two receptor molecules. A cartoon of the lipidic cubic phase used for crystallization of the receptor is shown in the background. See pages 1258 and 1266.

Image: Yekaterina Kadyshevskaya and the Stevens Laboratory, Scripps Research Institute

DEPARTMENTS

EDITORIAL

NEWS OF THE WEEK

NEWS FOCUS

LETTERS

BOOKS *ET AL.*

POLICY FORUM

PERSPECTIVES

CONTENTS continued >>

Science

SCIENCE EXPRESS

www.sciencexpress.org

GEOPHYSICS

BREVIA: Widespread Triggering of Nonvolcanic Tremor in California

J. Gomberg et al.

A large Alaskan earthquake triggered tremors along the San Andreas and other strike-slip faults in California, showing that this process is not specific to subduction zones.

10.1126/science.1149164

GEOPHYSICS

Tidal Modulation of Nonvolcanic Tremor

J. L. Rubinstein, M. La Rocca, J. E. Vidale, K. C. Creager, A. G. Wech

Small tremors and slow slip along the Cascadia subduction zone pulse every 12.4 and 24 to 25 hours, implying that lunar tides are driving this activity along weak faults.

10.1126/science.1150558

PHYSICS

Observation of Berry's Phase in a Solid-State Qubit

P. J. Leek et al.

A controllable geometric phase, or Berry's phase, is produced by moving a superconducting qubit along a path and may provide robust quantum information storage.

10.1126/science.1149858

DEVELOPMENTAL BIOLOGY >>

Induced Pluripotent Stem Cell Lines Derived from Human Somatic Cells

J. Yu et al.

Human fibroblasts transfected with four genes exhibit the properties of embryonic stem cells.

>> *News story p. 1224*

10.1126/science.1151526

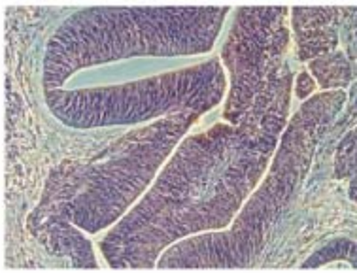

TECHNICAL COMMENT ABSTRACTS

GEOPHYSICS

BREVIA

PSYCHOLOGY

Contrary to current theory, two brain-injured patients who cannot remember their own past experiences can nevertheless infer the thoughts and beliefs of others.

RESEARCH ARTICLES

STRUCTURAL BIOLOGY

The 2.4 angstrom structure of the human β_2-adrenergic receptor displays an architecture and helical orientation distinct from that of rhodopsin, the prototypical member of this family.

>> *Perspective p. 1253*

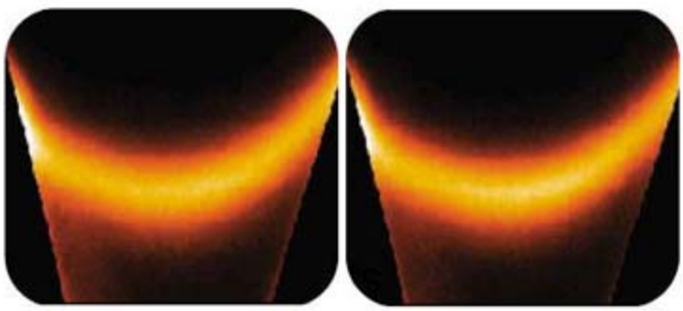

STRUCTURAL BIOLOGY

Replacing part of the β_2-adrenergic receptor allows an accurate determination of the receptor's structure, showing how ligand binding activates G proteins.

>> *Perspective p. 1253*

REPORTS

PHYSICS

The magnetoresistance of thin bismuth films perforated with nanometer holes shows that the paired electrons that produce superconductivity can also induce an insulator state.

CHEMISTRY

Known to form from long DNA segments, liquid crystalline phases can also be formed from short DNAs by stacking them into aggregates through adhesion of their end groups.

GEOCHEMISTRY

In the 2004, magnitude 6.0 Parkfield, California, earthquake the main rupture led 5 seconds later to increased slip from a secondary source 12 kilometers away.

GEOLOGY

Paleowind directions from aeolian sandstones imply that 180 million years ago, Pangea straddled the equator, rather than drifting northward as inferred from paleomagnetic data.

1287

CONTENTS continued >>

REPORTS *CONTINUED...*

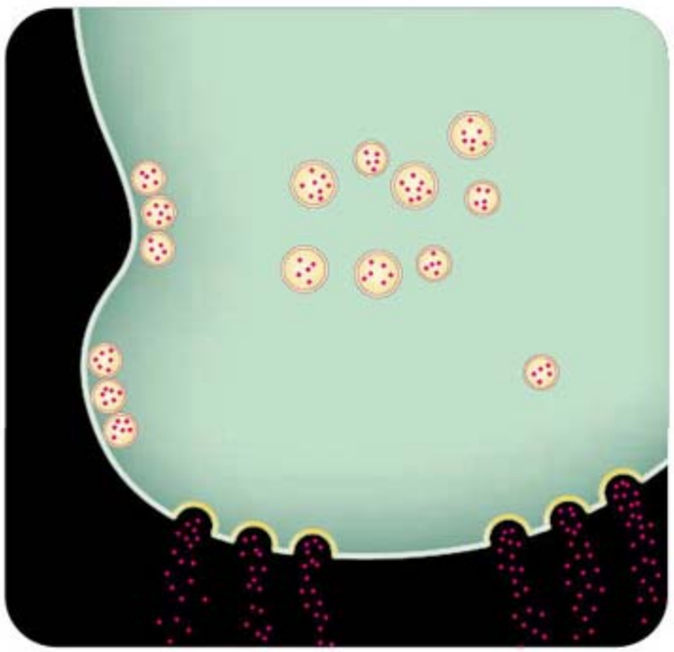

1249 & 1299

AAAS

ADVANCING SCIENCE, SERVING SOCIETY

SCIENCE (ISSN 0036-8075) is published weekly on Friday, except the last week in December, by the American Association for the Advancement of Science, 1200 New York Avenue, NW, Washington, DC 20005. Periodicals Mail postage (publication No. 484460) paid at Washington, DC, and additional mailing offices. Domestic individual membership and subscription (51 issue): $142 ($74 allocated to subscription). Domestic institutional subscription (51 issues): $710; Foreign postage extra: Mexico, Caribbean (surface mail) $55; other countries (air assist delivery) $85. First class, airmail, student, and emeritus rates on request. Canadian rates with GST available upon request, GST #1254 88122. Publications Mail Agreement Number 1069624. SCIENCE is printed on 30 percent post-consumer recycled paper. **Printed in the U.S.A.**

Change of address: Allow 4 weeks, giving old and new addresses and 8-digit account number. **Postmaster:** Send change of address to AAAS, P.O. Box 96178, Washington, DC 20090–6178. **Single-copy sales:** $10.00 current issue, $15.00 back issue prepaid includes surface postage; bulk rates on request. **Authorization to photocopy** material for internal or personal use under circumstances not falling within the fair use provisions of the Copyright Act is granted by AAAS to libraries and other users registered with the Copyright Clearance Center (CCC) Transactional Reporting Service, provided that $18.00 per article is paid directly to CCC, 222 Rosewood Drive, Danvers, MA 01923. The identification code for *Science* is 0036-8075. *Science* is indexed in the *Reader's Guide to Periodical Literature* and in several specialized indexes.

Printed on 30% post-consumer recycled paper.

CONTENTS continued >>

Deadly disease vector.

SCIENCENOW

www.sciencenow.org DAILY NEWS COVERAGE

Mutation Fired Outbreak of Deadly Tropical Virus
A simple genetic change enabled chikungunya to explode through an island population.

Flashes of Insight Into Mondo Supernova?
Astrophysicists propose explanations for record-breaking stellar explosion.

So Cute You Could Just Eat Them Up
In certain situations, it makes evolutionary sense for animals to eat their young.

Interactions between SOS and Ras.

SCIENCE'S STKE

www.stke.org SIGNAL TRANSDUCTION KNOWLEDGE ENVIRONMENT

PERSPECTIVE: Regeneration in Liver and Pancreas—Time to Cut the Umbilical Cord?
Y. Dor and B. Z. Stanger
Methods that enhance the proliferative and functional capacity of terminally differentiated cells may offer the greatest promise for creating tissues for human therapy.

PERSPECTIVE: New Insights into the Mechanisms of SOS Activation
L. A. Quilliam
Interplay between the guanine nucleotide exchange factors SOS and RasGRP1 regulates Ras activation.

PROTOCOL: Substrate-Bound Protein Gradients for Cell Culture Fabricated by Microfluidic Networks and Microcontact Printing
A. C. von Philipsborn, S. Lang, Z. Jiang, F. Bonhoeffer, M. Bastmeyer
Cellular responses to a defined microscopic pattern of a protein can be studied in a controlled in vitro environment.

Writing your thesis.

SCIENCECAREERS

www.sciencecareers.org CAREER RESOURCES FOR SCIENTISTS

GLOBAL: Mastering Your Ph.D.—Countdown to Your Thesis Defense
B. Noordam and P. Gosling
To start writing your thesis, assess what you've done, plan the last experiments, and set aside time to write.

EUROPE: A Family, a Laboratory, and an EMBO Award
E. Pain
A flair for research questions, independent work, and persuasiveness mark the career of French biologist Sandrine Etienne-Manneville.

MISCINET: Educated Woman, Postdoc Edition, Chapter 11—Breaking Free … Almost
M. P. DeWhyse
As the clock ticks, a more experienced Micella plots her escape differently than the last time.

US: From the Archives—Lucky Accidents, Chance Encounters, and the Prepared Job Seeker
P. Fiske
Good career outcomes are as likely to result from accidents as planning, but chance favors the prepared mind.

SCIENCEPODCAST

Download the 23 November *Science* Podcast to hear about induced human pluripotent stem cell lines, growing urgency about climate change, social comparison in the brain, and more.
www.sciencemag.org/about/podcast.dtl

CREDITS: (SCIENCE CAREERS) FRENKIEB/CREATIVE COMMONS; (SCIENCE NOW) JAMES GATHANY/CDC

Separate individual or institutional subscriptions to these products may be required for full-text access.

EDITED BY STELLA HURTLEY AND PHIL SZUROMI

CREDITS (TOP TO BOTTOM): SHIGEKI TAKEUCHI/HOKKAIDO UNIVERSITY; R. KLEINER

<< Short DNAs Stack and Order

For a material to form a liquid crystalline phase, it is generally believed that its constituent molecules need to have strong shape anisotropy (morphologies of rods or discs) and need to be fairly rigid. Long DNA fragments have been shown to form mesophases, but it is unclear that shorter fragments would do so. **Nakata *et al.*** (p. 1276) show that short DNA segments (6 to 20 base pairs) that lack shape anisotropy can form a wide range of ordered mesophases during the cooling of a solution of random fragments. Hydrophobic forces allow the base pairs to associate end-to-end to create long rod-shaped aggregates. By this route, it is possible that mixtures of fragments can undergo a separation as complementary fragments associate and locally concentrate into ordered droplets.

Insulating Cooper Pairs

The standard model of superconducting metals (the Bardeen-Cooper-Schreiffer, or BCS theory) describes how electrons pair up into a phase-coherent state and lose all of their electrical resistance. In the context of studying how quantum-driven phase transitions differ from thermally driven ones, a question now being addressed is what happens to the pairing gap and the long-range coherence when the superconductor is driven out of the superconducting regime by disorder or magnetic fields. **Stewart *et al.*** (p. 1273) present magnetoresistance measurements on amorphous ultrathin films of bismuth perforated with an array of nanometer-sized holes. Cooper pairs that give rise to zero resistance superconductors also give rise to high-resistance electrical insulators.

Reconsidering Supercontinent Movement

Paleomagnetic reconstructions of the latitudinal position of Pangea, the supercontinent that contained most of Earth's landmass for 100 million years from the Permian into the Jurassic, have been interpreted as showing that Pangea was originally centered roughly on the equator and moved northward by about 20° by the Early Jurassic. **Rowe *et al.*** (p. 1284) reconstructed apparent wind patterns derived from aeolian deposits in the southwestern United States and found that wind direction over the Colorado Plateau remained constant throughout the entire period, which indicates that Pangea remained at or near the equator. Among the several resolutions to this disagreement are that the latitudinal movement of Pangea based on paleomagnetic data is misinterpreted, our understanding of how winds shape sand dunes is incorrect, existing paleogeographic reconstructions cannot reproduce adequately the wind fields responsible for dune formation, or the climate controls on winds in the Jurassic were different than they are today.

Tracking Electrons on the Go

The detailed dynamics of current flow in a metal are challenging to study because the onset time of a potential gradient to drive the electrons forward tends to be much longer than the duration of the collisions and scattering events of interest. **Güdde *et al.*** (p. 1287) overcame this problem by inducing a transient current at a copper surface using the coherent interference effect of one- and two-photon laser excitation pathways, a phenomenon previously demonstrated in semiconductors. The femtosecond dynamics of transient current generated on an ultrashort time scale was tracked by imaging the momenta of photoelectrons ejected by a third laser pulse. The technique should generalize to a range of conducting and semiconducting substrates.

Superconducting Terahertz Generators

Practical sources of electromagnetic radiation between 0.5 to 2 terahertz have been lacking, but this frequency range has potential uses for molecular recognition, spectroscopy, and imaging applications. Josephson junctions, in which two superconducting layers sandwich an insulating layer, naturally oscillate with a frequency that depends on the superconducting gap and the applied bias, but this potential terahertz source cannot produce sufficient power for applications. With the clever design of the emitter geometry analogous to that of a laser cavity, **Ozyuzer *et al.*** (p. 1291; see the Perspective by **Kleiner**) report on the generation of intense terahertz radiation from a stack of Josephson junctions formed by the weakly coupled CuO_2 layers in the Bi_{2212} high-temperature superconductor.

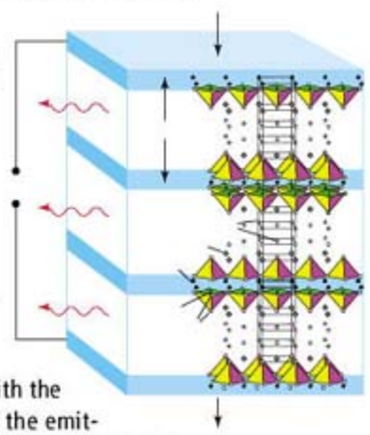

Energizing Polymer Shape-Memory Materials

In a shape-memory material, internal stresses that are captured during deformation processes are used to recover the shape of the material as it is heated above a transition temperature. For polymer-shape memory materials, large strain changes are possible, but

Continued on page 1215

Continued from page 1213

these changes are accompanied by only small recovery stresses. This combination leads to a low energy density and has made the polymer-based materials poor candidates for actuators. **Miaudet *et al.*** (p. 1294) formed a composite from poly(vinyl alcohol) and 20 weight percent carbon nanotubes whose stress recovery approaches that of metal-alloy shape-memory materials but still exhibit large strain capabilities.

β_2-Adrenergic Receptor Structures

G protein–coupled receptors (GPCRs) are transmembrane proteins that respond to diverse extracellular stimuli to trigger many different cellular responses. They are important pharmacological targets, but drug design has been hampered because structural information is only available for the rather distinctive member of this family, rhodopsin (see the Perspective by **Ranganathan**). Two studies now provide structural insights into another GPCR, the human β_2-adrenergic receptor. **Rosenbaum *et al.*** (p. 1266, published online 25 October) stabilized the protein for crystallization by protein engineering and analyzed mutagenesis data in the context of the structure to provide insight into how ligand binding is coupled. **Cherezov *et al.*** (p. 1258, published online 25 October; see the cover) describe in detail the 2.4 angstrom structure of the fusion protein and how it compares to the rhodopsin structure. It appears that conserved helices provide a common core in class A GPCRs while variable helices provide binding-site plasticity.

Nudging-In on Stem Cell Niches

The ability to transplant hematopoietic stem cells (HSCs) in bone marrow is of huge importance in a wide number of clinical settings. However, incoming HSCs do not easily conquer niches already occupied by host HSCs. **Czechowicz *et al.*** (p. 1296) use a mouse transplantation model to demonstrate that endogenous HSCs do indeed prevent the engraftment of donor HSCs through the occupancy of appropriate niches. However, by using an antibody that can transiently deplete endogenous HSCs, transplanted animals could be preconditioned to allow chimerism levels to rise to as much as 90%. Further work will be needed to determine if similar conditioning can improve HSC transplantation in humans.

Fair's Fair

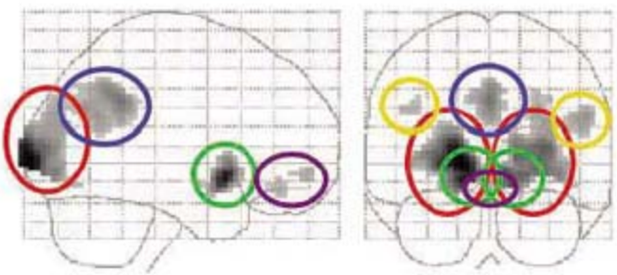

It is not uncommon for an employee to reflect both upon how much he or she has been paid, and on how much colleagues have received. A purely rational being would calculate the balance between income and expenses, in order to decide upon happiness or misery, yet ample experience suggests that we do care about our relative remuneration. **Fliessbach *et al.*** (p. 1305) used side-by-side brain imaging scanners and a behavioral task in which equal performance was rewarded inequitably. Neural activity in the ventral striatum, a brain area notable for its central role in responding to and predicting rewards, was indeed sensitive to the relative amount of money paid. Furthermore, this response occurred even when no decisions were made, which suggests that the calculation of social standing—as indexed by payment—may be automatic.

Decisions and Impulsivity

Deep brain stimulation of the subthalamic nucleus and dopaminergic medication both represent successful therapies for Parkinson's disease. However, both interfere with normal cognitive strategies, such as decision-making in conflict situations. **Frank *et al.*** (p. 1309, published online 25 October; see the 26 October news story by **Miller**) provide evidence for two distinct computational roles of these treatments in decision-making. Dopaminergic medication altered patients' relative tendency to learn from positive versus negative outcomes without impacting conflict-induced slowing. In contrast, deep-brain stimulation sped up high-conflict choices, without affecting learning biases. Both of these findings were predicted in a computational model of the basal ganglia in learning and decision-making.

CREDIT: FUESSBACH *ET AL.*

Donald Kennedy is the Editor-in-Chief of *Science*.

Toxic Dilemmas

AFTER ALL THESE YEARS OF ENVIRONMENTAL REGULATION, THE LAWS AND RULES REGARDING the introduction of toxic chemicals into consumer products and the environment are still ineffectual. After an earlier lifetime in which I worried about lead, polybrominated biphenyls in plastics, and the like, I got reacquainted with toxic dilemmas. It happened because of a reunion with an old friend who has a long familiarity with the use of toxic substances as fire retardants in consumer products. Here's the story.

In the early 1970s when I first got to know Arlene Blum, she was working with Bruce Ames at the University of California, Berkeley. They were applying the Ames test for mutagenicity to various lipid-soluble chlorinated and brominated compounds that are double trouble because they concentrate in food chains and wind up in people, and aren't biodegradable. They discovered widespread use of a compound called tris(2,3-ibromopropyl) phosphate as a fire retardant in children's sleepwear. A mutagen and putative human carcinogen, it leeched into children's bodies. After a 1977 paper by Blum and Ames in *Science*, that use was banned. Well, the alert chemical industry quickly substituted a dichlorinated tris, which Ames and Blum also found to be mutagenic and was subsequently removed from sleepwear.

The history of residential fire risk is an interesting one, because it involves the tobacco industry. Remember them? They designed cigarettes that when dropped or put down, would smolder long enough to start a fire. For years, cigarette-lit fires were the greatest cause of fire-related deaths in the United States. After three decades of opposition from tobacco lobbyists, 22 states and Canada finally passed laws requiring that cigarettes be made self-extinguishing. With fewer people smoking and better enforcement of building codes, fire-related deaths are decreasing.

I had missed this important development, having lost track of the topic. Arlene, a high-profile international mountaineer, was off leading expeditions in the Himalayas and elsewhere and writing a memoir about it. Meanwhile, I had left the U.S. Food and Drug Administration and was back at Stanford. I hadn't seen Arlene for 25 years or so, but a few months ago, she turned up with an extraordinary sequel to the tris story, which she tells of in a recent Letter in *Science*. Fire retardants are now widely used in furniture foam, and the second most-used compound is none other than chlorinated tris! In less than three decades, this highly toxic mutagen has moved from your child's nightgown to your sofa.

Arlene is scientific adviser for a bill in the California legislature called AB 706, which would ban the use of the most toxic fire retardants from furniture and bedding unless the manufacturers can show safety. It has a good chance of passage next year; even the firefighters support it. Not surprisingly, chemical manufacturers have launched a fear campaign in opposition, claiming that their products have dramatically reduced fire deaths in California, although the rate of decrease is about the same as that in states that do not regulate furniture flammability.

But the problem is a national one. The Consumer Product Safety Commission (CPSC) Reform Act (S 2045) toyed with a provision that would rush us into a national furniture flammability standard. That's premature, because it leaves no time to develop a safe way to reduce furniture flammability and puts potentially persistent toxic chemicals into U.S. homes. Congress should forget that approach. The real problem is that the U.S. regulatory system for toxic industrial chemicals is not effective and is a threat to public health.

In Europe, the chemical industry is required to establish safety before a product can continue to be marketed. The U.S. Toxic Substances Control Act (TOSCA) originally grandfathered existing chemicals, but none have been reexamined since the 1980s. Congress should abandon its attempt to attach a flammability standard to the CPSC, and instead turn to the real task of reforming TOSCA by introducing a real proof-of-safety provision. That would stop the chemical industry from continuing to make consumer protection look like a game of whack-a-mole.

– Donald Kennedy

10.1126/science.1151604

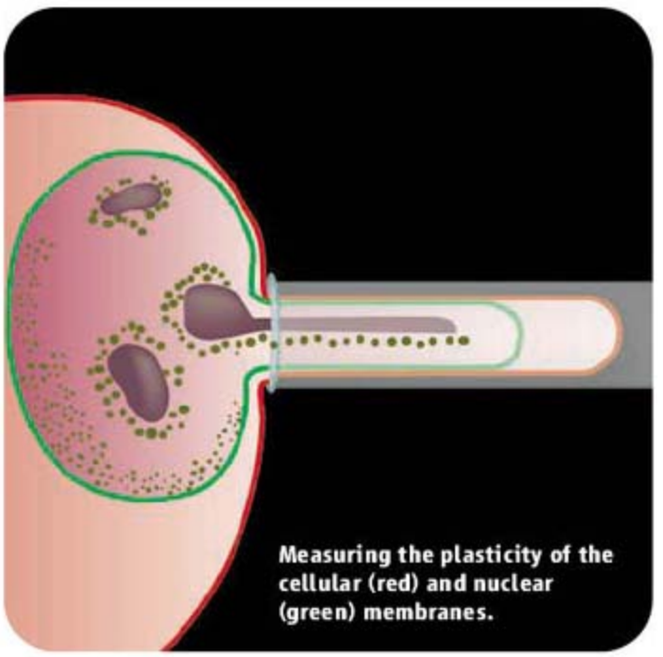

Measuring the plasticity of the cellular (red) and nuclear (green) membranes.

DEVELOPMENTAL BIOLOGY

A Loss of Flexibility with Age

As a cell transitions from an undifferentiated state to a differentiated cell type, its gene expression profile changes, which in part reflects physical changes in chromatin structure. In a complementary approach, Pajerowski *et al.* have examined the macroscopic properties of the nucleus during differentiation. Aspiration with a micropipette revealed that the nuclei of pluripotent human embryonic stem cells could be deformed relatively easily; however, as the cells differentiated, the nuclei became stiffer. Hematopoietic stem cells (from bone marrow) were able to differentiate into fewer cell types than embryonic stem cells and, similarly, showed an intermediate level of deformability. Progression toward the differentiated state was accompanied by an increase in the filamentous protein lamin A/C and greater condensation of chromatin. When lamin A/C was knocked down in epithelial cells, their flow behavior resembled that of hematopoietic stem cells. Further analysis showed that the fluid character of the nucleus is determined primarily by chromatin but that the degree of nuclear deformability is set by the lamina. Variations in the physical plasticity of the nucleus may be important for allowing less differentiated cells to move through tissues. — BAP

Proc. Natl. Acad. Sci. U.S.A. **104**, 15619 (2007).

ECOLOGY/EVOLUTION

Nasty, Brutish, and Short

Leaves are a vital organ for plants and for their environments. Their structure and life span influence photosynthesis, resource acquisition, and growth rates; they also influence the plant's ability to resist being eaten, for instance by insects. And leaves have important effects on the local ecosystem through leaf litter decomposition.

Knowing how leaves influenced paleoenvironments can provide key insights into past ecosystem functions. Leaf mass per area is a metric that correlates with various ecological traits but has not been applied systematically to fossil data. Royer *et al.* measure the petiole width (the petiole being the small stalk that attaches the leaf to the stem of the plant) and leaf area of fossil leaves and, through a scaling relationship they develop for these characteristics in extant leaves, use these to estimate fossil leaf mass per area. In a comparative analysis of two Eocene fossil lake floras (Republic, in the Klondike Mountains, and Bonanza, in Utah), the leaf mass per area was uniformly low at Republic, whereas Bonanza exhibited a broad range of values. These biosynthetic choices are consistent with the respective paleoclimates: The former was dominated by trees bearing short-lived leaves, which suffered fairly high levels of herbivory, and was associated with rapid leaf litter decomposition; whereas the latter showed wider ranges of these same traits. — GR

Paleobiology **33**, 574 (2007).

PHYSICS

Speeding Up Holography

The ability to produce ultrashort electron bunches and x-ray and optical pulses has allowed researchers to glimpse fleeting structural and electronic rearrangements occurring on femtosecond or shorter time scales. However, these pump-probe measurements often tend to provide a somewhat limited series of one- or two-dimensional (2D) snapshots of the processes at play. Two groups now show how holographic imaging—a technique in which the interference of two light beams encodes 3D information on a 2D detection surface—can be extended to the ultrafast regime, thereby raising the possibility of obtaining more detailed, fully dynamical 3D movies of processes taking place on these rapid time scales. Kubota *et al.* demonstrate the use of optical holography to track light images formed from femtosecond red light pulses as they are launched into an optical medium; the result is a spatially and temporally continuous movie of the images propagating, converging into a focal point, and then diverging again. Schlotter *et al.* extend ultrafast holography to shorter wavelengths in the x-ray regime. Using patterned masks to provide multiple x-ray sources, they demonstrate the ability to record images simultaneously at different parts of the sample. They note that combining this multi-spatial sampling with gated pump-probe illumination could extend the technique to 3D imaging of ultrafast processes. — ISO

Opt. Express **15**, 14348 (2007); *Opt. Lett.* **92**, 3110 (2007).

CELL BIOLOGY

To Spread or Not to Spread

When animal cells grow over a surface, they survey their surroundings and make decisions as to whether they should spread or retract from a certain path, processes that are central in cell migration and proliferation. Key to these decisions is the interaction of a group of membrane proteins, the integrins, with the surface on which the cells grow.

Flevaris *et al.* find that it is the calpain-dependent proteolytic cleavage of the integrin subunit β_3 at a specific tyrosine residue that acts as a molecular switch to help the cell change from spreading to retraction. In cells expressing a β_3 integrin that cannot be cleaved, spreading is enhanced in comparison to retraction. On the other hand, in cells expressing

CREDITS (TOP TO BOTTOM): ADAPTED FROM PAJEROWSKI ET AL., *PROC. NATL. ACAD. SCI. U.S.A.* **104**, 15619 (2007); SCHLOTTER ET AL., *OPT. LETT.* **92**, 3110 (2007)

only the cleaved form of β_3, retraction is favored—a defect that can be overcome by expressing the downstream signaling protein RhoA. The effects of β_3 appear to be mediated via an interaction of the intact integrin with the kinase c-Src at the plasma membrane, which in turn regulates RhoA-dependent contractile signaling. — SMH

J. Cell Biol. **179**, 553 (2007).

BIOMATERIALS

Nerves of Hair

Hair growth is a complex process involving more than 30 growth factors, cytokines, and signaling molecules. Both the alpha and gamma keratins, which respectively form the structure and cross-linking in the hair fibers, can be extracted from human hair. Sierpinski *et al.* explored the use of keratin-based hydrogels, which form on mixing extracts with water, for the rapid regeneration of peripheral nerves. At present, small nerve defects can be repaired using fillers to provide a structural support, but only short gaps are amenable to this approach. In vitro testing showed that the keratin hydrogels improved Schwann cell proliferation and migration and showed either no effect or some up-regulation in the production of certain

Regenerated nerve fiber.

key proteins. Using a nerve injury model in mice, the authors then proceeded to compare regeneration results from the keratin protocol with autografts (in which a different form of tissue is used to patch a defect site), as well as controls where no material was added to the defect site. The hair-based hydrogels outperformed the autografts in reducing electrical signal latency and showed a greater increase in overall nerve area, as well as comparable improvements in a number of other tests. The authors believe that the hydrogels provide a framework for the Schwann cells and also retain a number of the regulatory molecules needed for hair growth, which are also involved in nerve repair. — MSL

Biomaterials **29**, 118 (2008).

BIOTECHNOLOGY

Together We Shine

Green fluorescent protein (GFP) and its variants can be used in Förster resonance energy transfer (FRET) experiments (where emission is a function of the distance between donor and acceptor fluorophores) to monitor dynamic processes such as protein folding or association in intact cells. These experiments come with limitations, however, as the changes in fluorescence intensity may be smaller than cell-to-cell variations, and fusing GFP to the target protein may interfere with function. An alternative readout strategy uses the biarsenical reagents FlAsH –EDT_2 and ReAsH-EDT_2. These reagents selectively label recombinant proteins containing a tetracysteine sequence (CCPGCC), and only the protein-bound forms fluoresce.

Luedtke *et al.* show that polypeptides containing a split sequence, with the two cysteine pairs separated in linear sequence but close together when folded, can be labeled with FlAsH or ReAsH to give a fluorescent complex. Labeling of a dimer, where the two pairs were contained on different monomers, was also successful. Fluorescence intensity correlated with the stability of either protein folding or dimerization and allowed the detection of protein folding and assembly in live cells. — VV

Nat. Chem. Biol. **3**, 10.1038/nchembio.2007.49 (2007).

CHEMISTRY

Linking Up Cleanly

Selective coupling of aryl molecules is a crucial step in the preparation of a wide range of commercial organic compounds. The requisite selectivity has traditionally been achieved by appending mutually reactive groups (such as halides and boron- or tin-based substituents) to each partner, but the addition and elimination of such groups generate considerable waste material. Recent advances in transition metal catalysis have offered a promising alternative approach, in which C-H bonds on the aryl rings are oxidatively cleaved directly to yield a C-C bonded biaryl product and (ideally) water as the sole byproduct. Li *et al.* extend this method to the coupling of acetylated anilines with alkyl benzenes. The acetamide group directs a palladium catalyst to react selectively with an adjacent ortho C-H bond, and a second C-H scission links up the benzene partner. In the case of NH(acetyl) substrates, a subsequent sequence involving N-H and C-H scission leads efficiently to carbazole products with a fused central C_4N ring connecting the aromatic cycles on either side. The reactions proceed under oxygen at 120°C, with varying amounts of a cupric salt added as a co-catalyst depending on the substrates. — JSY

Angew. Chem. Int. Ed. **46**, 10.1002/anie.200704092 (2007).

CREDIT: SIERPINSKI *ET AL.*, *BIOMATERIALS* **29**, 118 (2008)

www.sciencemag.org

Science

1200 New York Avenue, NW
Washington, DC 20005
Editorial: 202-326-6550, FAX 202-289-7562
News: 202-326-6581, FAX 202-371-9227

Bateman House, 82-88 Hills Road
Cambridge, UK CB2 1LQ
+44 (0) 1223 326500, FAX +44 (0) 1223 326501

SUBSCRIPTION SERVICES For change of address, missing issues, new orders and renewals, and payment questions: 866-434-AAAS (2227) or 202-326-6417, FAX 202-842-1065. Mailing addresses: AAAS, P.O. Box 96178, Washington, DC 20090-6178 or AAAS Member Services, 1200 New York Avenue, NW, Washington, DC 20005

INSTITUTIONAL SITE LICENSES please call 202-326-6755 for any questions or information

REPRINTS: Author Inquiries 800-635-7181
Commercial Inquiries 803-359-4578

PERMISSIONS 202-326-7074, FAX 202-682-0816z

MEMBER BENEFITS AAAS/Barnes&Noble.com bookstore www.aaas.org/bn; AAAS Online Store http://www.apisource.com/aaas/ code MKB6; AAAS Travels: Betchart Expeditions 800-252-4910; Apple Store www.apple/eppstore/aaas; Bank of America MasterCard 1-800-833-6262 priority code FAA3YU; Cold Spring Harbor Laboratory Press Publications www.cshlpress.com/affiliates/aaas.htm; GEICO Auto Insurance www.geico.com/landingpage/go51.htm?logo=17624; Hertz 800-654-2200 CDP#343457; Office Depot https://bsd.officedepot.com/portalLogin.do; Seabury & Smith Life Insurance 800-424-9883; Subaru VIP Program 202-326-6417; VIP Moving Services http://www.vipmayflower.com/domestic/index.html; Other Benefits: AAAS Member Services 202-326-6417 or www.aaasmember.org.

science_editors@aaas.org (for general editorial queries)
science_letters@aaas.org (for queries about letters)
science_reviews@aaas.org (for returning manuscript reviews)
science_bookrevs@aaas.org (for book review queries)

Published by the American Association for the Advancement of Science (AAAS), *Science* serves its readers as a forum for the presentation and discussion of important issues related to the advancement of science, including the presentation of minority or conflicting points of view, rather than by publishing only material on which a consensus has been reached. Accordingly, all articles published in *Science*—including editorials, news and comment, and book reviews—are signed and reflect the individual views of the authors and not official points of view adopted by the AAAS or the institutions with which the authors are affiliated.

AAAS was founded in 1848 and incorporated in 1874. Its mission is to advance science and innovation throughout the world for the benefit of all people. The goals of the association are to: foster communication among scientists, engineers and the public; enhance international cooperation in science and its applications; promote the responsible conduct and use of science and technology; foster education in science and technology for everyone; enhance the science and technology workforce and infrastructure; increase public understanding and appreciation of science and technology; and strengthen support for the science and technology enterprise.

INFORMATION FOR AUTHORS

See pages 120 and 121 of the 5 January 2007 issue or access www.sciencemag.org/feature/contribinfo/home.shtml

BRAINS OVER BRAWN

How does Tiger Woods's brain behave before tapping the ball for a long putt? Neuroscientists from the University of Rome "La Sapienza" and from the Italian Olympic Committee's Institute of Medicine and Science of Sport in Rome are applying electrodes to expert golfers to find out why their games are so hot. Twelve right-handed golfers donned helmets that recorded their brain waves while they putted on a green in the lab.

Alpha waves, caused by rhythmic changes in the electrical activity of certain brain cells, usually fluctuate at frequencies of 8 to 12 cycles per second (Hz). High-amplitude alpha waves reflect a relaxed waking state, the brain's "idling" mode. When a golfer swings, alpha waves tighten up, decreasing in amplitude. "We noted that high-frequency alpha waves (10–12 Hz) over frontal motor areas were smaller in amplitude in the successful putts," says physiologist Claudio Babiloni of Sapienza University. The greater the amplitude reduction—reflecting the intensity of focus on the task—the closer the putt got to the hole.

The scientists, whose results are published online in *The Journal of Physiology*, say they see similar patterns in gymnasts, karate practitioners, and fencers. Fabrizio Eusebi, head of research at the Sport Medicine Institute, says golfers might be able to improve both their relaxation and concentration using video games. "It sounds like a promising and useful path to me," says professional golfer and trainer Gianluca Crespi. "Scientists keen on golf have been, so far, more interested in rehabilitation of joint-muscular function than enhancing players' cognitive skills."

CREDITS (TOP TO BOTTOM): FABRIZIO EUSEBI; MICHEL BREGER/UNIVERSITY OF VIENNA; IGNACIO ALVA/REUTERS/LANDOV

Star Wars

Astronomers in Vienna, Austria, last week clashed with astrologers at a demonstration against an astrology course offered by WIFI, an education institute funded by the city's Chamber of Commerce.

The 6-month course amounts to "government support for pseudoscience," says Michael Gruberbauer, an astronomy grad student at the University of Vienna. The astrologers, some of whom tried to shout down the researchers, countered that they have the right to study whatever they want. WIFI spokesperson Barbara Wichart said that "astrology is a recognized trade" like others for which courses are offered—including computer programming and secretarial work—and noted that the 135 enrollees are paying $2800 each for it.

"This is not just a local problem," says protest organizer Günter Wuchterl of the Tautenburg Observatory in Germany. "Astrology degrees are already offered at some U.K. universities, the largest astrology organization in Germany has stated that it wants to invade academia, and now Austria has fallen under their spell." For the duration of the course, astronomers are offering weekly public lectures at Vienna's Kuffner Observatory to explain astrology's "fundamental problems," says Wuchterl. "This is like offering a course for installing sewer pipes through which water cannot flow."

Astronomy student Michael Gruberbauer (*left*) and colleague at astrology protest.

Do the Math

Cutting up in class and ignoring the teacher get you in trouble but won't necessarily hurt your academic performance, according to a study covering more than 16,000 children.

An international team recently reanalyzed data from six longitudinal studies of schoolchildren in both the United States and the United Kingdom. The study sifted through evaluations of children's conduct starting at about age 5 through grade school and correlated them with later grades and test scores.

Assumptions that "social and emotional development" are as important as cognitive skills don't hold water, the authors report in the November issue of *Developmental Psychology*. Instead, most predictive of "later learning" was "knowledge of numbers and ordinality." That was more significant than reading ability and even trumped "attention skills."

Lead author Greg Duncan, an economist at Northwestern University in Evanston, Illinois, says the "biggest surprise" was to discover the relative unimportance of social training. Duncan says preschool programs should consider "channeling more resources" into helping children understand numbers and letters. Psychologist Karen Bierman of Pennsylvania State University says the data don't support that interpretation: "My big worry is that people will say we should be having preschoolers do flash cards."

Oldest Mural Found in Peru

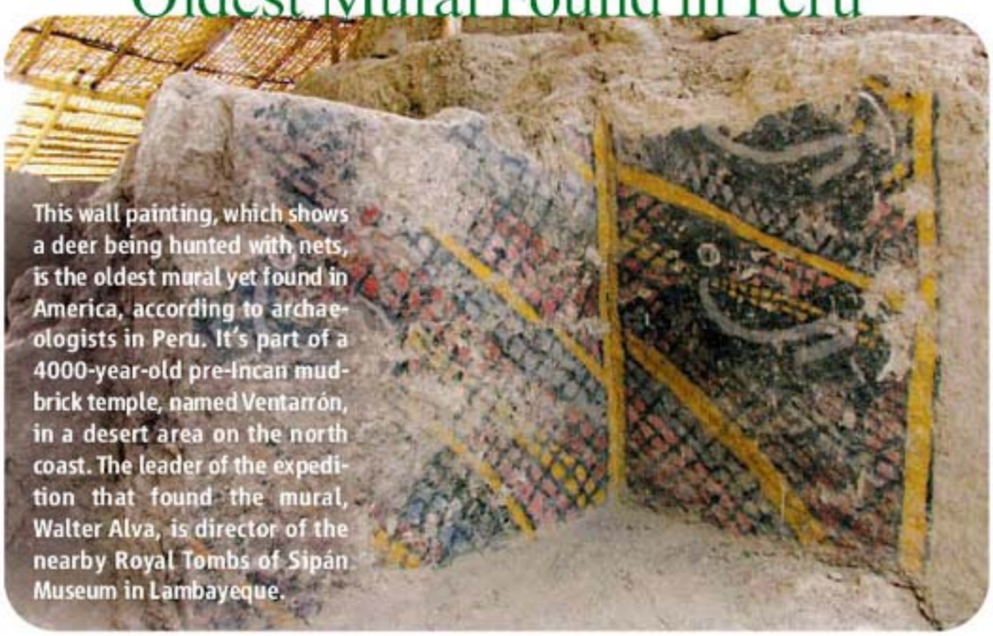

This wall painting, which shows a deer being hunted with nets, is the oldest mural yet found in America, according to archaeologists in Peru. It's part of a 4000-year-old pre-Incan mud-brick temple, named Ventarrón, in a desert area on the north coast. The leader of the expedition that found the mural, Walter Alva, is director of the nearby Royal Tombs of Sipán Museum in Lambayeque.

EDITED BY YUDHIJIT BHATTACHARJEE

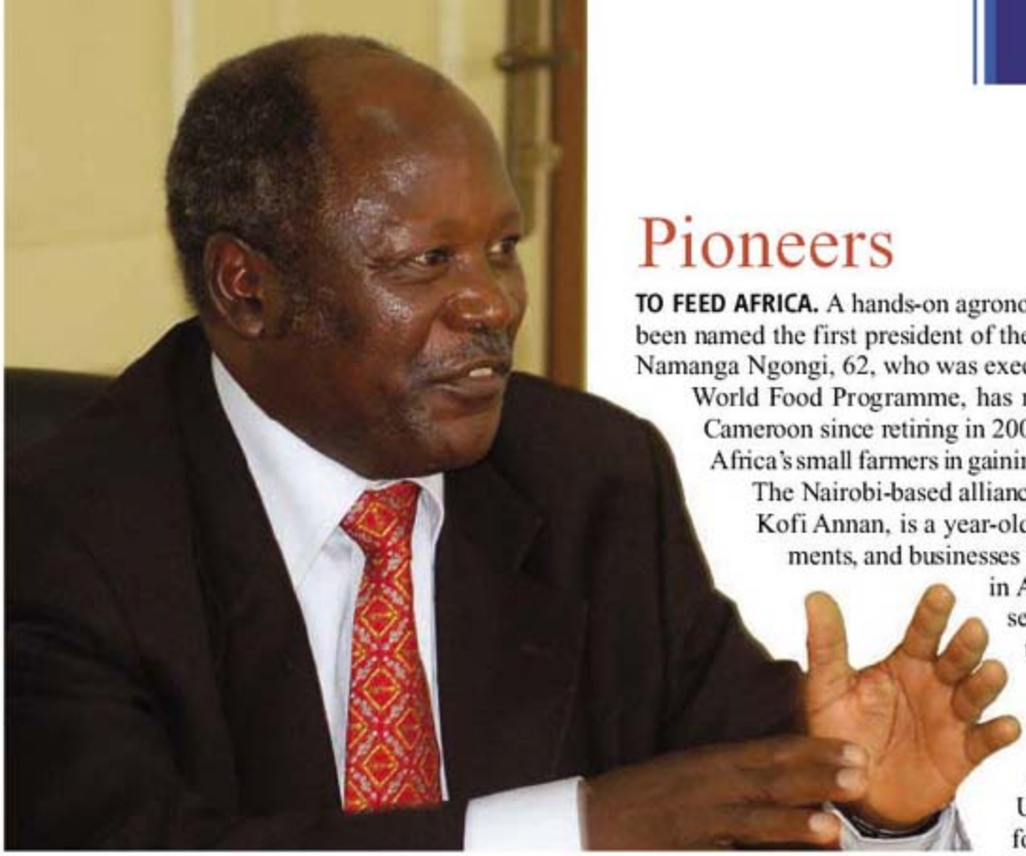

Pioneers

TO FEED AFRICA. A hands-on agronomist with wide international experience has been named the first president of the Alliance for a Green Revolution in Africa. Namanga Ngongi, 62, who was executive director of the United Nations (U.N.) World Food Programme, has run his own palm-oil and plantain farm in Cameroon since retiring in 2003. "As a farmer, I know the critical needs of Africa's small farmers in gaining access to equipment and finances," he says. The Nairobi-based alliance, chaired by former U.N. secretary-general Kofi Annan, is a year-old partnership of scientists, farmers, governments, and businesses that support innovative agricultural practices in Africa. It is developing programs to improve seeds, soil health, market access, and agricultural education, including graduate programs at African universities. The multiplicity of crops makes Africa more of a challenge than other parts of the world, says Ngongi, who earned a Ph.D. in agronomy from Cornell University in 1976. But he says he's looking forward to the challenge.

AWARDS

Sudanese molecular biologist **Hiba Mohamed** has won a $120,000 research prize from the Royal Society and Pfizer to continue her work on leishmaniasis, a disease borne by sand flies. Mohamed, a researcher at the Institute of Endemic Diseases in Khartoum, has been studying the genetic factors that determine an individual's susceptibility to the disease. The award was established last year to help boost research capacity in developing countries.

MOVERS

BIO GOLD. Neurobiologist and biotech entrepreneur Corey Goodman has been tapped to lead Pfizer Inc.'s new Biotherapeutics and Bioinnovation Center in South San Francisco, California. Goodman says his mission is to "supercharge" Pfizer's research on biological treatments such as antibodies and RNA interference until it matches the company's traditional strength in small-molecule drug discovery.

The New York City–based drug giant is looking for future blockbuster drugs to offset looming patent expirations. Goodman says the new center will employ only a few hundred scientists in order "to keep that biotech entrepreneurial spirit." He will also oversee alliances with biotech companies and scout for new collaborations or acquisitions.

Goodman's appointment comes as molecular geneticist Martin Mackay takes over the company's $7.6 billion global research and development effort. Goodman, who has co-founded two biotech firms in the past 13 years and has served on the faculties at Stanford University in Palo Alto, California, and the University of California, Berkeley, will keep a toe in the academic waters as an adjunct professor at UC San Francisco.

CREDITS (TOP TO BOTTOM): AGRA; SOURCE: COREY GOODMAN, WHOI

Got a tip for this page? E-mail people@aaas.org

THEY SAID IT

"If failure to compromise continues, the world community must accept responsibility and ensure that any cloned individual receives full human rights protections."

—Brendan Tobin, co-author of a United Nations report issued last week calling for a worldwide ban on human cloning.

NONPROFIT WORLD

BACK ON DECK. The former director of the Woods Hole Oceanographic Institution (WHOI) in Massachusetts has been named the first president of a new $120 million organization dedicated to increased support for U.S. ocean science. Robert Gagosian takes the reins of the Consortium for Ocean Leadership in Washington, D.C., formed earlier this year in a merger of the Consortium for Oceanographic Research and Education and the Joint Oceanographic Institutions.

WHOI grew significantly during his 12 years as its leader, adding labs and a new ship. Gagosian says that ocean research is being squeezed by rising oil prices and increased costs of ship maintenance and operations, but he's hopeful that greater awareness of climate change could mean a rising tide for the field. "If we can't get an increase for ocean science now, I don't know when we could," he says. He starts 1 December.

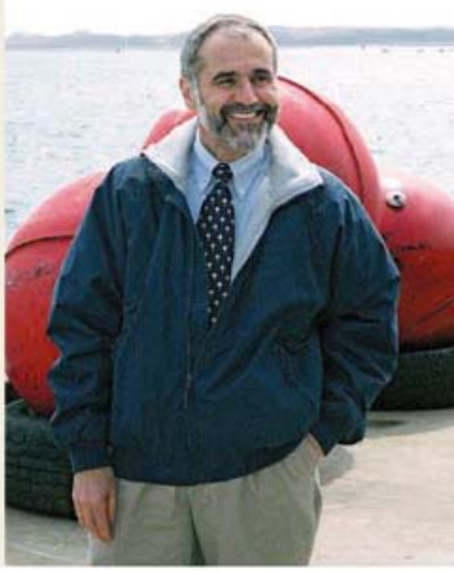

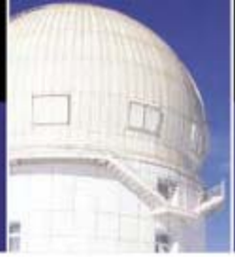

A king's birthday present 1228

Dispute over flu data escalates 1229

DEVELOPMENTAL BIOLOGY

Field Leaps Forward With New Stem Cell Advances

For a year and a half, stem cell researchers around the world have been racing toward a common goal: to reprogram human skin cells directly into cells that look and act like embryonic stem (ES) cells. Such a recipe would not need human embryos or oocytes to generate patient-specific stem cells—and therefore could bypass the ethical and political debates that have surrounded the field for the past decade.

The pace was set in June 2006, when Shinya Yamanaka of Kyoto University in Japan reported that his group had managed the feat in mice by inserting four genes into cells taken from their tails (*Science*, 7 July 2006, p. 27). Those genes are normally switched off after embryonic cells differentiate into the various cell types. The pace picked up in June this year, when Yamanaka and another group showed that the cells were truly pluripotent (*Science*, 8 June, p. 1404).

Now the race has ended in a tie, with an extra twist: Two groups report this week that they have reprogrammed human skin cells into so-called induced pluripotent cells (iPCs), but each uses a slightly different combination of genes. In a paper published online in *Cell* on 20 November, Yamanaka and his colleagues report that their mouse technique works with human cells as well. And in a paper published at the same time online in *Science* (www.sciencemag.org/cgi/content/abstract/1151526), James Thomson of the University of Wisconsin, Madison, and his colleagues report success in reprogramming human cells, again by inserting just four genes, but two of the genes are different from those Yamanaka uses.

Among stem cell scientists, the human cell reprogramming feats have somewhat overshadowed another major advance reported online in *Nature* last week: A team at the Oregon National Primate Research Center has officially become the first to obtain embryonic stem cells from cloned primate embryos, an advance that brings therapeutic cloning closer to reality for humans. Taken together, these feats suggest that scientists are getting very close to uncovering the secret of just what occurs in an oocyte to turn back the clock in the DNA of a differentiated cell.

The two human reprogramming papers could help solve some of the long-standing political and ethical fights about stem cells and cloning. The technique produces pluripotent cells, cells with the potential to become any cell type in the body, without involving either embryos or oocytes—two sticking points that have made embryonic stem cell research so controversial. Ian Wilmut of the University of Edinburgh, U.K., says that once he learned of Yamanaka's mouse work, his lab set aside its plans to work on human nuclear transfer experiments, otherwise known as research cloning. The new work now confirms that decision, he says. Direct reprogramming to iPCs "is so much more practical" than nuclear transfer, he says.

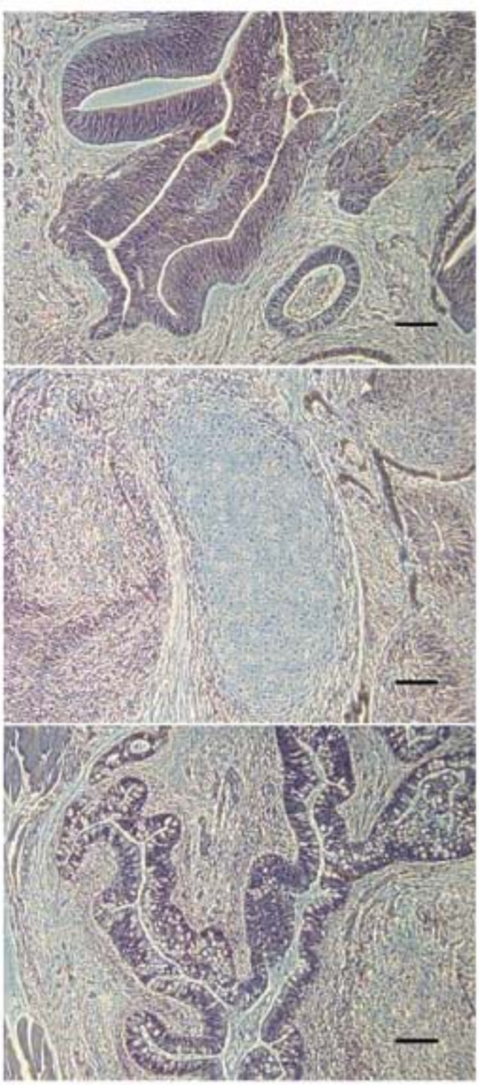

Full of potential. Human induced pluripotent cells form teratomas, tumors with multiple cell types.

CREDIT: J. YU ET AL., SCIENCE

In the new work, Yamanaka and his colleagues used a retrovirus to ferry into adult cells the same four genes they had previously employed to reprogram mouse cells: *OCT3/4*, *SOX2*, *KLF4*, and *c-MYC*. They reprogrammed cells taken from the facial skin of a 36-year-old woman and from the connective tissue of a 69-year-old man. Roughly one iPC cell line was produced for every 5000 cells they treated with the technique, an efficiency that enabled them to produce several cell lines from each experiment.

Thomson says he and his colleagues already had their own list of 14 candidate reprogramming genes when Yamanaka's mouse results were published. They, like Yamanaka's group, gradually whittled down the list through a systematic process of elimination. Thomson's experiments led to four factors as well: *OCT3* and *SOX2*, as Yamanaka used, and two different genes, *NANOG* and *LIN28*. *NANOG* is another gene associated with ES cells, and *LIN28* is a factor that seems to be involved in processing messenger RNA.

Instead of cells from adults, Thomson and his team reprogrammed cells from fetal skin and from the foreskin of a newborn boy. But Thomson says they are working on experiments with older cells, which so far look promising. Their experiments reprogrammed about one in 10,000 cells. The efficiency is less than that of Yamanaka's technique, Thomson says, but is still enough to create several cell lines from a single experiment.

Comparing the two techniques might help scientists learn how the inserted genes work to turn back the developmental clock, Yamanaka says. He says his team tried using *NANOG* but saw no effect, and *LIN28* was not in their initial screen. Thomson says his team tried Yamanaka's four genes without success, but that they may have tried the wrong relative doses.

The fact that Thomson's suite doesn't include a known cancer-causing gene is a

A time for action on climate
1230

Killing B cells relieves rheumatoid arthritis
1232

bonus, says Wilmut. (The *c-MYC* Yamanaka used is an oncogene.) But both techniques still result in induced cells that carry multiple copies of the retroviruses used to insert the genes. Those could easily lead to mutations that might cause tumors in tissues grown from the cells. The crucial next step, everyone agrees, is to find a way to reprogram cells by switching on the genes rather than inserting new copies. "It's almost inconceivable at the pace this science is moving that we won't find a way to do this without oncogenes or retroviruses," says stem cell researcher Douglas Melton of Harvard University. "It is not hard to imagine a time when you could add small molecules that would tickle the same networks as these genes" and produce reprogrammed cells without genetic alterations, he says.

Although the cells "act just like human ES cells," Thomson says, there are some differences between the cell types. Yamanaka's group reports that overall human iPC gene expression is very similar, but not identical, to human ES cell gene expression. "It will be probably a few years before we really understand these cells as well as we understand ES cells," Thomson says. But "for drug screening, they're already terribly useful. IVF embryos are very skewed ethnically," he says. But with the new iPC technique, "you can isolate cell lines that represent the genetic diversity of the United States. And I think it will be very straightforward to do."

The primate cloning success, although partially eclipsed by the human work, "is really a breakthrough," says primate stem cell researcher Jose Cibelli of Michigan State University in East Lansing. Although scientists have cloned a host of other animals, primates have proved to be particularly resistant—as demonstrated by the failure of Korean scientist Woo Suk Hwang, whose work with human embryos was shown to be fraudulent 2 years ago.

A group headed by Shoukhrat Mitalipov was able to generate two embryonic stem cell lines after injecting skin cells from a 9-year-old male rhesus macaque into 304 eggs collected from 14 female macaques. The cells showed all the requisite pluripotent stem cell markers; in lab dishes, they generated heart and brain neurons, and in live mice they formed teratomas—tumor tissues from all three germ layers.

Scientists such as Robin Lovell-Badge of the U.K. Medical Research Council have lauded the feat while pointing out that the low success rate—0.7%—means more primate work is needed before women should be asked to donate eggs for such research.

Mitalipov originally reported the achievement last June in Cairns, Australia, at the meeting of the International Society for Stem Cell Research. At the time, he met with some skepticism. Before publishing the paper, *Nature* took the unprecedented step of asking a group headed by David Cram of Monash University in Clayton, Australia, to be sure the cell lines had the same genotype as the donor of the skin cells. Their report is published in the same issue of *Nature*, which issued a statement declaring this a prudent step given the importance of the results and "recent history in the cloning field."

Scientists have discovered that the big peril in cloning, as the Hwang team ultimately discovered, is that what you may really come up with are parthenotes—that is, early embryos arising solely from the activated oocyte. Parthenotes—less useful than clones because they have only the genes of the egg donors—can result when the spindle containing the nuclear DNA is not completely removed before a foreign nucleus is introduced. The usual technique for locating the spindle is with a dye or ultraviolet light, which the researchers suspected could damage fragile primate oocytes. So instead, the Oregon group used a new noninvasive imaging system called Oosight to locate the spindle, then used a probe to suck it out and replace it with the skin cell. Enucleation of the oocyte is 100% efficient with this technique, said Mitalipov. The scientists also changed the culture medium, eliminating calcium and magnesium, which they believe cause premature activation of the oocyte and failure of the donor nucleus to become properly "remodeled."

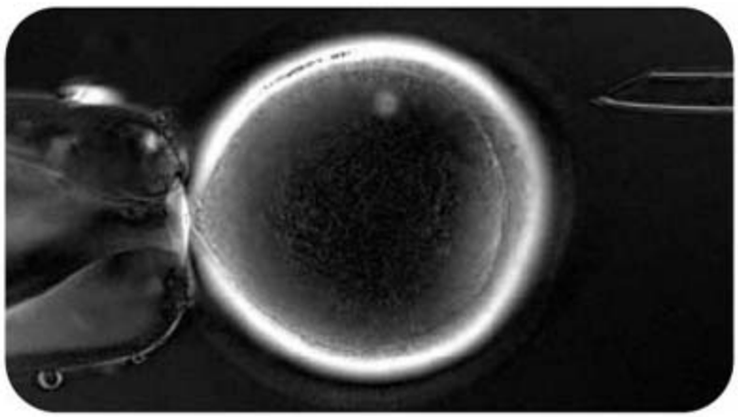

On target. Latest imaging technology clearly shows the egg's nucleus, to be withdrawn by pipette at right. Semos (*below*), the male macaque whose skin cells made history.

Although the cloning "efficiency is still low," Mitalipov said at a press conference, "I believe the technology we developed can be directly applicable to humans."

Robert Lanza of Advanced Cell Technology in Worcester, Massachusetts, calls the Oregon paper a "turnaround," saying that it marks a "recovery for the field," because the Hwang paper was retracted in January 2006. The next step, says Mitalipov, will be to test cloning for treatment of a disease, something that hitherto has been tried only in the mouse. A likely target is diabetes, says Mitalipov, who plans to inject cloned, genetically modified ES cells into a monkey model of the disease.

"I cannot emphasize enough how useful these [cloned primate ES] cells will be" for studying other diseases that also affect humans, says Cibelli. Another application, he says, will be to compare the cloned primate ES cells with cells reprogrammed by the methods Yamanaka and Thomson used. "If their method is as good as the oocyte" in reprogramming somatic cells, says Cibelli, "we will be no longer in need of oocytes, and the whole field is going to completely change. People working on ethics will have to find something new to worry about."

–GRETCHEN VOGEL AND CONSTANCE HOLDEN

CREDITS (TOP TO BOTTOM): SHOUKHRAT M. MITALIPOV, OHSU

CLINICAL RESEARCH

ALS Trial Raises Questions About Promising Drug

An antibiotic long thought to hold promise for treating neurologic diseases failed dramatically in a recent clinical trial; this news has sparked a debate about why the drug flopped and whether the results should be interpreted broadly. In a study of 412 people with amyotrophic lateral sclerosis (ALS), published earlier this month, scientists were startled to find that patients on the drug, minocycline, declined more quickly than those on a placebo. Now clinics are urgently tracking down ALS patients whose physicians have prescribed minocycline off label. Many have been taking the drug—approved in the 1970s to treat certain infections—because animal studies have shown it can slow the course of brain diseases, and some small human trials have suggested that it's safe. That did not appear to be the case here.

The disappointing outcome may affect new or ongoing trials of minocycline for other conditions, including multiple sclerosis (MS) and Huntington's disease. Researchers leading these trials generally reject the idea that the drug's showing in ALS, published online 1 November in *The Lancet Neurology*, has much bearing. "We don't really believe that the ALS data adds something, but when it's out there, you have to deal with it," says neurologist Luanne Metz of the University of Calgary in Canada, who is beginning a study of minocycline in 200 people at risk for MS. She argues that MS is very different from ALS—more autoimmune than neurodegenerative—and unlikely to respond in the same way. Still, Metz's trial has added extra safety monitoring.

In contrast, the authors of *The Lancet Neurology* paper are quite concerned, arguing that their trial "generates the need to re-examine … the justification for other trials of minocycline in patients with neurological disorders." Over 9 months of treatment, the ALS patients on minocycline declined 25% faster, as measured by a functional rating scale, than did those taking a placebo. But there was no significant difference in death rates between the two groups, and the patients rated quality of life equally, suggesting that the decline was subtle.

Exactly what went wrong remains a mystery. Merit Cudkowicz, a neurologist at Massachusetts General Hospital in Boston who is running a minocycline trial in 100 patients with Huntington's disease, believes the drug doses in the ALS study were too high, as much as double what she and Metz are using. But Paul Gordon, who led the ALS trial and works as a neurologist at Columbia University and at Hôpital de la Pitie-Salpêtrière in Paris, notes that patients on the higher doses did no worse than those on lower ones, nor did side effects appear to correlate with deterioration. "We're sort of left with scratching our heads," he says.

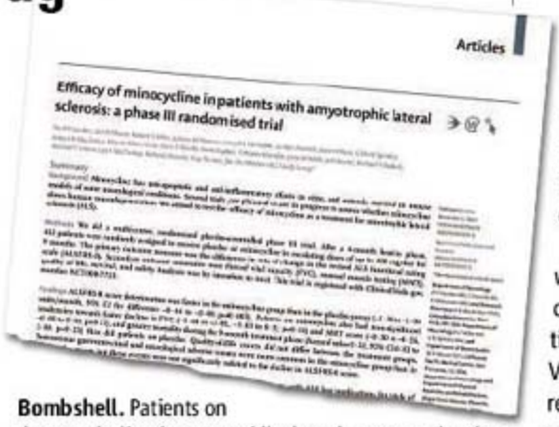
Articles

Efficacy of minocycline in patients with amyotrophic lateral sclerosis: a phase III randomised trial

Bombshell. Patients on therapy declined more rapidly than those on a placebo.

The results are especially confusing because published animal studies suggested that the drug can suppress neuroinflammation and inhibit cell death. But Gordon notes that mouse studies didn't really reflect the way ALS patients are treated. For example, the mice received minocycline before they began showing symptoms.

Animal experiments offer only a rough guide to human testing, says neurologist Nigel Leigh of King's College London, who still hopes that minocycline will prove useful for ALS. Leigh says it's possible that high doses of the antibiotic were neurotoxic for patients, whereas lower doses might be neuroprotective. He'd been planning with colleagues to launch a minocycline study in 1000 ALS patients; now he's seeking approval for a revised proposal to identify an ideal minocycline dose in a smaller group of patients.

"It would be hasty to stop every trial" testing the drug, agrees John Marler, an associate director for clinical trials at the U.S. National Institute of Neurological Disorders and Stroke in Bethesda, Maryland. Even very brief trials of minocycline, though, will consider whether to modify their protocols, says Marler, such as a 3-day acute stroke trial recently funded by the institute. Adds Marler: "We're not going to overlook any possible relief" for these patients.

–JENNIFER COUZIN

Church Blesses Stem Cell Studies

With the support of the pope and the Italian Episcopal Conference, which represents all the bishops of Italy, Bishop Vincenzo Paglia of Terni announced last week that he has provided University of Milan-Bicocca researcher Angelo Vescovi with €380,000 to isolate stem cells from naturally miscarried fetuses and test whether the cells can help people afflicted with multiple sclerosis or amyotrophic lateral sclerosis.

It's the first time Italy's Catholic Church, which has strongly opposed embryonic stem cell work and all in vitro fertilization practices, has funded any stem cell research, says Vescovi, who openly sided against ES cell research in a 2005 referendum in Italy. The overall project will cost about €2 million, and Vescovi says the remaining funds have been pledged by private and public sources. He now seeks regulatory approval in Europe or the United States to start clinical testing of his fetal stem cells in the next few months.

But University of Milan stem cell researcher Elena Cattaneo says, "scientists should have more data on stem cells from naturally miscarried fetuses before proceeding [to the clinic]." –FRANCESCO DE PRETIS

Brits Wish Scopes Farewell

The United Kingdom announced plans last week to withdraw from the Gemini Observatory, cutting the country off from two of the world's most advanced telescopes. Gemini's twin 26-foot telescopes in Hawaii and Chile allow astronomers from a seven-nation consortium an unobstructed view of the entire night sky. The United Kingdom had invested about £35 million in building Gemini. "No one was expecting this," says astronomer Roger Davies of the University of Oxford, U.K. The United Kingdom has other access to Southern Hemisphere telescopes, but Davies says the loss of access to the northern skies would jeopardize the country's extrasolar-planet detection and dark-energy research.

The U.K. Science and Technology Facilities Council, meeting this week to finalize the withdrawal, says the move will help it focus financial resources on the "highest priority programmes." But the council declined to explain how much money the decision will save. The United Kingdom pays about £4 million each year in Gemini operating costs, and under the consortium's 1992 agreement, a country that withdraws would lose its observing time and still be liable for those costs for 2 years, explains Jean-René Roy of the Gemini Observatory.

–ELIZABETH QUILL

ASTRONOMY

If You Build It, Will They Come?

CHIANG MAI, THAILAND—With an espresso stand, a gift shop, and a misty forest festooned with orchids and red rhododendrons, the 2550-meter summit of Inthanon Mountain lacks the grandeur of Fuji or the towering remoteness of Everest. But new construction atop Thailand's tallest peak is still making a statement: This Southeast Asian nation intends to become a serious player in global astronomy and a regional leader in the field.

Earlier this year, Thailand began building an observatory complex on Inthanon, about 100 kilometers west of the temple city of Chiang Mai in northern Thailand. The centerpiece of the $40 million program will be a 2.4-meter optical telescope for studying binary stars and searching for extrasolar planets. It will match the size of the largest instrument in mainland Asia—a newly installed 2.4-meter scope at Yunnan Observatory in Kunming, China, that is about to undergo a year of testing—and serve astronomers from across Southeast Asia and beyond. "It's a bold vision," says John Hearnshaw, an astronomer at the University of Canterbury in Christchurch, New Zealand, who assessed Thailand's ambitions on behalf of the International Astronomical Union.

Not everyone is enamored with the project, which is expected to be completed in March 2009. Some scientists have questioned such a large investment in astronomy by a country struggling to build capacity in biology and other fields more tightly coupled to economic growth. Others assail the telescope itself. "People in their right mind would not invest a huge sum of money to build an optical telescope in a tropical area with high humidity," says one Thai astronomer, who dismisses the project as "a white elephant."

Hearnshaw defends the decision. "Certainly the rainy season will curtail the observing season," he says. "But that won't be a disaster." He predicts that observing "should be reasonably good" for 9 months a year and that the telescope will be a valuable addition in tracking sudden events like gamma ray bursts and supernovae. "Many of the most exciting discoveries of the last 25 years in optical astronomy have come from small to medium telescopes on the ground," Hearnshaw says.

Thailand is home to only about a dozen research astronomers. Even so, the new telescope, to be dedicated to King Bhumibol Adulyadej, the world's longest serving head of state, won't be the first major astronomical facility on the mountain. Earlier this year, three universities—Mahidol, Chulalongkorn, and Ubon Rajathanee—used equipment donated by Japan's Shinshu University to build a cosmic-ray detector at a unique spot in Earth's geomagnetic profile.

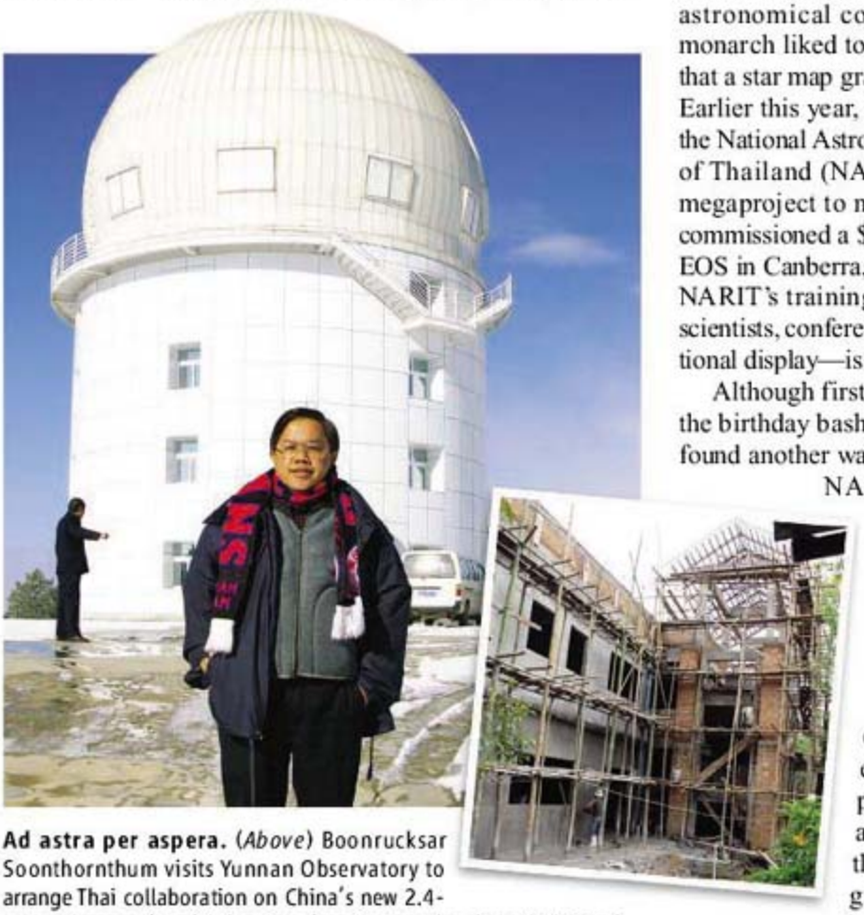

Ad astra per aspera. (*Above*) Boonrucksar Soonthornthum visits Yunnan Observatory to arrange Thai collaboration on China's new 2.4-meter telescope. (*Inset*) A dormitory for scientists takes shape in Thailand.

The neutron monitor is named after Princess Maha Chakri Sirindhorn, an astronomy buff, and situated on the grounds of a Royal Thai Air Force radar installation adjacent to the 2.4-meter telescope site. It studies solar cycles and serves as a space-weather sentinel. The geomagnetic equator passes through Thailand, and Earth's magnetic field bulges toward Southeast Asia, producing the strongest horizontal magnetic field on the planet. That dynamo allows only the toughest cosmic particles through. "Our station is registering the most energetic cosmic rays of any neutron monitor in the world," says astrophysicist David Ruffolo of Mahidol University in Bangkok. Such sensitivity, his group has shown, could provide a 4-hour warning of an oncoming geomagnetic storm—more than twice the lead time of space-weather satellites.

Four years ago, the Thai government requested proposals to commemorate King Bhumibol's 80th birthday this month. Astronomer Boonrucksar Soonthornthum, who has labored to raise education standards and the country's profile in the international astronomical community, noted that the monarch liked to stargaze in his youth and that a star map graces a ceiling in his palace. Earlier this year, the Thai cabinet approved the National Astronomical Research Institute of Thailand (NARIT) as the sole science megaproject to mark the birthday. NARIT commissioned a $7.8 million telescope from EOS in Canberra, Australia. Construction of NARIT's training center—dormitories for scientists, conference facilities, and an educational display—is in full swing.

Although first light will occur long after the birthday bash, Boonrucksar's outfit has found another way to celebrate. Next week, NARIT will host an International Olympiad here in astronomy and astrophysics. Some two dozen countries have agreed to send teams of five high school students.

Boonrucksar sees the Olympiad as part of a larger effort to "teach young people how to think critically and analytically." That's also the goal behind funding four graduate fellowships a year in astronomy, for study abroad, as part of the telescope project. Thailand hopes to lure foreign talent, too. Expanding the ranks of astronomers "is certainly necessary if the investment in the telescope is to be justified," Hearnshaw says.

Boonrucksar deserves credit for succeeding "against all odds" in putting Thailand on the astronomical map, says cosmologist Burin Gumjudpai of Naresuan University in Phitsanulok, Thailand. "It gives us hope," he says, "that astronomy can be a real career here."

–RICHARD STONE

CREDITS (TOP TO BOTTOM): COURTESY OF BOONRUCKSAR SOONTHORNTHUM; R. STONE/SCIENCE

Isolated. Indonesia has had the world's greatest number of H5N1 deaths, even while the country flip-flops on sharing flu samples with the World Health Organization.

CREDIT: TRISNADI/AP PHOTO

AVIAN INFLUENZA

More Bumps on the Road to Global Sharing of H5N1 Samples

A battle between Indonesia and the World Health Organization (WHO) is escalating. Indonesia's health minister, Siti Fadilah Supari, has claimed that WHO is refusing to return dozens of H5N1 influenza viruses isolated from Indonesian samples. WHO calls the claims baseless and says Indonesia can get back the viruses once it shows it can handle them safely. The clash promised to complicate what was already expected to be a difficult international meeting about pandemic preparedness, slated to start in Geneva, Switzerland, this week, after *Science* went to press.

At issue are 56 specimens from human H5N1 victims that Indonesia has shared with WHO as part of the Global Influenza Surveillance Network over the past few years. As usual, the samples have gone to WHO's four Collaborating Centres in London, Atlanta, Tokyo, and Melbourne, where researchers isolate and study the virus. Their analysis helps WHO monitor virus evolution, drug resistance, and pandemic risk, as well as aiding vaccine development. Indonesia, by far the most heavily afflicted country with 113 human cases and 91 deaths, has protested the scheme; the country worries that even if it collaborates, it will not have access to vaccines if a pandemic occurs. So far in 2007, Indonesia has shared only two samples, says David Heymann, who heads WHO's pandemic influenza efforts.

Heymann says that at Supari's request, on 31 October WHO sent Indonesia a list of the 56 specimens the country had submitted to the network prior to 2007. He says the four labs had isolated H5N1 virus from 40 of them. But according to a report in the *Jakarta Post*, Supari said at a press conference in Jakarta on 8 November that WHO refuses to send the samples back. "We keep asking [WHO] to return the samples because they belong to us. This is for the sake of our country's sovereignty," the newspaper quoted Supari as saying. Health ministry officials could not be reached to confirm the report. Heymann claims Supari is trying to cast WHO in a bad light. "She has always said she doesn't trust WHO, and she's finding new reasons not to trust us," he says.

Masato Tashiro, director of the WHO Collaborating Centre for Reference and Research on Influenza in Tokyo, says he believes Indonesia did not retain part of the samples, as countries usually do, because it previously did not have the biosafety level 3 (BSL-3) laboratories recommended for handling dangerous pathogens. Indonesia had cooperated with WHO's flu-sharing network until early this year when it learned that an Australian company had developed a vaccine using an Indonesian H5N1 strain. Fearing that such a vaccine made outside the country would be out of reach financially, Indonesia started developing its own research and development capabilities while withholding specimens and demanding capacity-building assistance from the international community. Tashiro says that when the institutions requesting viruses can certify that their planned BSL-3 labs are up and running, getting viruses returned from Japan—and probably other countries—would be routine.

Although Indonesia is the only country that has stopped sending samples, it is reportedly trying to persuade others to follow course. Widjaja Lukito, a physician at the University of Indonesia in Jakarta and a member of Indonesia's delegation to the Geneva meeting, says Indonesia would "clarify everything" in Geneva. Heymann and others say any interruption of the 55-year-old sharing system would create a huge risk for global health.

–MARTIN ENSERINK AND DENNIS NORMILE

SCIENCESCOPE

NIH Budget Boost Fails

The House last week failed to override a presidential veto of a 2008 spending bill, dashing hopes for a 3.8% budget boost for the National Institutes of Health (NIH). On 13 November, President George W. Bush vetoed the $151 billion bill funding labor, health, and education programs, calling it fiscally irresponsible. Although the Administration had asked for a $279 million cutback at NIH, this proposal included a $1.1 billion raise. The attempt to override the veto in the House on 15 November was close but fell two votes short of the two-thirds majority needed (277–141).

Lawmakers are now talking about meeting the president halfway, suggesting an increase of only $700 million for NIH, according to David Obey (D–WI), chair of the House Appropriations Committee. National Cancer Institute Director John Niederhuber told advisers last week that he expects the 2008 appropriation won't be finalized until February. For now, NIH and other agencies are operating at 2007 levels under a continuing resolution that expires on 14 December.

–JOCELYN KAISER

Reprieve Granted on Grants

The National Health Council (NHC) is on the prowl for $250,000 to fund a proposed database of rejected National Institutes of Health (NIH) grants. Under the plan, developed by NHC, a consortium of medical corporations and nonprofits based in Washington, D.C., investigators would submit the title, abstract, and other information from their rejected NIH proposals to a searchable database. Jo Anne Goodnight of NIH's Office of Extramural Research says the database would allow smaller organizations to leverage the NIH peer-review process. **–BENJAMIN LESTER**

Protesters Strike Again

PARIS—French academic life came to a partial standstill last week as students occupied or blocked access to faculty buildings at half of the country's 85 universities to demand the repeal of a law that gives those schools more freedom to handle budgets, staffing, and housing decisions. Many researchers applaud the reforms, which are slated for implementation in the coming months, but radical student unions fear they will increase inequality among universities and give business too much influence. A countermovement of students claiming the "right to study" has emerged. **–MARTIN ENSERINK**

How Urgent Is Climate Change?

Having issued their fair and balanced consensus document, many climate scientists now cite oft-overlooked reasons for immediate and forceful action to curb global warming

THE LATEST REPORTS FROM THE NOBEL Prize–winning Intergovernmental Panel on Climate Change (IPCC) were informative enough. Humans are messing with climate and will, sooner or later, get burned if they keep it up. But just how urgent is this global warming business?

IPCC wasn't at all clear on that, at least not in its summary reports. In the absence of forthright guidance from the scientific community, news about melting ice and starving polar bears has stoked the public climate frenzy of the past couple of years. Climate researchers, on the other hand, prefer science to headlines when considering just how imminent the coming climate crunch might be. With a chance to digest the detailed IPCC products that are now available (www.ipcc.ch), many scientists are more convinced than ever that immediate action is required. The time to start "is right now," says climate modeler Gerald Meehl of the National Center for Atmospheric Research in Boulder, Colorado. "We can't wait any longer."

What worries these researchers is the prospect that we've started a slow-moving but relentless avalanche of change. A warming may well arrive by mid-century that would not only do immediate grievous harm—such as increase drought in vulnerable areas—but also commit the world to delayed and even more severe damage such as many meters of sea-level rise. The system has built-in time lags. Ice sheets take centuries to melt after a warming. The atmosphere takes decades to be warmed by today's greenhouse gas emissions. And then there are the decades-long lags involved in working through the political system and changing the world energy economy. "If you want to be able to head off a few trillions of [dollars of climate] damages per year a few decades out," says glaciologist Richard Alley of Pennsylvania State University in State College, "you need to start now."

Bad things, soon

The disturbing message on the timing of global warming's effects comes in the IPCC chapters and technical summaries quietly posted online months after each of three working groups released a much-publicized Summary for Policymakers (SPM). An overall synthesis of the working group reports was released Saturday at the 27th session of IPCC. Earlier this year, only the SPMs went through the wringer of word-by-word negotiations with governments, which squeezed out a crucial table and part of another (*Science*, 13 April, p. 188). That information—which was always in the full reports—along with other report material, makes it clear that substantial impacts are likely to arrive sooner rather than later.

Early target. Some mountain-dwelling amphibians are already feeling the heat.

Table TS.3 of Working Group II's technical summary, for example, lays out projected warmings. The uncertainties are obvious. Decades ahead, models don't agree on the amount of warming from a given amount of greenhouse gas, and no one can tell which of a half-dozen emission scenarios—from unbridled greenhouse-gas production to severe restraint—will be closest to reality. But this table strongly suggests that a middle-of-the-road, business-as-usual scenario would likely lead to a 2°C warming by about the middle of this century.

Lined up beneath the projected warmings in the table are the anticipated effects of each warming. Beneath a mid-century, 2°C warming is a litany of daunting ill effects that had previously had no clear timing attached to them: increasing drought in mid-latitudes and semiarid low latitudes, placing 1 billion to 2 billion additional people under increased water stress; most corals bleached, with widespread coral mortality following within a few decades; and decreases in low-latitude crop productivity,

CREDITS (TOP TO BOTTOM): HANS STRAND/CORBIS; CHARLES H. SMITH/U.S. FISH AND WILDLIFE SERVICE

A goner? Time may have run out to prevent the disappearance of summertime Arctic sea ice.

as in wheat and maize in India and rice in China, among other pervasive impacts.

At the bottom of the same table is a category of effects labeled "Singular Events," most dramatically sea level rise. The table shows a "Long term commitment to several metres of sea-level rise due to ice sheet loss" falling between the middle-of-the-road 2°C warming and a 3°C warming, which without drastic emissions reductions might well come by the end of the century. The report calls it a "commitment" because although the temperatures needed to melt much of the Greenland ice sheet might be reached in the next 50 to 100 years, the ice sheet, similar to an ice cube sitting on a countertop, will take time to melt even after the surrounding air is warm enough. Its huge thermal inertia means a lag of at least several centuries before it would largely melt away, flooding much of South Florida, Bangladesh, and major coastal cities.

A laggard system

Ice sheets aren't the only thing that stretches out the time between an action—say, building a coal-fired power plant—and a global warming impact. For example, the atmosphere is slow to warm because the oceans are absorbing some of the heat trapped by the strengthening greenhouse. IPCC estimates that even if no greenhouse gases were added after the year 2000, the oceans' heat would warm the atmosphere 0.6°C by the end of the century, or as much as it warmed in the last century. So the world is already committed to almost one-quarter of the warming that can be expected late in the century. And half the warming of the next couple of decades will be carried over from emissions in the past century.

Then there are the lags that come into play ahead of the climate system. The technological infrastructure that does most of the emitting—the gasoline-fed cars and coal-fired power plants, primarily—will have to be radically altered if greenhouse emissions are to be drastically reduced. The speed at which infrastructure can be changed depends on the perceived urgency, says energy-climate analyst James Edmonds of the Pacific Northwest National Laboratory's office in College Park, Maryland. Past transitions from one energy source to another—say, wood to coal—took upward of 50 to 100 years, he notes. But even with a Manhattan Project imperative—something nowhere in sight—weaning cars off oil, building nuclear power plants, and rigging coal power plants to shoot the carbon dioxide into the ground will take decades, not years.

And there's the lag while governments crank up the will to fundamentally alter the global energy system. "The biggest lag is in the political system," says geoscientist Michael Oppenheimer of Princeton University. A couple of decades have already passed discussing the seriousness of the threat, as he sees it, and at the present rate it could be another 20 years before a worldwide program up to the task is in place.

Yet another lag would enter the calculation for taking action if policymakers waited for more research to narrow the scientific uncertainties. In the 1980s, for example, the biggest uncertainty in climate science was clouds and how they would react to climate change.

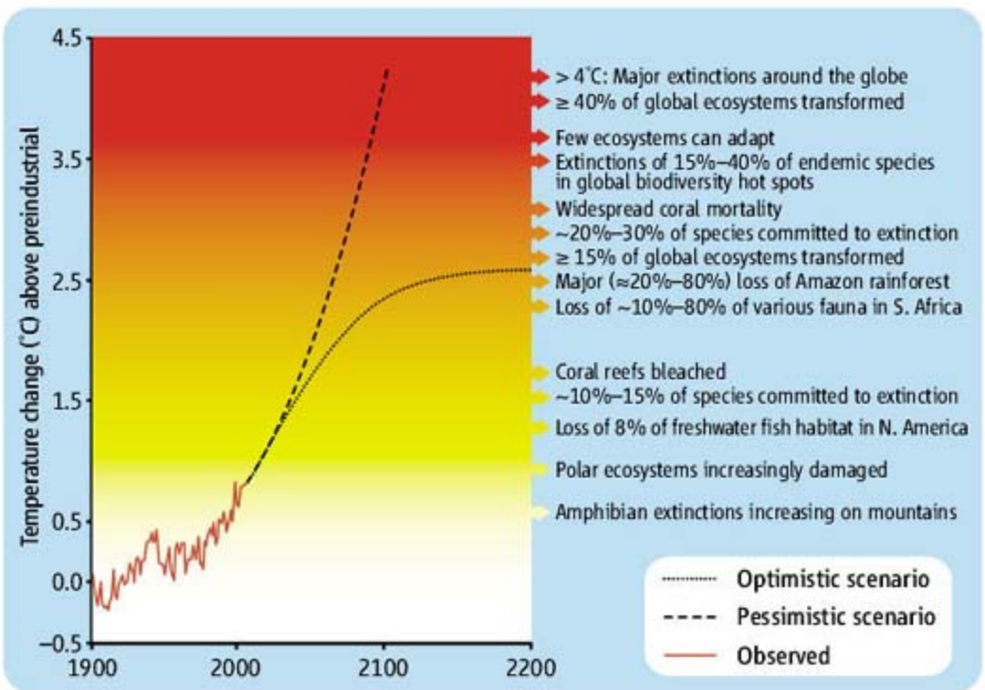

SOURCE: MODIFIED FROM IPCC WORKING GROUP II'S 2007 TECHNICAL SUMMARY, FIGURE TS.6

Fifteen years later, "we are essentially where we were then," says atmospheric scientist Robert Charlson of the University of Washington, Seattle. Clouds are still poorly understood, as are pollutant hazes, another collection of microscopic particles with a highly uncertain effect on future climate.

With all these known time lags adding up to many decades, a lot of climate scientists say that the time for serious action is now. "We can't really afford to do a 'wait and learn' policy," says Oppenheimer. "The most important question is, when do we commit to 2°? Really, there isn't a lot of headroom left. We better get cracking."

Fear of the unknown

Physics and socioeconomics may make piloting the ponderous ship of climate a cumbersome business, but researchers are also worried about navigating around the hazards they fear may be lurking unseen beneath the surface. They've hit hidden obstacles before. Back in the 1970s, atmospheric chemists were worrying that pollutant chlorine might be destroying stratospheric ozone over their heads. Yet all the while, that chlorine was teaming up with ice-cloud particles over Antarctica to wipe out stratospheric ozone through a mechanism that scientists had overlooked.

Prestigious committees have been warning for 25 years that similar surprises could spring from the climate system. A few may be starting to show themselves. Arctic sea ice took a nosedive last summer, prompting concerns that feedbacks not properly included in models are taking hold and accelerating ice loss (*Science*, 5 October, p. 33). Glaciers draining both southern Greenland and West Antarctic have suddenly begun rushing to the sea, and glaciologists aren't sure why (*Science*, 24 March 2006, p. 1698). And theorists recently reminded their colleagues that they will never be able to eliminate the small but very real chance that the climate system—contrary to most modeling—is hypersensitive to greenhouse gases.

The uncertainties are adding up. "You can hope the uncertainties are going to break your way," says policy analyst Roger Pielke Jr. of the University of Colorado, Boulder. "There have been times they did. But if you play that game often enough, you're going to lose some pretty big bets sometimes." In the case of global warming, Pielke says, "we don't have a lot of time to wait around." Edmonds agrees. If avoiding a 2°C warming is the goal, "the world really has to get its act together pretty damn fast. The current pace isn't going to do it."

–RICHARD A. KERR

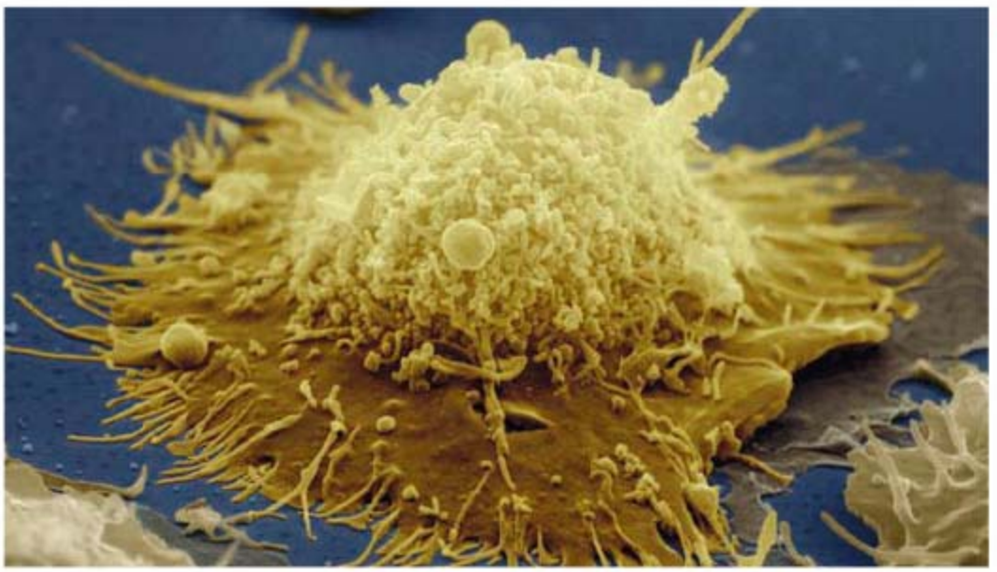

B gone. Killing B cells (*left*) could be a treatment for autoimmune diseases.

AUTOIMMUNE DISEASES

The B Cell Slayer

It took nearly a decade for Jonathan Edwards to persuade people that killing B cells could relieve symptoms of rheumatoid arthritis. Multiple sclerosis is his next target

LONDON—For someone who has just seen his ideas for treating a crippling disease vindicated after years of rejection, Jonathan Edwards is remarkably self-effacing. Asked whether he feels he has brought hope to some of the millions with rheumatoid arthritis (RA), the 57-year-old rheumatologist tends to look at his shoes or up at the ceiling. Edwards would much rather talk about where he plans to go next than to dwell on how his University College London (UCL) team's decade-long pursuit of an unfashionable idea has now led to a new RA therapy approved in the United States and in Europe.

The unfashionable idea advocated by Edwards is that RA stems from the misbehavior of denizens of the bloodstream known as B cells. These white blood cells play a key role in the body's immune system, releasing disease-fighting antibodies that have exquisite specificity for molecular targets, normally those on pathogens. B cells are also obvious suspects in autoimmune conditions such as RA, in which the immune system goes haywire and starts unleashing friendly fire within normal healthy tissue. Yet the idea of their involvement fell out of favor in the 1970s when autoimmune researchers interested in RA turned their attention to a different white blood cell, the T cell.

Edwards, however, has breathed new life into the B cell theory of RA by providing evidence that eliminating these cells in patients can ease their symptoms. "Edwards deserves great personal credit; … he was a strong, consistent voice at a time when most others were not looking at B cells as central to rheumatoid arthritis pathogenesis," says rheumatologist Gregg Silverman of the University of California, San Diego.

B cell–depletion therapy doesn't work for every RA patient, and questions remain about how long the relief it brings lasts. Still, once again challenging conventional wisdom, Edwards is now arguing that B cells hold the key to another autoimmune affliction: multiple sclerosis (MS). And there is already tantalizing clinical evidence that the outcome could be the same—namely, a new therapy for a notoriously recalcitrant disease.

> **"Edwards put B cells back on the agenda."**
>
> —Alan Silman, U.K. Arthritis Research Campaign

The return of B cells

When Edwards began his career in rheumatology in the 1970s, B cells seemed a prime suspect in the cause of RA, as they are the source of so-called rheumatoid factor (RF), a variety of antibody found in high levels in patients with the disease. Yet about 20% of RA patients don't have RF in their blood, and the level of RF doesn't correlate perfectly with the severity of disease.

As researchers struggled to link B cells with what they were seeing in their patients, attention shifted to the behavior of T cells instead. These white blood cells help control B cells and turn up in joint tissue damaged by RA in larger quantities than B cells do. "By the late 1970s, B cells didn't seem to have anything to say. They'd become boring," says Edwards. T cells "were just much more interesting."

For the next 20 years, T cells dominated the research agenda on autoimmune diseases. Yet it became clear, at least to Edwards, that the excitement about T cells was largely misplaced. Anti–T cell therapies failed to work for RA. It also remained unclear that T cells could cause inflammation without the involvement of B cells. Nor, he argued, could T cells account for the persistence of RA.

All this prompted Edwards and his UCL colleague Geraldine Cambridge to begin pondering alternatives in the late 1990s—including the old idea that B cells held the key to therapy. The pair had been struck by the discovery that joint tissue attacked in RA contained two molecules—VCAM-1 and DAF—known to promote the persistence of B cells.

By 1998, Edwards and Cambridge had the framework of a new explanation for RA based on B cells. Put simply, they suspected that the problem was a few bad apples. The body maintains a vast array of B cells, each producing an antibody with a unique shape, many of which prove useful in fighting disease. By chance, however, some B cells inadvertently produce antibodies that attack healthy tissue. Normally, the B cells producing these "autoantibodies" are destroyed. But in a disastrous twist in some people, the UCL team proposed, some of these autoantibodies undermine the weeding-out process, keeping the bad-apple B cells alive and also prompting T cells to help these B cells make yet more of their destructive antibodies. "The result is a vicious cycle," says Edwards.

The test of this hypothesis was obvious: Eliminate B cells from people with RA and let the immune system "reboot" with new B cells. The odds that the same bad apples would arise again and survive weeding out would be very small. As luck would have it, a drug capable of killing B cells but sparing

the stem cells that make them had just reached the market. Approved in 1997 for use with B cell lymphomas, rituximab is a monoclonal antibody specially designed to home in on and knock out the immune cells. If Edwards and Cambridge were right, rituximab could also be the basis of a treatment for RA. A largely safe one, moreover: Studies of rituximab in hundreds of cancer patients had produced relatively few side effects and shown that people could temporarily lose all their B cells without suffering too many problems from suppression of their immune systems.

The pair tried to publish their B cell theory—only to encounter responses from journals ranging from lukewarm to cryogenic. "We were told there was already a perfectly good explanation—based on T cells," recalls Edwards. "The major medical journals wouldn't take it at all." Their proposal finally appeared in *Immunology* in 1999 and provoked no response at all.

Undeterred, the UCL team set up a pilot trial, giving B cell–depleting drugs, including rituximab, to five people with especially severe RA. Once their B cells disappeared, the patients' symptoms improved dramatically, and three continued to do well even after their B cells returned, 6 months or so later. Although journals dismissed the results on so few patients as inconclusive, Edwards scraped together more money from departmental funds and recruited more patients. At a 2000 meeting, the UCL team was able to present data on 20 patients, all but two of whom had shown major improvements, some for as long as 18 months.

The media picked up on the apparent success, but the resulting headlines sparked accusations of hype, with the *British Medical Journal* condemning the "irresponsibility" of the UCL team in talking to the press about preliminary results from such a small trial. Still, Edwards got the support of the drug company Roche, which owns the European rights to rituximab, to push ahead. By 2002, the UCL team had the results of a randomized, controlled trial involving 161 patients, which showed that more than 40% of those receiving rituximab with methotrexate, a conventional anti-inflammatory agent, had experienced major improvements in symptoms at the end of 24 weeks, compared to just 13% of those receiving MTX alone. The relief continued even when the patients were checked 48 weeks after the B cell–depletion therapy. "When I presented these results, I think the penny finally dropped within the research community," says Edwards. Indeed, *The New England Journal of Medicine* ultimately published the study's results in 2004.

The success prompted further, larger trials, and last year, the regulatory authorities in both the United States and Europe approved rituximab for use with MTX in severe cases of RA. And in August, the United Kingdom concluded that the therapy was sufficiently cost-effective to be made available free of charge through the National Health Service.

RA patient groups are understandably delighted about the new therapy, with the U.K. charity Arthritis Care describing it as "a triumph." The RA research community is also excited. "I grew up thinking rheumatoid arthritis was a kind of classic B cell disease, and then the T cell people moved in," says Alan Silman of the University of Manchester, U.K., who is medical director of the U.K. Arthritis Research Campaign. "Edwards put B cells back on the agenda."

CREDIT: UNIVERSITY COLLEGE LONDON

Seeking approval. Jonathan Edwards's efforts resulted in B cell–depletion therapy being approved for rheumatoid arthritis.

Remaining doubts, new disease

Yet Silman isn't totally won over. He and others continue to argue that most of RA's inflammation is caused by a direct effect of T cells. "B cells don't correlate perfectly with the disease," says Silman.

There have also been new safety concerns about rituximab, as two lupus patients receiving the drug last year died of a rare viral infection. But no link with the drug has been proven. Overall, says Silverman, almost a decade of rituximab use has shown the drug to have a good safety profile, with no increase in opportunistic infections among those receiving it.

Edwards accepts that questions remain about the role of B cells in RA: Why do fewer than half of patients respond to rituximab, for example? Nevertheless, Edwards and his colleagues have become interested in whether B cell–depletion therapy can treat MS, a neurodegenerative condition stemming from the destruction of the myelin insulation surrounding vital nerve cells. This myelin loss triggers a host of symptoms, from muscle spasms and pain to loss of bladder and speech control.

Many scientists have argued that T cells drive the myelin breakdown in MS, but no effective therapy has yet resulted from pursuing that theory. Edwards notes, however, that studies in the mid-1980s found that in the early stages of MS, the damage to nervous tissue seemed linked to the local accumulation of offspring of B cells known as plasma cells. Indeed, back in 1999, Edwards tried to interest neurologists in testing B cell–depletion therapy on MS patients but found no takers.

Given the poor prognosis of many people with MS and the apparently low risks involved in rebooting the B cell system, Edwards has continued to lobby that rituximab is worth a try. And some MS researchers have started to agree. "There's strong circumstantial evidence implicating antibodies" and thus B cells in MS, says immunologist Christopher Linington of the University of Aberdeen, U.K. "Rituximab will almost certainly help some patients. The problem is, you cannot predict which ones."

In May at a neurology meeting, a team at the University of California, San Francisco (UCSF), unveiled preliminary results from an ongoing rituximab trial involving more than 100 patients with so-called remitting-relapsing MS. The data, primarily magnetic resonance imaging scans of the patients' nervous systems, indicated that the drug has dramatically reduced the nerve damage caused by the disease. "It's no longer a question of 'Do B cells contribute to MS?' " but rather how, says Amit Bar-Or of McGill University in Montreal, Canada, who worked with the UCSF team assessing the safety of the potential new therapy.

The UCL team is playing down any suggestion that they've been proved right again. Edwards says it's far too early for that, although he's hopeful. "The longer we stay in this business, the more we realize there may be further twists to the tale," he says.

–ROBERT MATTHEWS

Robert Matthews is a freelance writer based in Oxford, U.K.

BIOMEDICAL RESEARCH

Cell Biology Meets Rolfing

A diverse group of researchers wants to create a new discipline from scratch by bringing together experts in fascia and deep-tissue massage

BOSTON—Peter Huijing was far from enthusiastic when he received an invitation to speak at the Fascia Research Congress. The meeting, held here last month, would be the first dedicated to the soft part of the body's connective tissue system—an important but medically neglected organ. It would bring together top scientists from fields as diverse as cell biology and biophysics, but it would also include alternative medicine practitioners, such as chiropractors and deep-tissue manipulators known as Rolfers. "I had a fear of damaging my reputation," says Huijing, a world-renowned biomechanics researcher at Vrije Universiteit in Amsterdam, the Netherlands, who, despite his hesitation, decided to attend. By the time the conference was over, Huijing had agreed to organize the next one.

The conference was the brainchild of Thomas Findley, an M.D.-Ph.D. co-director of research at the VA Medical Center in East Orange, New Jersey. For 30 years, Findley has been studying the science behind rehabilitation medicine; he is also director of research at the Rolf Institute of Structural Integration in Boulder, Colorado, which trains and certifies Rolfers. He became convinced early on that fascia—which weaves its way through the body like a gossamer blanket, cradling organs, ensheathing bones, and providing structural support—plays a key role in how patients respond to treatment. He wanted to learn more, but there were no identifiable fascia researchers.

Frustrated, Findley began e-mailing scientists like Huijing in 2005. He knew that researchers around the world had been studying fascia in some form—MEDLINE references to it have spiked in the past 3 years—but that they didn't see themselves as part of a coherent field. Huijing, for example, looks at how the body generates force via the interactions between muscles and fascia, but he was unaware of cell biologists who were studying how fascial cells respond to movement. Findley hoped that bringing such scientists together would stimulate new research collaborations and shed light on the mysterious tissue.

Findley also wanted to bring in clinicians, but he knew that M.D.s wouldn't cut it. Some researchers have speculated that fascial anomalies may be responsible for black box disorders like fibromyalgia and lower back pain, yet doctors have traditionally ignored the tissue. Medical books barely mention fascia, and anatomical displays remove it. "It's just not sexy," says Elizabeth Montgomery, a pathologist who specializes in soft tissue at Johns Hopkins University in Baltimore, Maryland.

So Findley turned to the alternative-medicine community. Findley knew that Rolfers and other alternative therapists held fascia in high regard: They believe that rubbing and stretching the tissue brings about the improvements they see in clients.

Yet they don't have the tools or data to prove their claims. "Practitioners want to know the science behind what they're doing," says Findley, "and scientists want to see clinical applications of their work." Combining the two groups to create a new field seemed natural. But as the meeting in Boston revealed, bridging the gap won't be easy.

Pervasive. Fascia shown here is from a lower leg muscle, dissected by Peter Huijing (*inset*).

CREDITS: RON THOMPSON; GUUS C. BAAN (INSET)

The great divide

Frederick Grinnell picked up on the gap right away when he heard the applause—in the middle of a talk. It was 9:00 in the morning on the first day of the conference, and Paul Standley, a vascular physiologist at the University of Arizona College of Medicine in Phoenix, was describing his work on fibroblasts, the chief type of cell found in fascia. When Standley's team placed the cells on flexible collagen and stretched the collagen in ways that replicated repetitive motion strains on the body, many cells died. But when the team followed the strains by stretching the collagen in ways that approximate techniques like Rolfing, more cells survived. The audience erupted.

"It's rare to see such enthusiasm at a conference," says Grinnell, a cell biologist at the University of Texas (UT) Southwestern Medical Center in Dallas. "I was really struck by it." The audience was composed mostly of alternative-medicine practitioners—chiropractors, massage therapists, and Rolfers—who signed up in droves when Findley first advertised the meeting in the fall of 2006. Within 5 months, the 500-seat venue at Harvard Medical School had sold out.

The scientists took more convincing. In addition to Findley's aggressive e-mail campaign, a 51-year-old graduate student named Robert Schleip (see sidebar, p. 1235) traveled to labs around the world looking for plenary speakers. Some, like Grinnell, saw the conference as an opportunity to learn from other basic researchers. "I never realized my work on cell mechanics related to tissue mechanics until I heard about this meeting," he says. But others, like Huijing, were turned off at first: "I had never heard of

FROM ROLFER TO RESEARCHER

Robert Schleip remembers the moment he became a "born-again scientist." For 13 years, he had been teaching Rolfing—a technique that involves rubbing and stretching a bodywide network of soft connective tissue known as fascia—when he began to question his lesson plans. "I found there was a pseudoscientific mentality behind what I was doing," says Schleip, who in 1978 became Germany's first licensed Rolfer. "I thought, 'I'd better check this stuff out.' "

So Schleip turned to the scientific literature on fascia. "When I did my homework, I discovered that some of [the Rolfing dogma] didn't look so good." For example, as part of their training, Rolfers assume that if they apply enough force to an area of fascia, they can lengthen it and remove tension. "But the science says you would have to apply a ton of pressure to effect these changes," Schleip says.

The literature also provided insight: Schleip discovered, for example, that fascia is highly innervated, and that might explain why manipulating the tissue could ease pain. "I knew there were many gold mines waiting," Schleip says. So he stopped teaching and pursued a scientific career.

Getting a research position wasn't easy. Ten professors turned Schleip down before one at Ulm University gave him a chance—but no lab space. Schleip spent his first year conducting experiments in his kitchen and in a storage room he rented from a nearby pharmacy. He began to study the ability of fascial tissue to contract—a property that could play a role in stiffness and lower back pain. "The professor was so impressed with how much I did on my own that he let me work in his lab," Schleip says.

Schleip now has a lab of his own. He earned his Ph.D. with honors in 2006 at the age of 52, and shortly thereafter established the Fascia Research Project at Ulm University. He's continuing his work on fascial contraction and has begun collaborating with Giulio Gabbiani, a preeminent cell biologist at the University of Geneva in Switzerland. Now Schleip says that when he calls professors to discuss research projects, they call him back. **–D.G.**

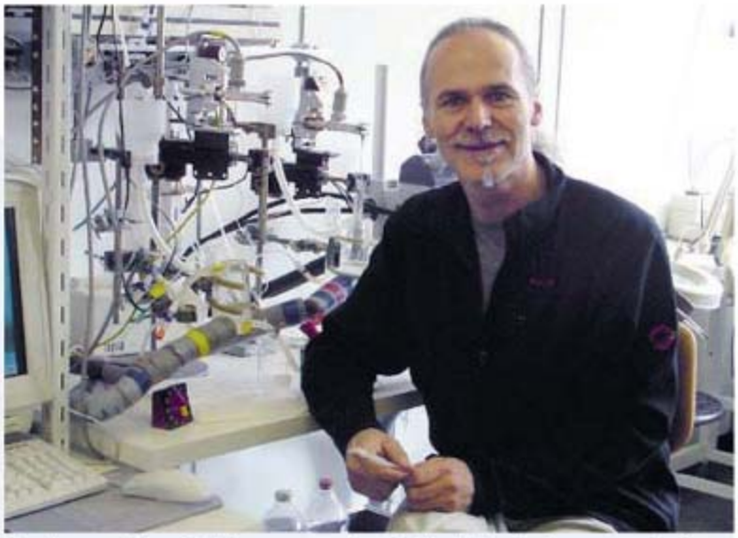

Sea change. Robert Schleip was a prominent Rolfer before he became a scientist.

CREDIT: RAABE MUNICH GERMANY

things like Rolfing before," he says. "I didn't see the relevance." In the end, 58 scientists signed up for the meeting—along with 51 M.D.s. Most of them took the podium, whereas the practitioners filled the seats.

Clapping aside, many of the practitioners struggled with the science. Findley was adamant that the talks not be "watered down," and intricate presentations on the first day pulled no punches. Cell biologists spoke about how fascial cells alter gene expression in response to force, while biomechanics researchers detailed how interactions between fascial cells and the extracellular matrix contribute to whole body mobility. By the afternoon, the auditorium was noticeably emptier. "My frontal lobe was tired," says Briah Anson, a St. Paul, Minnesota–based Rolfer.

For their part, the scientists had some problems connecting with the clinicians. Huijing's fears of stigma seemed to be borne out when he interacted with one group of attendees. "They started talking about aura," he says. "I don't want my name associated with that." And Giulio Gabbiani, a cell biologist at the University of Geneva in Switzerland who studies connective tissue and wound healing, acknowledged difficulty discussing some concepts with the practitioners. "It's like we were talking two different languages," he says.

All of this prompts Wallace Sampson to question whether putting the two camps together is a good idea. "Fascia is a legitimate target of study, but a field like this has to be generated organically," says the alternative-medicine skeptic and professor emeritus at Stanford University in Palo Alto, California. "You have to do the basic science and see what evolves. You can't force the clinical side."

Partap Khalsa strongly disagrees. "It's not only valid to bring these groups together, it's essential," says the program officer with the U.S. National Institutes of Health (NIH) National Center for Complementary and Alternative Medicine (NCCAM), which, along with organizations such as the Rolf Institute and the Evanston, Illinois–based Massage Therapy Foundation, provided funding for the meeting. "You need people who can do good basic science and clinicians who can inform them about their experiences," he says. "It's the only way to advance the field."

Bridging the gap

By the second day of the conference, things began to gel. A clinician-scientist panel fostered a dialogue between the two groups, and a networking lunch sparked new collaborations. "I heard clinicians talking about how manipulating fascial stiffness was key to their interventions," says UT Southwestern's Grinnell. Now he plans to study the cell biological basis of stiffness and how it might contribute to wound repair and scarring. Huijing says he also learned new things from the alternative therapists—and he found that he had something to teach them as well. Establishing fascia research as a legitimate field, he says, will guarantee that these interactions continue.

Findley knows it won't be easy. First, he'll need to attract more scientists. Publishing fascia research in top journals would help. He'll also need to cultivate a stable source of funding. Through the Rolf Institute, Findley has helped establish the Ida P. Rolf Research Foundation (named after the institute's founder), which is raising funds in hopes of awarding $200,000 in grants per year in 2 to 3 years. That's still a pittance compared to the millions NIH can provide, and NCCAM's Khalsa says he likes what he saw at the meeting. "There's a lot of potential here," he says.

But Findley's greatest challenge will be keeping everyone happy. Practitioners want to see more of their own up on the podium, and scientists want assurances that everything will remain respectable.

It's a tightrope Huijing looks forward to walking in 2009 when he puts together the next conference, to be held in Amsterdam. Huijing plans to give a larger spotlight to practitioners and to explore even more of the basic science. He's adding days, and he's reserved an auditorium for 1000 people—twice the size of the room at this year's event. "I have a feeling it could be very big," he says. **–DAVID GRIMM**

Did Horny Young Dinosaurs Cause Illusion of Separate Species?

Of all the strange-headed dinosaurs, the prize for toughest, prickliest noggins probably belongs to the pachycephalosaurs—literally, the "thick-headed lizards." Some sported domed skulls, and all had bony spikes studding their long snouts. Four species are known from roughly 65-million-year-old rocks in Wyoming, Montana, and South Dakota alone. It's an impressive display of diversity for the waning days of the dinosaurs.

Or maybe not. At the Society of Vertebrate Paleontology's annual meeting here last month, Jack Horner of Montana State University (MSU) in Bozeman argued that three of the species are just one. What were thought to be two unique species, he says, are in fact juveniles of different ages that would have grown up to be bony-headed *Pachycephalosaurus*. "It's a dramatic remake," says Peter Dodson of the University of Pennsylvania.

The revision would remove two particularly colorful characters from the paleontological bestiary, and not everyone is convinced. Getting the taxonomy right has major implications, says David Evans of the Royal Ontario Museum in Toronto: "It's really important for understanding a whole range of evolutionary phenomena."

First described in 1931, *Pachycephalosaurus wyomingensis* has such a prodigious pate that paleontologists speculated males butted heads with each other, although many now doubt it (*Science*, 5 November 2004, p. 962). In 1983, a related species made its debut. *Stygimoloch spinifer* ("horned devil from the river of death") had a smaller dome but fearsome spikes. The newest addition was introduced last year: *Dracorex hogwartsia* has a flat head with telltale nasal horns. The dragon-king was named in honor of J. K. Rowling, whose *Harry Potter* novels feature the Hogwarts School of Witchcraft and Wizardry.

Horner and colleagues—MSU doctoral student Holly Woodward and Mark Goodwin of the University of California, Berkeley—suspected that young dinosaurs might have been misidentified as adults. During previous work on another pachycephalosaur, *Stegoceras*, they noticed that the bone of smaller specimens was full of radial canals, a spongelike texture that indicates rapidly growing bone and suggests that they were juveniles.

The team cut open skulls of *Pachycephalosaurus* and found dense bone without canals, suggesting that the specimens were full-grown adults. *Stygimoloch* bone was full of canals. "This is not even close to being full-grown," Horner says. The spikes had a spongy texture and showed signs that the bone was being resorbed—suggesting it was a juvenile *Pachycephalosaurus*.

There is only one specimen of *Dracorex*, housed in the Children's Museum of Indianapolis, so Horner couldn't cut it open to look at the tissue. Horner notes that little bumps on the top of the head of *Dracorex* resemble those that give rise to radial bone growth in *Stygimoloch*. Two large holes in the top of the skull are another characteristic of juveniles that haven't finished growing. Given the lack of a dome and the shorter skull, Horner suspects that *Dracorex* is an even younger *Pachycephalosaurus*. He says the hypothesis could be falsified if researchers were to discover, say, a new skull of *Dracorex* that is as big as *Pachycephalosaurus* or that has mature bone.

The argument makes sense to Robert Sullivan of the State Museum of Pennsylvania in Harrisburg, who co-authored a paper describing *Dracorex* published last year in the *New Mexico Museum of Natural History and Science Bulletins*. In another talk at the meeting, Sullivan speculated that juvenile pachycephalosaurs in Asia may have been misidentified as new species. But another author, Robert Bakker of the Houston Museum of Natural Science in Texas, adamantly opposes lumping together the three North American species. "The differences are [so] astonishing," he says, that he can't imagine that one could have grown into the other. Evans, on the other hand, says such big changes are possible. "What dinosaurs teach us is that relative growth can be extreme, particularly in the skull," he says.

What's needed are careful measurements of many specimens to see how shape changes with size, Evans says; this can help reveal whether various specimens all belong to a so-called growth series. If some features, such as the height of the dome, do not depend on size, it would suggest they rightly belong to different species. Because juveniles tend to start out with features of their evolutionary ancestors and modify them as they grow, it's important to distinguish juveniles from adults or family trees may get confused. That would give researchers a skewed picture of how various pachycephalosaurs are related to one another and to more distant taxa.

If Horner turns out to be right, the diversity of pachycephalosaurs would be 50% lower than previously thought for the latest Cretaceous. "It makes a lot more sense," he says, because other kinds of dinosaurs were also declining in diversity at the time. Not even an honorary degree in wizardry, it seems, was enough to save them. **–ERIK STOKSTAD**

E pluribus unum. Three species of pachycephalosaurs may actually be just one that changed drastically during adolescence.

CREDIT: HOLLY N. WOODWARD

Sensational. Ancestors of the duck-billed platypus may have had the same electrosensory bill.

Jaw Shows Platypus Goes Way Back

When scientists first laid eyes on the duck-billed platypus and the echidnas in the late 18th century, they were so baffled by these bizarre egg-laying mammals that some considered the specimens a hoax. Modern researchers have uncovered other implausible features, including 40,000 tiny glands in the broad bill that sense electric currents, which may help the platypus catch prey underwater. The ant-eating echidna has about 100 in its tiny snout. The platypus and echidna are so unusual that they were assigned an order—the Monotremata—separate from the more common marsupial and placental mammals.

The fossil record of monotremes is also sparse. The oldest known specimen is a single tooth from Patagonia, about 62 million years old, with a distinctive compressed shape like that of juvenile platypuses before they lose their teeth. A reanalysis of fossil jaws from Australia, reported at the meeting, suggests it belonged to a platypus that lived at least 112 million years ago. "It's really, really old for a monotreme," Timothy Rowe of the University of Texas (UT), Austin, told the audience.

Teinolophos trusleri was discovered near Inverloch, Australia, in 1997 and described by Thomas Rich of the Museum Victoria in Melbourne, Pat Vickers-Rich of Monash University, and colleagues. The specimens consist of jaws and teeth.

Looking for more anatomical clues to the evolution of mammals, Rich's team took fossil jaws to Rowe, a paleontologist who also runs a computed tomography–scanning facility at UT Austin. Scans of three specimens revealed a large internal canal along the entire length of the jaw, like the canal in a modern platypus that carries nerve fibers from the electrosensory glands in the bill to the brain. "There's no other mammal that has a canal this size," Rowe said. Even back in the early Cretaceous, it seems, the platypus was using electrosensation. "This is the most compelling evidence to us that *Teinolophos* is a platypus."

That would push back the fossil record of the platypus quite a bit; the next youngest fossil is *Obdurodon dicksoni* from 15-million-year-old rocks in Australia. It is also much older than current estimates from DNA of when platypuses and echidnas diverged from their most recent common ancestor. Molecular clocks put that date somewhere between 17 million and 80 million years ago. Rowe speculated that one reason for the underestimate may be that monotremes evolve at slower rates than other mammals do, an idea that fits with their lower diversity.

Grand canal. The dark gray area in the CT scan (*above*) of a jaw marks the path of nerve fibers.

Zhe-Xi Luo of the Carnegie Museum of Natural History in Pittsburgh, Pennsylvania, agrees that the canal in *Teinolophos* resembles that of a modern platypus: "I'm leaning toward accepting Rowe's idea." **–ERIK STOKSTAD**

Snapshots From the Meeting >>

Hopping toward frogs. About 340 million years ago, amphibians began to evolve into an amazing array of now-extinct forms. Some grew 3 meters long; others developed armor. One of the most diverse groups, called the Dissorophoidea, also concocted some more familiar shapes that resemble modern amphibians. Jason Anderson of the University of Calgary in Canada described an unnamed fossil that strengthens the case that dissorophoids gave rise to frogs and salamanders.

The 12-centimeter-long fossil was discovered in Texas in 1995. The nearly complete specimen is housed in the collections of the Smithsonian Institution's National Museum of Natural History. The skull looks froglike enough that the fossil was dubbed "Froggy," and the number of bones in the digits are also froglike. The short ribs and fused bones in the ankle are like those of salamanders. A classic dissorophoid called *Amphibamus* had 21 vertebrae, the oldest fossil frog had 14 vertebrae, and Froggy fits in between with 17. All told, Anderson says, Froggy is the closest fossil relative to frogs and salamanders. "It really neatly fills the gap," says Rainer Schoch of Staatliches Museum für Naturkunde in Stuttgart, Germany.

Flight first. A stunning new fossil unveiled at the meeting suggests that bats evolved flight before they began to echolocate. "We're all excited about it," says Nicholas Czaplewski of the Oklahoma Museum of Natural History in Norman. "There's a lot you can learn from a specimen that well preserved."

In her presentation, Nancy Simmons of the American Museum of Natural History in New York City described the 52-million-year-old bat, which came from Green River Formation in Wyoming and is now housed in the Royal Ontario Museum in Toronto, Canada. "When we first saw it, we knew it was special," she recalled. The bat has traits that make it the most primitive yet discovered. For example, there are claws on all five digits; modern bats have claws on at most two fingers of each hand. The claws could have made the bat a skilled climber.

Long fingers, a keeled sternum, and other features suggest that the bat could flutter under its own power. It probably couldn't fly as far or as fast as other fossil bats, because of the stubby wings, but it would have been able to maneuver well. The skull lacks the features of echolocation, such as an enlarged cochlea, found in modern bats. "It finally gives us an answer: Flying evolved first, echolocation second," Simmons said. **–E.S.**

CREDITS (TOP TO BOTTOM): NICOLE DUPLAIX/NATIONAL GEOGRAPHIC/GETTY IMAGES; TIMOTHY ROWE/PNAS

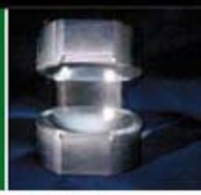

LETTERS

edited by Jennifer Sills

Mixing It Up with Krill

THE PERSPECTIVE "BIOMIXING OF THE OCEANS?" BY A. W. VISSER (11 May, p. 838) challenged the suggestion that dense swarms of vertically migrating krill could generate substantial mixing (*1*–*3*). Visser asserted that 1- to 2-cm-long krill are too small to generate turbulence at the larger scales needed to mix water efficiently.

Our study of intense turbulence associated with vertically migrating krill in Saanich Inlet (*3*) addresses Visser's objection. Both the range of length scales and the distribution of shear resembled those of shear-driven turbulence, and the density overturns we observed were consistent with our interpretation of turbulent mixing. The measurements showed all the characteristics of turbulent mixing, including shear fluctuations on length scales of 0.01 to 1 m distributed as expected for turbulence (*4*) and regions of unstable density (i.e., where heavy water was located above light water), on scales much larger than individual krill. The presence of these established signatures of turbulent mixing suggests that mixing was occurring.

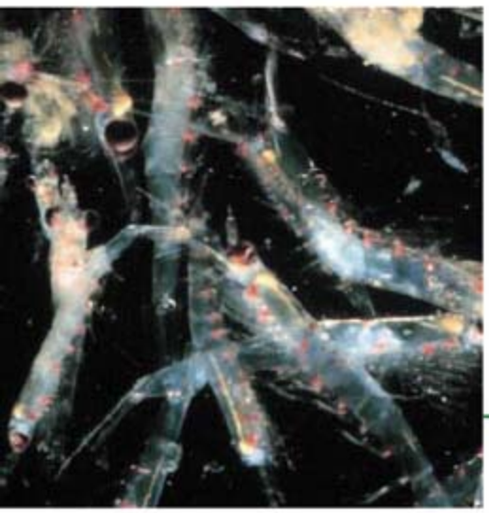

The mechanism by which swarms of small krill can create turbulence with scales of 1 to 10 m remains a mystery. Krill swarms have very patchy distributions (*5*), so the mixing action may be manifested at the scale of the swarm patchiness (i.e., tens of meters) rather than that of an individual krill. The effect of krill may be analogous to large downdrafts that are generated by the collective drag of falling raindrops (*6*).

It may well be that swimming marine organisms do not swarm or school densely enough in most of the ocean to excite substantial turbulent mixing. Regardless, the primary objection raised by Visser does not hold up against our observations.

E. KUNZE,[1] J. F. DOWER,[1] R. DEWEY,[1] E. A. D'ASARO[2]

[1]School of Earth and Ocean Sciences, University of Victoria, Victoria, BC V8W 3P6, Canada. [2]Applied Physics Laboratory, University of Washington, Seattle, WA 98195, USA.

References

1. M. E. Huntley, M. Zhou, *Mar. Ecol. Prog. Ser.* **273**, 65 (2004).
2. W. K. Dewar *et al.*, *J. Mar. Res.* **64**, 541 (2006).
3. E. Kunze *et al.*, *Science* **313**, 1768 (2006).
4. N. S. Oakey, *J. Phys. Oceanogr.* **12**, 256 (1982).
5. M. Barange *et al.*, *Mar. Ecol. Prog. Ser.* **99**, 205 (1993).
6. R. A. Houze Jr., *Cloud Dynamics*, vol. 53 of *International Geophysics Series* (Academic Press, San Diego, CA, 1993).

Response

IN MY PERSPECTIVE (11 MAY, P. 838), I pointed out that even in well-developed, isotropic turbulence, mixing efficiency is not a global constant. It depends critically on the length scale at which turbulent energy is imparted to the flow compared with the buoyancy length scale. In most physical oceanographic applications, this scale dependence goes unnoticed because these length scales are generally commensurate and mixing efficiency is near its maximum. This is not true for biomixing, and studies that ignore mixing efficiency (*1*–*3*) in all likelihood overstate the case for the biosphere's role in mixing the world's oceans.

In biomixing, turbulent kinetic energy due to the drag and thrust of swimming animals is imparted at the scale of individuals. Schools, swarms, and shoals of swimming animals may very well introduce larger-scale structures to the flow, but there is no reason to suppose that the turbulent dissipation rate at these scales is identical to the rate at microscales. The idea that the larger-scale turbulent structures induced by swimming animals "resemble" or "are consistent with" oceanic turbulence is not a sufficient argument to prop up a global relationship between microscale dissipation rates and turbulent mixing.

ANDRÉ W. VISSER

Department of Marine Ecology and Aquaculture, Technical University of Denmark, Danish Institute for Fisheries Research, DK-2920 Charlottenlund, Denmark.

References

1. M. E. Huntley, M. Zhou, *Mar. Ecol. Prog. Ser.* **273**, 65 (2004).
2. W. K. Dewar *et al.*, *J. Mar. Res.* **64**, 541 (2006).
3. E. Kunze, J. F. Dower, I. Beveridge, R. Dewey, K. P. Bartlett, *Science* **313**, 1768 (2006).

Estrogen and Tumors: For Better or for Worse?

IN THER REPORT "GENDER DISPARITY IN LIVER cancer due to sex differences in MyD88-dependent IL-6 production" (6 July, p. 121), W. E. Naugler *et al.* clearly demonstrated the role of IL-6 in the development of hepatocellular carcinoma (HCC) in mice. In addition, a single estradiol injection in male mice reduced the acute phase response to a carcinogenic injection to levels observed in female mice, in terms of IL-6 production and liver cell damage. However, great caution should be taken before concluding that estrogen-mimetic compounds could prevent progression to HCC in male patients with chronic liver disease.

First, it has been hypothesized that sex steroids are actually contributing to hepato-

carcinogenesis. Although not revealing a statistically significant effect, randomized trials with tamoxifen have aimed at blocking estrogen because male patients with chronic hepatitis present with a relatively hyperestrogenic phenotype (*1*).

Second, exogenous estrogen therapy by means of oral contraceptives in women is the major risk factor for the development of hepatocellular adenoma (HA) (*2*), a benign liver tumor with malignant potential. In men, cases of HA after the chronic intake of exogenous steroid hormones have been reported (*3*).

Third, given that the development of HCC in men with hepatitis B or C viral infections or cirrhosis occurs after years of chronic inflammation, we imagine that chronic suppression of IL-6 levels by an estrogen mimetic in those patients would be necessary, and long-term estrogen treatment leads to an even greater risk of HA. In a cohort recently investigated at our institution, 94% of women with HA reported the use of oral contraceptives for a median duration of 15 years (*4*). Long-term estrogen treatment in males may also contribute to the development of liver masses. Tumor induction, even if benign, would complicate the clinical management, as any solid tumor in a patient with a history of chronic liver disease should primarily be considered malignant and would be an indication for surgical resection.

DIRK J. VAN DER WINDT, NIELS F. M. KOK, JAN IJZERMANS

Department of Surgery, Erasmus University Medical Center Rotterdam, Rotterdam 3015 CE, Netherlands.

References

1. Cancer of the Liver Italian Programme, *Lancet* **352**, 17 (1998).
2. H. A. Edmondson, B. Henderson, B. Benton, *N. Engl. J. Med.* **294**, 470 (1976).
3. E. A. Psatha *et al.*, *J. Magn. Reson. Imag.* **22**, 258 (2005).
4. D. J. van der Windt *et al.*, *Br. J. Surg.* **93**, 1495 (2006).

Response

THE CONTRIBUTIONS OF SEX STEROID DYSregulation to the development of hepatocellular cancer (HCC) has been debated for decades, spawning several trials studying estrogen modulators (such as tamoxifen) in the treatment of HCC. None of the trials has convincingly shown any benefit of tamoxifen in the treatment of HCC, as Van der Windt and colleagues note. Our study, however, does not address the treatment of existent HCC; it focuses instead on the factors that influence HCC incidence.

We found that estrogen administration markedly diminished the inflammation and injury associated with a chemical carcinogen, which translated much later into a decreased incidence of HCC in mice. Furthermore, when we administered tamoxifen prior to chemical injury, the injury was amplified rather than diminished, suggesting that tamoxifen, already known to be useless in the treatment of established HCC, is also unlikely to prevent the occurrence of HCC.

Although the malignant potential of hepatic adenomas is controversial (*1*), there is little question that these neoplasms are associated with prior oral contraceptive use in women (*2*). As Van der Windt *et al.* point out, the use of estrogen mimetics for prevention of HCC in clinically relevant situations (e.g., chronic liver inflammation such as that produced by hepatitis B or C infection) would be long-term and could lead to the development of adenomas. We agree that this would complicate the care of such patients, likely precluding the use of such a strategy.

Another risk of an estrogen mimetic would be the feminizing side effects in extrahepatic tissues. This includes not only the breasts and testes but also the coagulation system, as estrogens predispose to thrombus formation.

Our results suggest a possible alternative to estrogen-mimetic therapy. The mechanism by which estrogens diminish liver injury is through down-regulation of IL-6 production, indicating that strategies to decrease IL-6 signaling in the setting of chronic liver inflammation may decrease HCC development. Down-modulation of the IL-6 signaling pathway may circumvent the problems of possible adenoma development and feminization inherent in long-term estrogen use, while still providing the benefit of decreasing HCC incidence in men.

MICHAEL KARIN

Laboratory of Gene Regulation and Signal Transduction, Department of Pharmacology and Cancer Center, University of California, San Diego, CA 93093, USA.

References

1. L. C. Tao, *Acta Cytol.* **36**, 338 (1992).
2. H. A. Edmondson, B. Henderson, B. Benton, *N. Engl. J. Med.* **294**, 470 (1976).

CORRECTIONS AND CLARIFICATIONS

Letters: "Response to 'Shopping for explanations'" by M. M. Krasnow *et al.* (2 November, p. 745). The first line in the fourth paragraph was incorrect, due to an editorial error. The line should have been, "Finally, only a weak commitment to egalitarianism depends on claims of biological identity."

TECHNICAL COMMENT ABSTRACTS

COMMENT ON "Roadless Space of the Conterminous United States"

Evan H. Girvetz, Jochen A. G. Jaeger, James H. Thorne

Watts *et al.* (Reports, 4 May 2007, p. 736) introduced a metric of landscape pattern called roadless volume (RV). However, as with most previous metrics, RV does not explicitly address ecological processes. We demonstrate that RV can produce results inconsistent with the notion of landscape connectivity and contend that more ecologically relevant metrics are available.

Full text at www.sciencemag.org/cgi/content/full/318/5855/1240b

RESPONSE TO COMMENT ON "Roadless Space of the Conterminous United States"

Raymond D. Watts, Roger W. Compton, John H. McCammon, Carl L. Rich, Stewart M. Wright, Tom Owens, Douglas S. Ouren

Girvetz *et al.* criticize our work and the value of the roadless volume (RV) metric, basing their arguments on the artificial imposition of wildlife habitat connectivity as the context. We counter that in our intended contexts, both practical and geographic theoretical considerations make RV an appropriate measure of the space between roads.

Full text at www.sciencemag.org/cgi/content/full/318/5854/1240c

Virtual Reality and Telepresence

IN THE 24 AUGUST ISSUE, TWO TEAMS OF cognitive neuroscientists used video-based immersive virtual reality systems to induce an "out-of-body" experience in healthy volunteers (Brevia, H. H. Ehrsson, p. 1048; Reports, B. Lenggenhager *et al.*, p. 1096).

An important implication of this work, not fully discussed in the papers, is the role of virtual reality (VR) in inducing these experiences. VR is usually presented as a collection of technological hardware, such as computers and head-mounted displays. However, as underlined by Steuer (*1*) more than 15 years ago, the core of VR is more experiential than technological; "virtual reality" can be defined as a simulated environment in which a perceiver experiences the feeling of presence by means of a communication medium, a phenomenon referred to as telepresence.

Using this definition, the outcome of the two studies is immediately clear: During the experiment, the subjects were no longer present in their real body but were instead in the synthetic body produced by VR. In short, the researchers used virtual reality to induce telepresence. But what is "presence," and what is it for?

One group of researchers describes the sense of presence as a function of our experience of a given medium (*2*). The main result of this approach is the definition of presence as the perceptual illusion of nonmediation (*2*), produced by means of the disappearance of the medium from the conscious attention of the subject. A second approach (*3*) based on principles of Embodied Cognition, defines presence as the nonmediated perception of successfully transforming an intention into action.

A better understanding of presence will be an important future goal for cognitive science. This is why the European Community has been funding, since 2002, the "Future and Emerging Technologies—Presence" research program (*4*).

GIUSEPPE RIVA

Applied Technology for Neuro-Psychology, Istituto Auxologico Italiano, Milan 20145, Italy.

References

1. J. S. Steuer, *J. Commun.* **42**, 73 (1992).
2. M. Lombard, T. Ditton, *J. Comput. Mediated Commun.* **3** (1997); available at http://jcmc.indiana.edu/vol3/issue2/lombard.html.
3. G. Riva, M. T. Anguera, B. K. Wiederhold, F. Mantovani, *From Communication to Presence: Cognition, Emotion and Culture Towards the Ultimate Communicative Experience*, G. Riva, F. Davide, Eds. (IOS Press, Amsterdam, 2006); available at www.emergingcommunication.com/volume8.html.
4. Information Society Technologies (www.cordis.lu/ist/fet/pr.htm).

Response

WE WELCOME RIVA'S DISCUSSION OF PRESence, virtual reality (VR), and their relevance with respect to our experimental findings on bodily self-consciousness. We also recognize that there is currently no agreement on how to conceptualize and how to measure presence and related aspects such as bodily self-consciousness, whether in the field of engineering, computer science, psychology, or physiology.

It seems to us that Riva overinterprets our data to a certain extent. Unlike Ehrsson (Brevia, 24 August, p. 1048), we did not report that we induced full-blown out-of-body experiences. True, our participants identified with the virtual body and also experienced touch on the virtual body. They also mislocalized their own bodily selves as they drifted toward their virtual bodies and thus to a position outside their bodily borders. Yet, as we argued in our Report (24 August, p. 1096), this should not be mistaken for full-blown experiences of disembodiment that are typically reported during spontaneous out-of-body experiences. The responses in Ehrsson's study differed from ours: The participants did not feel present in the virtual body, as argued by Riva, but felt located at a distance from their body. Thus, drawing parallels between the two studies and linking them to presence, VR, and bodily self-consciousness is perhaps not as simple as Riva states. Nevertheless, both studies show that experimental paradigms involving multisensory processing in combination with VR might turn out to be an important tool for studying bodily self-consciousness and presence. Experimental psychology and cognitive neuroscience will certainly help to define presence and distinguish between different theoretical accounts.

With respect to one such theory cited by Riva, our data demonstrate that presence (as quantified in our study by the measures of self-location and self-attribution) is not necessarily related to the "perception of successfully transforming an intention in action." We did not modulate motor or intentional mechanisms experimentally and only modified multisensory bodily information. When investigating complex phenomena, such as human bodily self-consciousness or presence, we feel that it is methodologically important to isolate the simplest form of the target phenomenon (in our case, phenomenal selfhood).

We agree that our participants felt some aspects of out-of-body experiences (*1*). Tackling issues of bodily self-consciousness and presence with different behavioral and neuroimaging techniques is timely, and we expect cognitive science and neuroscience to play a major part in this endeavor.

BIGNA LENGGENHAGER,[1] TEJ TADI,[1] THOMAS METZINGER,[2,3] OLAF BLANKE[1,4]

[1]Laboratory of Cognitive Neuroscience, Ecole Polytechnique Fédérale de Lausanne, Swiss Federal Institute of Technology, 1015 Lausanne, Switzerland. [2]Philosophical Seminar, Johannes Gutenberg-Universität Mainz, 55099 Mainz, Germany. [3]Frankfurt Institute for Advanced Studies, Johann Wolfgang Goethe University, 60438 Frankfurt am Main, Germany. [4]Department of Neurology, University Hospital, 1214 Geneva, Switzerland.

Reference

1. G. Miller, *Science* **317**, 1020 (2007).

Letters to the Editor

Letters (~300 words) discuss material published in *Science* in the previous 3 months or issues of general interest. They can be submitted through the Web (www.submit2science.org) or by regular mail (1200 New York Ave., NW, Washington, DC 20005, USA). Letters are not acknowledged upon receipt, nor are authors generally consulted before publication. Whether published in full or in part, letters are subject to editing for clarity and space.

Response

I DO NOT SHARE RIVA'S IDEA THAT THE concept of telepresence, as formulated in his Letter, will become a useful theoretical framework in cognitive neuroscience. Presence research has been restricted to technologically oriented research departments, and the term has not been used in neuroscience (*1*). The concept of presence is a "feeling of being there" (in the simulated environment), which leads to the participant responding realistically to events and situations in the virtual environment (*1*). However, there are many other broader definitions ranging over many possible media—from reading a book or using a mobile phone, to full immersive virtual reality. Steuer (*2*) described how any technologically mediated communication involves a degree of telepresence, including speaking to someone on the phone, listening to a live music recording, or playing a videogame. For cognitive neuroscientists, this looser definition—together with the fact that this approach to presence relates to many different technological, perceptual, and cognitive factors—becomes a serious limitation. Therefore, I think that it is unlikely that cognitive neuroscientists would find this type of vague definition of telepresence to be very useful in the design and interpretation of experiments investigating specific perceptual and cognitive processes.

Indeed, presence research would benefit from working more closely with cognitive neuroscience to relate presence to psychological or physiological models of perception, action, spatial awareness, body self-representation, and social interaction (*3*). This could lead to the engineering of the next-generation virtual reality applications in which the simulated sensory data fully replace the input from physical reality, and the feeling of being, acting, and interacting "as if you were there" becomes complete.

H. HENRIK EHRSSON

The Wellcome Trust Center for Neuroimaging, University College London, London WC1N3BG, UK.

References

1. M. V. Sanchez-Vives, M. Slater, *Nat. Rev. Neurosci.* **6**, 332 (2005).
2. J. Steuer, *J. Commun.* **42**, 73 (1992).
3. M. Slater *et al.*, *IEEE Comput. Graph. Appl.* **27**, 90 (2007).

GENOMICS

Adventurer in Genome Science

Stephen Hilgartner

For readers of *Science*, J. Craig Venter, one of the most famous biologists alive today, needs no introduction. Owing to his scientific accomplishments and penchant for inspiring debate, Venter's name has repeatedly graced both the news and the technical sections of this journal. Much of his notoriety stems from his starring role in the acrimonious race between the publicly funded Human Genome Project and Celera, a private company founded to sequence the human genome before the public project could. Moreover, some of Venter's most notable publications—including the 1991 paper on expressed sequence tags (ESTs) (*1*), the 1995 paper describing the first complete genome sequence of a free-living organism (*2*), and the 2001 paper announcing Celera's version of the human sequence (*3*)—appeared here. Among scientists and more broadly, Venter is as controversial as he is famous. Observers have cast him as a brilliant maverick, an opportunistic egomaniac, and a badass (a term usually meant as a compliment). With his countless admirers and critics, he is probably the closest thing biology has to a Hollywood celebrity.

The conflicting characterizations of Venter make it likely that his autobiography, *A Life Decoded: My Genome: My Life*, will attract a broad audience of scientists and science watchers. In addition, the launch of the book has been cleverly stage managed. A few weeks prior to its release, the J. Craig Venter Institute announced the publication of the first true diploid genome of a single individual—the sequence of all 46 chromosomes from Venter himself (*4*). (Early assessments suggest that the data are of the highest quality.) Not only does the coincident timing enhance the newsworthiness *of A Life Decoded*, but the book also draws on the sequence to claim a literary innovation: in Venter's words, it is "the first biography to benefit from having six billion base pairs of the author's genetic code as an essential appendix." Throughout the text, Venter splices fragments of genetic information into his story, speculating about how his genome may have shaped his life. The effort is preliminary (if not gimmicky), and Venter acknowledges that genetic insights shed "only a weak light on my destiny." Nonetheless, the book raises the question of how future writers will use genome data to produce what one might call molecular biographies.

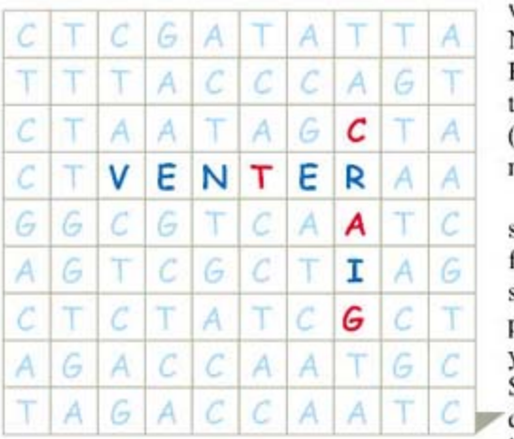

A Life Decoded
My Genome: My Life
by J. Craig Venter
Viking, New York, 2007. 416 pp. $25.95, C$31. ISBN 9780670063581.
Allen Lane, London. £25. ISBN 9780713997248.

A Life Decoded can be decrypted into several messages. On one level, it offers a window into the life and mind of a scientist who, however one perceives him, has indisputably become an extraordinary figure. On another, the book can be read as a fresh salvo in the ongoing battle between Venter and his critics, and no doubt many genomics insiders will quickly flip to the index to learn what Venter has said about whom. But the most interesting interpretations will view the book as being about something bigger than Venter himself. *A Life Decoded* can be treated as an account that, like a sociological tracing agent, charts a course through the world of genomics, highlighting structural features and tensions.

Born in 1946, Venter grew up in a military family outside San Francisco and served as a medic in Vietnam. After completing a Ph.D. at the University of California, San Diego, in 1975, he began his career as an independent scientist at the State University of New York at Buffalo. His work on adrenaline receptors landed him a research post at the National Institutes of Health (NIH) in 1984. He acquired his first DNA sequencing machine in February 1987 and within a few years had shifted completely into the field of genome research, where he quickly became an increasingly important player. In 1990, his laboratory launched a sequencing strategy that soon had it cranking out large numbers of ESTs—a success that entangled him in an international controversy about genome patents. In 1992, with backing from venture capital, Venter left NIH to found The Institute for Genomic Research (TIGR), a nonprofit organization tied to the company Human Genome Sciences (HGS)—which enjoyed rights to exploit commercially TIGR's discoveries.

At TIGR, Venter achieved some notable scientific successes, securing his stature in the field. But ongoing tensions with HGS, which sought more control over the publication and patenting of TIGR data than Venter wanted to yield, led him to negotiate a split in June 1997. Shortly thereafter, he took part in a series of discussions with Applied Biosystems and its parent company, Perkin-Elmer, that ultimately led to the 1998 founding of Celera. The ensuing race between Celera and the public project was temporarily declared a draw in June 2000, when a ceremony featuring President Bill Clinton and British Prime Minister Tony Blair celebrated the completion of the "first draft" of the human sequence. Celera fired Venter in 2001 during a period that coincided with a move to shift its business model away from selling access to genome data, much of which was by then available from the public project for free.

Since leaving Celera, Venter has been busy. He embarked on a project to sequence seawater in order to identify hitherto-unknown microorganisms; began a research program in synthetic biology; merged TIGR and several other organizations to form the J. Craig Venter Institute, a nonprofit with some 500 scientists and staff; and launched a new company called Synthetic Genomics. Meanwhile, the public project announced the completion of the human sequence in 2003; many see it as the winner of the competition, a characterization that Venter and some of his fans dispute.

A Life Decoded depicts Venter as a rugged individualist and passionate lover of the ocean, happiest when sailing on the open waters of the high seas or conducting science unencumbered by institutional constraints or conventional wisdom. Whether racing toward a new scientific "first" or speeding toward victory in a transatlantic yacht race, Venter also fashions himself as a man who thrives on competition. He narrates his scientific life as a course that tacks between an exhilarating voyage of discovery and an intense struggle against narrow-minded, territorial people and rigid institutions. For example, the chapter "Scientific Heaven, Bureaucratic Hell"

The reviewer is at the Department of Science and Technology Studies, 306 Rockefeller Hall, Cornell University, Ithaca, NY 14853, USA. E-mail: shh6@cornell.edu

BROWSING

Hispaniola. A Photographic Journey Through Island Biodiversity, Biodiversidad a Través de un Recorrido Fotográfico. Eladio Fernández, Ed. Translated into Spanish by Irina Ferreras and Gustavo A. Romero-González. Harvard University Press, Cambridge, MA, 2007. 394 pp. $60, £38.95, €55.30. ISBN 9780674026285.

Haiti and the Dominican Republic share the second largest island in the Caribbean. Hispaniola includes the region's lowest and highest points: the hypersaline Lago Enriquillo, 40 m below sea level, and Pico Duarte, 3087 m. This wide altitudinal range and the island's 40 million-year history have fostered the Caribbean's greatest variety of habitat types and a diverse insular flora and fauna. Despite the impacts of an accelerated degradation of natural resources, pollution, and the rapidly expanding human population, Hispaniola retains a number of wild places. Fernández, a Dominican-based conservationist and photographer, takes the reader on a circuit of protected areas and biodiversity hotspots. His images include dramatic landscapes (such as Parque Nacional Lago Enriquillo, above), closer views of habitats (from mountain forests to estuaries and coastal mangroves), and field portraits of animals, plants, and fungi. Researchers provide introductory essays (in Spanish and English) on the island's birds, mammals, amphibians, reptiles, insects, vegetation, and the "woefully understudied" macrofungi. In his foreword, Edward O. Wilson notes both the beauty and vulnerability of this island biota and hopes that more will be done to save it.

CREDIT: ELADIO FERNÁNDEZ/COURTESY HARVARD UNIVERSITY PRESS

recounts his experiences at NIH, contrasting the feverish excitement of knowing his laboratory was "going to turn biology upside down" with depressing encounters with the "one-size-fits-all mentality that plagues any bureaucracy" and peer reviewers who "seemed to be united by one purpose: to stop anyone else from getting any money before they did." Venter applies this basic narrative to his experiences in a range of institutional environments, using it to frame his struggle with the head of HGS, to attack the public genome project as dogmatic, and to describe his bosses during his falling out with Celera.

Like many autobiographers, Venter uses *A Life Decoded* to aggressively present his version of events. He perceives himself as having been misunderstood and unfairly demonized by his critics in the research community, and he seeks to correct the record, justify some of his decisions, and settle some old scores. Not surprisingly, he is particularly concerned with revisiting the conflict between Celera and the public genome project, which featured a complex tangle of intertwined issues involving intellectual property, data access, sequencing methods, and scientific priority—not to mention mutual distrust. His account, although rich with details from backstage maneuvers, is clearly a continuation of the debate rather than an analysis of it. Readers who seek a fuller understanding of the controversies Venter describes will want to compare *A Life Decoded* with additional perspectives drawn from other books on the genome project, including works by Robert Cook-Deegan (*5*) and John Sulston and Georgina Ferry (*6*).

A Life Decoded is most revealing when read not as a portrait of a man but as an account of the environment in which genome research is taking place. Venter's story includes a goodly number of scientists, but they are joined by venture capitalists, business executives, corporate lawyers, government officials, politicians, members of the intelligence community, publicists, and others. Moreover, hybrids—such as contractually mediated assemblages of nonprofit organizations and private companies—are abundant. Like Venter's career, genome science seems to be continually overflowing its institutional containers, and managerial devices like five-year plans and business models often seem incapable of keeping pace with the accelerating speed of the action. If this image of the new biology is roughly accurate, then we can expect this domain of sociotechnical change to remain more unruly than even its most iconoclastic individual participants.

References

1. M. D. Adams *et al.*, *Science* **252**, 1651 (1991).
2. R. D. Fleischman *et al.*, *Science* **269**, 496 (1995).
3. J. C. Venter *et al.*, *Science* **291**, 1304 (2001).
4. S. Levy *et al.*, *PLoS Biol.* **5**, e254 (2007).
5. R. Cook-Deegan, *The Gene Wars: Science, Politics, and the Human Genome* (Norton, New York, 1994); reviewed by J.-P. Gaudillière, *Science* **265**, 685 (1994).
6. J. Sulston, G. Ferry, *The Common Thread* (Corgi, London, 2003).

10.1126/science.1150191

MOLECULAR BIOLOGY

Manners, Good and Bad

Sydney Brenner

All of us have received those scoring guidelines from funding agencies that begin with outstanding; proceed through excellent, very good, and good; and terminate (at least in America) with average. Absent are poor, bad, awful, and disgusting. I have always felt that only two categories are required: interesting and boring. Boring and being bored figure large in Jim Watson's new book *Avoid Boring People*, and the double meaning of the title is make explicit by the insertion of a ghostly "other" on the dust jacket.

I must confess that I had been sent parts of the book sometime ago, when its title was going to be *Manners*. Thus, when the new title was announced, I thought a good title for a review would be "Avoid boring books." But after reading the book, I quickly changed my mind. It is interesting because it fills out the parts of Jim's life missing from his previous books.

I learned many things about Jim that

The reviewer is at the Howard Hughes Medical Institute, Janella Farms Research Campus, 19700 Helix Drive, Ashburn, VA 20147, USA. E-mail: Brenner@salk.edu

exploded several of my theories about him. For example, when Jim and I were stopped by the police in Kansas in 1954, Jim expressed great irritation at being addressed as Mr. Dewey, his middle name. I always thought that this name stemmed from John Dewey, the philosopher, whose books occupied the top shelf of the large bookcase I had seen a few days before in his father's study in their home in Chicago. In fact, Dewey is a family name of Jim's grandmother, brought to America in the 17th century. There are also many other interesting connections of his family, including that Jim and Orson Welles are related. From the information given in the book, they could share as much as 6% of their genomes—but we can definitely exclude that they have the same Y chromosome.

The early chapters of the book take us through Jim's undergraduate education at the University of Chicago, his graduate work in Bloomington, his encounter with the phage group, and the influences of Max Delbrück and Salva Luria on his intellectual development. After a somewhat hilarious first postdoc with Herman Kalckar in Copenhagen, he arrives in Cambridge in 1951, and we are soon back in the familiar country of *The Double Helix* (*1*), with a detailed history of the discovery.

Watson in 1962. That year he "got a Nobel Prize but no raise from Harvard."

The remainder of the book deals with Jim's years at Harvard, which he joined as an untenured professor in 1956, 3 years after making the discovery of the century. He resigned in 1976, when he found that combining his Harvard duties with the directorship of Cold Spring Harbor Laboratory (which he had taken up in 1967) was proving difficult. At Harvard between writing *The Molecular Biology of the Gene* (*2*) and *The Double Helix*, Jim emerged as a leader in molecular biology, a great mentor of his students, and the force behind the appointments of many colleagues who collectively made Harvard a leading center for the new molecular biology. Unlike Delbrück, who was nearly always wrong, Jim was nearly always right in his scientific choices. And also unlike Delbrück (who could be ruthlessly dismissive in his criticism and wounded many young people), Jim was constructive, even though some of his ideas could be eccentric. Jim also knew what it was like to be a young person in a competitive field of science.

Jim gives an account of what he claims to be his prior discovery of messenger RNA. Although this is not the place for a discussion of this matter, I was interested to learn that Leo Szilard was not convinced by the experiment and that Jim then followed his advice to try to demonstrate messenger RNA in bacteria before publishing it. It was difficult at the time to change everybody's standard views, which is why François Jacob and I took enormous pains with the experiments we carried out. We withdrew our completed paper to wait for Jim's manuscript, which we assumed was ready but was delayed 4 months. Jim does not deny the delay but claims it irrelevant because he got there first. However, the delay had certain consequences of which I am sure he is aware.

If Jim's first autobiographical book (*The Double Helix*) is a story of success, his second, *Genes, Girls and Gamow* (*3*), is one about failure. In it, Jim fails to solve the structure of RNA and is only a spectator in the quest for the genetic code. He also fails to get his girl; indeed, he fails to get any girl at all. Whereas *Avoid Boring People*, I think, is about fulfillment. Jim does get his girl as well as the Nobel Prize. He emerges a leader of the field of molecular biology, a great defender of basic research, and the source of much welcome encouragement for young scientists working at the frontiers of knowledge. The Human Genome Project, which Jim led in its early years, has had one bad—one might say, boring—consequence in generating factory science that I have called "low input, high throughput, no output" biology. Such biology is a theme addressed in the Epilogue, which discusses the demise of Larry Summers, the previous president of Harvard University. Summers was forced to resign after making some ill-chosen remarks about genes and the academic skills of women. That, Jim asserts, was his personal fault, but he deserved to fail because of his contributions to the destruction of biological research in Harvard.

Avoid Boring People
Lessons from a Life in Science / And Other Lessons from a Life in Science

by James D. Watson

Knopf, New York, 2007. 365 pp. $26.95, C$34.95. ISBN 9780375412844. Oxford University Press, Oxford. £14.99. ISBN 9780192802736.

I almost forgot to mention that each of the book's chapters is followed by a set of lessons and manners learned. The 108 "remembered lessons" are then provided again at the end of the book. I am afraid that most of them are boring. They are in no way "an indispensable guide to anyone plotting [note: not planning, or entertaining] a career in science." There are better lessons to be learned from reading *Avoid Boring People*.

Epilogue. While I wrote this review in a hospital bed, there flashed across the television screen the news of Jim's recent activities in London. It was an uncanny replay of what had happened to Larry Summers. Jim made some remarks about genes and black people (he's done the women one before), and those raised an uproar. Branded as a racist, he had to abandon his lecture, and Cold Spring Harbor had to censure him and relieve him of his administrative duties. Manners are social codes that enable us to operate in society in acceptable ways. There are good manners and bad manners. But this and the Summers episode go much more deeply than the display of bad manners, for which one can always apologize. The Greeks had a word for it: hubris, the self-confidence and arrogance that always leads to disastrous retribution. If Euripides were with us, he would have said "Whom the gods wish to destroy, they first expose to the public press."

References

1. J. D. Watson, *The Double Helix: A Personal Account of the Discovery of the Structure of DNA* (Atheneum, New York, 1968); reviewed by E. Chargaff, *Science* **159**, 1448 (1968).
2. J. D. Watson, *The Molecular Biology of the Gene* (Benjamin, New York, 1965); reviewed by T. M. Sonneborn, *Science* **150**, 1282 (1965).
3. J. D. Watson, *Genes, Girls and Gamow*, (Oxford Univ. Press, Oxford, 2001); reviewed by R. A. Ankeny, *Science* **295**, 977 (2002).

10.1126/science.1151032

ECOLOGY

Managing Evolving Fish Stocks

Christian Jørgensen,[1*] Katja Enberg,[1,2] Erin S. Dunlop,[2,1] Robert Arlinghaus,[3,4] David S. Boukal,[2,1] Keith Brander,[5] Bruno Ernande,[6,7] Anna Gårdmark,[8] Fiona Johnston,[7,3] Shuichi Matsumura,[7,3] Heidi Pardoe,[9,10] Kristina Raab,[11,10] Alexandra Silva,[12] Anssi Vainikka,[8] Ulf Dieckmann,[7] Mikko Heino,[2,1,7] Adriaan D. Rijnsdorp[13]

Evolutionary impact assessment is a framework for quantifying the effects of harvest-induced evolution on the utility generated by fish stocks.

Darwinian evolution is the driving process of innovation and adaptation across the world's biota. Acting on top of natural selection, human-induced selection pressures can also cause rapid evolution. Sometimes such evolution has undesirable consequences, one example being the spreading resistance to antibiotics and pesticides, which causes suffering and billion-dollar losses annually (*1*). A comparable anthropogenic selection pressure originates from fishing, which has become the main source of mortality in many fish stocks, and may exceed natural mortality by more than 400% (*2*). This has, however, been largely ignored, even though studies based on fisheries data and controlled experiments have provided strong empirical evidence for fisheries-induced evolution over a range of species and regions (see table, page 1248). These evolutionary changes are unfolding on decadal time scales—much faster than previously thought.

Life-history theory predicts that increased mortality generally favors evolution toward earlier sexual maturation at smaller size and elevated reproductive effort. Fishing that is selective with respect to size, maturity status, behavior, or morphology causes further evolutionary pressures (*3*). Evidence that harvesting can bring about genetic changes comes from breeding programs in aquaculture, which have shown heritable genetic variation in numerous traits (*4*), and from experiments showing harvest-induced evolution in just a few generations (table S1). Furthermore, analyses of fisheries data spanning a few decades have detected widespread changes in maturity schedules that are unlikely to be explained by environmental influences alone (table S2). Although alternative causal hypotheses can be difficult to rule out, fisheries-induced evolution consistently arises as the most parsimonious explanation after environmental factors have been accounted for. The question is not whether such evolution will occur, but how fast fishing practices bring about evolutionary changes and what the consequences will be.

Life-history traits are among the primary determinants of population dynamics, and their evolution has repercussions for stock biomass, demography, and economic yield (*5*, *6*). Fisheries-induced evolution may also be slow to reverse or even irreversible (*5*), with implications for recruitment and recovery (*7*). Consequently, predator-prey dynamics, competitive interactions, relative species abundances, and other ecological relationships will systematically change over time. Current management reference points are thus moving targets: Stocks may gradually become less resilient or may be erroneously assessed as being within safe biological limits. Some evolutionary trait changes will even have the potential to cause nonlinear ecological transitions and other unexpected outcomes (*8*). Fisheries-induced evolutionary changes are therefore pertinent beyond single-species management.

An evolutionarily enlightened management approach is needed (*5*, *6*, *9*). Although

[1]Department of Biology, University of Bergen, N-5020 Bergen; [2]Institute of Marine Research, Bergen, Norway. [3]Department of Biology and Ecology of Fishes, Leibniz-Institute of Freshwater Ecology and Inland Fisheries, Berlin; [4]Humboldt-University of Berlin, Institute of Animal Sciences, Berlin, Germany. [5]International Council for the Exploration of the Sea (ICES), Copenhagen, Denmark. [6]Laboratoire Ressources Halieutiques, Institut Français de Recherche pour l'Exploitation de la Mer (IFREMER), Port-en-Bessin, France. [7]Evolution and Ecology Program, International Institute for Applied Systems Analysis (IIASA), Laxenburg, Austria. [8]Institute of Coastal Research, Swedish Board of Fisheries, Öregrund, Sweden. [9]Marine Research Institute, Reykjavik; [10]University of Iceland, Institute of Biology, Sturlugata 7, Reykjavik; [11]Hólaskóli, Sauðarkrókur, Iceland. [12]INRB-IPIMAR National Institute for Agriculture and Fisheries, Lisboa, Portugal. [13]Wageningen Institute for Marine Resources and Ecosystem Studies (IMARES), Ijmuiden, the Netherlands.

*Author for correspondence. E-mail: christian.jorgensen@bio.uib.no

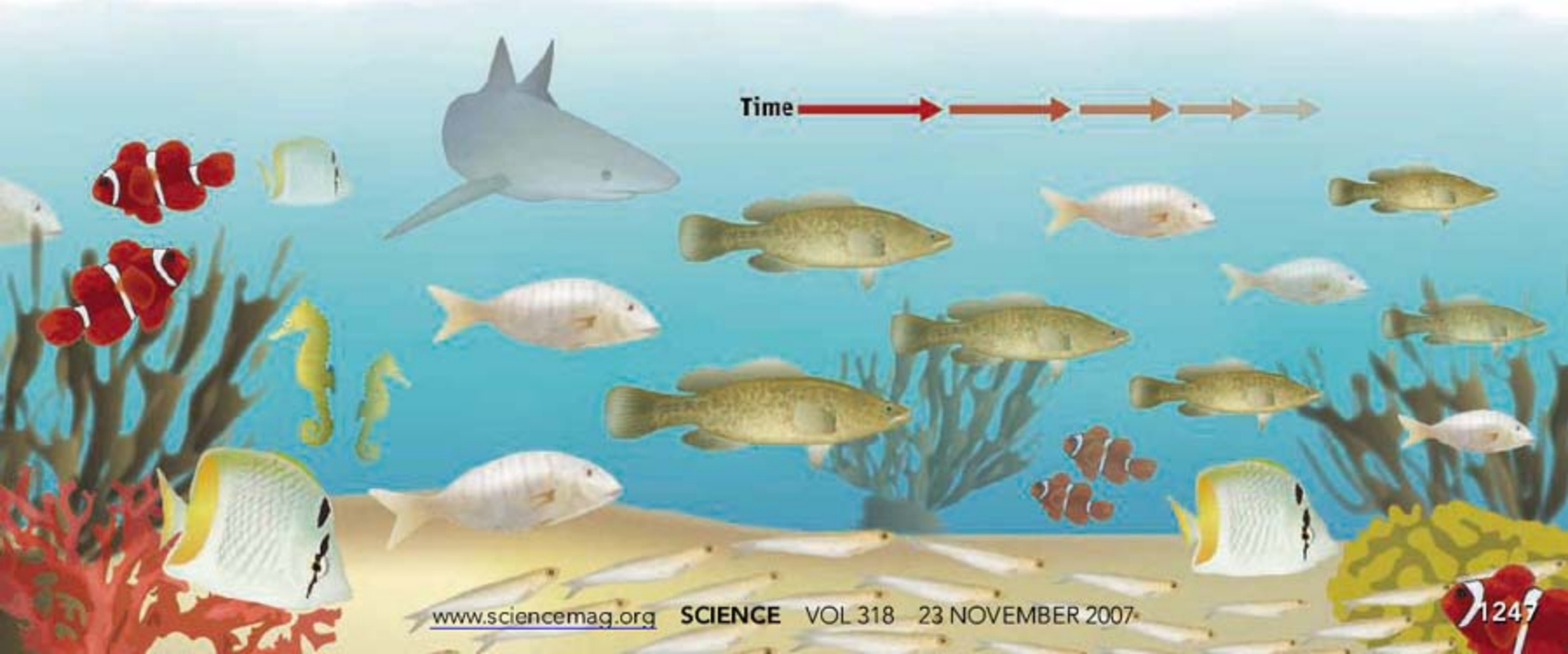

CREDIT: N. KEVITIYAGALA/SCIENCE

Moving targets. Fishing not only reduces the number of fish in the sea, but also changes their heritable features. This may reduce the body size of the fish.

some fish stocks will be managed primarily to maximize sustainable yield, successful management of fisheries-induced evolution will generally benefit from the recognition of a broader range of ecological services generated by living aquatic resources (fig. S1). This perspective emphasizes that evolution underlies ecology and influences economies. An evolutionary perspective will, therefore, (i) support the ecosystem approach to fisheries management (*10*–*13*) by considering how evolution alters ecological relations and management reference points, (ii) comply with the precautionary approach (*14*) by accounting for uncertainty and risk, and (iii) respect the Johannesburg summit's commitment to the restoration of sustainable fisheries (*15*).

Harvest-induced evolutionary changes in marine and freshwater fish.

Evolutionary change	No. of species	No. of studies	Change % (*n*)
Maturation at lower age	6	10	23–24 (1)
Maturation at smaller size	7	13	20–33 (3)
Lower PMRN midpoint	5	10	3–49 (13)
Reduced annual growth	6	6	15–33 (3)
Increased fecundity	3	4	5–100 (3)
Loss of genetic diversity	3	3	21–22 (2)

Fisheries-induced evolution has been demonstrated in several species and studies, for some stocks (*n*) the magnitude of change could also be quantified. Analyzed time series covered between 13 and 125 years. PMRN, probabilistic maturation reaction norm (*18*). The documented evolutionary changes potentially affect fishery yield, recreational fishing experience, tourism revenue, trophic interactions, resilience to fishing, resilience to environmental fluctuations, and adaptability (e.g., to climate change). Further details are given in table S2 and fig. S1.

Environmental impact assessments are commonly used to evaluate the consequences of human activities for ecosystems and society. We propose evolutionary impact assessment (EvoIA) as a tool for the management of evolving resources. Conceptually, an EvoIA involves two major steps. The first relies on biological information and describes how human actions, such as fishing, lead to trait changes. The second step addresses how trait changes affect the stock's utility to society. Any definition of utility has to reflect management objectives and needs to be developed with stakeholder involvement. Evolutionary impact is then assessed as the change in utility of a stock as a result of fisheries-induced evolution.

Economically valuable stocks typically have a long history of exploitation; for such stocks, a natural starting point to help prioritize management efforts is a retrospective assessment of past evolutionary change [e.g., (*16*, *17*)]. Given suitable fisheries data, new statistical techniques can assess the extent to which evolutionary changes may have occurred (*18*).

A more detailed understanding will typically rely on evolutionary models. For example, Northeast Arctic cod was identified as being susceptible to large evolutionary changes in maturation, because offshore trawling, introduced in the 1920s, reversed earlier selection pressures (*5*).

An EvoIA goes a step further, linking evolution to an impact on utility. EvoIAs that look forward in time and compare alternative management options will have to rely on evolutionary models to provide quantitative predictions. In these prospective EvoIAs, projections of future utility depend not only on how fishing affects traits, but also on how trait changes alter ecological relations, which in turn affect utility (fig. S2). Empirical and theoretical studies have shown that many life-history traits are prone to rapid harvest-induced evolution. These traits are important because they influence a population's demography and harvestable biomass. However, life-history traits are also shaped by, and have implications for, density-dependence, trophic interactions, geographical distribution, migration patterns, behavior, and sexual selection. Furthermore, the risk of adverse ecological consequences intensifies, because of nonlinear effects, as traits evolve further away from their historic distributions. Prospective EvoIAs will thus rely on life-history models that, ultimately, should address a broad range of mechanisms and traits influenced by fishing (*19*).

A baseline for comparison is the continuation of a business-as-usual scenario, with evolutionary and utility projections based on the current fishing regime. This allows the cost of inaction to be quantified for different time horizons. Further, utility can be calculated for alternative management scenarios. This identifies management regimes that have the least negative, or even positive, effects on utility (fig. S2). Cumulative utility and its net present value will depend on the choice of time horizons and discounting rates (*20*).

A central challenge to all EvoIAs is to define evolutionarily enlightened management objectives that can be translated into unified utility metrics integrating disparate social values. Pragmatically, such objectives are more likely to be implemented if they harmonize with the pressing short-term goals of traditional fisheries management (*21*). In the context of fisheries-induced evolution, utility metrics might include yield and its variability and sustainability, conservation of genetic and phenotypic diversity, the role of a harvested species in ecosystem functioning, and implications for recreational fishing and tourism. The current state of each of these factors may be eroded either directly through fisheries-induced evolution or indirectly through the ecosystem-level implications of such evolution.

Fisheries-induced evolution is likely to diminish yield and degrade ecological services within decades, having an impact on species, ecosystems, and societies. Evolutionary effects could magnify the ecological challenges that already threaten sustainable harvesting. Successful management, therefore, will require the ecological and evolutionary consequences of fishing to be evaluated and mitigated. Adopting EvoIAs will enable fisheries managers to rise to this challenge.

References and Notes

1. S. R. Palumbi, *Science* **293**, 1786 (2001).
2. G. Mertz, R. A. Myers, *Can. J. Fish. Aquat. Sci.* **55**, 478 (1998).
3. M. Heino, O. R. Godø, *Bull. Mar. Sci.* **70**, 639 (2002).
4. T. Gjedrem, *Aquaculture* **33**, 51 (1983).
5. R. Law, D. R. Grey, *Evol. Ecol.* **3**, 343 (1989).
6. D. O. Conover, S. B. Munch, *Science* **297**, 94 (2002).
7. M. R. Walsh *et al.*, *Ecol. Lett.* **9**, 142 (2006).
8. M. Scheffer, S. Carpenter, B. de Young, *Trends Ecol. Evol.* **20**, 579 (2005).
9. M. V. Ashley *et al.*, *Biol. Conserv.* **111**, 115 (2003).
10. U.N. Food and Agriculture Organization (FAO), *Fisheries Management 2: The Ecosystem Approach to Fisheries* (FAO Technical Guidelines for Responsible Fisheries No. 4, Suppl. 2, FAO, Rome, 2003).
11. E. K. Pikitch *et al.*, *Science* **305**, 346 (2004).
12. R. C. Francis *et al.*, *Fisheries* **32**, 217 (2007).
13. J. R. Beddington, D. J. Agnew, C. W. Clark, *Science* **316**, 1713 (2007).
14. FAO, *Precautionary Approach to Capture Fisheries and Species Introductions* (FAO Technical Guidelines for Responsible Fisheries, No. 2, FAO, Rome, 1996).
15. The United Nations 2002 World Summit on Sustainable Development in Johannesburg, South Africa, declared that fish stocks shall be restored to produce the maximum sustainable yield by 2015.
16. A. D. Rijnsdorp, *Oecologia* **96**, 391 (1993).
17. E. M. Olsen *et al.*, *Nature* **428**, 932 (2004).
18. U. Dieckmann, M. Heino, *Mar. Ecol. Progr. Ser.* **335**, 253 (2007).
19. W. C. Lewin, R. Arlinghaus, T. Mehner, *Rev. Fish. Sci.* **14**, 305 (2006).
20. C. W. Clark, *The Worldwide Crisis in Fisheries* (Cambridge Univ. Press, Cambridge, UK, 2006).
21. R. Law, *Mar. Ecol. Progr. Ser.* **335**, 271 (2007).

22. We thank A. James, M. Jöstl, and K. Platzer at IIASA for help with graphics and formatting. The authors are members of the ICES Group on Fisheries-Induced Adaptive Change. Please contact the chairs M.H., U.D., or A.D.R. for information.

Supporting Online Material

www.sciencemag.org/cgi/content/full/318/5854/1247/DC1

10.1126/science.1148089

CELL BIOLOGY

IP_7 Debut in Insulin Release

An inositol compound determines the capacity of the pancreas to release insulin and may function similarly in other secretory cells.

Shinya Nagamatsu and Mica Ohara-Imaizumi

In a healthy individual, the pancreas is poised to release the hormone insulin when the concentration of blood glucose rises, causing muscle and liver cells to take up and store the nutrient as a future energy source. This release occurs in two phases: a rapid and transient first phase, followed by a sustained second phase (*1*–*3*). This biphasic response maintains blood glucose homeostasis by priming peripheral tissues for glucose uptake and preventing overinsulinization (and subsequent hypoglycemia). Type 2 diabetes correlates with an aberration in this biphasic pattern, including a selective loss of the first-phase (*4*). So clarifying how biphasic insulin release occurs is essential to understanding the pathogenesis of this complex disease. On page 1299 of this issue, Illies *et al.* (*5*) describe a new factor in pancreatic β cells that controls the exocytosis (release) of insulin storage granules.

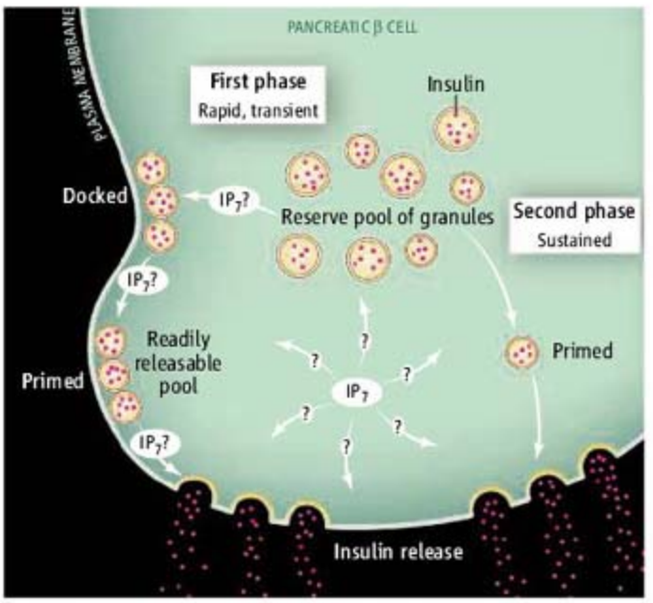

Mechanism of glucose-induced insulin release. The inositol phosphate IP_7 controls the rapid release phase of insulin from pancreatic cells, but its mechanism of action remains unclear.

More than 30 years ago, a mathematical model described biphasic insulin secretion involving two compartments of limited insulin storage (*6*). More recently, a combination of capacitance measurements (an indicator of exocytosis) and electron microscopy of pancreatic β cells (*2*) suggested a model in which secretory granules containing insulin are divided into two distinct functional pools. In this case, a readily releasable pool constitutes a subset of granules that are "docked" at the plasma membrane, and can undergo exocytosis immediately when the cell is stimulated with a factor, such as glucose (see the figure). A reserve pool of granules is located in the cytoplasm, and those granules are recruited to replenish the readily releasable pool (*7*, *8*). The first phase of insulin release is largely attributable to fusion of previously docked granules from the readily releasable pool, as observed through imaging studies of live pancreatic β cells (*9*). These docked granules localize with syntaxin 1A, a membrane protein involved in the docking and fusion of granules in many secretory cell types, including neurons. During the second phase of insulin release, "newcomer" granules, absent at the plasma membrane before cell stimulation, participate in fusion (without syntaxin 1A association) (*10*). Thus, marked differences in the first and second phase of insulin release have been visually observed.

Phosphorylated inositol compounds regulate insulin release from pancreatic β cells (*11*). These compounds, which are ubiquitously expressed in mammalian cells, include inositol 1,4,5-trisphosphate (IP_3), which regulates Ca^{2+} release from intracellular stores (Ca^{2+} can trigger granule fusion) (*12*) and is also a precursor to more highly phosphorylated inositol phosphate molecules, such as inositol tetrakis- (IP_4), pentakis- (IP_5), and hexakis- (IP_6) phosphates. IP_6 activates voltage-dependent L-type Ca^{2+} channels, exocytosis, and endocytosis (uptake of extracellular material) in pancreatic β cells (*11*). Additional phosphorylation of IP_6 produces inositol pyrophosphates, diphosphoinositol pentakisphosphate (PP-IP_5, or IP_7) and bis-(diphospho)inositol tetrakisphosphate [$(PP)_2$-IP_4 or IP_8]. Furthermore, inositol pyrophosphates have been linked to a wide range of biological processes, including vesicle trafficking, programmed cell death, DNA repair, telomere maintainance, and responses to stress (*13*). Notably, inositol pyrophosphates contain highly energetic pyrophosphate bonds, with a free energy of hydrolysis similar to that of adenosine 5′-triphosphate (ATP) (*13*). Therefore, IP_7 can directly phosphorylate proteins in an ATP- and enzyme-independent manner (*14*). Thus, it appears that inositol pyrophosphates have many potential actions, although the underlying molecular mechanisms and physiological targets are obscure.

A putative disruption of the gene that encodes inositol hexakisphosphate kinase 1 (IP6K1), the enzyme that produces IP_7 from IP_6, was identified in a family with type 2 diabetes (although the association to the disease in this case is not clear) (*15*). On the other hand, Illies *et al.* show that an increase in IP_7 concentration in pancreatic β cells increases the size of the readily releasable pool of insulin-containing granules, leading to enhanced exocytosis. Because the readily releasable pool is essential for the first-phase of insulin release (*7*, *8*, *10*), and a reduced size of this pool correlates with a decrease in first-phase insulin release (as seen in the diabetic Goto-Kakizaki rat model of human type 2 diabetes) (*9*), Illies *et al.* have addressed a key feature of impaired insulin release in diabetes.

How does this ascribed role for IP_7 fit into the overall sequence of steps that control insulin release? IP_7 could conceivably act at three points in exocytosis (see the figure): by accelerating the translocation of granules from the reserve pool to the plasma membrane, by enhancing the priming step, or by acting directly on the fusion process during exocytosis. IP_7 interacts with several proteins that contain pleckstrin homology domains, although the functions of these interactions are unclear (*13*). Hence, for example, IP_7 may interact with a pleckstrin homology domain–containing protein called Ca^{2+}-dependent activator protein for secretion (*16*) to activate the priming step of docked insulin granules. In addition, IP_7 may bind to IP_6-binding proteins such as C2-domain–containing proteins (*17*). Several proteins bearing C2 domains, such as protein kinase C, synaptotagmin, rabphilin, Doc2, RIM, and Munc13, are thought to have roles in exocytosis (*17*, *18*). The interaction of IP_7 with these proteins could increase the size of the readily releasable pool. Alternatively, IP_7 could phosphorylate other proteins that

The authors are in the Department of Biochemistry, Kyorin University School of Medicine, Shinkawa 6-20-2, Mitaka, Tokyo 181-8611, Japan E-mail: shinya@kyorin-u.ac.jp

control the size of this granule pool. Illies *et al.* do show that IP_7 has little effect on the second phase of insulin release, though this should be firmly established.

The precise steps in insulin release that IP_7 controls, and the mechanisms, remain speculative. Nevertheless, the addition of this factor to our understanding of insulin secretion provides a foundation for further studies. Moreover, because IP_7 is widely present in other cell types, it is likely to have physiological function in other secretory cell types.

References and Notes

1. D. L. Curry, L. L. Bennett, G. M. Grodsky *Endocrinology* **83**, 572 (1968).
2. P. Rorsman *et al.*, *News Physiol. Sci.* **15**, 72 (2000).
3. J. C. Henquin *Diabetes* **49**, 1751 (2000)
4. E. Cerasi, in *Insulin: Molecular Biology to Pathology*, F. M. Ashcroft, S. J. H. Ashcroft, Eds. (IRL, Oxford, UK, 1994), pp. 347–392.
5. C. Illies *et al.*, *Science* **318**, 1299 (2007).
6. G. M. Grodsky, *J. Clin. Invest.* **51**, 2047 (1972).
7. S. G. Straub, G. W. G. Sharp, *Diabetes Metab. Res. Rev.* **18**, 451 (2002).
8. P. Rorsman, E. Renström, *Diabetologia* **46**, 1029 (2003).
9. M. Ohara-Imaizumi *et al.*, *Biochem. J.* **381**, 13 (2004).
10. M. Ohara-Imaizumi *et al.*, *J. Cell Biol.* **177**, 695 (2007).
11. C. J. Barker, I. B. Leibiger, B. Leibiger, P.-O. Berggren, *Am. J. Physiol. Endocrinol. Metab.* **283**, E1113 (2002).
12. M. J. Berridge, P. Lipp, M. D. Bootman, *Nat. Rev. Mol. Cell. Biol.* **1**, 11 (2000).
13. M. Bennett, S. M. N. Onnebo, C. Azevedo, A. Saiardi, *Cell. Mol. Life Sci.* **63**, 552 (2006).
14. A. Saiardi, R. Bhandari, A. C. Resnick, A. M. Snowman, S. H. Snyder, *Science* **306**, 2101 (2004).
15. J. Kamimura *et al.*, *J. Hum. Genet.* **49**, 360 (2004).
16. R. N. Grishanin *et al.*, *Neuron* **43**, 551 (2004).
17. M. Fukuda, K. Mikoshiba, *Bioessays* **19**, 593 (1997).
18. R. D. Burgoyne, A. Morgan, *Physiol. Rev.* **83**, 581 (2003).

19. We thank M. Fukuda (Graduate School of Life Sciences, Tohoku University) for helpful comments.

10.1126/science.1151361

CHEMISTRY

Chemicals from Biomass

Many chemicals used by the chemical industry can be derived from biomass, potentially reducing the industry's reliance on petroleum.

David R. Dodds and Richard A. Gross

Recently, there has been a strong political and technical focus on using biomass to produce transportation fuels (*1*, *2*). Much less attention has been given to biomass as a feedstock for organic chemicals. Replacement of petroleum-derived chemicals with those from biomass will play a key role in sustaining the growth of the chemical industry.

Currently, ~13% of the crude oil consumed by the United States is used for nonfuel chemical production (*3*). Biomass-based processes that could replace crude oil harness enzymatic methods, microbiology, and metabolic engineering to direct the transformation of sugars, lipids, and other biomass-derived molecules to the desired small molecules and polymers.

The biological production of commodity chemicals has considerable history. Between 1945 and 1950, 66% of the *n*-butanol and 10% of acetone in the United States were produced by fermentation of molasses and starch. Other commodity products produced by fermentation in the first half of the 20th century include acetic acid, citric acid, lactic acid, and itaconic acid (*4*). Increased prices of sugar feedstock and decreased prices of petrochemical feedstock ended the fermentative production of these commodities.

Now, the situation has reversed. A 2004 report by the U.S. Department of Energy (DOE) identified high-volume commodity chemicals that could be produced from biomass and can serve as starting materials for many chemical products via biological processes (*5*). A joint report by the DOE and the U.S. Department of Agriculture (*6*) concluded that U.S. agricultural and forest sources can renewably supply a billion tons per year of lignocellulosic biomass. This amount of biomass would not satisfy U.S. fuel demands, but could theoretically replace petrochemical feedstocks for chemical production. Several commodity chemicals are already produced by fermentation, including glutamic acid (~1.7 billion kg/year worldwide), citric acid (~1.6 billion kg/year), and lysine (~850 million kg/year).

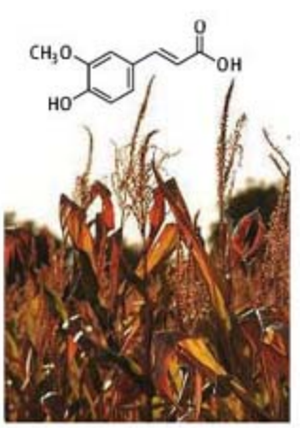

New feedstocks for the chemical industry. Ferulic acid, a precursor for numerous aromatic chemicals used in the chemical industry, can be extracted from corn fiber. Many other important precursors can also be obtained from biomass.

In addition to these commodity chemicals, commodity polymers may also be produced using biologically produced monomers combined with classical chemical methods, as well as through biological polymerization methods, either with isolated enzymes or in actively growing cells.

For example, lactic acid produced by fermentation (*7*) can be converted chemically to methyl lactate, lactide, and polylactic acid (PLA). The latter polymer—commercially available under different trade names—is a fully biodegradable replacement for polyethylene terephthalates (PETs) (*8*). Efforts are also under way to develop efficient processes for converting biologically produced lactic and hydroxypropionic acids to methacrylic and acrylic acids, respectively, both major commodity monomers consumed at ~1.6 billion kg/year worldwide.

Another well-known example is work by scientists at Genencor and DuPont, who have developed a cost-effective fermentative route to 1,3-propanediol (1,3PDO), the key building block in poly(propyleneterephthalate) (PPT, Sorona 3GT), which is not readily available from petrochemical feedstocks (*9*).

Immobilized enzyme catalysts have also been used to polymerize bio-derived monomers. For example, by using a commercially available lipase catalyst, direct polycondensations can be performed between sorbitol and/or glycerol with chemically or biologically produced diacids (*10*). This method dramatically reduces reaction temperatures and energy consumption relative to chemical polymerization processes, while also controlling branching during polymerization.

Fermentation by various microorganisms has been used to produce succinic acid (*11*, *12*), which may potentially replace maleic anhydride, now produced from butane at ~1.8 billion kg/year worldwide. (Maleic anhydride is the starting material for various polymers and industrial solvents.) In another example of microorganism-based production, the shikimic acid pathway in *Escherichia coli* has been reengineered to transform glucose to catechol and other aromatic alcohols (*13*); these indus-

D. R. Dodds is with Dodds & Associates LLC, Manlius, NY 13104, USA. R. A. Gross is at the NSF Center for Biocatalysis and Bioprocessing of Macromolecules, Polytechnic University, Brooklyn, NY 11201, USA. E-mail: rgross@poly.edu

trial chemicals are currently produced from benzene. Further manipulation of this metabolic pathway leads to *cis,cis*-muconic acid, which can be converted chemically to adipic acid. The latter is one of two components required to produce Nylon 6,6 (*14*).

Polymers from biomass have also been produced completely within microbial cells. A notable example is the microbial synthesis of poly-3-hydroxyalkanoates (PHAs) (*15*).

Nor is fermentation a required action for the use of biomass-derived feedstock. Fischer-Tropsch chemistry has been run on pyrolysed biomass, and some commodity chemicals could be derived directly from biomass via conventional extraction methods. For example, corn fiber contains a high percentage of ferulic acid (see the figure), a flexible feedstock for various fine chemicals such as vanillin and guaicol. An estimated 1 billion kg/year of ferulic acid could be recovered from corn fiber separated in current corn-milling operations (*16*).

The rapid growth in the biodiesel industry, which uses chemical methods to synthesize its product, has decreased the market price of glycerol; many biodiesel production facilities now view crude glycerol as waste. Chemical companies can use this glycerol as a low-cost chemical building block. Dow Chemical Company, Huntsman Corporation, Cargill, and Archer Daniels Midland Corporation have begun, or announced plans, to chemically convert glycerol to propylene glycol (*17*). Dow Chemical Company and Solvay plan to build plants that use glycerol to produce epichlorohydrin (*18*).

Other innovative chemical methods convert fatty acids to polymer building blocks. For example, Cargill, working with the Kansas Polymer Research Center, has developed a bio-derived polyol (BiOH) by the chemical conversion of triglyceride carbon-carbon double bonds to alcohol and methoxy groups. Polyols are important precursors to numerous polyurethane materials (*19*).

Despite these achievements, the transition of industrial chemical production from petrochemical to biomass feedstock faces real hurdles. Biological processes do not require the high pressures and temperatures associated with most nonbiological chemical processes and thus have the potential to reduce costs. However, current processes for production of commodity chemicals have evolved through considerable investment to become highly efficient, often continuous, and well integrated. To be successful, new biological processes must rapidly approach similar levels of efficiency and productivity. Nevertheless, economic opportunities, available technologies, and environmental imperatives make the use of biomass and biological methods for industrial chemical production not only feasible but highly attractive from multiple perspectives.

References

1. Special Issue on Sustainability and Energy, *Science* **315** (9 February 2007).
2. N. S. Lewis, *Science* **315**, 798 (2007).
3. See www.eia.doe.gov.
4. E. S. Lipinsky, *Science* **212**, 1465 (1981).
5. T. Werpy, P. Petersen, *Top Value Added Chemicals from Biomass. Volume I: Results of Screening for Potential Candidates from Sugars and Synthesis Gas* (www1.eere.energy.gov/biomass/pdfs/35523.pdf).
6. *Biomass as Feedstock for a Bioenergy and Bioproducts Industry: The Technical Feasibility of a Billion-Ton Annual Supply* (feedstockreview.ornl.gov/pdf/billion_ton_vision.pdf).
7. T. L. Carlson, E. M. Peters, U.S. Patent application US2006/094093 A1, published 4 May 2006.
8. P. Lorenz, H. Zinke, *Trends Biotechnol.* **23**, 570 (2005).
9. M. Emptage, S. Haynie, L. Laffend, J. Pucci, G. Whited, European Patent Application 1586647A1, published 19 October 2005.
10. A. Kumar, A. S. Kulshrestha, W. Gao, R. A. Gross, *Macromolecules* **36**, 8219 (2003).
11. M. V. Guettler, M. K. Jain, B. K. Soni, U.S. Patent 5504004 (1996).
12. M. Donnelly, C. S. Millard, L. Stols, U.S. Patent 5770435 (1998).
13. J. W. Frost, K. M. Draths, U.S. Patent 5629181 (1997).
14. J. W. Frost, K. M. Draths, U.S. Patent 5487987 (1996).
15. G. Q. Chen *et al.*, *Appl. Microbiol. Biotechnol.* **57**, 50 (2001).
16. I.-Y. Lee, T. G. Volm, J. P. N. Rosazza, *Enzyme Microb. Technol.* **23**, 261 (1998).
17. M. McCoy, *Chem. Eng. News* **85**, 12 (19 March 2007).
18. A. H. Tullo, *Chem. Eng. News* **85**, 14 (7 May 2007).
19. S. K. Ritter, *Chem. Eng. News* **85**, 35 (9 July 2007).

10.1126/science.1146356

PHYSICS

Better Computing with Photons

New findings in quantum optics reported at a recent conference are stimulating advances in quantum computing.

Timothy C. Ralph and Robert W. Boyd

For decades, researchers have been fascinated by the ways in which light acts as a quantum particle (photon). For almost as long, they have also pursued schemes in which photons can be used as information carriers and processors. As they have done every 6 years since the 1960s, the quantum optics community gathered to hear the latest results at the CQO (Coherence and Quantum Optics) and ICQI (International Conference on Quantum Information) conferences held 11 to 15 June 2007 at the University of Rochester in Rochester, New York, USA (*1*, *2*). This year's meeting did not disappoint, with a number of exciting developments combining quantum optics with quantum information.

Quantum optics (*3*–*5*) plays an important role in quantum information science (*6*–*9*) not only because light can manipulate matter with high precision, but also because the photon is so versatile as a quantum bit (qubit). The polarization of photons in a light beam acts as an ideal quantum mechanical two-level system that can be easily controlled and measured. For example, we can assign logical bit values of 0 and 1 to horizontal and vertical polarizations, respectively. Diagonal and elliptical polarizations, which are superpositions of the vertical and horizontal polarizations, then represent qubit states. Photons are also robust; when they travel through free space, their polarization is stable. Optics therefore represents an ideal way to transmit quantum information over large distances. For communication through an optical fiber, which tends not to preserve the polarization state, other variables such as timing or frequency can be used.

Although photons have their quantum information virtues, they also have their vices. First, they are very difficult to store. Thus, although great communicators, photons are not very good as quantum information memories. Second, it is difficult to make photons interact; in the absence of matter, photons take little notice of each other. Yet such interactions are required for processing quantum information, and without them it will be impossible to build large-scale quantum processors (also known as quantum computers). Third, and perhaps most important, high-quality single-photon states are difficult to produce on demand. The goal is to produce one and only one photon in successive identical pulses.

T. C. Ralph is in the Department of Physics, University of Queensland, Brisbane QLD 4072, Australia. R. W. Boyd is at the Institute of Optics, University of Rochester, Rochester, NY 14627, USA. E-mail: boyd@optics.rochester.edu

To achieve this, it is necessary to introduce matter, which can mediate interactions between photons and facilitate storage. Remarkable progress has been made in this domain.

A long-held dream of the quantum optics community is to have single photons and single atoms strongly and efficiently interact with each other. This is the realm of cavity quantum electrodynamics (CQED). The idea is to have a single atom held in a very-high-quality optical cavity [that is, a storage device with extremely low energy loss (see the figure)]. This ensures that the coupling between the field and the atom is so strong that the state of the single atom can completely change the dynamics of the cavity field. Conversely, the presence of a single photon in the field can completely change the dynamics of the atom. Reaching this so-called strong coupling regime has proved technically challenging, but at the conference we learned about several major advances involving both traditional systems and entirely new approaches.

The traditional approach to CQED is to drop or fire atoms through a cavity constructed with mirrors of extremely high reflectivity. At optical frequencies it is now possible to trap a single atom in the cavity mode for seconds, as discussed by H. J. Kimble (Caltech). In a further break with traditional techniques, Kimble and K. Vahala have now also managed to achieve strong coupling of atoms to microtoroidal cavities. The promise of this technology is scalability, as many microtoroids can be created on a single chip.

Typically we think of atoms as the objects to be studied with photon probes. In certain cases, these usual roles are reversed. This was the case in the CQED experiments involving microwave photons reported by M. Brune and S. Haroche (École Normale Supérieure, Paris) in which atoms are used to count the number of photons in a cavity mode. In a particularly spectacular result, they were able to observe quantum jumps between states consisting of up to seven photons, down to zero photons, contained in their microwave cavity. This provides a new understanding of the boundary between quantum and classical phenomena and may be useful in manipulating quantum interactions among multiple atoms.

The most radical departure from the traditional approach to CQED came from R. Schoelkopf (Yale), who described forming high-quality microwave cavities from strip lines on chips and achieving strong coupling of the microwave photons to artificial atoms formed from superconducting Cooper pair boxes. This represents the first steps toward integrated, hybrid quantum optical solid-state circuits.

Another way to achieve light storage is through the use of "slow-light" and "stopped-light" methods. In these experiments, a light pulse at just the right frequency interacts with matter so that the group velocity (the speed of the entire pulse) slows to a snail's pace. J. Howell (Univ. of Rochester) reported an especially intriguing result in which an extremely weak image-bearing beam was slowed down by a factor of 30 in an atomic vapor and emerged intact.

Arguably the most useful interaction between light and atoms is currently afforded by trapped single ions, which can be controlled by electric fields. R. Blatt (Univ. of Innsbruck) showed us the rich landscape of interactions afforded by the calcium-43 ion and the detailed control possible through optical manipulations, including the recent demonstration of a quantum byte—an 8-qubit entangled state.

Achieving efficient interactions between single ions and single photons remains challenging because of the technical problems involved in combining mirrors and charged particles. Nonetheless, C. Monroe (Univ. of Michigan) showed us that even if only inefficient coupling is possible, some startling results can be achieved. In particular, by simultaneously measuring photons arising from the spontaneous decay of two separate ions, his group was able to produce entanglement (i.e., an intrinsic quantum link) between ions lying a meter apart.

The experimental ability to generate, distribute, and use optical entanglement has steadily been improving over recent years. At the meeting, we heard of various advances in this field from P. Kwiat (Univ. of Illinois), A. Furusawa (Univ. of Tokyo), and H.-A. Bachor (Australian National Univ.). In particular, P. Kumar (Northwestern Univ.) described his group's optical fiber–based entanglement source, promising the possibility of integration of quantum communication applications into standard telecom infrastructure. He presented results on a telecom-wavelength quantum controlled-NOT gate, which is perhaps the essential logic device necessary to build a quantum computer.

Quantum information science, and quantum computation in particular, took off in the mid-1990s with the discovery of two key algorithms: Shor's algorithm for factoring primes, and Grover's algorithm for quantum search of a database. Two groups reported small-scale optical demonstrations of these algorithms. A. Zeilinger's group (Univ. of Vienna) used an optical cluster state to demonstrate Grover's quantum search. In addition, A. White's group (Univ. of Queensland) demonstrated a concatenated (and simplified) version of Shor's algorithm using a quantum circuit implementation.

The results presented (*1*, *2*) in Rochester this year show that these are exciting times in the fields of quantum optics and quantum information science. We can be assured that many new advances in these fields will be presented at the next gathering at Rochester in 6 years.

Quantum resonator. Two mirrored half-sections are opened to show the interior of a high-quality microwave cavity. Such storage chambers are used to control and study the interaction between single atoms and single photons.

CREDIT: M. BRUNE/ECOLE NORMALE SUPERIEURE, PARIS

References

1. www.osa.org/meetings/archives/2007/ICQI/ICQIArchive2007.pdf
2. *Coherence and Quantum Optics IX*, N. P. Bigelow, J. H. Eberly, C. R. Stroud Jr., Eds. (Optical Society of America, Washington, DC, 2007).
3. L. Mandel, *Rev. Mod. Phys.* **71**, S274 (1999).
4. H.-A. Bachor, T. C. Ralph, *A Guide to Experiments in Quantum Optics* (Wiley-VCH, Weinheim, Germany, 2004).
5. A. Zeilinger, G. Weihs, T. Jennewein, M. Aspelmeyer, *Nature* **433**, 250 (2005).
6. D. Bouwmeester, A. Ekert, A. Zeilinger, *The Physics of Quantum Information* (Springer, Berlin, 2000).
7. M. Nielsen, I. Chuang, *Quantum Computation and Quantum Information* (Cambridge Univ. Press, Cambridge, 2000).
8. H. J. Kimble, S. J. van Enk, *Nature* **429**, 712 (2004).
9. V. Giovannetti, S. Lloyd, L. Maccone, *Science* **306**, 1330 (2004).

10.1126/science.1150968

BIOCHEMISTRY

Signaling Across the Cell Membrane

Structural and functional studies shed light on how G protein–coupled receptors sense external stimuli.

Rama Ranganathan

Cells contain a panoply of transmembrane receptor molecules that can recognize external signals and initiate intracellular signaling events. G protein–coupled receptors (GPCRs)—the largest and most diverse group of these receptors—occur in nearly every eukaryotic cell and can sense photons, cations, small molecules, peptides, and proteins (*1*, *2*). Understanding how GPCRs operate has therefore been a major goal in signaling research for more than two decades (*3*). Two research articles in this issue (*4*, *5*) and a recent article in *Nature* (*6*) report important steps toward this goal.

How can GPCRs recognize such a diversity of extracellular stimuli? How is information about ligand binding (or light absorption) at a site facing the outside of the cell transferred to sites within the cell that mediate interaction with downstream signaling proteins? The structure of the inactive state of bovine rhodopsin (*7*)—a light-sensing GPCR—provided a critical initial step in addressing these questions. Together with functional studies, it led to basic models of GPCR action (*8*). However, it has been difficult to solve structures of more typical GPCRs that bind to diffusible ligands.

In addition to the usual problems encountered in producing membrane proteins suitable for crystallization, many GPCRs have an inherent conformational plasticity (*9*, *10*). Unlike rhodopsin, which is tightly locked into an inactive state by its covalently bound ligand, 11-*cis*-retinal, more typical GPCRs that are activated by diffusible molecules may assume an ensemble of different inactive and active states. This property could be physiologically important, accounting for the ability of different ligands to elicit a range of biological responses from the same GPCR by stabilizing different conformational states within these ensembles.

Given all this, the high-resolution structure determination of an engineered β_2-adrenergic receptor (β_2AR), a canonical GPCR family member activated by diffusible ligands, represents a spectacular advance (*4*–*6*). To minimize conformational heterogeneity and maximize crystal contacts, the authors made several modifications to the receptor that included cocrystallization with the ligand carazolol, removal of a flexible C-terminal tail, and either binding of a Fab fragment of a monoclonal antibody (*11*) or insertion of a small globular protein (T4 lysozyme, T4L) into the flexible third intracellular loop. Further key technical features included addition of cholesterol (known to stabilize β_2AR) as a crystallization additive and the use of the lipidic cubic phase to facilitate crystal growth (*12*). The structure determination itself was a tour de force of advanced techniques in crystal growth, screening, and diffraction. The current papers describe two structures of β_2AR bound to carazolol—a lower-resolution complex with Fab (*6*) and a high-resolution chimera with T4L reported by Cherezov *et al.* [p. 1258, (*4*)]—and a detailed functional characterization of the β_2AR-T4L protein by Rosenbaum *et al.* [p. 1266, (*5*)].

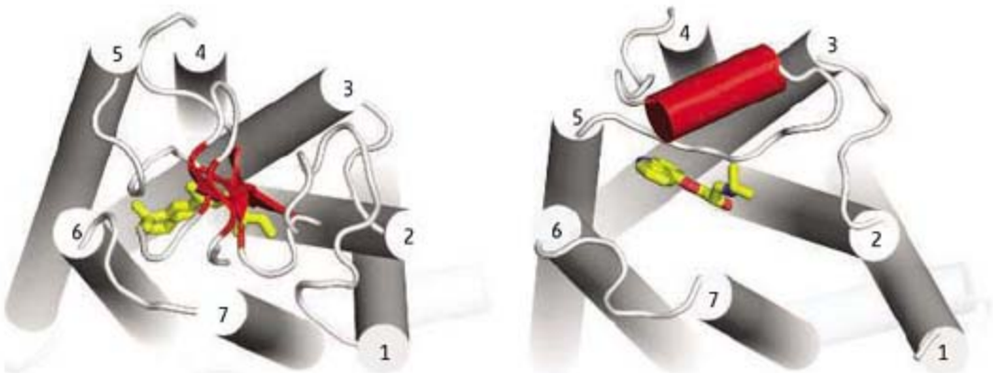

Similar yet different. Rhodopsin **(left)** and the β_2AR **(right)** share overall structural features and a binding pocket for their cognate ligands, 11-*cis*-retinal and carazolol, respectively (in yellow), at a site located deep within the transmembrane helices. However, the extracellular loops are distinctly structured, a result that may explain how diffusible ligands gain access to the binding pocket in the β_2AR.

Although the structures are similar in overall fold to rhodopsin—a roughly ellipsoid arrangement of seven membrane-spanning α-helical segments surrounding the ligand binding site (see the figure)—there are several new findings. With regard to ligand binding, carazolol is located deep within the transmembrane helices, at a site that is consistent with the retinal binding pocket, and some key interactions are consistent with findings in the rhodopsin structure. For example, the inactive state of rhodopsin maintained by 11-*cis*-retinal is thought to be stabilized in part by direct conformational restriction of a conserved tryptophan side chain (*13*). The analogous tryptophan in the β_2AR is similarly restrained (although indirectly) by carazolol. This finding provides a structural basis for interpreting prior mutation studies, which showed that signal propagation mechanisms are largely conserved in members of the GPCR family.

However, the data also indicate variation that may permit specialized responses to specific ligands. A helical structure in the second extracellular loop (ECL2) of β_2AR-T4L makes direct contact with carazolol. This feature is not conserved in rhodopsin. Cherezov *et al.* and Rosenbaum *et al.* suggest that the novel structure in ECL2 and disorder in the N-terminal region of β_2AR may provide a path for diffusible ligands to the binding pocket and contribute to ligand selectivity. Thus, although conformational changes associated with GPCR activation might be conserved in the family, specific kinetic and thermodynamic details of ligand recognition might be specified through modular variation of extracellular loop regions.

A particularly interesting feature is found in the intracellular part of the β_2AR structures. In the inactive state of rhodopsin, a network of hydrogen-bonding interactions links the cytoplasmic end of helix III with a residue in helix VI in a so-called "ionic lock" (*8*). This interaction is broken in both β_2AR structures. This ionic lock–deficient state may represent stabilization of one molecular configuration in the inactive-state ensemble by carazolol, and may explain why this ligand only partially shuts off

The author is at the Green Center for Systems Biology and Department of Pharmacology, University of Texas Southwestern Medical Center, Dallas, TX 75390, USA. E-mail: rama.ranganathan@utsouthwestern.edu

basal β_2AR activity. In this view, the ionic-locked state of rhodopsin is an extreme case—a specialized, more fully inactivated state that provides for the remarkable level of silencing of receptor activity required to suppress noise in the dark-adapted state of photoreceptor neurons. Structure determination of additional ligand-receptor complexes may help test the model of a conformationally heterogeneous inactive-state ensemble in β_2AR.

Rosenbaum *et al.* report a systematic functional analysis of β_2AR bound to T4L to establish its physiological relevance. The engineered receptor displays wild-type binding to antagonists and inverse agonists but increased affinity for agonists, a profile similar to that of constitutively active mutants. Thus, although the receptor chimera is similar to the wild-type β_2AR in many ways, this finding also illustrates potential complexities of working with engineered proteins. In this regard, the functional characterization by Rosenbaum *et al.* plays an important role in the interpretation of the atomic structure.

A major next goal is a structure of the agonist-bound active state of the receptor, work that may require formation of a ternary complex with the cognate G protein or with the inhibitory protein arrestin. The modifications made in the β_2AR-T4L complex preclude interaction with these target proteins. Thus, new strategies will be necessary that will require more of the kind of creativity and dedication that led to the present structures. This work would pave the way for a deeper mechanistic understanding of the GPCR family.

References

1. P. S. Park, D. T. Lodowski, K. Palczewski, *Annu. Rev. Pharmacol. Toxicol.*, 10.1146.annurev.pharmtox.48.113006.094630 (2007).
2. Y. Zhang, M. E. DeVries, J. Skolnick, *PLoS Comput. Biol.* **2**, e13 (2006).
3. E. Jacoby, R. Bouhelal, M. Gerspacher, K. Seuwen, *ChemMedChem* **1**, 761 (2006).
4. V. Cherezov *et al.*, *Science* **318**, 1258 (2007); published online 25 October 2007 (10.1126/science.1150577).
5. D. M. Rosenbaum *et al.*, *Science* **318**, 1266 (2007); published online 25 October 2007 (10.1126/science.1150609).
6. S. G. Rasmussen *et al.*, *Nature*, 10.1038/nature06325 (2007).
7. K. Palczewski *et al.*, *Science* **289**, 739 (2000).
8. K. Palczewski, *Annu. Rev. Biochem.* **75**, 743 (2006).
9. B. K. Kobilka, X. Deupi, *Trends Pharmacol. Sci.* **28**, 397 (2007).
10. E. C. McCusker, S. E. Bane, M. A. O'Malley, A. S. Robinson, *Biotechnol. Prog.* **23**, 540 (2007).
11. P. W. Day *et al.*, *Nat. Methods* **4**, 927 (2007).
12. E. M. Landau, J. P. Rosenbusch, *Proc. Natl. Acad. Sci. U.S.A.* **93**, 14532 (1996).
13. T. W. Schwartz, T. M. Frimurer, B. Holst, M. M. Rosenkilde, C. E. Elling, *Annu. Rev. Pharmacol. Toxicol.* **46**, 481 (2006).

10.1126/science.1151656

APPLIED PHYSICS

Filling the Terahertz Gap

A device made from a layered superconductor emits electromagnetic waves in a frequency range for which good radiation sources had been lacking.

Reinhold Kleiner

At almost every frequency, we have good methods to generate and detect electromagnetic radiation. One crucial exception is the low terahertz range, where despite intensive research there is a severe lack of devices such as oscillators and detectors. With better terahertz technology, researchers could develop new kinds of nondestructive imaging for materials testing and medical diagnosis, and carry out novel spectroscopic studies of materials and molecules. On page 1291 of this issue, Ozyuzer *et al.* (*1*) report an important step toward filling this "terahertz gap." The authors detected relatively strong continuous-wave terahertz radiation emitted by devices made from a cuprate superconductor. In the future, such structures may serve as useful micrometer-sized terahertz devices.

These devices, called Josephson junctions (formed by two superconducting electrodes separated by a thin nonsuperconducting barrier), generate current oscillations when a static voltage is applied between the electrodes. For example, Josephson tunnel junctions with niobium as the superconductor and aluminum oxide as the insulating barrier can generate radiation up to 600 GHz (*2*). In this case, vortices of magnetic flux moving along the junction excite internal resonances (cavity modes). Although the operation frequency can be tuned only moderately on such a resonance, there are many cavity modes, such that the device can be operated over a wide frequency range.

Josephson tunnel junctions based on conventional superconductors like niobium are restricted to sub-terahertz operation. In addition, the output power of a single Josephson junction is typically below 1 μW close to the device and well below 1 nW farther away. One way to increase the power is to use coherently oscillating junction arrays. Just as a laser has increased brightness from coherent oscillation, coherent Josephson arrays can emit much more powerful terahertz radiation. Such arrays have been intensively studied with both low-temperature and high-temperature superconductors (*3*); however, it turned out to be hard to synchronize a large number of junctions at high frequencies.

Recently, a different kind of device called the intrinsic Josephson junction (*4*, *5*) has offered solutions to limitations on power and frequency. Intrinsic Josephson junctions form naturally between the superconducting CuO_2 layers in cuprate materials such as $Bi_2Sr_2CaCu_2O_8$ (BSCCO), with the

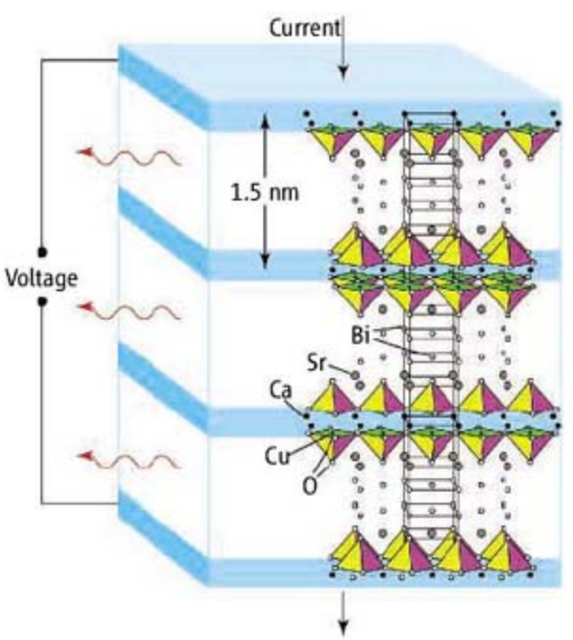

Working together. Sketch of intrinsic Josephson junctions in BSCCO. Blue layers indicate the superconducting sheets (CuO_2 layers), and transparent layers in between are the insulating barriers. The crystal structure is superimposed on the diagram. The junctions forming the stack can be individually switched between the zero voltage state and the resistive state where the Josephson current oscillates. In the experiments by Ozyuzer *et al.*, strong THz emission was found at voltages where hundreds of junctions were resistive.

The author is at the Physikalisches Institut, Universität Tübingen, D-72076 Tübingen, Germany. E-mail: kleiner@uni-tuebingen.de

BiO and SrO layers acting as the tunnel barrier. A single intrinsic Josephson junction in BSCCO has a thickness of 1.5 nm. A device of approximately 1 μm thickness consists of a stack of about 670 of these junctions. The figure shows a schematic diagram of the crystal structure superimposed on a drawing of the layered films.

As with conventional Josephson tunnel junctions operating within a particular current range, each intrinsic junction is bistable. That is, the junction can either carry a zero-resistance current at zero dc voltage or it can be in its resistive state, where the Josephson current oscillates, emitting terahertz radiation. At low temperatures with a BSCCO superconductor, the best intrinsic junctions may be capable of frequencies near 10 THz.

Having stacks of thousands of intrinsic junctions oscillating coherently offers fascinating possibilities. Ozyuzer *et al.* were able to obtain coherent oscillation of many junctions by a method similar to the way a laser works. The boundaries of the whole structure define an electromagnetic cavity that acts to synchronize all of the individual intrinsic junctions, just as light bouncing between the mirrors of laser synchronizes all the atoms to emit coherently. In contrast to all but the earliest previous experiments, Ozyuzer *et al.* used comparatively huge stacks having lateral dimensions in the 100-μm range.

Unfortunately, if too many junctions are in the resistive state at the same time, the stack may heat to temperatures above the superconducting transition, shutting down the Josephson oscillation. Ozyuzer *et al.* were able to control the heating problem so that in their measurements they could drive the whole 1-μm stack resistive. By comparison, most experiments within the past decade have used structures with smaller lateral dimensions of a few μm or less and thicknesses corresponding to only tens of intrinsic Josephson junctions. For such structures, the presence of the ac Josephson effect at THz frequencies has been confirmed with microwave irradiation up to 2.5 THz (*6*) and by measurement of microwave emission up to 0.5 THz (*7*). In the latter experiment, the emission was probably generated by a single intrinsic junction.

In earlier work, cavity modes at 0.5 to 1 THz have been excited in external magnetic fields by moving flux vortices (fluxons) (*8*). However, further analysis indicated that adjacent junctions oscillated out of phase instead of coherently. Cavity modes at zero magnetic field have been excited and imaged under microwave irradiation (*9*). There was indication for an in-phase oscillation, although the resonance frequency was below 0.3 THz. An arrangement of two stacks of nearby intrinsic junctions, one acting as a fluxon oscillator and one as the detector, was studied in (*10*). Electromagnetic emission was detected in the range between 0.7 and 1 THz, with an estimated maximum power of about 15 nW.

This list of experiments—which is far from complete—shows that that the ac Josephson effect at terahertz frequencies is present in intrinsic Josephson junction stacks. These experiments also showed how difficult it is to realize and then unambiguously identify high-frequency coherent emission. Ozyuzer *et al.* measured electromagnetic radiation without an applied magnetic field at frequencies up to 0.85 THz (by contrast, to excite cavity modes by moving fluxons one must apply a magnetic field in the tesla range and orient it with high accuracy parallel to the layer structure). Analyzing the polarization of the detected electromagnetic radiation allowed the authors to clearly distinguish Josephson radiation from thermal radiation, and driving the whole stack resistive excited the fundamental in-phase cavity mode. The authors estimate that up to 20 μW have been pumped into this resonance, which suggests the power level that might be achieved (the actual detected power was in the 0.5 μW range).

In their experiments, Ozyuzer *et al.* have produced coherent radiation in a range of sample sizes that was abandoned by most researchers in the field a long time ago. Of course, many questions remain open, such as whether different cavity modes can be excited (to increase the accessible frequency range and tunability of a given sample), what their stability might be, and the precise mechanism of excitation. The experiment by Ozyuzer *et al.* will clearly stimulate the field, and interesting results are sure to follow, possibly filling the terahertz gap.

References

1. L. Ozyuzer *et al.*, *Science* **318**, 1291 (2007).
2. V. P. Koshelets, S. V. Shitov, *Supercond. Sci. Technol.* **13**, R53 (2000).
3. M. Darula, T. Doderer, S. Beuven, *Supercond. Sci. Technol.* **12**, R1 (1999).
4. R. Kleiner, F. Steinmeyer, G. Kunkel, P. Müller, *Phys. Rev. Lett.* **68**, 2394, (1992).
5. A. Yurgens, *Supercond. Sci. Technol.* **13**, R85 (2000).
6. H. B. Wang, P. H. Wu, T. Yamashita, *Phys. Rev. Lett.* **87**, 107002 (2001).
7. I. Batov *et al.*, *Appl. Phys. Lett.* **88**, 262504 (2006).
8. H. B. Wang *et al.*, *Appl. Phys. Lett.* **89**, 252506 (2006).
9. T. Clauss, T. Ushida, M. Mößle, D. Koelle, R. Kleiner, *Appl. Phys. Lett.* **85**, 3166, (2004).
10. M. H. Bae, H.-J. Lee, J.-H. Choi, *Phys. Rev. Lett.* **98**, 027002 (2007).

10.1126/science.1151373

PHYSIOLOGY

Still Pondering an Age-Old Question

Thomas Flatt and Daniel E. L. Promislow

A theory of trade-offs to explain why we age has spurred 50 years of interdisciplinary research in evolution and molecular genetics.

Why do we age? Exactly 50 years ago, the visionary evolutionary biologist George C. Williams proposed the "antagonistic pleiotropy" theory of aging—aging evolves because natural selection favors genes that confer benefits early in life, even though those genes may prove detrimental to an organism later in life (*1*). In other words, aging evolves as an inevitable consequence of trade-offs. Williams's landmark 1957 paper offered a possible genetic explanation for why organisms experience a decline in physiological function with advancing age. His notion has inspired much of today's integrative aging research—a convergence of evolutionary, molecular, and genetic studies that has led to the discovery of numerous genes affecting aging. In light of the molecular and genetic insights that one could not possibly have known about 50 years ago, is antagonistic pleiotropy still a sufficient explanation for how aging has evolved?

Prior to Williams, evolutionary biologists had already established that the force of selection declines with age (*2*, *3*), which could explain why aging evolved. Consider a deleterious mutation, inherited through the germ line, which reduces the probability of survival in just one age class. If the effects of that mutation are confined to some late age, individuals carrying the mutation will likely have already passed it on to their offspring by the time it is expressed, and natural selection will be relatively ineffective in eliminating it. By contrast, a deleterious mutation that acts early in

T. Flatt is in the Department of Ecology and Evolutionary Biology, Brown University, Providence, RI 02912, USA. D. E. L. Promislow is in the Department of Genetics, University of Georgia, Athens, GA 30602–7223, USA. E-mail: thomas_flatt@brown.edu, promislow@uga.edu

life will quickly be eliminated by selection, because carriers will be less likely to survive and breed compared to those without the mutant gene. In 1952, Peter Medawar concluded that the accumulation of these late-acting deleterious genetic variants over time would lead to the evolution of aging (*3*).

Building on Medawar's "mutation accumulation" theory, Williams suggested that selection might actually favor deleterious mutations if they have beneficial pleiotropic effects early in life, when the force of selection is strong. Aging and its attendant symptoms, including cardiovascular disease, cancer, and diabetes, might thus be a maladaptive by-product of selection for genetic variants that aid development, reproduction, and survival during youth.

Fifty years later, how much empirical support is there for Williams's idea? Numerous evolutionary genetic studies have found that trade-offs indeed exist, and that the evolution of increased longevity comes at the cost of reduced fecundity (*4*–*7*). For example, fruit flies (*Drosophila melanogaster*) selected for late-life reproductive success are long-lived but lay relatively few eggs early in life, whereas flies bred for increased early reproduction evolve a shorter life span and reduced fecundity at old age (*4*, *5*). Remarkably, even in humans, reproduction might shorten life span (*8*).

Why we age. In 1957, George C. Williams offered a compelling argument for why we age: Negative effects on fitness late in life are outweighed by positive effects on fitness early in life.

The trade-offs that Williams envisaged are common, but are they caused by antagonistic pleiotropic genes, as he postulated? Over the past 20 years, and in a nod back to Williams, molecular biologists have begun to unravel the complex genetics of aging in yeast, worms, flies, and mice. Although several studies confirm Williams's prediction of trade-offs, only in a few cases can we point to specific genes that exhibit antagonistic pleiotropy (*9*, *10*). For example, among 16 insulin-like receptor (*daf-2*) mutant alleles in the nematode *Caenorhabditis elegans*, there is a striking negative correlation between fecundity and longevity (*11*). Likewise, fruit flies with mutated insulin receptors live longer but have reduced reproduction (*12*). Flies also live longer if the gene for a heat shock protein, *hsp70*, is transgenically overexpressed, but this reduces egg hatchability (*13*). However, for most mutations that increase life span, we know little about the fitness consequences (*9*, *10*).

So far, it seems that when we look carefully, Williams's prediction often holds true, but not always. Many molecular genetic studies have challenged the antagonistic pleiotropy theory. Numerous mutants in flies and worms appear to enjoy increased life span without paying any obvious costs in terms of early-life fitness (*9*). For example, certain mutants of the genes *age-1* and *daf-2* are long-lived, but have normal developmental rates, activity levels, and fertility (*11*, *14*). Moreover, impairing *daf-2* function only in adults increases life span without reducing reproduction, whereas the absence of *daf-2* in pre-adult stages increases life span but decreases fertility (*15*). Thus, because the effects of *daf-2* on reproduction and aging can be decoupled, this gene might affect both traits independently. These observations are clearly at odds with Williams's antagonistic pleiotropy theory—or are they?

Whereas long-lived mutants may appear to gain a free and long-lasting lunch under benign laboratory conditions, when these organisms come up against the cut-and-thrust of a competitive environment, the benefits of long life span are suddenly outweighed by early-age costs. When long-lived *age-1* mutants are nutritionally stressed, they have lower fitness than wild-type worms (*14*). Similarly, when long-lived *daf-2* mutants without apparent fitness costs are competed against wild-type animals, the mutants become extinct in four generations (*16*).

It is still too early to tell how many of the genes that affect aging exhibit the sort of pleiotropic effects predicted by Williams's theory. Population genetic models, quantitative genetic data, and evolutionary selection experiments clearly suggest that antagonistic pleiotropy might be pervasive (*4*–*7*, *10*). For the few genes and molecular pathways in which Williams's notion has been examined, the data are consistent with antagonistic pleiotropy (*5*, *10*). But not all genes affecting aging will necessarily exhibit this phenomenon. First, the strong, laboratory-induced mutations studied by molecular geneticists might not have the same properties as weaker genetic variants found in real-world populations subject to natural selection. Second, not all genes affecting aging are necessarily pleiotropic—life span can also be affected by mutations that have no effect early in life, but detrimental effects at advanced age, as suggested by Medawar (*3*, *5*, *7*).

Among scientists working on aging, Williams's and Medawar's ideas continue to inspire questions at many levels, from molecules to entire populations. Molecular biologists are trying to understand the mechanisms by which trade-offs work, and the physiological pathways that are central to these trade-offs. At the same time, evolutionary biologists are still asking whether variation within and among populations in the rates of aging is best accounted for by antagonistic pleiotropy or mutation accumulation. And at the broadest, phylogenetic level, we are still a long way from understanding why some species live for hundreds of years (tortoises), or even thousands (bristlecone pine), whereas others live for days or weeks. Perhaps our greatest challenge is to determine whether the genes that influence longevity in model organisms are evolutionary cousins of those that might have helped Jeanne Calment, the longest-lived human, to live to the age of 122 (*17*). Regardless of whether or not Williams's theory prevails for another 50 years, the notion of antagonistic pleiotropy has fueled a half-century of inquiry, and Williams's ideas continue to spark our curiosity.

References

1. G. C. Williams, *Evolution* **11**, 398 (1957).
2. R. A. Fisher, *The Genetical Theory of Natural Selection* (Clarendon, Oxford, UK, 1930).
3. P. Medawar, *An Unsolved Problem of Biology* (Lewis, London, 1952).
4. M. Rose, B. Charlesworth, *Nature*, **287**, 141 (1980).
5. S. C. Stearns, L. Partridge, in *Handbook of the Biology of Aging*, E. Masoro, S. Austad, Eds. (Academic Press, New York, 2001), pp. 353–368.
6. M. R. Rose, *Evolutionary Biology of Aging* (Oxford Univ. Press, New York, 1991).
7. B. Charlesworth, *Evolution in Age-Structured Populations* (Cambridge Univ. Press, Cambridge, UK, 1994).
8. R. G. J. Westendorp, T. B. L. Kirkwood, *Nature* **396**, 743 (1998).
9. L. Partridge, D. Gems, D. J. Withers, *Cell* **120**, 461 (2005).
10. A. M. Leroi *et al.*, *Mech. Ageing Dev.* **126**, 421 (2005).
11. D. Gems *et al.*, *Genetics* **50**, 129 (1998).
12. M. Tatar *et al.*, *Science* **292**, 107 (2001).
13. R. Silbermann, M. Tatar, *Evolution* **54**, 2038 (2000).
14. D. W. Walker, G. McColl, N. L. Jenkins, J. Harris, G. J. Lithgow, *Nature* **405**, 297 (2000).
15. A. Dillin, D. K. Crawford, C. Kenyon, *Science* **298**, 830 (2002).
16. N. L. Jenkins, G. McColl, G. J. Lithgow, *Proc. R. Soc. London Ser. B.* **271**, 2523 (2004).
17. J. J. McElwee *et al.*, *Genome Biol.* **8**, R132 (2007).

10.1126/science.1147491

Theory of Mind Is Independent of Episodic Memory

R. Shayna Rosenbaum,* Donald T. Stuss, Brian Levine, Endel Tulving

As humans, we are intrigued by who we are and how we differ from other creatures of evolution. Among the capacities thought to be uniquely human are autonoetic consciousness, the aspect of self-awareness that allows us to imagine our own experiences in different places at other times, and theory of mind (ToM), which allows us to infer other people's current mental states. The idea that ToM is closely related to, and that it may depend on, episodic memory and autonoetic consciousness seems perfectly natural: that in order to imagine and make sense of other people's thoughts, feelings, intentions, and actions, we must rely on our autobiographical recollections (*1*). The ability to consciously recollect past personal happenings has been shown to be necessary for imagining coherent and detailed personal happenings in the future (*2*, *3*). Both episodic memory and ToM emerge close in time in ontogenetic development (*4*). The neural substrate on which the two abilities rely is in many ways strikingly similar (*1*).

In order to test the hypothesis that ToM requires autonoetic consciousness, it is necessary to administer objective ToM tests to participants without autonoetic abilities. Such tests are available, but individuals without autonoetic consciousness are rare. Here, we describe the result of an investigation of the matter with the help of two such rare participants, K. C. and M. L., who, as a result of severe traumatic brain injury (fig. S1), lost their ability to consciously recollect personal happenings from their own lives (*5*, *6*). In both, this loss stands in stark contrast to their preserved ability to think of personal and public facts learned before they suffered brain damage (table S1). Casual observations, especially of K. C.'s clear appreciation of humor and sarcasm (*5*), suggest that ToM does not require autonoetic consciousness, but in the absence of more extensive, objective evidence the matter has remained unclear.

A variety of the most widely used tests known to be sensitive to perspective-taking and ToM impairment (*7*) was administered to assess systematically the extent to which K. C., M. L., and 14 control participants can reason about other people's thoughts and feelings (*8*). K. C.'s and M. L.'s performance was indistinguishable from that of controls on all measures (Table 1).

The current findings are at variance with the idea that the ability to simulate or reconstruct one's own past mental states is necessary to imagine the contents of other people's minds (*1*, *2*). Both K. C. and M. L. suffer from severe difficulties in consciously (autonoetically) recollecting any events from any period of their lives. Yet they have no apparent difficulty in taking other persons' perspectives and inferring other people's thoughts, feelings, and intentions, as revealed by the ToM tests. The findings imply that K. C.'s and M. L.'s ToM ability may depend on semantic memory and general knowledge abilities that are largely preserved in both cases (*5*, *6*).

Cases such as those of K. C. and M. L. allow for the study of ToM in isolation of autonoetic consciousness. Because these cases are rare, the relevant literature on the topic is sparse. The only other related piece of evidence of which we are aware is a report of a participant with a large medial prefrontal lesion who nonetheless performed well on several of the ToM tests used here. However, the extent to which his autobiographical memory impairment reflects a tendency to confabulate is unclear (*7*).

Our two cases do not shed any light on the extent to which fully functioning autonoetic ability is necessary for the development of ToM, because both K. C. and M. L. may have acquired ToM ability premorbidly. Our findings do, however, allow the conclusion that an existing severe impairment of episodic memory and autonoetic consciousness does not compromise the expression of ToM abilities. The dissociation we report here is important both theoretically and practically.

Table 1. Performance of all participants on theory of mind (ToM) tests (*8*). Numbers in parentheses in left-hand column indicate maximum scores for each section.

	K. C.	M. L.	Controls [mean (SD)]
False belief			
First-order (/10)	10	10	10 (0)
Second-order (/10)	10	10	8.79 (1.05)
Faux pas (/30)	29	29	23 (4.67)
Reading the mind in the eyes (/36)	26	31	26.07 (3.77)
Animations			
Random appropriateness (/3)	3	3	2.64 (0.46)
Random intentionality (/5)	0	0	0.48 (0.58)
Goal-directed appropriateness (/3)	3	2.75	2.36 (0.41)
Goal-directed intentionality (/5)	2.75	2.5	2.64 (0.29)
ToM appropriateness (/3)	3	2.5	2.2 (0.5)
ToM intentionality (/5)	4.5	4.5	3.66 (0.7)
Sarcasm and empathy			
First-order (/12)	12	11	11 (1.24)
Second-order (/12)	12	12	10.86 (0.95)
Visual perspective-taking/deception			
Transfer of inference (/6)	6	6	5.93 (0.27)
Deception (first trial of five consecutive correct)	7	6	6.5 (5.44)
Emotional situations			
Self (/8)	7	8	7.64 (0.5)
Other (/8)	8	8	7.93 (0.27)

References and Notes

1. R. L. Buckner, D. C. Carroll, *Trends Cogn. Sci.* **11**, 49 (2007).
2. D. Hassabis, E. A. Maguire, *Trends Cogn. Sci.* **11**, 299 (2007).
3. D. L. Schacter, D. R. Addis, *Nature* **445**, 27 (2007).
4. J. Perner, T. Ruffman, *J. Exp. Child Psychol.* **59**, 516 (1995).
5. R. S. Rosenbaum *et al.*, *Neuropsychologia* **43**, 989 (2005).
6. B. Levine *et al.*, *Brain* **121**, 1951 (1998).
7. C. M. Bird, F. Castelli, O. Malik, U. Frith, M. Husain, *Brain* **127**, 914 (2004).
8. Materials and methods are available on *Science* Online.

9. This research was supported by a Focus on Stroke Award from the Heart and Stroke Foundation (HSF) of Canada and the Canadian Institutes of Health Research and by grants from HSF of Ontario Centre for Stroke Recovery and Louis and Leah Posluns Centre for Stroke and Cognition at Baycrest. We thank R. Bloom, S. Gillingham, and L. Zackheim for technical assistance and F. Castelli and U. Frith for making available the animations test.

Supporting Online Material

www.sciencemag.org/cgi/content/full/318/5854/1257/DC1
Materials and Methods
Fig. S1
Table S1
References

3 August 2007; accepted 10 October 2007
10.1126/science.1148763

Department of Psychology, York University and Rotman Research Institute, Baycrest, Toronto, Ontario M3J 1P3, Canada.

*To whom correspondence should be addressed. E-mail: shaynar@yorku.ca

High-Resolution Crystal Structure of an Engineered Human β_2-Adrenergic G Protein–Coupled Receptor

Vadim Cherezov,[1]* Daniel M. Rosenbaum,[2]* Michael A. Hanson,[1] Søren G. F. Rasmussen,[2] Foon Sun Thian,[2] Tong Sun Kobilka,[2] Hee-Jung Choi,[2,3] Peter Kuhn,[4] William I. Weis,[2,3] Brian K. Kobilka,[2]† Raymond C. Stevens[1]†

AUTHORS' SUMMARY

The largest family of integral membrane proteins coded by the human genome comprises G protein–coupled receptors (GPCRs), with almost 1000 members (*1*, *2*). These receptors communicate signals across cell membranes in response to an astonishing variety of extracellular stimuli—light, proteins, peptides, small molecules, hormones, and ions. Once activated, GPCRs trigger a cascade of responses inside the cell, primarily through interactions with their G protein partners, three-subunit regulators that are switched on and off by binding guanosine triphosphate (GTP) (thus accounting for their name). In addition, these receptors have been found to activate other, G protein–independent, signaling pathways. Their combined effects yield an amazingly diverse network of signals that must be exquisitely coordinated to ensure proper cellular function (*3*, *4*).

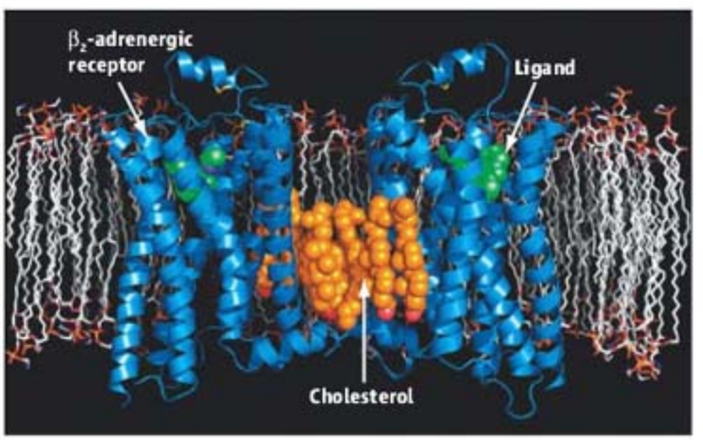

Structure of the human β_2-adrenergic receptor (blue) embedded in a lipid membrane and bound to a diffusible ligand (green), with cholesterol and palmitic acid (orange) between the two receptor molecules.

Although drugs that act on GPCRs command more than 50% of the current market for human therapeutics, with annual revenues in excess of $40 billion, these drugs interact with only a fraction of the available receptors. Because of the importance of this protein family, there is an ongoing search for new drugs that act on GPCRs and that combine potent efficacy with high specificity. Of particular interest are the class A adrenergic receptors that respond to the hormones adrenaline and noradrenaline. These are the targets of current cardiac and asthma drugs that often have undesirable side effects. In addition, improved asthma drugs are needed in developing countries where the population and pollution levels are rapidly rising, along with the incidence of asthma. Structures of GPCRs can guide the development of more specific drugs and can be combined with traditional chemical screening methods to improve and accelerate drug discovery.

For protein structures to effectively guide drug design, it is critically important to maximize the available detail, as low-resolution structures can be ambiguous at best and misleading at worst. However, it remains a formidable challenge to obtain high-resolution structural data for membrane proteins. To accomplish this, we engineered the β_2-adrenergic receptor to include lysozyme in place of one of the intracellular loops, which reduced conformational heterogeneity and facilitated crystal nucleation [see (*5*)]. Crystals were grown in a cholesterol-doped lipidic cubic phase that stabilized the receptor in a more natural membrane-like environment. We used a robot to set up more than 15,000 trials to optimize crystal growth in the extremely viscous lipidic cubic mesophase. We then evaluated the micrometer-size transparent crystals with a 10-μm x-ray beam. Our resulting 2.4 Å crystal structure of the human β_2-adrenergic receptor successfully provides high-resolution detail.

The crystal structure of this important human membrane receptor reveals the details of its interactions with a diffusible ligand (the partial inverse agonist carazolol). In examining the structure, one can begin to appreciate the amazing structural plasticity of the GPCRs and how this allows them to recognize such a wide range of ligands critical for function within the human body. The ligand-binding site of the β_2-adrenergic receptor is located in a position similar to that of the covalently bound ligand of rhodopsin, the light-absorbing, G protein–coupled receptor responsible for human vision. Key differences from rhodopsin are also observed, particularly in several of the kinked transmembrane helices and in the second extracellular loop, which in the β_2-adrenergic receptor contains an unusual pair of disulfide bonds and an extra helix. This loop and the absence of structure in the N-terminal region of the receptor may be important for ligand binding.

Although this structure of a GPCR that recognizes a diffusible ligand furthers understanding of signal transduction and should facilitate the design of new drugs with fewer side effects, the structure alone cannot fully explain how ligand binding on the outside surface of a cell triggers internal signaling pathways. This will require characterization of how the receptor changes its conformation as it is activated. Follow-up structures or receptors bound to other ligands will be required to understand the different conformational states and how they transduce signals. It is possible that the active state will only be understood when a structure is obtained for a GPCR–G protein signaling complex with an agonist bound to the receptor. In addition, structural and complementary biophysical techniques (e.g., nuclear magnetic resonance) will help to resolve other key biological questions, including the effects of homodimerization or heterodimerization of the receptor, the nature of class B and C GPCR structures, and elucidation of cholesterol's role in GPCR function.

Summary References

1. S. Takeda, S. Kadowaki, T. Haga, H. Takaesu, S. Mitaku, *FEBS Lett.* **520**, 97 (2002).
2. R. Fredriksson, M. C. Lagerstrom, L. G. Lundin, H. B. Schioth, *Mol. Pharmacol.* **63**, 1256 (2003).
3. K. L. Pierce, R. T. Premont, R. J. Lefkowitz, *Nat. Rev. Mol. Cell Biol.* **3**, 639 (2002).
4. R. J. Lefkowitz, S. K. Shenoy, *Science* **308**, 512 (2005).
5. D. M. Rosenbaum *et al.*, *Science* **318**, 1266 (2007); published online 25 October 2007 (10.1126/science.1150609).

FULL-LENGTH ARTICLE

Heterotrimeric guanine nucleotide–binding protein (G protein)–coupled receptors constitute the largest family of eukaryotic signal transduction proteins that communicate across the membrane. We report the crystal structure of a human β_2-adrenergic receptor–T4 lysozyme fusion protein bound to the partial inverse agonist carazolol at 2.4 angstrom resolution. The structure provides a high-resolution view of a human G protein–coupled receptor bound to a diffusible ligand. Ligand-binding site accessibility is enabled by the second extracellular loop, which is held out of the binding cavity by a pair of closely spaced disulfide bridges and a short helical segment within the loop. Cholesterol, a necessary component for crystallization, mediates an intriguing parallel association of receptor molecules in the crystal lattice. Although the location of carazolol in the β_2-adrenergic receptor is very similar to that of retinal in rhodopsin, structural differences in the ligand-binding site and other regions highlight the challenges in using rhodopsin as a template model for this large receptor family.

G protein–coupled receptors (GPCRs) constitute the largest integral membrane protein family in the human genome, with almost 1000 members (*1*, *2*). GPCRs are major contributors to the information flow into cells and, as such, are associated with a multitude of diseases that make members of this family important pharmacological targets (*3*–*6*).

GPCRs have been grouped into five classes (*2*) on the basis of sequence conservation, with class A being the largest and most studied. Class A receptors are further divided into groups associated with particular ligand specificity, such as the opsin, amine, peptide, cannabinoid, and olfactory receptors. The adrenergic receptors in the amine group are among the most thoroughly investigated class A GPCRs (*7*–*12*) and consist of two main subfamilies, α and β, which differ in tissue localization and ligand specificity as well as in G protein coupling and downstream effector mechanisms (*13*). Genetic modifications of adrenergic receptors are associated with diseases as diverse as asthma, hypertension, and heart failure (*14*). β_2-Adrenergic receptors (β_2ARs) reside predominantly in smooth muscle throughout the body, and β_2AR agonists are used in the treatment of asthma and preterm labor (*15*–*17*).

Despite extensive efforts, structural information for only one member of the eukaryotic GPCR family, bovine rhodopsin, is available to date (*18*–*21*). Rhodopsin is unusual in that it is highly abundant from natural sources and is structurally stabilized by the covalently bound ligand 11-*cis*-retinal, which maintains the receptor in a dark-adapted, nonsignaling conformation. In contrast, all other GPCRs are activated by diffusible ligands and are expressed at relatively low levels in native tissues. These receptors are structurally more flexible and equilibrate among multiple conformational states, some of which are prone to instability (*22*). Although the structure determination of rhodopsin was important, many questions remain concerning the conformational changes between different activation states for each receptor, as well as the structural differences among receptors that accommodate the very large diversity of ligands. What structural features enable GPCRs to recognize and bind diffusible ligands? How structurally conserved are the class A GPCRs, and what is the importance of their similarities and differences?

To address these questions, we modified the human β_2AR to facilitate the growth of diffraction-quality crystals by inserting T4 lysozyme (T4L) in place of the third intracellular loop (β_2AR-T4L) and solved the three-dimensional crystal structure in the presence of a partial inverse agonist, carazolol (2-propanol, 1-9*H*-carbazol-4-yloxy)-3-[(1-methylethyl)amino]) at 2.4 Å resolution (*23*, *24*). We provide a comprehensive analysis of the crystal packing and intramolecular contacts between the β_2AR and

Table 1. Data collection and refinement statistics.

	β_2AR-T4L
*Data collection (APS GM/CA CAT 23ID-B, 10-μm beam)**	
Space group	*C*2
Cell dimensions	
a, *b*, *c* (Å)	106.3, 169.2, 40.2
β (°)	105.62
Number of reflections processed	245,571
Number of unique reflections	26,574
Resolution (Å)	50 to 2.4 (2.5 to 2.4)
R_{sym}†	12.7 (67.8)
Mean $I/\sigma(I)$	9.6 (2.2)
Completeness (%)	99.5 (99.1)
Redundancy	9.4 (4.8)
*Refinement**	
Resolution (Å)	20 to 2.4 (2.46 to 2.4)
Number of reflections (test set)	25,247 (1310)
R_{work} / R_{free}	19.8 (27.0) / 23.2 (30.1)
Number of atoms	3805
Protein	3544
Ions, lipids, ligand, and other	213
Water	48
Overall *B* values (Å^2)	82
β_2AR	77
T4 lysozyme	75
Carazolol	55
Lipid	100
RMSD	
Bond lengths (Å)	0.013
Bond angles (°)	1.5
Ramachandran plot statistics (%) (excluding Gly, Pro):	
Most favored regions	94.8
Additionally allowed regions	5.0
Generously allowed regions	0.2
Disallowed regions	0

*Highest-resolution shell is shown in parentheses. †$R_{sym} = \Sigma_{hkl}\ I(hkl) - \langle I(hkl)\rangle / \Sigma_{hkl} I(hkl)$, where $\langle I(hkl)\rangle$ is the mean of the symmetry-equivalent reflections of $I(hkl)$.

[1]Department of Molecular Biology, Scripps Research Institute, La Jolla, CA 92037, USA. [2]Department of Molecular and Cellular Physiology, Stanford University School of Medicine, Stanford, CA 94305, USA. [3]Department of Structural Biology, Stanford University School of Medicine, Stanford, CA 94305, USA. [4]Department of Cell Biology, Scripps Research Institute, La Jolla, CA 92037, USA.

*These authors contributed equally to this work.
†To whom correspondence should be addressed. E-mail: stevens@scripps.edu (R.C.S.); kobilka@stanford.edu (B.K.K.)

T4L to identify potential receptor-perturbing interactions. The overall receptor topology and the ligand-binding pocket are described, as are the main similarities and differences between β_2AR-T4L and rhodopsin.

Structure determination. The engineering, functional properties, expression, and purification of crystallization-grade β_2AR-T4L protein are described fully in the companion paper (*24*, *25*). Briefly, β_2AR-T4L was expressed in Sf9 insect cells, solubilized in 1% dodecylmaltoside, and purified by sequential antibody and ligand affinity chromatography. Following the reported success with microbial rhodopsins in lipidic cubic phase (LCP) (*26*), we were able to produce crystals of β_2AR-T4L that diffracted to a resolution of 2.2 Å with a modified LCP procedure, and we solved and refined the structure at 2.4 Å resolution (*27*). Relative to crystallization in detergents, LCP provides a more native, lipid environment for crystallization, as well as a confinement of protein molecules to two-dimensional membrane sheets that may facilitate the crystallization process through the formation of type I packing interactions (*28*–*30*). In agreement with prior biological evidence that cholesterol improves β_2AR stability (*31*) and may mediate receptor-receptor interactions, crystals were grown from a cholesterol-doped monoolein cubic phase. An automated, nanovolume LCP crystallization protocol (*32*) substantially reduced the time and amount of protein required for the exhaustive, multidimensional optimization trials needed to arrive at these conditions. Crystals of β_2AR-T4L were also obtained in lipid bicelles, but they did not diffract as well as those obtained in LCP (*27*).

Diffraction data for β_2AR-T4L were measured to a resolution of 2.4 Å from a total of 27 microcrystals (average size 30 μm by 15 μm by 5 μm) using a high-intensity, highly parallel minibeam with a diameter of 10 μm at the GM/CA-CAT beamline of the Advanced Photon Source, Argonne National Laboratory (*33*). Phase information was obtained by molecular replacement using both T4L (PDB ID code 2LZM) and a polyalanine model of the transmembrane regions of rhodopsin (PDB ID code 1U19) as search models. Additional crystallization, data collection, processing, and refinement statistics are reported in Table 1 and discussed in (*27*).

Overall receptor topology. The final model of β_2AR-T4L includes 442 amino acids. The model also includes a palmitic acid covalently bound to Cys^{341} and an acetamide molecule bound to $Cys265^{6.27}$ (residues are designated by their position within the β_2AR sequence; where applicable, their Ballesteros-Weinstein designations appear as superscripts) (*34*, *35*), as well as one carazolol molecule, three cholesterol molecules, two sulfate ions, and two butanediol molecules that interact with β_2AR. There are also four sulfate ions, a putative disaccharide (modeled as maltose), and a molecule of polyethylene glycol 400 bound to T4L. For β_2AR, excellent electron density was observed for residues 29 to 342, including the ligand carazolol and the two disulfide bonds $Cys106^{3.25}$-$Cys191^{5.30}$ and $Cys184^{4.76}$-$Cys190^{5.29}$. The palmitic acid at Cys^{341} was clearly visible in $F_{obs} - F_{calc}$ omit maps; however, the quality of the electron density was lower than for the rest of the receptor. The N terminus (residues 1 to 28) and the majority of the C terminus (residues 343 to 365) were disordered and not visible in the structure.

The β_2AR has a fold composed of seven transmembrane helices forming a helical bundle (Fig. 1A). The residues that make up the helices (I to VII) in β_2AR are as follows: helix I, positions $29^{1.28}$ to $60^{1.59}$; helix II, positions $67^{2.38}$ to $96^{2.67}$; helix III, positions $103^{3.22}$ to $136^{3.55}$; helix IV, positions $147^{4.39}$ to $171^{4.63}$; helix V, positions $197^{5.36}$ to $229^{5.68}$; helix VI, positions $267^{6.29}$ to $298^{6.60}$; and helix VII, positions $305^{7.32}$ to $328^{7.55}$. The residues forming the intracellular loops (ICLs) and extracellular loops (ECLs) of β_2AR are as follows: ICL1, positions $61^{1.60}$ to $66^{2.37}$; ECL1, positions $97^{2.68}$ to $102^{3.21}$; ICL2, positions $137^{3.56}$ to $146^{4.38}$; ECL2, positions

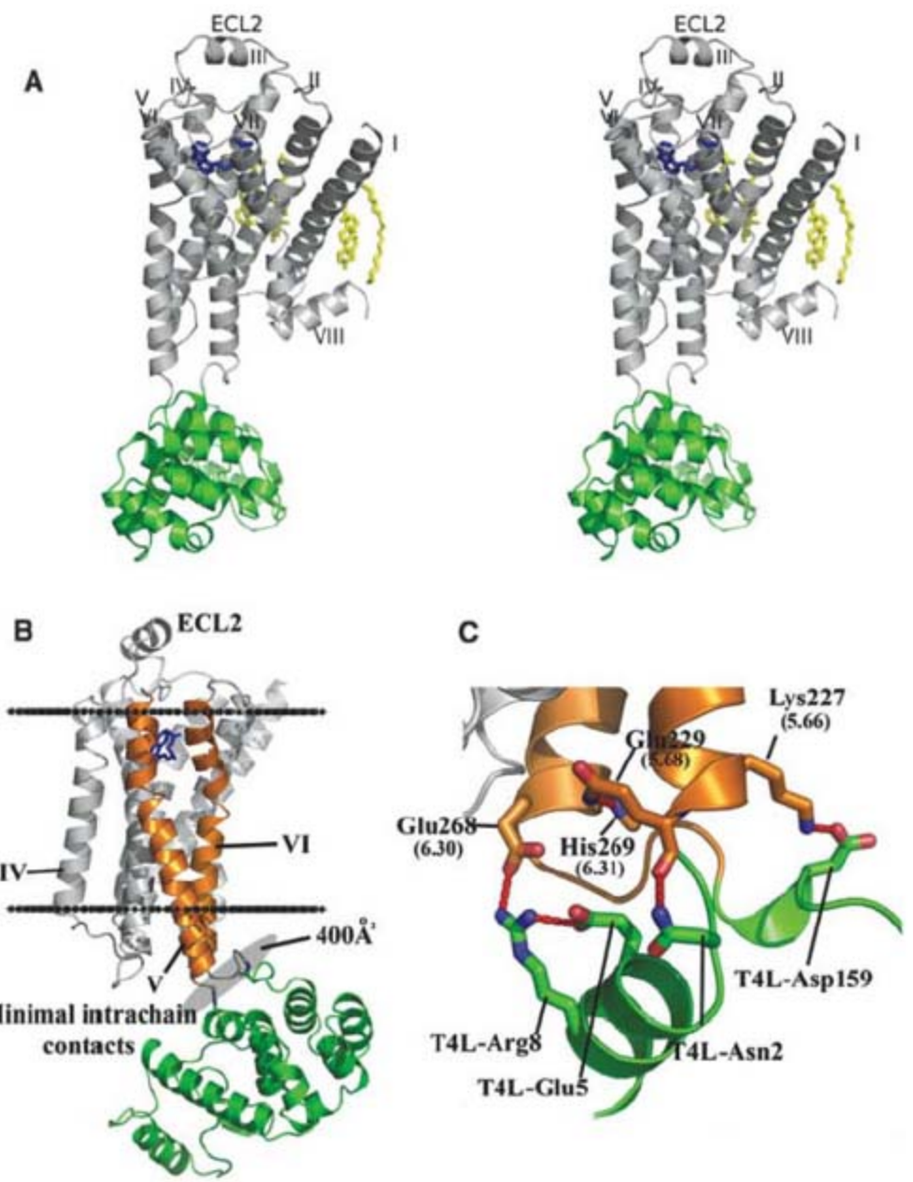

Fig. 1. Overall fold of the β_2AR-T4L fusion with its predicted orientation in the plasma membrane and key intramolecular interactions. **(A)** Stereoview of the overall fold of β_2AR-T4L. The receptor and T4L are colored gray and green, respectively. Carazolol is shown in blue; the lipid molecules bound to the receptor are in yellow. **(B)** The receptor is aligned to a rhodopsin model that was positioned in a lipid membrane (boundaries indicated by horizontal black lines) as found in the Orientations of Proteins in Membranes database (*74*). T4L is fused internally into the third intracellular loop of β_2AR and maintains minimal intramolecular packing interactions by tilting away from the receptor. **(C)** Specific intramolecular interactions between β_2AR and T4L.

$172^{4.64}$ to $196^{5.35}$; ICL3, positions $230^{5.69}$ to $266^{6.28}$ (residues 231 to 262 are replaced by T4L residues 2 to 161); and ECL3, positions $299^{6.61}$ to $304^{7.31}$. Helices II, V, VI, and VII each have a proline-induced kink at conserved positions along the span of the transmembrane segments. These kinks are thought to enable the structural rearrangements required for activation of G protein effectors (*36*). In addition to the seven membrane-spanning helices, β_2AR has two other helical segments: helix VIII, which is believed to be common to all rhodopsin-like GPCRs (*37*), and an unexpected, short helical segment in the middle of ECL2, which is not present in rhodopsin and was not predicted by computational secondary structure analysis (Fig. 1A).

In the β_2AR-T4L construct, T4L is fused to the truncated cytoplasmic ends of helices V and VI. In the crystal structure, the T4L moiety is tilted slightly away from the center axis of β_2AR drawn normal to the membrane (Fig. 1B). As a result, interactions between T4L and β_2AR are minimal, with only 400 $Å^2$ of surface area buried between them. The intramolecular contacts between T4L and β_2AR include salt bridges between the side chains of T4L-Asp^{159} and the side-chain amine of β_2AR-$Lys227^{5.66}$ (distance 3.4 Å) and between the guanidinium group of T4L-Arg^{8} and the side-chain carboxyl of β_2AR-$Glu268^{6.30}$ on helix VI (distance 3.2 Å) (Fig. 1C and table S2). The latter interaction is noteworthy, because in rhodopsin $Glu^{6.30}$ forms an ionic bond with $Arg^{3.50}$ of the conserved Asp-(Glu)-Arg-Tyr motif (*18*). This interaction is postulated to be important for maintaining rhodopsin in the inactive state, but the charged groups of the two residues [$Arg131^{3.50}$ (NH1) and $Glu268^{6.30}$ (OE1)] are 10 Å apart in the β_2AR-T4L structure. Possible functional implications of this disruption are discussed in (*24*). The remainder of the lysozyme molecule provides important crystal-packing interactions but does not appear to influence the receptor structure.

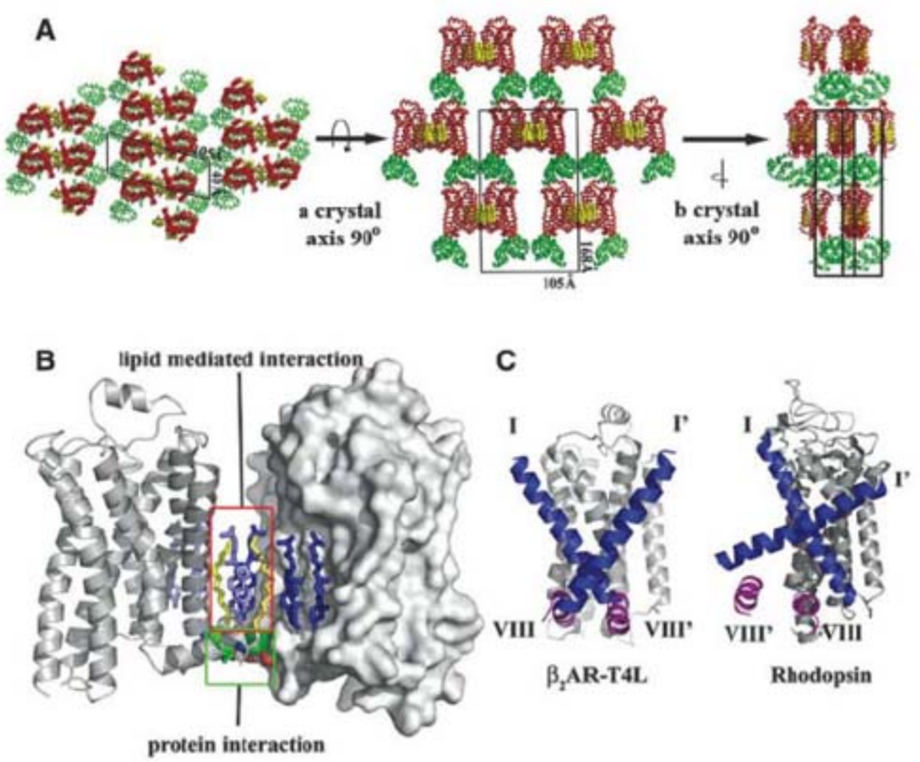

Fig. 2. Crystal-packing interactions in the lipidic mesophase–crystallized β_2AR-T4L. (**A**) There are four main contact areas, two of which are mediated by T4L in the plane of the membrane with itself through a two-fold symmetry axis and translation. The third interaction is normal to the membrane plane between T4L and lumen-exposed loops of β_2AR. The fourth interaction is generated by the two-fold symmetry axis, packing one receptor to another in the plane of the membrane. (**B**) The receptor crystal-packing interface is composed mainly of lipids, with two cholesterol molecules and two palmitic acid molecules forming the majority of the interactions. A network of ionic charge interactions exists on the cytoplasmic end of the interface, forming the only interreceptor protein contacts. (**C**) Comparison between β_2AR-T4L and rhodopsin (PDB ID code 2I35) parallel receptor association interface. Helices I (blue) and VIII (magenta) are highlighted in both structures. Only one monomer is shown for each receptor representation, along with helices I′ and VIII′ only from the opposing symmetry-related molecule. The rhodopsin interface is twisted relative to β_2AR-T4L, resulting in a substantial offset from the parallel orientation required for a physiological dimer interface. β_2AR-T4L–associated monomers are in a highly parallel orientation.

Crystal-packing interactions. The β_2AR-T4L protein is packed in a C-centered monoclinic lattice with one molecule per asymmetric unit (Fig. 2A). As observed in all previous lipidic mesophase–grown crystals (*38*), the β_2AR-T4L crystals adopt type I packing (*39*), featuring a multilayered arrangement in accordance with a proposed crystallization mechanism (*28*, *40*). Within each layer, protein molecules form arrays of parallel, symmetry-related dimers. There are four distinct crystal-packing interactions within each layer, three of which are mediated by T4L. The fourth interaction in the array is between two receptor molecules related by a crystallographic two-fold rotation axis. This is the sole interaction between symmetry-related receptors and is mediated primarily by ordered lipids consisting of six cholesterol and two palmitic acid molecules, the latter being covalently attached to Cys^{341} in the C-terminal portion of the receptor (*41*) (Fig. 2B). These eight lipid molecules form a two-fold symmetric sheet between receptors. The only direct receptor-receptor contact involves a 2.7 Å pair of ionic interactions between the charged amine group of $Lys60^{1.59}$ in helix I and the carboxylate of Glu^{338} in helix VIII from the symmetry-related receptor. Remarkably, of the 515 $Å^2$ buried at the receptor symmetry interface, 73% of the crystal contact surface area is mediated by ordered lipid, whereas only 27% is contributed by protein-protein contacts. The stacking interactions between layers are formed between T4L and extracellular loops ECL2 and ECL3 of the receptor (Fig. 2A). Because of the small size of ECL3 and the rigid architecture of ECL2, it is unlikely that these contacts affect the orientation of these loops.

Lipid-mediated receptor association. Many GPCRs including β_2AR are thought to exist as dimers in the plasma membrane, although the location of the dimer interface and the functional importance of dimerization are not clear (*42*). The observation of ordered lipids in the helix I–helix VIII interface between two symmetry-related molecules makes it tempting to speculate on the physiological relevance of this association (*43*–*45*). Associations between the equivalent regions of rhodopsin have been found in crystal structures (*21*, *46*) (Fig. 2C). On the other hand, studies in native membranes suggest that helix VI may form the dimer interface for the β_2AR (*47*), and helix IV may form the dimer interface for the closely related D_2 dopamine receptor (*48*).

Although the role of cholesterol in promoting β_2AR association is speculative, its role in the physiologic function of β_2AR is well documented. Depletion of cholesterol from the membranes of neonatal cardiac myocytes alters the signaling behavior of endogenous β_2AR (*49*). In untreated cells, activation of β_2AR results in sequential coupling to the G

proteins G_s and G_i, producing a biphasic effect on myocyte contraction rate. Upon depletion of cholesterol, the β_2AR couples more strongly to G_s. This effect may be due to a role of cholesterol in regulating interactions between the β_2AR and G proteins, or possibly to the effect of cholesterol on β_2AR dimerization. The β_2AR couples efficiently to G_s as a monomer (*50*), so it is possible that cholesterol-mediated association (dimerization) reduces the efficiency of β_2AR coupling to G_s. The effects of cholesterol depletion on β_2AR signaling may also be a secondary effect of altering subcellular signaling compartments. There is evidence that cells may concentrate signaling molecules, such as GPCRs and their cognate G proteins, by way of membrane microdomains or compartments such as caveolae (*51*). This compartmentalization may be a major regulator of receptor-effector coupling. Thus, the importance of cholesterol in forming the observed crystallographic association is consistent with its role in β_2AR signaling. Additional experiments will be required to determine whether the association of monomers observed in the crystal is relevant to β_2AR packing within membrane microdomains.

Electrostatic charge distribution. Electrostatic charge distribution was calculated using the program APBS (*52*) and mapped onto a molecular surface representation of β_2AR. The analysis reveals three polarized areas within the molecule (Fig. 3A). First, the cytoplasmic face of the receptor is involved in G protein interaction and carries a net positive charge even in the absence of ICL3, which also has a predicted overall positive charge (Fig. 3B). The second site is an electrostatically negative region located within the membrane between helices III, IV, and V potentially exposed to the lipid alkyl chains, which is unexpected because the burial of charge within the plasma membrane is thermodynamically unfavorable. A Glu residue at position $122^{3.41}$ may partially account for the observed charge distribution. Finally, the binding-site cleft is negatively charged and exposed to solvent by an unusual ECL2 architecture and a lack of N-terminal interactions. This negative charge may facilitate ligand binding through electrostatic funneling of positively charged catecholamines (Fig. 3B).

Extracellular region. The ECLs and N termini of GPCRs, together with the extracellular halves of the transmembrane helices, are believed to define the ligand-binding site of each receptor (*43*). Therefore, the ECLs may play an important role in the overall pharmacology of any particular receptor. In general, small-molecule ligands are thought to bind deeper within the space created by the transmembrane domain helices, whereas larger ligands such as peptides bind closer to the membrane surface near the ECLs (*53*, *54*). Mutagenesis studies suggest that the β_2AR binds its ligand deep within the transmembrane helix bundle, which may be related to the observation that the extracellular regions have a rather simple structure with short loops connecting transmembrane helices II and III with helices VI and VII (Fig. 4A). ECL2, which links helices IV and V, has a somewhat more extensive architecture that is unanticipated. In contrast to the buried β-sheet structure of this loop in rhodopsin (Fig. 4B), ECL2 in β_2AR is more exposed to the solvent and contains an extra helical segment. Additional-

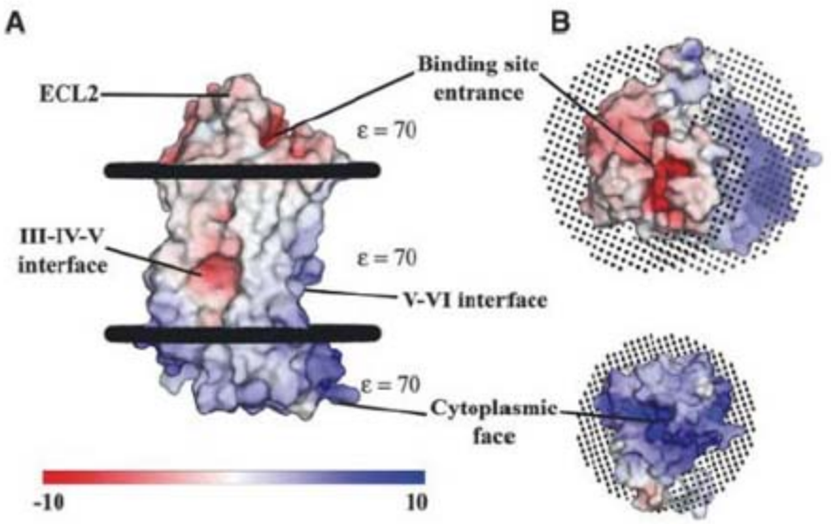

Fig. 3. Surface representation of β_2AR colored by calculated charge from red (−10 k_bT/e_c) to blue (+10 k_bT/e_c) using a dielectric constant of 70. (**A**) Three main areas of interest are indicated. The binding-site cleft is negatively charged, as is a groove between helices III, IV, and V. The third region is an overall positive charge in the region of the ionic lock and Asp-Arg-Tyr motif on the cytoplasmic face. The overall result is a highly polarized molecule that may use its negative charge to facilitate binding of catecholamine ligands. The presence of a negative charge in the groove between helices III, IV, and V is unexpected, as it is in the middle of the lipid membrane. This charge may be partially derived from the presence of an unpaired glutamate at position $122^{3.41}$. The effective charge in this region is likely greater than shown here because of its location in the low-dielectric environment of the lipid membrane. (**B**) View rotated 90° from (A), showing the negatively charged binding-site cleft (top) and the positively charged cytoplasmic face (bottom). Poisson-Boltzmann electrostatics were calculated using APBS (*52*) as implemented in PyMOL (*75*). PyMOL was used exclusively in the preparation of all figures.

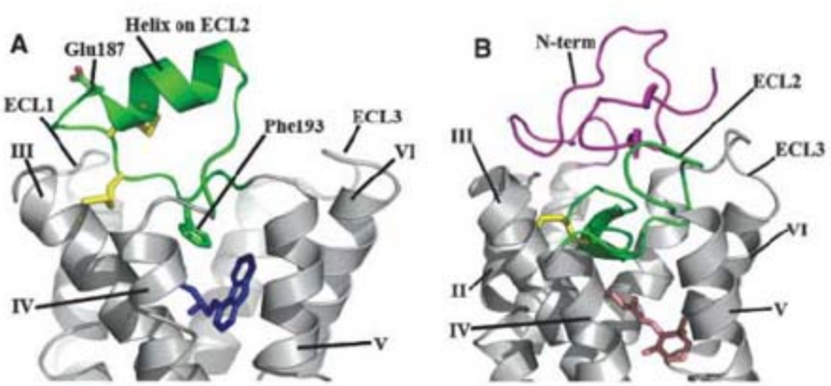

Fig. 4. Comparison of the extracellular sides of β_2AR-T4L and rhodopsin. (**A**) The N terminus is missing from the experimental density in the β_2AR-T4L structure and is not shown. ECL2 is shown in green and contains a short α helix and two disulfide bonds (yellow). The intraloop disulfide bond constrains the tip of ECL2, which interacts with ECL1. The second disulfide bond links ECL2 with helix III. There is one interaction between ECL2 and carazolol (blue) through $Phe193^{5.32}$. The entire loop is held out of the ligand-binding site by a combination of the rigid helical segment and the two disulfide bonds. (**B**) In contrast, ECL2 (green) in rhodopsin assumes a lower position in the structure that occludes direct access to the retinal-binding site and forms a small β sheet in combination with the N-terminal region (magenta) directly above the bound retinal (pink).

ly, there is an intraloop disulfide bond between Cys184$^{4.76}$ and Cys190$^{5.29}$ that may help stabilize the more exposed ECL2. A second disulfide bond between Cys191$^{5.30}$ and Cys106$^{3.25}$ in helix III effectively ties ECL2 to the transmembrane core (*55*). The distal portion of ECL2 makes close contacts with ECL1 and contains a glycosylation site at Asn187$^{5.26}$ (*56*), which may serve to mask a grouping of aromatic residues on ECL1; in this construct, Asn187$^{5.26}$ has been mutated to Glu to aid in crystallization.

Electron density corresponding to the N terminus was not apparent in the maps, and therefore residues 1 to 28 are not included in the model. This disorder contrasts with rhodopsin, in which the N terminus interacts extensively with the ECLs, forming a small four-strand β sheet in conjunction with ECL2. This sheet structure forms a cap that effectively isolates the retinal-binding site in a hydrophobic pocket (Fig. 4B). The lack of interactions between the N terminus of β_2AR and ECL2 further enables diffusible ligand access to the binding site. However, a completely disordered N terminus may be an artifact induced by the presence of the N-terminal Flag tag, which carries an overall positive charge and may disrupt N-terminal interactions.

The short helical region on ECL2 adds a rigid structural element that, along with the two disulfide bonds, constrains the loop to a small range of conformations and helps stabilize the receptor by linking three transmembrane helices (Fig. 4A). This rigid conformation may help to stabilize the core of the receptor and lock ECL2 in a conformation that does not hinder access to the binding pocket.

Ligand-binding site and comparison to rhodopsin. Carazolol is a partial inverse agonist that binds with picomolar affinity to β_2AR-T4L, producing a reduction of the basal activity of the receptor (*57*). The crystal structure reveals extensive interactions between the receptor and carazolol that position the carbazole moiety adjacent to Phe289$^{6.51}$, Phe290$^{6.52}$, and Trp286$^{6.48}$ (Fig. 5A, fig. S1, and table S3). In contrast, 11-*cis*-retinal is a full inverse agonist covalently bound to rhodopsin, which suppresses all activity toward transducin (*58*). Carazolol and retinal occupy similar spaces in their respective receptors, with substantial overlap of the nonaromatic regions of carazolol. However, the β-ionone ring of retinal extends deep into the binding pocket of rhodopsin and contacts residues on helices V and VI, where it is sandwiched between Phe212$^{5.47}$ and Tyr268$^{6.51}$ and interacts with the highly conserved Trp265$^{6.48}$ (Fig. 5B). It has been proposed that changes in the rotamer of Trp265$^{6.48}$ occur upon activation of rhodopsin and related family members, and that these changes constitute the "toggle switch" for receptor activation (*59*). Accordingly, the interactions between 11-*cis*-retinal and Trp265$^{6.48}$ are likely to contribute to the absence of basal activity in rhodopsin. Carazolol does not interact directly with the toggle switch on helix VI; however, it lowers the basal activity of the receptor, and may do so by interacting with Phe289$^{6.51}$ and Phe290$^{6.52}$, which form an extended aromatic network surrounding the highly conserved Trp286$^{6.48}$. As a result, Trp286$^{6.48}$ adopts the rotamer associated with the inactive state. Thus, the steric constraints imposed by Phe290$^{6.52}$ appear to structurally mimic the interaction of the β-ionone ring of retinal with the conserved Trp286$^{6.48}$ and Phe212$^{5.47}$ on rhodopsin (*60*) (Fig. 5C).

Structural alignment and helix bundle reorganization. It has long been thought that class A GPCRs share a similar architecture as a result of their predicted seven-transmembrane helical bundles and sequence conservation within the membrane-spanning regions (*61*). To learn more about the structural similarities and differences in class A GPCRs, we aligned the structure of β_2AR-T4L to highest-resolution structure of rhodopsin (PDB ID code 1U19). We used difference distance matrices to select nondivergent areas between the two structures that align to reveal the differences in helix orientation between β_2AR-T4L and rhodopsin (*62*).

Relative to rhodopsin, the following helical shifts are seen in β_2AR-T4L: The extracellular portions of helices I and III angle away from the center of the receptor, helix IV is translated away from the center of the receptor, helix V is translated closer to the center of the receptor, and helix VI angles away from the receptor on the cytoplasmic end (Fig. 6). The largest difference is in helix I, which lacks a proline-induced kink found in rhodopsin and is comparatively straight. The angle between the rhodopsin and β_2AR positions of helix I is about 18° with a shift of 7 Å at the apex on the extracellular face. This structural difference may arise from the need for an accessible binding site in β_2AR, which is provided in part by a lack of interactions between the N terminus and extracellular loop segments. In contrast, the N-terminal

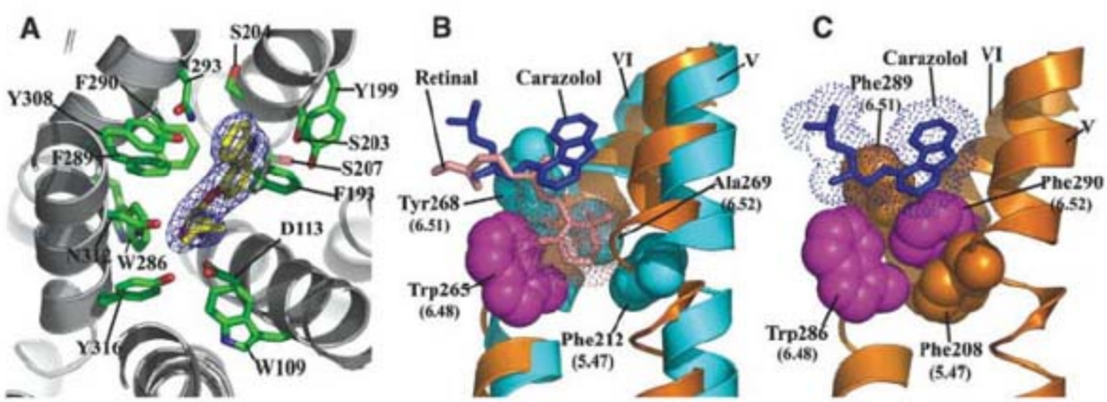

Fig. 5. Ligand-binding characterization and comparison to rhodopsin. **(A)** View looking down on the plane of the membrane from the extracellular surface, showing a detailed representation of the carazolol-binding site in β_2AR-T4L. Carazolol is shown as sticks with carbon atoms colored yellow. β_2AR-T4L residues contributing to carazolol binding are shown in green and labeled. Electron density is contoured at 5σ from an $F_{obs} - F_{calc}$ omit map calculated without the contribution of carazolol. Abbreviations: D, Asp; F, Phe; N, Asn; S, Ser; W, Trp; Y, Tyr. **(B)** Binding orientation comparison between 11-*cis*-retinal in rhodopsin and carazolol in β_2AR-T4L. Van der Waals surfaces for carazolol and retinal are represented as dots to accentuate the close-packing interactions. Retinal in the 11-cis conformation (pink) binds deep in the active site of rhodopsin as compared to carazolol (blue), packing its β-ionone ring between Tyr268$^{6.51}$ and Phe212$^{5.47}$ (cyan) and blocking movement of Trp265$^{6.48}$ (magenta) into the space. The β-ionone ring of all-*trans*-retinal in activated rhodopsin would not block Trp265$^{6.48}$ from rotating into the space, allowing a rotameric shift into its proposed active form. **(C)** Four residues are involved in the toggle switch mechanism of β_2AR-T4L. Phe290$^{6.52}$ (magenta) is sandwiched between Phe208$^{5.47}$ (tan) and Phe289$^{6.51}$ (tan), forming a ring-face aromatic interaction. Like rhodopsin, an activation step is thought to occur by a rotameric change of Trp286$^{6.48}$ (magenta), which would displace Phe290$^{6.52}$. Carazolol is shown to interact extensively with the sandwich motif; however, few interactions are seen with Trp286$^{6.48}$. The 6.52 position in β_2AR-T4L is occupied by Phe290$^{6.52}$, as opposed to Ala269$^{6.52}$ in rhodopsin, where the β-ionone ring replaces an aromatic protein side chain in forming the sandwich interactions. The aromatic character of the sandwich is otherwise maintained by Phe289$^{6.51}$ and Phe208$^{5.47}$ in β_2AR-T4L.

region in rhodopsin occludes the retinal-binding site through extensive interactions with the extracellular loops (Fig. 4B). Helix V of β_2AR is closer to the binding pocket by about 3.5 Å on average, and its lumenal end is angled more toward helix VI. Helix IV of β_2AR is farther from the binding site, possibly to remove steric clashes resulting from the modified position of helix V (Fig. 6, B and C). Helix III pivots farther from the binding site about a fulcrum located close to the cytoplasmic end (Fig. 6C). The angle formed between rhodopsin helix III and β_2AR helix III is about 7°, yielding a 4 Å displacement out of the binding pocket at the cytoplasmic end of the helix. Relative to rhodopsin, helix VI of β_2AR is positioned farther from the center of the receptor at the cytoplasmic end; this is caused by a slight difference in the angle about the proline-induced kink in the helix (Fig. 6C).

The ligand-binding pocket is formed by both structurally conserved and divergent helices, in the context of their positions in rhodopsin (Fig. 6D). Helices III and V are two of the most conformationally shifted helices and contain the canonical catecholamine-binding residues associated with activation of the adrenergic family of receptors (*63*–*65*). The comparison with rhodopsin suggests that the structurally conserved helices provide a common core present throughout the class A GPCRs, whereas the variable helices confer binding-site plasticity with a resulting architecture capable of binding a large spectrum of ligands.

Comparison to rhodopsin-based GPCR models. Since the determination of the inactive dark-state rhodopsin structure (*18*), a number of homology models of other class A GPCRs have been reported (*66*–*70*). Typically, homology models start by alignment of so-called fingerprint motifs that are common among the family. These fingerprint motifs are extrapolated to assign coordinates for the entire helical bundle. Loop regions are either ignored or modeled on the basis of databases of loop conformations, depending on the application (*66*). A number of models exist for β_2AR, some of which have been improved upon with supporting biochemical data (*66*, *70*–*73*). When compared to the β_2AR structure reported here, however, all of these models were more similar to rhodopsin, as were models for other receptors (e.g., dopamine, muscarinic, and chemokine) (*27*). This is not entirely surprising but highlights a general shortcoming in homology models generated from a single structural template. The structural divergence between β_2AR and rhodopsin would be quite difficult to predict accurately using only rhodopsin as a template. The addition of a second class A GPCR structure should make it possible to correlate the sequence differences between rhodopsin and β_2AR with the observed structural differences, enabling extrapolation to other class A GPCRs. Highlighting interactions that constrain class A receptors into each of the two observed states will allow a more comprehensive analysis of structural divergence and should result in more accurate models. Furthermore, evidence provided in (*24*) indicates that β_2AR-T4L may not be in a completely inactive conformation like rhodopsin, providing an alternative signaling state on which to base homology models that will be more relevant for virtual ligand screening and structure-based drug design (*66*, *73*). The addition of further structural templates and conformational states to the pool of information on GPCRs should pave the way to a new generation of more potent therapeutics targeting this expansive receptor family and enhance our understanding of the signaling properties within their associated pathways.

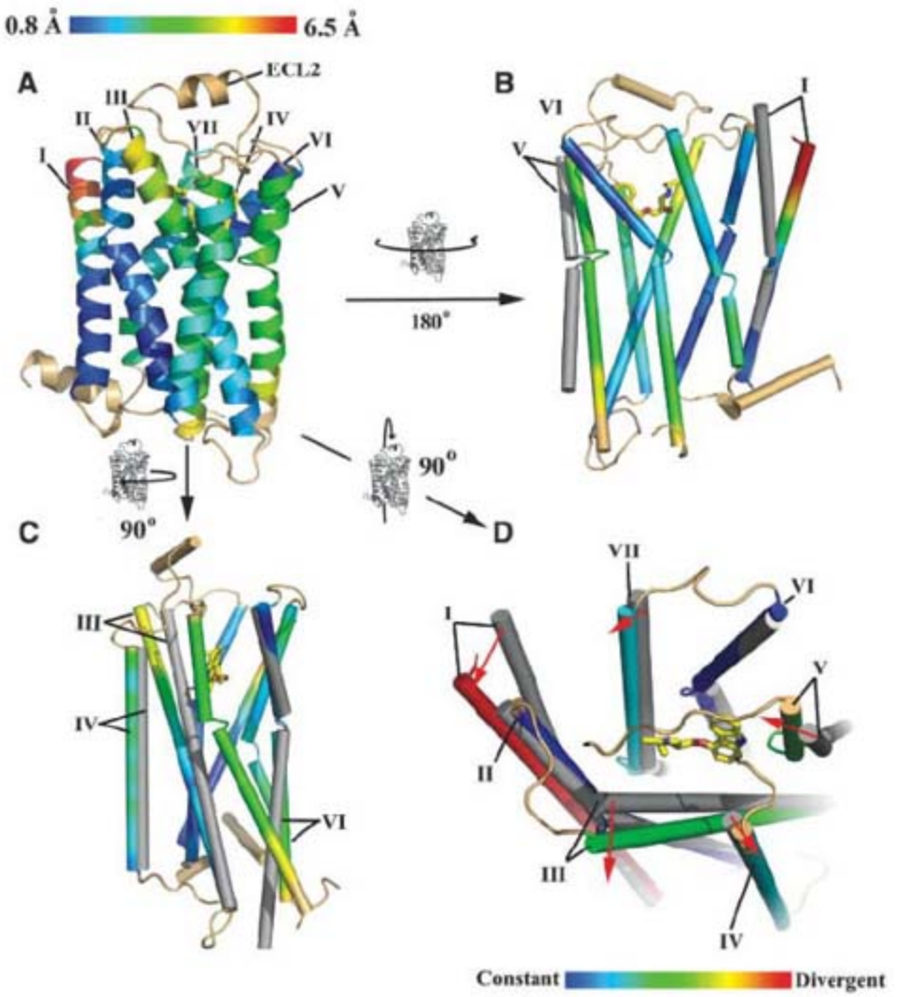

Fig. 6. Comparison of β_2AR-T4L helical orientations with those of rhodopsin (PDB ID code 1U19). **(A)** β_2AR-T4L is rendered as a ribbon trace colored with a blue-to-red spectrum corresponding to observed distances between Cα positions in the two structures [root mean square deviation (RMSD) 2.7 Å between all residues in the transmembrane region]. Helix II shows very little movement, whereas the entire lengths of helices III, IV, and V shift substantially. Helix VIII and loops were not included in the comparison and are colored tan. **(B)** Movements of helices I and V of rhodopsin (gray) are shown relative to β_2AR-T4L. **(C)** Movements of helices III, IV, and VI. **(D)** Ligand-binding site representation. Carazolol is shown with yellow carbons. Entire helices are assigned a single designation on the basis of their divergence from the rhodopsin position in the area of the ligand-binding site as shown. Helix I is highly divergent; helices II and VI are similar to rhodopsin. Helices IV and VII are moderately constant. Helices III and V are moderately divergent.

References and Notes

1. S. Takeda, S. Kadowaki, T. Haga, H. Takaesu, S. Mitaku, *FEBS Lett.* **520**, 97 (2002).
2. R. Fredriksson, M. C. Lagerstrom, L. G. Lundin, H. B. Schioth, *Mol. Pharmacol.* **63**, 1256 (2003).
3. K. L. Pierce, R. T. Premont, R. J. Lefkowitz, *Nat. Rev. Mol. Cell Biol.* **3**, 639 (2002).
4. R. J. Lefkowitz, S. K. Shenoy, *Science* **308**, 512 (2005).
5. Y. Sun *et al.*, *EMBO J.* **26**, 53 (2007).
6. J. Drews, *Science* **287**, 1960 (2000).
7. B. Kobilka, *Annu. Rev. Neurosci.* **15**, 87 (1992).

8. M. G. Caron, R. J. Lefkowitz, *Recent Prog. Horm. Res.* **48**, 277 (1993).
9. A. D. Strosberg, *Protein Sci.* **2**, 1198 (1993).
10. L. Hein, B. K. Kobilka, *Trends Cardiovasc. Med.* **7**, 137 (1997).
11. D. K. Rohrer, *J. Mol. Med.* **76**, 764 (1998).
12. Y. Xiang, B. Kobilka, in *The Adrenergic Receptors in the 21st Century*, D. M. Perez, Ed. (Humana, Totowa, NJ, 2006), pp. 267–292.
13. G. Milligan, P. Svoboda, C. M. Brown, *Biochem. Pharmacol.* **48**, 1059 (1994).
14. M. R. Taylor, *Pharmacogenomics J.* **7**, 29 (2007).
15. T. R. Bai, *Lung* **170**, 125 (1992).
16. P. J. Barnes, *Life Sci.* **52**, 2101 (1993).
17. R. M. Smiley, M. Finster, *J. Matern. Fetal Med.* **5**, 106 (1996).
18. K. Palczewski *et al.*, *Science* **289**, 739 (2000).
19. T. Okada *et al.*, *J. Mol. Biol.* **342**, 571 (2004).
20. J. Li, P. C. Edwards, M. Burghammer, C. Villa, G. F. Schertler, *J. Mol. Biol.* **343**, 1409 (2004).
21. D. Salom *et al.*, *Proc. Natl. Acad. Sci. U.S.A.* **103**, 16123 (2006).
22. B. K. Kobilka, X. Deupi, *Trends Pharmacol. Sci.* **28**, 397 (2007).
23. Inverse agonists act to reduce the basal activity of a receptor through interactions that shift the equilibrium to more of an inactive state. In contrast, antagonists bind to and block the active site but do not affect the equilibrium between inactive and active states, and agonists shift the equilibrium to an active receptor state.
24. D. M. Rosenbaum *et al.*, *Science* **318**, 1266; published online 25 October 2007 (10.1126/science.1150609).
25. β_2AR-T4L was generated by three distinct modifications to β_2AR: (i) A fusion protein was created by replacement of the third intracellular loop with T4L, (ii) the C-terminal 48 amino acids were deleted, and (iii) a glycosylation site at Asn^{187} was eliminated through a Glu substitution. This modified version was created to assist in improved crystal formation.
26. E. M. Landau, E. Pebay-Peyroula, R. Neutze, *FEBS Lett.* **555**, 51 (2003).
27. See supporting material on *Science* Online.
28. M. Caffrey, *Curr. Opin. Struct. Biol.* **10**, 486 (2000).
29. J. Deisenhofer, H. Michel, *EMBO J.* **8**, 2149 (1989).
30. E. M. Landau, J. P. Rosenbusch, *Proc. Natl. Acad. Sci. U.S.A.* **93**, 14532 (1996).
31. Z. Yao, B. Kobilka, *Anal. Biochem.* **343**, 344 (2005).
32. V. Cherezov, A. Peddi, L. Muthusubramaniam, Y. F. Zheng, M. Caffrey, *Acta Crystallogr. D* **60**, 1795 (2004).
33. The successful diffraction screening and data collection that led to the structure determination of β_2AR-T4L required overcoming a number of technological barriers that encompassed the growth and harvest of microcrystals, crystal imaging, and collection of diffraction data. Because of their transparency, crystals were often visually obstructed by the frozen lipidic mesophase material and therefore could not be confidently imaged by traditional beamline cameras; moreover, their extremely small size made them susceptible to rapid radiation damage (*27*).
34. GPCRs are frequently posttranslationally modified with palmitoylate on cysteine residues at the C-terminal tail. Furthermore, β_2AR-T4L was treated with iodoacetamide during purification to eliminate free thiols.
35. In Ballesteros-Weinstein numbering, a single most conserved residue among the class A GPCRs is designated x.50, where x is the transmembrane helix number. All other residues on that helix are numbered relative to this conserved position.
36. S. Yohannan, S. Faham, D. Yang, J. P. Whitelegge, J. U. Bowie, *Proc. Natl. Acad. Sci. U.S.A.* **101**, 959 (2004).
37. M. Katragadda, M. W. Maciejewski, P. L. Yeagle, *Biochim. Biophys. Acta* **1663**, 74 (2004).
38. V. Cherezov *et al*, *J. Mol. Biol.* **364**, 716 (2006).
39. Membrane proteins generally can form two types of crystal packing. Type I represents stacks of two-dimensional crystals ordered in the third dimension via interactions of hydrophilic parts of membrane proteins. Type II crystals are composed of membrane proteins whose hydrophobic part is shielded by a detergent micelle, and all crystal contacts are formed through hydrophilic, solvent-exposed parts of protein molecules.
40. P. Nollert, H. Qiu, M. Caffrey, J. P. Rosenbusch, E. M. Landau, *FEBS Lett.* **504**, 179 (2001).
41. B. F. O'Dowd, M. Hnatowich, M. G. Caron, R. J. Lefkowitz, M. Bouvier, *J. Biol. Chem.* **264**, 7564 (1989).
42. G. Milligan, *Mol. Pharmacol.* **66**, 1 (2004).
43. S. Angers *et al.*, *Proc. Natl. Acad. Sci. U.S.A.* **97**, 3684 (2000).
44. J. A. Javitch, *Mol. Pharmacol.* **66**, 1077 (2004).
45. J. F. Mercier, A. Salahpour, S. Angers, A. Breit, M. Bouvier, *J. Biol. Chem.* **277**, 44925 (2002).
46. G. F. Schertler, *Curr. Opin. Struct. Biol.* **15**, 408 (2005).
47. T. E. Hebert *et al.*, *J. Biol. Chem.* **271**, 16384 (1996).
48. W. Guo, L. Shi, J. A. Javitch, *J. Biol. Chem.* **278**, 4385 (2003).
49. Y. Xiang, V. O. Rybin, S. F. Steinberg, B. Kobilka, *J. Biol. Chem.* **277**, 34280 (2002).
50. M. R. Whorton *et al.*, *Proc. Natl. Acad. Sci. U.S.A.* **104**, 7682 (2007).
51. R. S. Ostrom, P. A. Insel, *Br. J. Pharmacol.* **143**, 235 (2004).
52. N. A. Baker, D. Sept, S. Joseph, M. J. Holst, J. A. McCammon, *Proc. Natl. Acad. Sci. U.S.A.* **98**, 10037 (2001).
53. T. H. Ji, M. Grossmann, I. Ji, *J. Biol. Chem.* **273**, 17299 (1998).
54. U. Gether, *Endocr. Rev.* **21**, 90 (2000).
55. K. Noda, Y. Saad, R. M. Graham, S. S. Karnik, *J. Biol. Chem.* **269**, 6743 (1994).
56. J. Mialet-Perez, S. A. Green, W. E. Miller, S. B. Liggett, *J. Biol. Chem.* **279**, 38603 (2004).
57. S. G. F. Rasmussen *et al.*, *Nature*, published online 21 October 2007 (10.1038/nature06325).
58. K. Palczewski, *Annu. Rev. Biochem.* **75**, 743 (2006).
59. T. W. Schwartz, T. M. Frimurer, B. Holst, M. M. Rosenkilde, C. E. Elling, *Annu. Rev. Pharmacol. Toxicol.* **46**, 481 (2006).
60. L. Shi *et al.*, *J. Biol. Chem.* **277**, 40989 (2002).
61. R. J. Lefkowitz, *Nat. Cell Biol.* **2**, E133 (2000).
62. For the alignment, residues on β_2AR were aligned to equivalent residues on rhodopsin: Residues 43 to 59 were aligned to residues 47 to 63; residues 67 to 95 were aligned to residues 71 to 99; residues 122 to 135 were aligned to residues 126 to 139; and residues 285 to 296 were aligned to residues 264 to 275.
63. C. D. Strader *et al.*, *J. Biol. Chem.* **263**, 10267 (1988).
64. C. D. Strader, M. R. Candelore, W. S. Hill, I. S. Sigal, R. A. Dixon, *J. Biol. Chem.* **264**, 13572 (1989).
65. G. Liapakis *et al.*, *J. Biol. Chem.* **275**, 37779 (2000).
66. C. Bissantz, P. Bernard, M. Hibert, D. Rognan, *Proteins* **50**, 5 (2003).
67. A. Fano, D. W. Ritchie, A. Carrieri, *J. Chem. Inf. Model.* **46**, 1223 (2006).
68. J. V. Hobrath, S. Wang, *J. Med. Chem.* **49**, 4470 (2006).
69. M. Nowak, M. Kolaczkowski, M. Pawlowski, A. J. Bojarski, *J. Med. Chem.* **49**, 205 (2006).
70. Y. Zhang, M. E. Devries, J. Skolnick, *PLoS Comput. Biol.* **2**, e13 (2006).
71. P. L. Freddolino *et al.*, *Proc. Natl. Acad. Sci. U.S.A.* **101**, 2736 (2004).
72. K. E. Furse, T. P. Lybrand, *J. Med. Chem.* **46**, 4450 (2003).
73. P. R. Gouldson *et al.*, *Proteins* **56**, 67 (2004).
74. M. A. Lomize, A. L. Lomize, I. D. Pogozheva, H. I. Mosberg, *Bioinformatics* **22**, 623 (2006).
75. W. L. DeLano, The PyMOL Molecular Graphics System (2002) (www.pymol.org).

76. Author contributions: R.C.S. and B.K.K. independently pushed the GPCR structural biology projects for more than 15 years. B.K.K. managed the protein design, production, and purification. R.C.S. managed novel crystallization and data collection methods development and experiments. V.C. developed novel methods for and performed LCP crystallization, LCP crystal mounting, LCP data collection, and model refinement, analyzed the results, and was involved in manuscript preparation. D.M.R. supplied protein materials for all crystallization trials, grew and collected data from the bicelle crystals, collected, processed and refined the 3.5 Å LCP structure, refined the 2.4 Å structure, analyzed the results, and was involved in manuscript preparation. M.A.H. designed the blind crystal screening protocol and collected the 2.4 Å data set, processed the 2.4 Å data, solved the structure by molecular replacement at 3.5 Å and 2.4 Å resolution, wrote the initial draft of the manuscript, and created all figures. S.G.F.R. assisted with the final stages of β_2AR-T4L purification. F.S.T. expressed β_2AR-T4L in insect cells and, together with T.S.K., performed the initial stage of β_2AR purification. H.-J.C. assisted with the refinement. P.K. assisted in developing novel methods to screen the transparent crystals, data collection, and refinement, and was involved in manuscript preparation. W.I.W. assisted with low-resolution data collection and processing, solved the β_2AR-T4L molecular replacement problem at 3.5 Å, participated in the 2.4 Å refinement process, and participated in structure analysis and manuscript preparation. B.K.K. additionally assisted with β_2AR-T4L purification, β_2AR-T4L 3.5 Å synchrotron data collection, structure analysis, and manuscript preparation. B.K.K. and D.M.R. designed the β_2AR-T4L fusion protein strategy. R.C.S. additionally assisted with β_2AR-T4L crystallization, 2.4 Å data collection, structure solution, refinement, structure analysis, and manuscript preparation. Supported by NIH Roadmap Initiative grant P50 GM073197 and Protein Structure Initiative grants U54 GM074961 and P50 GM062411 (R.C.S.), NIH Roadmap Initiative grant R21 GM075811 and National Institute of Neurological Disorders and Stroke grant NS028471 (B.K.K.), NIH grant F32 GM082028 (D.M.R.), the Lundbeck Foundation (S.G.F.R.), and NIH grant R01 GM056169 (H.-J.C. and W.I.W.). The GM/CA-CAT beamline (23-ID) at the Advanced Photon Source is supported by National Cancer Institute grant Y1-CO-1020 and National Institute of General Medical Sciences grant Y1-GM-1104. We thank J. Smith, R. Fischetti, and N. Sanishvili at the GM/CA-CAT beamline for assistance in development and use of the minibeam and beam time; G. Schertler for help with the initial diffraction experiments on LCP crystals, performed at ID-13 at the European Synchrotron Radiation Facility; K. Wüthrich and R. Horst for initial NMR analysis of samples; C. Roth, V.-P. Jaakola, A. Alexandrov, E. Chien, M. Bracey, V. Katritch, I. Wilson, and M. Yeager for careful review of the manuscript; Y. Zheng (Ohio State University) and M. Caffrey (University of Limerick) for use of the *in meso* robot [built with support from NIH (GM075915), NSF (IIS0308078), and SFI (02-IN1-B266)]; and A. Walker for assistance with manuscript preparation. Coordinates and structure factors have been deposited in the Protein Data Bank with identification code 2RH1.

Supporting Online Material

www.sciencemag.org/cgi/content/full/1150577/DC1
Materials and Methods
Figs. S1 to S4
Tables S1 to S3
References

17 September 2007; accepted 11 October 2007
Published online 25 October 2007;
10.1126/science.1150577
Include this information when citing this paper.

GPCR Engineering Yields High-Resolution Structural Insights into β_2-Adrenergic Receptor Function

Daniel M. Rosenbaum,[1*] Vadim Cherezov,[2*] Michael A. Hanson,[2] Søren G. F. Rasmussen,[1] Foon Sun Thian,[1] Tong Sun Kobilka,[1] Hee-Jung Choi,[1,3] Xiao-Jie Yao,[1] William I. Weis,[1,3] Raymond C. Stevens,[2†] Brian K. Kobilka[1†]

AUTHORS' SUMMARY

Heterotrimeric guanine nucleotide–binding protein (G protein) coupled receptors (GPCRs) are a remarkably versatile family of transmembrane signaling molecules that present extraordinary therapeutic potential as drug targets for a wide spectrum of diseases (*1*). A better understanding of GPCR structure will help to elucidate the mechanism by which they transmit signals across the plasma membrane and will facilitate the development of more effective and selective drugs. Rhodopsin, the light-sensitive photoreceptor found in the mammalian eye, is also a GPCR, and its structure has been determined. Obtaining high-resolution structures of GPCRs other than rhodopsin, however, has been challenging because of their low natural abundance and inherent structural flexibility and instability (*2*). As a result, the application of structure-based drug discovery to GPCRs has largely been limited to the use of rhodopsin-based homology models. We have applied targeted protein engineering to make other GPCRs better candidates for crystallographic structure analysis, using the human β_2-adrenergic receptor as an initial candidate. The β_2-adrenergic receptor binds the hormones adrenaline and noradrenaline to regulate cardiovascular and pulmonary function. Our results show that targeted protein engineering can be used to obtain high-resolution structures of GPCRs.

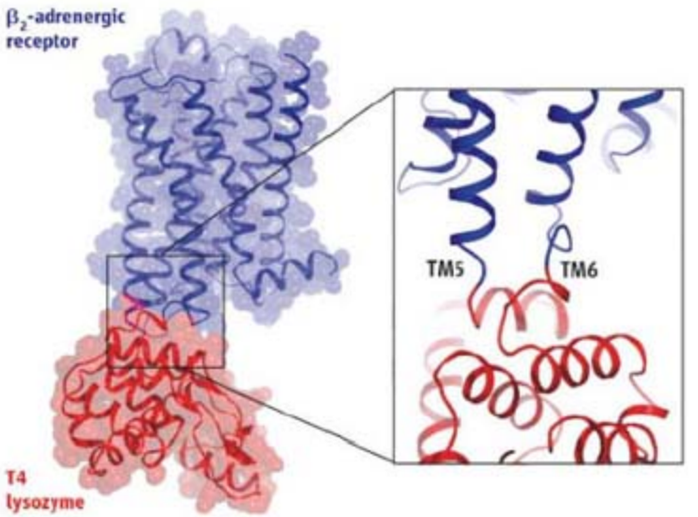

Replacement of an intracellular loop of the β_2-adrenergic receptor with lysozyme stabilized two flexible helices (5 and 6), allowing crystallization of the fusion protein and determination of the structure of this medically important membrane receptor.

Efforts to crystallize the wild-type (WT) β_2-adrenergic receptor have been unsuccessful. We identified the third intracellular loop (ICL3) as a possible contributor to the difficulties in crystallization. This region interacts with signaling molecules such as G proteins. ICL3 is poorly structured and contributes to the relatively unrestricted movement of the transmembrane helices, which leads to the receptor's conformational heterogeneity and crystallization problems. Truncation of ICL3 could reduce the movement of the helices, but this would also reduce the polar surface area that is important for forming crystal-lattice contacts. Thus, we replaced ICL3 with T4 lysozyme (T4L), a well-folded protein that adds a polar surface and simultaneously restricts the movement of transmembrane helices linked by the inserted sequence (see the figure). The resulting fusion protein could be efficiently expressed in insect cells and purified. It also retained ligand binding affinities near those of the WT receptor and could undergo conformational changes upon agonist binding.

The engineered protein formed crystals in two different lipid environments: bicelles and lipidic cubic phase. Crystals grown in lipidic cubic phase yielded a 2.4 Å x-ray diffraction data set from which we determined the structure by molecular replacement, using T4 lysozyme and a polyalanine model of the transmembrane regions of rhodopsin as search models [see (*3*)].

One must be concerned that the structural modifications that facilitated crystal formation could produce a high-resolution structure that does not reflect the WT β_2-adrenergic receptor. The fusion protein exhibited slightly elevated agonist binding affinities; however, antagonist binding affinities were normal, and only minor differences were observed when the β_2-adrenergic receptor–T4L structure was compared to a 3.4 Å structure of the WT β_2-adrenergic receptor crystallized in complex with an antibody fragment (*4*). Therefore, with the exception of ICL3, the structure of β_2-adrenergic receptor–T4L probably reflects that of the native receptor.

Although we know the structure of the GPCR rhodopsin, our structure of the β_2-adrenergic receptor now provides a high-resolution view of a GPCR that binds diffusible hormones and neurotransmitters and should facilitate structure-based drug development. Moreover, it can help to reveal how structural changes are propagated from the agonist binding site to the G protein–coupling domains. The methods that we used to obtain these crystals will probably be applicable to other GPCRs, allowing the determination of their structures and increasing our understanding of transmembrane signal transduction and drug discovery for this important class of molecules.

Nevertheless, a full understanding of the structural basis of GPCR activation will require a high-resolution structure of a complex between a receptor with an agonist bound and its G protein, as well as methods to assess the dynamics of their interaction that cannot be captured by the static snapshots provided by x-ray crystallography. Future nuclear magnetic resonance (NMR) experiments, which capture some of the dynamics, could identify key GPCR residues: those critical for binding different classes of ligands, propagating conformational changes, and forming allosteric interaction sites for signaling partners such as G proteins and arrestins. When interpreted in the context of high-resolution crystal structures, NMR and other dynamics experiments will lead to a better understanding of GPCR signaling and how such signaling can be manipulated with small molecules to therapeutic effect.

Summary References

1. K. L. Pierce, R. T. Premont, R. J. Lefkowitz, *Nat. Rev. Mol. Cell Biol.* **3**, 639 (2002).
2. B. K. Kobilka, X. Deupi, *Trends Pharmacol. Sci.* **28**, 397 (2007).
3. V. Cherezov *et al.*, *Science* **318**, 1258, (2007); published online 25 October 2007 (10.1126/science.1150577).
4. S. G. F. Rasmussen *et al.*, *Nature*; published online 21 October 2007; 10.1038/nature06325.

FULL-LENGTH ARTICLE

The β_2-adrenergic receptor (β_2AR) is a well-studied prototype for heterotrimeric guanine nucleotide–binding protein (G protein)–coupled receptors (GPCRs) that respond to diffusible hormones and neurotransmitters. To overcome the structural flexibility of the β_2AR and to facilitate its crystallization, we engineered a β_2AR fusion protein in which T4 lysozyme (T4L) replaces most of the third intracellular loop of the GPCR ("β_2AR-T4L") and showed that this protein retains near-native pharmacologic properties. Analysis of adrenergic receptor ligand-binding mutants within the context of the reported high-resolution structure of β_2AR-T4L provides insights into inverse-agonist binding and the structural changes required to accommodate catecholamine agonists. Amino acids known to regulate receptor function are linked through packing interactions and a network of hydrogen bonds, suggesting a conformational pathway from the ligand-binding pocket to regions that interact with G proteins.

The adrenergic receptors make up a class of heterotrimeric guanine nucleotide–binding protein (G protein)–coupled receptors (GPCRs) that play a central role in mediating the effects of catecholamine hormones. In contrast to rhodopsin, which is expressed at very high levels in photoreceptor cells and has the ligand retinal covalently bound (*1*), other GPCRs such as the β_2-adrenergic receptor (β_2AR) generally express at low levels, bind diffusible ligands, and exhibit greater functional and structural plasticity (*2*). The β_2AR was the first non-rhodopsin GPCR to be cloned and has been one of the most extensively studied members of this large receptor family.

To obtain high-resolution structural information on the β_2AR, we increased its proteolytic stability and crystallizability by eliminating the C-terminal tail and replacing most of the third intracellular loop (ICL3) with the protein T4 lysozyme (T4L). The optimized β_2AR-T4L protein was crystallized in lipidic cubic phase, as described in the companion paper by Cherezov *et al.* (*3*), and the resulting 2.4 Å resolution crystal structure reveals the interface between the receptor and the ligand carazolol, a partial inverse agonist (*4*). Analysis of mutagenesis data in light of the structure clarifies the roles of different amino acids in inverse-agonist binding and implies that rearrangement of the binding pocket accompanies agonist binding. In addition, the structure reveals how mutations known to cause constitutive activity or uncoupling of agonist binding and G protein activation are distributed between the ligand-binding pocket and the cytoplasmic surface of the protein, such that changes in side chains due to interaction with the ligand can be transmitted through the structure to the site of G protein interaction.

β_2AR-T4L: A crystallizable GPCR fusion protein. The conformational complexity that makes GPCRs versatile signaling molecules may contribute to the difficulty of crystallizing these proteins (*2*). Despite substantial efforts, we were unable to grow diffraction-quality crystals from purified, homogeneous wild-type (WT) β_2AR. This was probably due to conformational variability of the flexible ICL3 and C terminus, as well as the relatively small polar surface available for crystal contacts. Fluorescence resonance energy transfer experiments show that the C-terminal portion of the β_2AR is in an extended conformation (*5*), a property that may be important for the role of this region in interacting with signaling and scaffold proteins, but one that would probably interfere with crystal-lattice formation. ICL3, which links the cytoplasmic ends of helices V and VI, is functionally important both for the specificity of receptor–G protein interactions and for G protein activation. In the β_2AR, this domain is susceptible to proteolysis; however, proteolytic cleavage does not lead to dissociation of the transmembrane segments linked by the ICL3. In fact, β_2AR helices I to V and helices VI and VII behave as independent folding domains that can be expressed on separate plasmids and assemble to form a functional "split" receptor (*6*). Therefore, we speculated that ICL3 links two domains with a relatively dynamic interface, which could be important for function but may also contribute to greater instability.

Because the majority of membrane protein crystals form through contacts of the nonmembranous portions of the molecule, we sought to improve the chances of β_2AR crystallization by replacing ICL3 with a well-structured, soluble domain that might aid in the formation of lattice contacts. The initial criteria for choosing the inserted soluble protein were that the N and C termini would approximate the predicted distance between the cytoplasmic ends of helix V and helix VI and that the protein would crystallize under a variety of conditions. T4L is a small, stable protein that fulfills these criteria (*7*). The N and C termini of WT T4L are 10.7 Å apart in Protein Data Bank (PDB) structure 2LZM (*8*), compared with a distance of 15.9 Å between the carbonyl carbon of residue $228^{5.63}$ (*9*) and the amide nitrogen of residue $241^{6.24}$ in the high-resolution structure of rhodopsin (PDB 1U19) (*10*).

DNA encoding the T4L protein ($Cys^{54} \rightarrow Thr^{54}$, $Cys^{97} \rightarrow Ala^{97}$) (*11*) was initially cloned into the human β_2AR gene, guided by a comparison of ICL3 length and sequence among class A GPCRs (*12*): residues $234^{5.73}$ to $259^{6.21}$ of the β_2AR were replaced by residues 2 to 164 of T4L (construct "E3" in Fig. 1A). In addition, the receptor was truncated at position 365, which aligns approximately with the position of the rhodopsin C terminus. Although these modifications resulted in a receptor that was expressed efficiently in Sf9 cells, further optimization was carried out to reduce the length of the junction between the receptor and the T4L termini (*13*). Several candidate constructs are illustrated in Fig. 1A, and selected immunofluorescence images of transfected, permeabilized human embryonic kidney (HEK) 293 cells are shown in Fig. 1B. Relative to the initial construct, we could remove three residues from the cytoplasmic end of helix V, three from the C-terminal end of T4L, and three from the N terminus of helix VI, all without losing substantial cell-surface expression. The final construct used for crystallization trials (β_2AR-T4L) has residues $231^{5.70}$ to $262^{6.24}$ of the β_2AR replaced by amino acids 2 to 161 of T4L (D1 in Fig. 1A). Similar reduction of flexibility through minimization of linker length has been important in previous crystallization studies on soluble fusion proteins (*14*).

Functional properties of β_2AR-T4L. We measured saturation binding of [^{3}H]DHA to the β_2AR-T4L, as well as competition binding of the inverse agonist ICI-118,551 and several agonists (Fig. 2A, fig. S1, and table S1). The results show that β_2AR-T4L has WT affinity for the antagonist [^{3}H]DHA and the inverse agonist ICI-118,551, whereas the affinity for both agonists (e.g., isoproterenol, epinephrine, formoterol) and a partial agonist (salbutamol) is two-to-threefold higher relative to WT β_2AR. Higher agonist binding affinity is a property associated with constitutively active mutants (CAMs) of GPCRs. CAMs of the β_2AR also exhibit elevated basal, agonist-independent activation of the stimulatory G protein for adenylyl cyclase (Gs) and typically have lower expression levels and reduced stability (*15*, *16*). β_2AR-T4L exhibits binding properties of a CAM, but it expresses at levels exceeding 1 mg/liter of Sf9 cell culture, is more resistant to trypsin proteolysis than the WT β_2AR (fig. S2), and retains binding activity in detergent at 37°C, as well as the WT receptor (fig. S3).

β_2AR-T4L did not couple to Gs, as expected, because of the replacement of ICL3 by T4L. To assess whether the fused protein alters receptor function at the level of its ability to undergo conformational changes, we used a covalently attached fluorescent probe as a reporter for ligand-induced structural changes. Fluorophores attached at $Cys265^{6.27}$, at the cytoplasmic end of helix VI, detect agonist-induced conformational changes that correlate with the efficacy of the agonist toward G protein activation (*17*–*20*). Detergent-

[1]Department of Molecular and Cellular Physiology, Stanford University School of Medicine, Stanford, CA 94305, USA. [2]Department of Molecular Biology, The Scripps Research Institute, La Jolla, CA 92037, USA. [3]Department of Structural Biology, Stanford University School of Medicine, Stanford, CA 94305, USA.

*These authors contributed equally to this work.
†To whom correspondence should be addressed. E-mail: stevens@scripps.edu (R.C.S.); kobilka@stanford.edu (B.K.K.)

solubilized β_2AR365 (WT receptor truncated at 365) and β_2AR-T4L were each labeled with monobromobimane, which has been used previously to monitor conformational changes of the β_2AR (*21*). The addition of the agonist isoproterenol to purified β_2AR365 induces a decrease in fluorescence intensity and a shift in the wavelength at maximum intensity (λ_{max}) for the attached bimane probe (Fig. 2B and table S2). These changes in intensity and λ_{max} are consistent with an agonist-induced increase in polarity around bimane. A smaller change is observed with the partial agonist salbutamol, whereas the inverse agonist ICI-118,551 had little effect. For the β_2AR-T4L, there are subtle differences in the baseline spectrum of the bimane-labeled fusion protein, as might be expected if the environment around Cys265$^{6.27}$ is altered by T4L. However, the full agonist isoproterenol induces a qualitatively similar decrease in intensity and rightward shift in λ_{max}. Thus, the presence of the fused T4L does not prevent agonist-induced conformational changes. The partial agonist salbutamol induced larger responses in β_2AR-T4L than were observed in WT β_2AR, and there was a small increase in fluorescence in response to the inverse agonist ICI-118,551. These properties are observed in CAMs (*15*, *22*) and are consistent with the higher affinities for agonists and partial agonists exhibited by β_2AR-T4L. Therefore, we conclude that the T4L fusion induces a partial constitutively active phenotype in the β_2AR, probably caused by changes at the cytoplasmic ends of helices V and VI.

Comparison between β_2AR-T4L and β_2AR-Fab structures. The β_2AR-T4L fusion strategy is validated by a comparison of its structure to that of WT β_2AR complexed with a Fab that recognizes a three-dimensional epitope consisting of the N- and C-terminal ends of ICL3, determined at an anisotropic resolution of 3.4 Å/3.7 Å (*23*). Figure 3A illustrates the similarity between the fusion and antibody complex approaches to β_2AR crystallization, in that both strategies rely on attachment (covalent or noncovalent, respectively) of a soluble protein partner between helices V and VI. A major difference between the two structures is that the extracellular loops and the carazolol ligand could not be modeled in the β_2AR-Fab complex, whereas these regions are resolved in the structure of β_2AR-T4L. Nonetheless, it is clear that the T4L insertion does not substantially alter the receptor. Superposition of the two structures (fig. S4) illustrates that the transmembrane helices of the receptor components are very similar (root mean square deviation = 0.8 Å for 154 common modeled transmembrane Cα positions versus 2.3 Å between β_2AR-T4L and the 154 equivalent residues in rhodopsin), especially when the modest resolution of the Fab complex is taken into account.

There is one major difference between the Fab-complex and chimeric-receptor structures that can be attributed to the presence of T4L. The cytoplasmic end of helix VI is pulled outward as a result of the fusion to the C terminus of T4L, which alters the packing of Phe264$^{6.26}$ at the end of helix VI (Fig. 3B). In the Fab-complex β_2AR, interactions between Phe264$^{6.26}$ and residues in helix V, helix VI, and ICL2 may be important in maintaining the β_2AR in the basal state. The loss of these packing interactions in β_2AR-T4L could contribute to the higher agonist binding affinity characteristic of a CAM.

An unexpected difference between the structure of rhodopsin and the β_2AR-T4L involves the sequence E/DRY (*24*) found at the cytoplasmic end of helix III in 71% of class A GPCRs. In rhodopsin, Glu134$^{3.49}$ and Arg135$^{3.50}$ form a network of hydrogen bond and ionic interactions with Glu247$^{6.30}$ at the cytoplasmic end of helix VI. These interactions have been referred to as an "ionic lock" that stabilizes the inactive state of rhodopsin and other class A members (*25*). However, the arrangement of the homologous residues is considerably different in β_2AR-T4L: Arg131$^{3.50}$ interacts primarily with Asp130$^{3.49}$

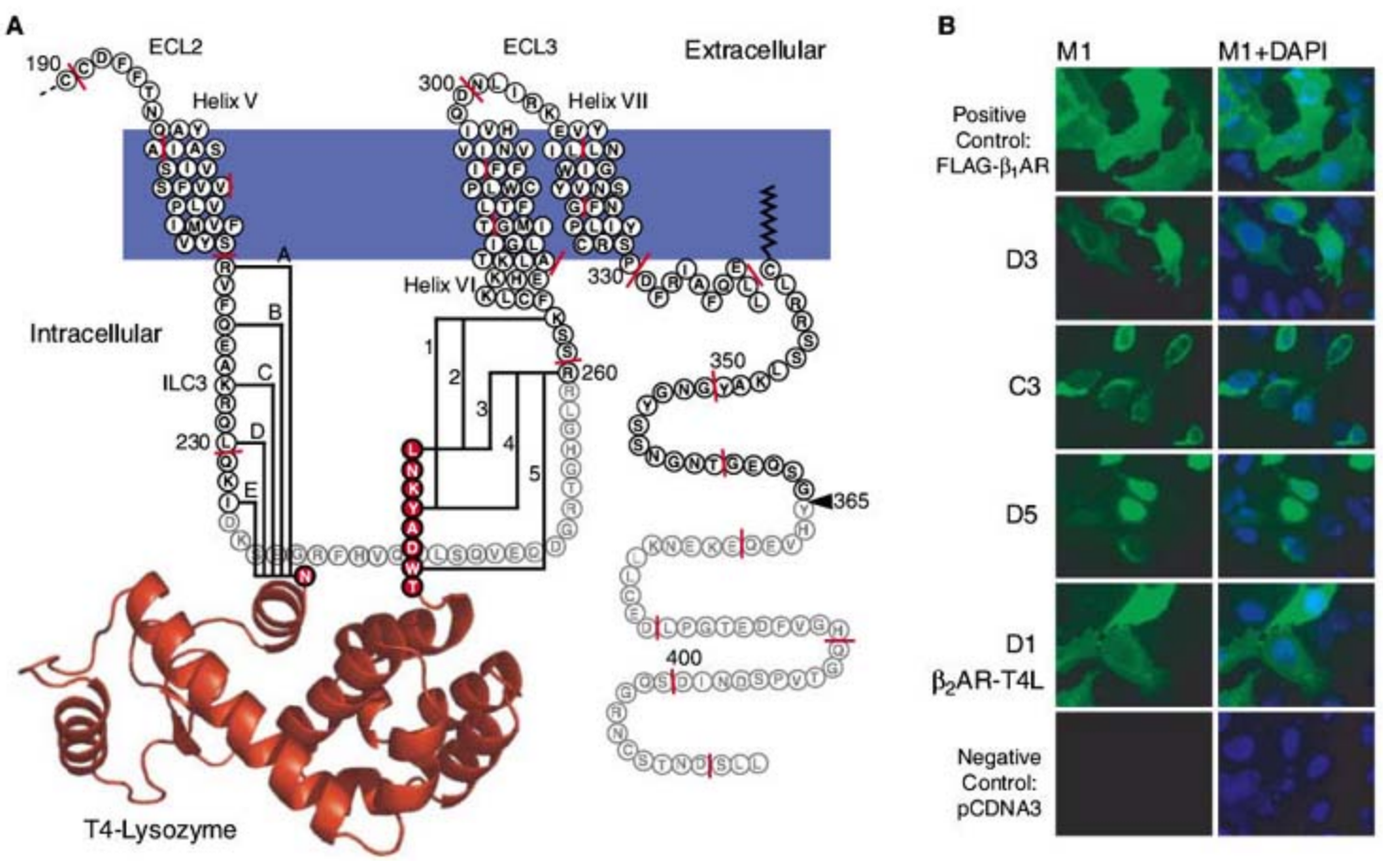

Fig. 1. Design and optimization of the β_2AR-T4L fusion protein. (**A**) The sequence of the region of the β_2AR targeted for insertion of a crystallizable domain is shown, and the positions of the junctions between the receptor and T4L (red) for various constructs are indicated. The sequences that were initially replaced or removed are faded. Red lines are shown after every tenth residue. ECL, extracellular loop. (**B**) Immunofluorescence images of HEK293 cells expressing selected fusion constructs. (Left) M1 anti-FLAG signal corresponding to antibody bound to the N terminus of the receptor. (Right) Same signal merged with blue emission from 4′,6′-diamidino-2-phenylindole (nuclear staining for all cells). Plasma membrane staining is observed in the positive control, D3, and D1, whereas C3 and D5 are retained in the endoplasmic reticulum.

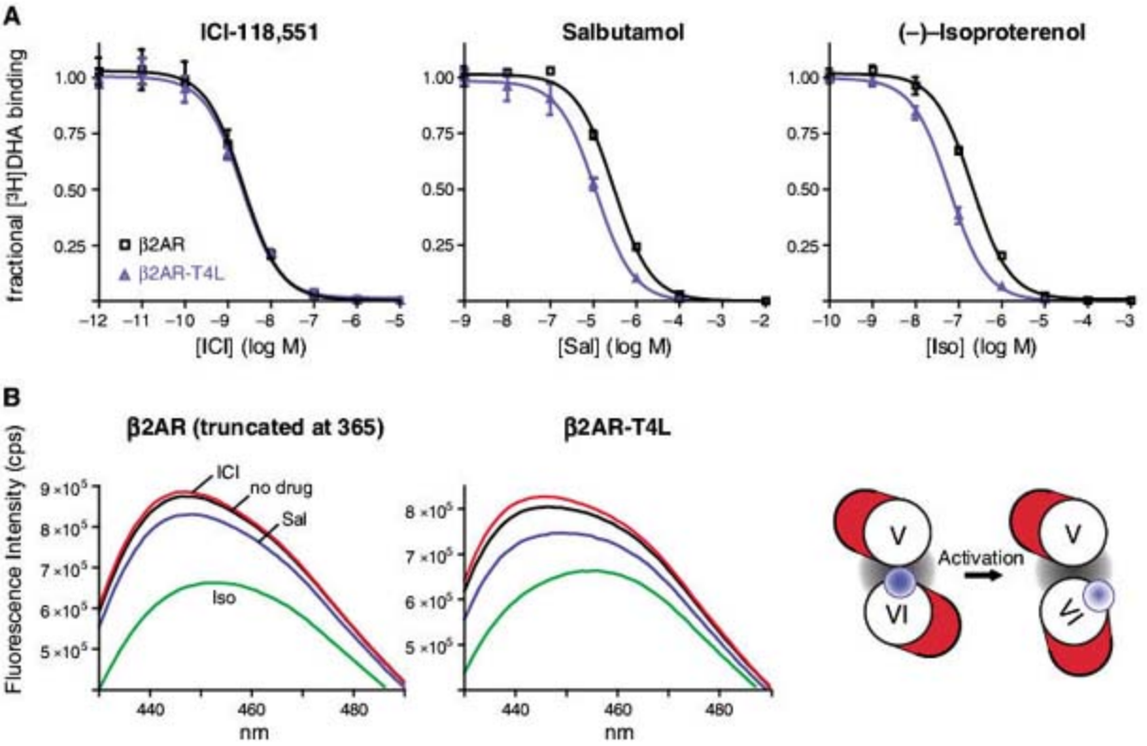

Fig. 2. Functional characterization of β_2AR-T4L. **(A)** Affinity competition curves for adrenergic ligands binding to β_2AR-T4L and WT β_2AR. Binding experiments on membranes isolated from Sf9 insect cells expressing the receptors were performed as described (*13*). **(B)** β_2AR-T4L is still able to undergo ligand-induced conformational changes. Bimane fluorescence spectra (excitation at 350 nm) of detergent-solubilized β_2AR-T4L and WT β_2AR truncated at 365, labeled under conditions that selectively modify Cys265$^{6.27}$ (*13*), were measured after incubating the unliganded receptors with compounds for 15 min at room temperature. The cartoon illustrates that the observed changes in fluorescence can be interpreted as a movement of the bimane probe from a more buried, hydrophobic environment to a more polar, solvent-exposed position. cps, counts per second.

and a sulfate ion rather than with Glu268$^{6.30}$, and the distance between helix III and helix VI is greater than in rhodopsin (Fig. 3C). This difference might be explained by the interaction between Glu268$^{6.30}$ and Arg8 of T4L; however, the arrangement of Asp130$^{3.49}$ and Arg131$^{3.50}$ and the distance between helix III and helix VI is very similar to that observed in the β_2AR-Fab structure. Although the presence of an antibody or T4L at the ICL3 region could potentially affect the arrangement of these residues, the fact that similar ionic-lock structures were obtained using two different approaches suggests that a broken ionic lock may be a genuine feature of the carazolol-bound state of the receptor.

Ligand binding to the β_2AR. The β_2AR-T4L fusion protein was purified and crystallized in complex with the inverse agonist carazolol. Carazolol stabilizes the β_2AR against extremes of pH and temperature, perhaps related to its unusually high binding affinity (equilibrium dissociation constant $K_d < 0.1$ nM) and slow dissociation kinetics (half-time $t_{1/2} \sim 30$ hours) (fig. S5). The interactions between carazolol and β_2AR-T4L are depicted schematically in Fig. 4. The carbazole ring system is oriented roughly perpendicular to the plane of the membrane, and the alkylamine chain (atoms 15 to 22 in the model) is nearly parallel to the heterocycle (Fig. 5, A and B). Carazolol was modeled into the electron density (*3*) as the (S)-(–) isomer because of the higher affinity of this enantiomer, despite the fact that a racemic mixture of the ligand was used in crystallization. Asp113$^{3.32}$, Tyr316$^{7.43}$, and Asn312$^{7.39}$ present a constellation of polar functional groups to the alkylamine and alcohol moieties of the ligand, with the Asp113$^{3.32}$ and Asn312$^{7.39}$ side chains forming close contacts (<3 Å) with the

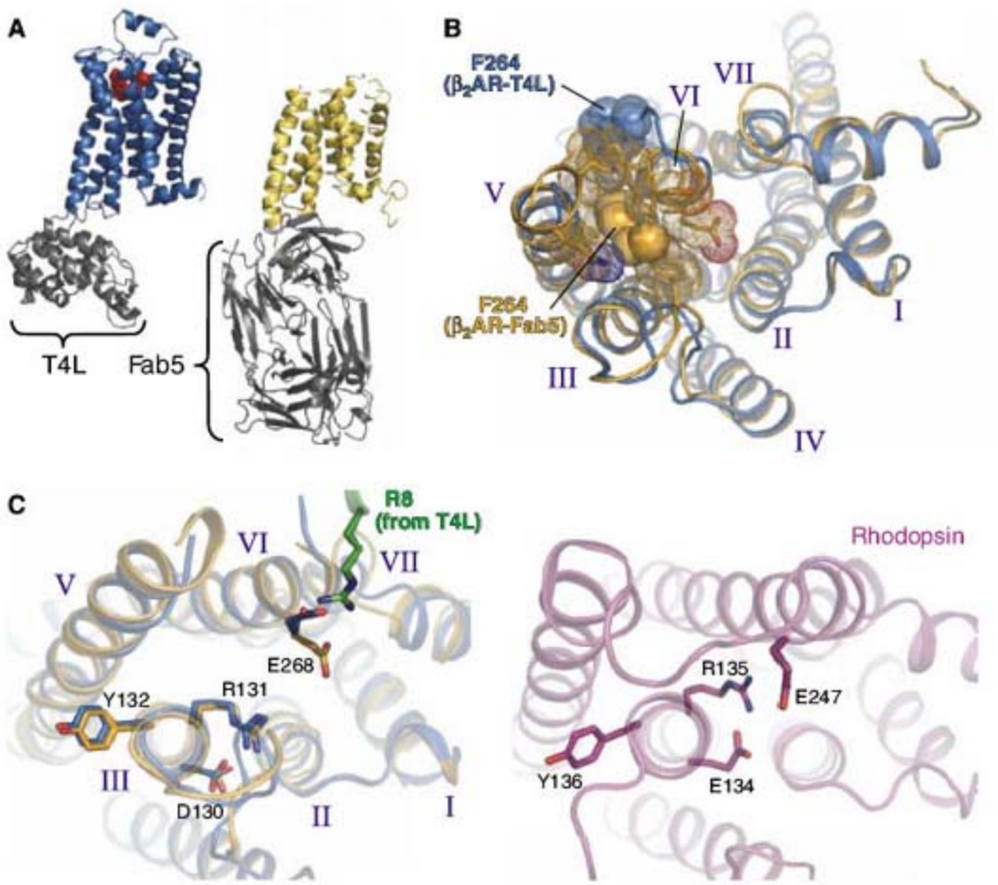

Fig. 3. **(A)** Side-by-side comparison of the crystal structures of the β_2AR-T4L fusion protein and the complex between β_2AR365 and a Fab fragment. The receptor component of the fusion protein is shown in blue (with modeled carazolol as red spheres), whereas the receptor bound to Fab5 is yellow. **(B)** Differences in the environment surrounding Phe264$^{6.26}$ (shown as spheres) for the two proteins. **(C)** Analogous interactions to the ionic lock between the E(D)RY motif and Glu247$^{6.30}$ seen in rhodopsin (right panel, purple) are broken in both structures of the β_2AR (left panel, blue and yellow as above). PyMOL (*43*) was used for the preparation of all figures.

O_{17} and N_{19} atoms of carazolol (Figs. 4 and 5, A and B). Asp113$^{3.32}$ was one of the first β_2AR residues shown to be important for ligand binding; the D113N mutation causes a complete loss of detectable affinity for antagonists (*26*) and a decrease in the potency of agonists toward cell-based G protein activation by over four orders of magnitude (*27*). Likewise, mutations of Asn312$^{7.39}$ perturb β_2AR binding to agonists and antagonists: Changes to nonpolar amino acids (Ala or Phe) reduce affinities to undetectable levels, whereas retention of a polar functionality (Thr or Gln) gives partial affinity (*28*). On the opposite end of the ligand near helix V, N_7 of the carbazole heterocycle forms a hydrogen bond with the side-chain hydroxyl of Ser203$^{5.42}$. Mutations of Ser203$^{5.42}$ specifically decrease β_2AR affinity toward catecholamine agonists and aryloxyalkylamine ligands with nitrogen-containing heterocycles such as pindolol (*29*) and, by implication, carazolol. Thus, the polar interactions between carazolol and the receptor observed in the crystal structure agree with the known biochemical data. The contribution of Tyr316$^{7.43}$ to antagonist and

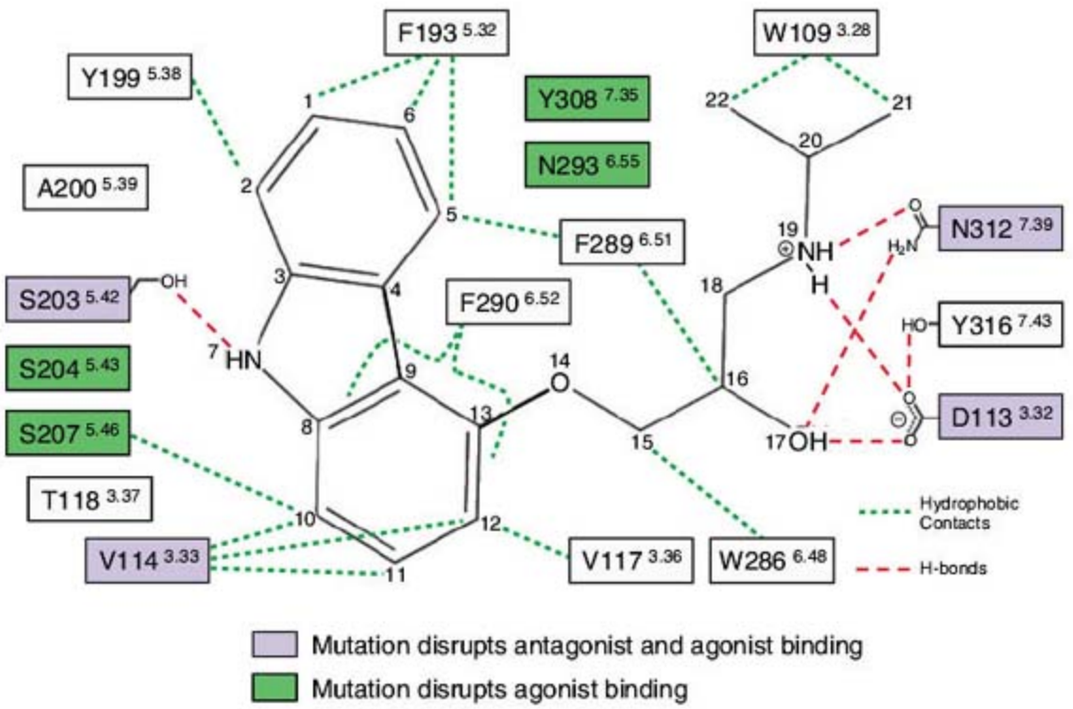

Fig. 4. Schematic representation of the interactions between β_2AR-T4L and carazolol at the ligand binding pocket. The residues shown here have at least one atom within 4 Å of the ligand in the 2.4 Å resolution crystal structure.

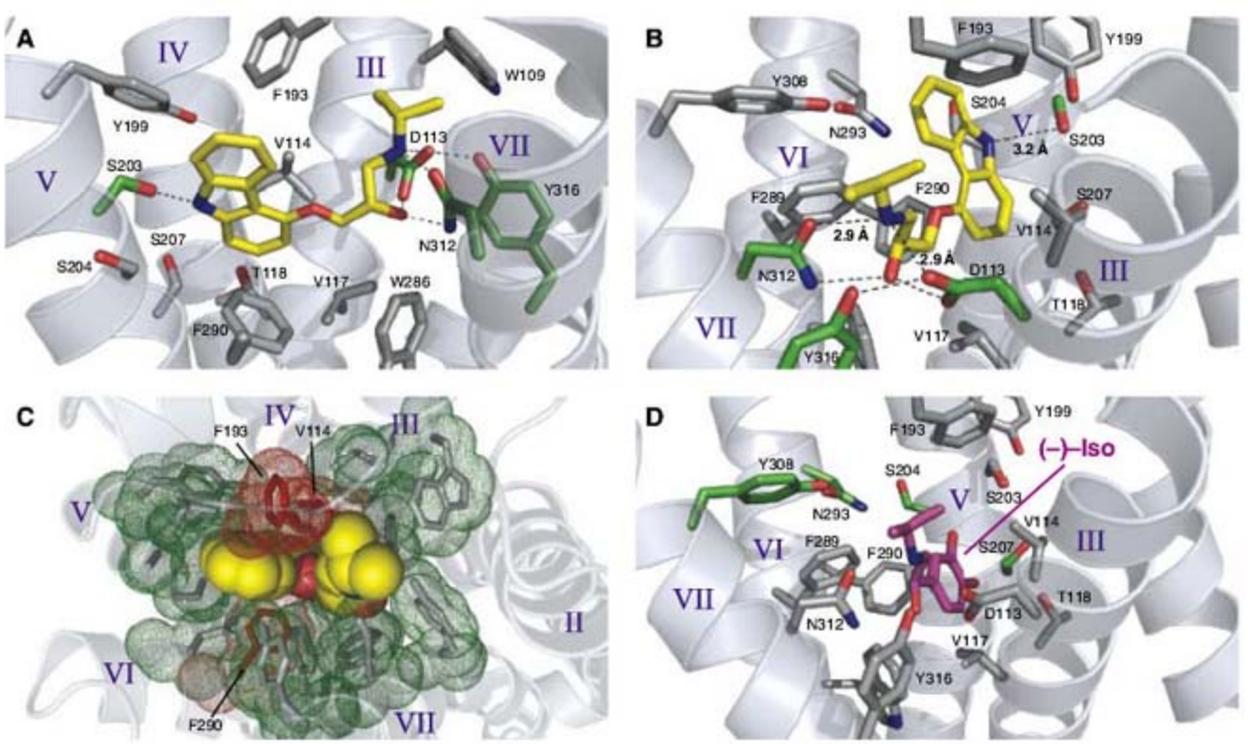

Fig. 5. Ligand binding pocket of β_2AR-T4L with carazolol bound. (**A**) Residues within 4 Å of the ligand are shown as sticks, with the exception of A200, N293, F289, and Y308. Residues that form polar contacts with the ligand (distance cutoff: 3.5 Å) are shown in green, other residues are gray, and carazolol is yellow (in all panels, oxygens are red and nitrogens are blue). (**B**) Same as (A), except that the ligand is oriented with its amine facing out of the page. W109 is not shown. (**C**) Packing interactions between carazolol and all residues within 5 Å of the ligand. The view is from the extracellular side of the membrane. Carazolol is shown as yellow spheres, and receptor residues are shown as sticks within van der Waals dot surfaces. Val114$^{3.33}$, Phe193$^{5.32}$, and Phe290$^{6.52}$ are red, and all other residues are gray. (**D**) Model of (–)-isoproterenol (magenta sticks) in the ligand binding pocket observed in the crystal structure. A model of the agonist with optimal bond lengths and angles was obtained from the PRODRG server (*44*), and the dihedral angles were adjusted to the values observed in the homologous atoms of bound carazolol (16 to 22 in Fig. 4). The one remaining unaccounted dihedral in (–)-isoproterenol was adjusted in order to place the catechol ring in the same plane as the C_{16}–C_{15}–O_{14} plane in carazolol. Residues known to specifically interact with agonists are shown as green sticks.

agonist affinity remains to be tested; this residue is conserved as Tyr in all sequenced adrenergic receptor genes (*12*).

Figure 5C shows the tight packing between carazolol and surrounding amino acids that buries 790 Å^2 of surface area from solvent; specific contacts are depicted schematically in Fig. 4. Notable among the hydrophobic residues contacting carazolol are Val114$^{3.33}$, Phe290$^{6.52}$, and Phe193$^{5.32}$. The side chain of Val114$^{3.33}$ from helix III makes multiple contacts with the C_8-to-C_{13} ring of the carbazole heterocycle, and Phe290$^{6.52}$ from helix VI forms an edge-to-face aromatic interaction with the same ring. As a result, these two amino acids form a hydrophobic "sandwich" with the portion of the aryl moiety that is common to many adrenergic antagonists. The mutation of Val114$^{3.33}$ to Ala was shown to decrease β_2AR affinity toward the antagonist alprenolol by one order of magnitude, as well as to lower affinity for the agonist epinephrine 300-fold (*30*). Phe193$^{5.32}$ is different from other carazolol contact residues in that it is located on the second extracellular loop, in the path of hormone accessibility to the binding pocket. This amino acid contributes more buried surface area than any other residue to the interface between β_2AR-T4L and carazolol (table S3). Therefore, Phe193$^{5.32}$ is likely to contribute substantially to the energy of β_2AR-carazolol complex formation, and the position of this residue on the extracellular side of the binding site may allow it to act as a gate that contributes to the unusually slow dissociation of the ligand (fig. S5).

Analysis of the binding pocket provides insights into the structural basis for pharmacologic selectivity between the β_2AR and closely related adrenergic receptors such as the β_1AR. The affinities of these two receptors for certain ligands, such as ICI-118,551, betaxolol, and RO363 (*31*), differ by up to 100-fold. Curiously, all of the amino acids in the carazolol binding pocket are conserved between the β_1AR and β_2AR [fig. S6 in (*13*)]. The majority of the 94 amino acid differences between the β_1AR and β_2AR are found in the cytoplasmic and extracellular loops. Whereas residues that differ in the transmembrane segments generally face the lipid bilayer, eight residues lie at the interface between helices and may influence helix packing. The structural basis for pharmacologic differences between β_1AR and β_2AR must, therefore, arise from amino acid differences in the entrance to the binding pocket or subtle differences in the packing of helices. Evidence for the latter comes from chimeric-receptor studies (*32*) in which successive exchange of helices between β_1AR and β_2ARs led to a gradual change in affinity for the β_2AR selective ICI-118,551 and the β_1AR selective betaxolol.

As discussed above, β_2AR-T4L shows CAM-like properties with respect to agonist binding affinities, suggesting that the unliganded β_2AR-T4L may exist in a more active conformation than the WT β_2AR. Nevertheless, as shown in Fig. 2B, β_2AR-T4L can be stabilized in an inactive conformation by an inverse agonist. Because β_2AR-T4L was crystallized with bound carazolol, a partial inverse agonist, the structure most likely represents an inactive state. This is consistent with the similarity of the β_2AR-T4L and β_2AR-Fab5 carazolol-bound structures. To assess whether conformational changes are required to accommodate catecholamines, a model

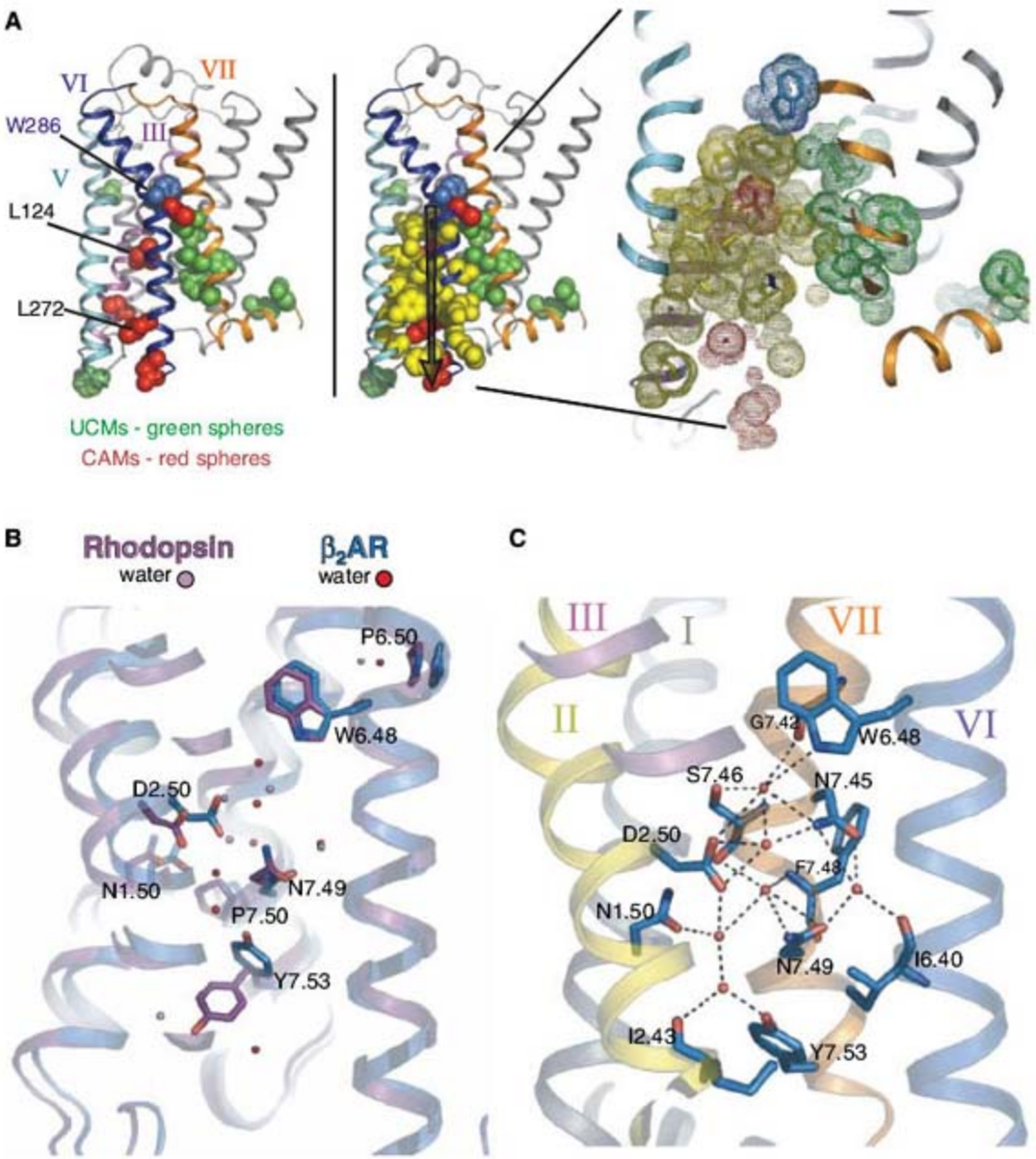

Fig. 6. Packing interactions in the β_2AR that are likely to be modulated during the activation process. (**A**) (Left) Residues previously demonstrated to be CAMs (*16*, *25*, *37*–*39*, *45*) or UCMs (*26*, *41*, *46*–*49*) are shown as van der Waals spheres mapped onto a backbone cartoon of the β_2AR-T4L structure. (Right) Residues that are found within 4 Å of the CAMs Leu124$^{3.43}$ and Leu272$^{6.34}$ are shown as yellow spheres or dot surfaces. A vertical cross section through the structure illustrates that these surrounding residues connect the CAMs on helices III and VI with the UCMs on helix VII through packing interactions. (**B**) In both β_2AR-T4L (blue) and rhodopsin (purple), a network of ordered water molecules is found at the interface between the transmembrane helices at their cytoplasmic ends. (**C**) Network of hydrogen bonding interactions between water molecules and β_2AR-T4L residues (side chains shown as blue sticks), notably three UCMs on helix VII (orange) and one on helix II (yellow). In (B) and (C), only Ballesteros-Weinstein numbers (9) are used to identify amino acids.

of isoproterenol was placed in the binding site such that common atoms (16 to 22 in Fig. 4) were superimposed onto the analogous carazolol coordinates in the crystal structure (Fig. 5D). Residues $Ser204^{5.43}$ and $Ser207^{5.46}$ are critical for catecholamine binding and activation of the β_2AR, with $Ser204^{5.43}$ hydrogen bonding to the meta-hydroxyl and $Ser207^{5.46}$ to the para-hydroxyl of the catechol ring, respectively (*33*). In our model, the catechol hydroxyls of isoproterenol face the appropriate Ser residues on helix V, but the distances are too long for hydrogen bonding (6.8 Å from the meta-hydroxyl oxygen to the side-chain oxygen of $Ser204^{5.43}$ and 4.8 Å from the para-hydroxyl oxygen to the side-chain oxygen of $Ser207^{5.46}$). In addition, $Asn293^{6.55}$ and $Tyr308^{7.35}$, two residues expected to form selective interactions with agonists based on the literature (*34*, *35*), are too distant to form productive polar or hydrophobic contacts with the modeled isoproterenol molecule. These observations suggest that agonist binding requires changes in the binding site relative to the carazolol-bound structure, unless common structural components of agonists and inverse agonists bind in a considerably different manner.

Structural insights into β_2AR activation. Biophysical studies provide evidence that conformational changes associated with activation of the β_2AR are similar to those observed for rhodopsin (*2*, *18*, *21*, *36*). Yet the highly efficient process of light activation of rhodopsin through the cis-trans isomerization of covalently bound retinal is very different from activation of the β_2AR and other GPCRs by diffusible hormones and neurotransmitters (*2*). Despite representing a static picture of the inverse agonist–bound state, the crystal structure of β_2AR-T4L may still provide clues as to how agonist binding is translated into structural changes in the cytoplasmic domains of receptor. Agonist binding occurs at the extracellular ends of helices III, IV, V, and VII, and G protein activation is mediated by the cytoplasmic ends. Whereas the structure is open at the extracellular face to form the ligand binding pocket, the helices are more closely packed in the intracellular half of the receptor. This close packing implies that isolated rigid-body movement of any of these helices is unlikely and that conformational changes can be accomplished only by rearrangement of the side chains forming the network of interactions between the helices. Biophysical studies show that structurally different agonists stabilize distinct active states (*17*, *20*), suggesting that different ligands could stabilize different combinations of side-chain rearrangements.

Analysis of mutations that affect β_2AR function provides insights into structural rearrangements that are likely to occur during receptor activation. Figure 6A illustrates the location of amino acids for which mutations lead to elevated basal, agonist-independent activity (CAMs), as well as amino acids for which mutations impair agonist activation [uncoupling mutations (UCMs)]. Residues for which CAMs have been described are likely to be involved in interactions that maintain the receptor in the inactive conformation. These amino acids are centrally located on helices III and VI. In contrast, positions in which UCMs have been observed are likely to form intramolecular interactions that stabilize the active state. A cluster of UCMs is found at the cytoplasmic end of helix VII. Neither CAMs nor UCMs are directly involved in agonist binding. Although the CAMs and UCMs are not directly connected in sequence, it is evident from the structure that they are linked through packing interactions, so that movements in one will probably affect the packing of others. For example, Fig. 6A (right panel) shows all amino acids with atoms within 4 Å of the two centrally located CAMs, $Leu124^{3.43}$ (*37*) and $Leu272^{6.34}$ (*38*). Several amino acids that pack against these CAMs also interact with one or more UCMs. $Trp286^{6.48}$ lies at the base of the binding pocket. It has been proposed that agonist binding leads to a change in the rotameric state of $Trp286^{6.48}$, with subsequent changes in the angle of the helical kink formed by $Pro288^{6.50}$ (*39*). It is likely that an agonist-induced change in the rotameric state of $Trp286^{6.48}$ will be linked to changes in side chains of CAMs and UCMs through packing interactions and propagated to the cytoplasmic ends of the helices and the associated intracellular loops that interact with G proteins and other signaling molecules.

In the structures of both rhodopsin and the β_2AR, a cluster of water molecules lies near the most highly conserved class A GPCR residues (Fig. 6B). It has been proposed that these water molecules may play a role in the structural changes involved in receptor activation (*40*). Figure 6C shows the network of potential hydrogen bonding interactions that link $Trp286^{6.48}$ with conserved amino acids extending to the cytoplasmic ends of helices. UCMs have been identified for four amino acids linked by this network: $Asp79^{2.50}$, $Asn318^{7.45}$, $Asn322^{7.49}$, and $Y326^{7.53}$ (*41*). This relatively loose-packed, water filled region is probably important in allowing conformational transitions, as there will be fewer steric restraints to side-chain repacking. Future structures of the agonist-bound state of the β_2AR will help to clarify the precise rearrangements that accompany activation of the receptor.

Although crystallization of β_2AR-T4L in the presence of other ligands remains an exciting prospect, future efforts to obtain structures of the catecholamine-bound receptor will be challenging because of the relatively low affinity of these compounds in the absence of G protein and their chemical lability. Moreover, biophysical studies indicate that agonist binding and activation is a multistep process involving distinct conformational intermediates (*2*, *17*, *19*–*21*, *42*), which produces structural heterogeneity even at saturating concentrations of agonist. It is therefore possible that structural elucidation of the active state of the β_2AR will be possible only through crystallization of the complex between agonist, β_2AR, and Gs.

References and Notes

1. H. G. Khorana, *J. Biol. Chem.* **267**, 1 (1992).
2. B. K. Kobilka, X. Deupi, *Trends Pharmacol. Sci.* **28**, 397 (2007).
3. V. Cherezov *et al.*, *Science* **318**, 1258 (2007); published online 25 October 2007 (10.1126/science.1150577).
4. The efficacy of a ligand describes the effect of the ligand on the functional properties of a GPCR. Agonists are defined as ligands that fully activate the receptor, partial agonists induce submaximal activation even at saturating concentrations, and inverse agonists inhibit basal receptor activity. Antagonists have no effect on basal activity but competitively block access of other ligands. Carazolol is defined as a partial inverse agonist because it suppresses only 50% of the basal activity of the β_2AR.
5. S. Granier *et al.*, *J. Biol. Chem.* **282**, 13895 (2007).
6. B. K. Kobilka *et al.*, *Science* **240**, 1310 (1988).
7. X. J. Zhang, J. A. Wozniak, B. W. Matthews, *J. Mol. Biol.* **250**, 527 (1995).
8. L. H. Weaver, B. W. Matthews, *J. Mol. Biol.* **193**, 189 (1987).
9. Ballesteros-Weinstein numbering is used throughout the text as superscripts to the protein numbering. Within each helix is a single, most conserved residue among the class A GPCRs. This residue is designated x.50, where x is the number of the transmembrane helix. All other residues on that helix are numbered relative to this conserved position.
10. T. Okada *et al.*, *J. Mol. Biol.* **342**, 571 (2004).
11. M. Matsumura, W. J. Becktel, M. Levitt, B. W. Matthews, *Proc. Natl. Acad. Sci. U.S.A.* **86**, 6562 (1989).
12. F. Horn *et al.*, *Nucleic Acids Res.* **31**, 294 (2003).
13. Materials and methods and supplementary figures are available as supporting material on *Science* Online.
14. D. R. Smyth, M. K. Mrozkiewicz, W. J. McGrath, P. Listwan, B. Kobe, *Protein Sci.* **12**, 1313 (2003).
15. U. Gether *et al.*, *J. Biol. Chem.* **272**, 2587 (1997).
16. S. G. Rasmussen *et al.*, *Mol. Pharmacol.* **56**, 175 (1999).
17. P. Ghanouni *et al.*, *J. Biol. Chem.* **276**, 24433 (2001).
18. P. Ghanouni, J. J. Steenhuis, D. L. Farrens, B. K. Kobilka, *Proc. Natl. Acad. Sci. U.S.A.* **98**, 5997 (2001).
19. G. Swaminath *et al.*, *J. Biol. Chem.* **279**, 686 (2004).
20. G. Swaminath *et al.*, *J. Biol. Chem.* **280**, 22165 (2005).
21. X. Yao *et al.*, *Nat. Chem. Biol.* **2**, 417 (2006).
22. P. Samama, S. Cotecchia, T. Costa, R. J. Lefkowitz, *J. Biol. Chem.* **268**, 4625 (1993).
23. S. G. F. Rasmussen *et al.*, *Nature*, published online 21 October 2007; 10.1038/nature06325.
24. Single-letter abbreviations for the amino acid residues are as follows: A, Ala; C, Cys; D, Asp; E, Glu; F, Phe; G, Gly; H, His; I, Ile; K, Lys; L, Leu; M, Met; N, Asn; P, Pro; Q, Gln; R, Arg; S, Ser; T, Thr; V, Val; W, Trp; and Y, Tyr.
25. J. A. Ballesteros *et al.*, *J. Biol. Chem.* **276**, 29171 (2001).
26. C. D. Strader *et al.*, *Proc. Natl. Acad. Sci. U.S.A.* **84**, 4384 (1987).
27. C. D. Strader *et al.*, *J. Biol. Chem.* **263**, 10267 (1988).
28. S. Suryanarayana, B. K. Kobilka, *Mol. Pharmacol.* **44**, 111 (1993).
29. G. Liapakis *et al.*, *J. Biol. Chem.* **275**, 37779 (2000).
30. P. Chelikani *et al.*, *Proc. Natl. Acad. Sci. U.S.A.* **104**, 7027 (2007).
31. Y. Sugimoto *et al.*, *J. Pharmacol. Exp. Ther.* **301**, 51 (2002).
32. T. Frielle, K. W. Daniel, M. G. Caron, R. J. Lefkowitz, *Proc. Natl. Acad. Sci. U.S.A.* **85**, 9494 (1988).
33. C. D. Strader, M. R. Candelore, W. S. Hill, I. S. Sigal, R. A. Dixon, *J. Biol. Chem.* **264**, 13572 (1989).
34. K. Wieland, H. M. Zuurmond, C. Krasel, A. P. Ijzerman, M. J. Lohse, *Proc. Natl. Acad. Sci. U.S.A.* **93**, 9276 (1996).
35. H. Kikkawa, M. Isogaya, T. Nagao, H. Kurose, *Mol. Pharmacol.* **53**, 128 (1998).
36. U. Gether *et al.*, *EMBO J.* **16**, 6737 (1997).
37. Y. X. Tao, A. N. Abell, X. Liu, K. Nakamura, D. L. Segaloff, *Mol. Endocrinol.* **14**, 1272 (2000).
38. A. D. Jensen *et al.*, *J. Biol. Chem.* **276**, 9279 (2001).
39. L. Shi *et al.*, *J. Biol. Chem.* **277**, 40989 (2002).
40. L. Pardo, X. Deupi, N. Dolker, M. L. Lopez-Rodriguez, M. Campillo, *ChemBioChem* **8**, 19 (2007).
41. L. S. Barak, L. Menard, S. S. Ferguson, A. M. Colapietro, M. G. Caron, *Biochemistry* **34**, 15407 (1995).
42. M. J. Lohse, C. Hoffmann, V. O. Nikolaev, J. P. Vilardaga, M. Bunemann, *Adv. Protein Chem.* **74**, 167 (2007).
43. W. L. DeLano, The PyMOL Molecular Graphics System (DeLano Scientific, Palo Alto, CA, 2002), www.pymol.org.
44. A. W. Schüttelkopf, D. M. F. van Aalten, *Acta Crystallogr. D Biol. Crystallogr.* **D60**, 1355 (2004).

45. M. J. Zuscik, J. E. Porter, R. Gaivin, D. M. Perez, *J. Biol. Chem.* **273**, 3401 (1998).
46. F. Z. Chung, C. D. Wang, P. C. Potter, J. C. Venter, C. M. Fraser, *J. Biol. Chem.* **263**, 4052 (1988).
47. O. Moro, M. S. Shockley, J. Lameh, W. Sadee, *J. Biol. Chem.* **269**, 6651 (1994).
48. S. A. Green, G. Cole, M. Jacinto, M. Innis, S. B. Liggett, *J. Biol. Chem.* **268**, 23116 (1993).
49. A. M. Gabilondo *et al.*, *Proc. Natl. Acad. Sci. U.S.A.* **94**, 12285 (1997).
50. B.K.K. managed the protein design, production, and purification. R.C.S. managed lipidic cubic phase (LCP)–based crystallization and data collection methods development and experiments. D.M.R. designed, engineered, and characterized the β_2AR-T4L fusion protein; supplied protein materials for all crystallization trials; grew and collected data from the bicelle crystals; collected, processed, and refined the 3.5 Å LCP structure; refined the 2.4 Å structure; analyzed the results; and wrote the initial draft of the manuscript. V.C. developed methods for and performed LCP crystallization, LCP crystal mounting, LCP data collection, model refinement, analyzed the results, and was involved in manuscript preparation. M.A.H. designed the blind crystal screening protocol, collected the 2.4 Å data set, processed the 2.4 Å data, solved the structure by molecular replacement at 3.5 Å and 2.4 Å resolution, and was involved in manuscript preparation. S.G.F.R. assisted with β_2AR-T4L characterization and purification, as well as manuscript preparation. F.S.T. expressed β_2AR-T4L in insect cells and, together with T.S.K., performed the initial stage of β_2AR purification. H.-J.C. assisted with the refinement and comparison with the β_2AR-Fab5 structure. X.-J.Y. developed the bimane fluorescence assay. W.I.W. assisted with low-resolution data collection and processing, solved the β_2AR-T4L molecular replacement problem at 3.5 Å, supervised the 2.4 Å refinement process, and participated in structure analysis and manuscript preparation. R.C.S. additionally assisted with β_2AR-T4L crystallization, 2.4 Å data collection, structure solution, refinement, structure analysis, and manuscript preparation. B.K.K. additionally assisted with the design of the β_2AR-T4L fusion strategy, β_2AR-T4L purification, β_2AR-T4L 3.5 Å synchrotron data collection, structure analysis, and manuscript preparation. The authors thank G. Schertler for help with initial diffraction experiments on LCP crystals performed at ID-13 at the European Synchrotron Radiation Facility and P. Day for help with cell culture and immunofluorescence experiments. The use of T4L insertions in membrane proteins has also been reported by Privé and co-workers for lactose permease. This work was supported by NIH grant F32 GM082028 (to D.M.R.); the Lundbeck Foundation (to S.G.F.R); NIH Roadmap Initiative grant P50 GM073197 and Protein Structure Initiative P50 GM62411 (to R.C.S.); National Institute of Neurological Disorders and Stroke grant NS028471, the Mather Charitable Foundations, Lundbeck, and the NIH Roadmap Initiative grant R21 GM075811 (to B.K.K.). H.-J.C. and W.I.W. were supported in part by NIH grant R01 GM056169. Coordinates and structure factors for β_2AR-T4L have been deposited in the Protein Data Bank with identification code 2RH1.

Supporting Online Material

www.sciencemag.org/cgi/content/full/1150609/DC1
Materials and Methods
Figs. S1 to S6
Tables S1 to S3
References

17 September 2007; accepted 11 October 2007
Published online 25 October 2007;
10.1126/science.1150609
Include this information when citing this paper.

REPORTS

Superconducting Pair Correlations in an Amorphous Insulating Nanohoneycomb Film

M. D. Stewart Jr.,[1] Aijun Yin,[2] J. M. Xu,[1,2] James M. Valles Jr.[1]*

The Cooper pairing mechanism that binds single electrons to form pairs in metals allows electrons to circumvent the exclusion principle and condense into a single superconducting or zero-resistance state. We present results from an amorphous bismuth film system patterned with a nanohoneycomb array of holes, which undergoes a thickness-tuned insulator-superconductor transition. The insulating films exhibit activated resistances and magnetoresistance oscillations dictated by the superconducting flux quantum $h/2e$. This $2e$ period is direct evidence indicating that Cooper pairing is also responsible for electrically insulating behavior.

The 50-year-old Bardeen Cooper Schrieffer (BCS) theory (*1*) provides a microscopic description of superconductivity in metals that also generally applies to superfluidity in other systems of fermions, including liquid ^{3}He (*2*) and ultracold atomic gases (*3*). BCS theory introduced a novel phase of matter consisting of weakly bound Cooper pairs of conduction electrons that condense into a single quantum state. This phase exhibits zero dc resistance because correlations among the Cooper pairs inhibit the scattering processes normally responsible for electrical dissipation (*1*). Counterintuitively, Cooper pair formation has also been invoked to account for recently uncovered high-resistance states of matter (*4*–*8*). Moreover, these states appear in amorphous ultrathin films (*5*, *7*–*9*), where the factors favoring insulating behavior can compete with Cooper pair formation (*10*).

The question of whether Cooper pairing occurs in systems with a resistive ground state is at the heart of discussions of the insulator–to-superconductor quantum phase transition (IST). Numerous systems, including ultrathin amorphous films (*11*) and wires (*12*) and high-temperature superconducting oxides (*8*), can be tuned from an insulating phase, which has a resistance that asymptotically approaches infinity in the zero temperature limit, to a superconducting phase, which has zero resistance. The tuning parameters, which include film thickness (*11*), magnetic field (*6*), and magnetic impurities (*13*), determine the quantum ground state of the system. Consequently, the transformation is deemed a quantum, rather than a thermal, phase transition (*4*). Models of ISTs broadly separate into those that do or do not presume that Cooper pairs exist in the insulating phase. If Cooper pairs are present, then models include only Bose degrees of freedom and Cooper pairs and vortices, and the IST occurs through Bose condensation (*4*). If not, then the microscopic interactions among the fermionic degrees of freedom, electrons, must be considered, and the very formation of pairs can dominate the IST (*14*). Intermediate models of bosons within a dissipative background of fermions have also been developed (*15*). However, opinions differ widely on which scenario applies for amorphous film systems, because some experiments support a boson-only picture and others do not. Electron tunneling measurements suggest that Cooper pairs first appear at the same thickness as superconductivity in thin elemental films, in support of fermionic models (*16*). On the other hand, signatures in the magnetoresistance of other amorphous films suggest that vortices (*17*) and/or Cooper pairs (*5*–*7*) can persist well into an insulating phase.

We have studied a set of films that undergo an IST and can be probed directly for Cooper pairs in their insulating phase. Our films consist of an ultrathin amorphous metal patterned with a nanometer honeycomb (NHC) array of holes, which are tuned to pass from an insulating to a superconducting state by increasing their thickness. The resistive phases of systems that also exhibit a superconducting phase have been scrutinized for Cooper pairs using Nernst-effect measurements of vortex motion (*18*), electron tunneling measurements of the density of states (*16*), and ac conductivity measurements (*19*). These reveal at least the presence of pairing fluctuations. It is desirable, however, to devise a detection scheme that is sensitive to the spatial phase coherence of the pair wavefunction and thus to long-lived Cooper pairs. We constructed a simple but effective platform, which relies on the magnetic field dependence of the pair wavefunction phase

[1]Department of Physics, Brown University, 182 Hope Street, Providence, RI 02912, USA. [2]Division of Engineering, Brown University, 182 Hope Street, Providence, RI 02912, USA.

*To whom correspondence should be addressed. E-mail: valles@physics.brown.edu

(*20*–*22*). In a magnetic vector potential $\vec{A}$, the phase varies in space according to $\phi_2 - \phi_1 = \frac{2e}{\hbar}\int(\vec{A} + \mu_0\lambda^2\vec{J}_s)\cdot d\vec{x}$, where $\vec{J}_s$ is the superfluid current and λ is the penetration depth. This relation plus the requirement that the phase be single-valued at any point leads to magnetic flux quantization. For superconductors patterned with an ordered array of holes, this combination causes their free energy and transport properties to oscillate in an applied magnetic field with a period of $h/2eS$, where S is the area of a unit cell. Nonsuperconducting systems containing Cooper pairs can also exhibit magneto-oscillations, provided that the pair phase-coherence length exceeds the hole spacing. Correspondingly, patterning the holes as closely spaced as possible enhances the sensitivity to Cooper pairs.

To create films with a nanometer-scale hole array, we used a templated growth method analogous to that used to form metal nanowires on carbon nanotubes (*12*). We quenched deposit from vapor Sb followed by Bi onto a cooled [temperature (T) = 8 K] anodized aluminum oxide substrate previously structured with an NHC array of holes (*23*). The data presented here primarily come from a series of films with hole radius (r_{hole}) = 27 nm and thicknesses (d_{Bi}) $1.09 < d_{Bi} < 1.3$ nm (*23*).

With increasing Bi thickness, both the unpatterned and NHC films pass from insulating to superconducting states (Fig. 1, A and B, respectively). In each case, the sheet resistance $R(T)$ transitions from insulating-like ($dR/dT < 0$) to superconducting-like ($dR/dT > 0$) at the lowest temperatures, but the transitions differ in important details. The IST of the unpatterned film occurs first at $d_{Bi} = 0.72$ nm. Nearest its IST, the conductance of its insulating phase decreases logarithmically with decreasing temperature, in agreement with previous results on these amorphous films (*24*). In contrast, the IST for NHC films occurs at $d_{Bi} = 1.27$ nm, and its superconducting state emerges from an insulator whose resistance rises exponentially to the lowest measurement temperatures (Fig. 1C). In the thinnest films, this rise is monotonic, whereas closer to the IST, a minimum intercedes. The lowest-temperature data fit well to $R = R_0\exp(T_0/T)^{\chi}$, with $\chi = 1$ and a single $R_0 \sim 6.2\ k\Omega$. Data from the series of NHC films with $r_{hole} = 23$ nm show that the activated behavior extends to at least 0.1 K. The activation energies, T_0, decrease from 4 K in the thinnest film to nearly zero at the IST.

The magnetoresistances, $R(H)$, of insulating NHC films near the IST oscillate with a well-defined period, $H_M = 0.23$ T, which we have used to normalize the H axis in Fig. 2A. Each $R(H)$ exhibits six or more discernible oscillations that decay into a rising background. The oscillations first appear at $d_{Bi} \approx 1.16$ nm, near where the minimum in the $R(T)$ is developed. However, experiments on the smaller hole size indicate that the oscillations need not be associated with the development of the minimum. Figure 2, B and C, show the $R(T)$ at $H = 0$, $H_M/2$, and H_M for a film with and without a minimum, respectively, each showing that the $R(T)$ maintains an activated form $H \neq 0$, but T_0 varies and is larger at $f = 1/2$ than at $f = 0$ or 1, where $f = H/H_M$. By comparison, the prefactor R_0 varies only slightly with field. Thus, the $R(H)$ oscillations primarily reflect T_0 oscillations and correspondingly, their amplitude grows exponentially as T decreases. In addition, Fig. 2, B and C, show that the amplitude of the magneto-oscillations decreases with increasing normal state resistance. Finally, Fig. 3 exhibits the variation of $T_0(0)$, $T_0(1/2)$ and the

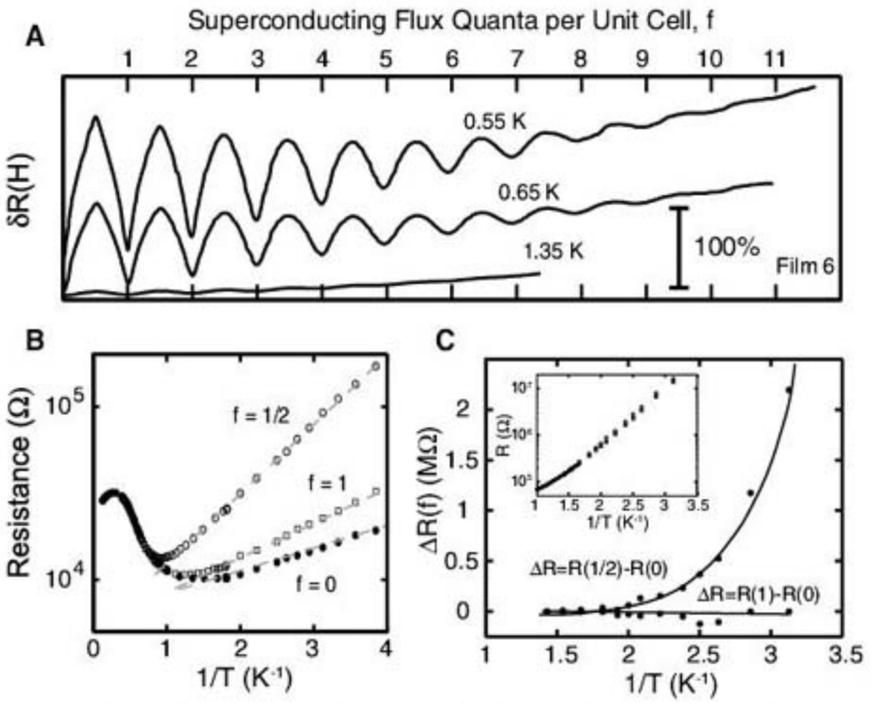

Fig. 2. Magnetic field effects on transport. **(A)** Normalized magnetoresistance oscillations for one of the NHC films (no. 6) at three different temperatures. The frustration axis has been normalized by $h/2eS$, where S is the area of a unit cell (see Fig. 1B). **(B)** Arrhenius plot of resistance for the same film, showing that the magnetoresistance oscillations in (A) arise as a result of oscillations of the activation energy with magnetic field. Dashed gray lines are fits to the data. $f = 0$ data are shown as solid circles, $f = 1/2$ as open circles, and $f = 1$ as squares. **(C)** Difference in resistance observed in different fields as a function of temperature in a film with $r_{hole} = 23$ nm and no minimum in the $R(T,H = 0)$ shown as an inset.

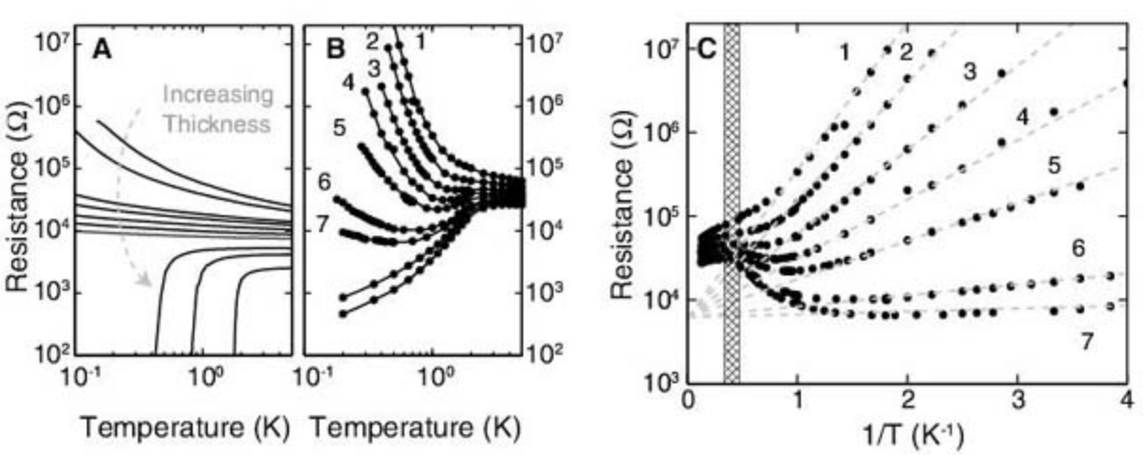

Fig. 1. Electronic transport. **(A)** IST of unpatterned a-Bi/Sb films produced simultaneously with NHC films. From top to bottom, d_{Bi} = 0.57, 0.59, 0.63, 0.65, 0.67, 0.69, 0.7, 0.74, 0.81, and 0.95 nm. There is no deviation in this data from that in the literature. **(B)** IST of a-Bi/Sb NHC films with d_{Bi} = 1.09, 1.13, 1.16, 1.17, 1.20, 1.24, 1.27, 1.3, and 1.32 nm from top to bottom. Lines are guides to the eye. **(C)** Arrhenius plot of resistance versus inverse temperature for the insulating films in (B) and fits to the Arrhenius form (gray dashed lines). The hatched area reflects the range of transition temperatures for the unpatterned films for this range of thickness. Films 1 to 7 have activation energies T_0 = 4.05, 3.30, 2.30, 1.62, 1.05, 0.30, and 0.08 K, respectively.

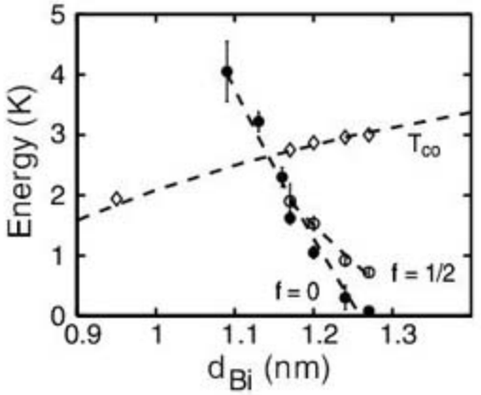

Fig. 3. Energy scales derived from the data (r_{hole} = 27 nm). Activation energies in $f = 0$ are shown as solid circles. For those films exhibiting magnetoresistance oscillations, activation energies for $f = 1/2$ are shown as open circles. The critical temperature for unpatterned films is shown as diamonds.

mean field transition temperature of the reference film T_{c0} (*24*) with d_{Bi}. It illustrates the range over which the combination of oscillations and exponential localization has been observed and suggests that the IST occurs as $T_0(0) \rightarrow 0$ with metallicity $[R(T, f = 0) = R_C \approx R_0]$ at the critical point.

These observations imply that the insulating phase near the IST consists of localized Cooper pairs that are phase-coherent over distances exceeding the interhole spacing. The period $H_M \approx h/2eS$ corresponds to one superconducting flux quantum, $\phi_0 = h/2e$, per unit cell area, S, of the array (fig. S1B), consistent with Cooper pairing (*20*, *21*). In the range of d_{Bi} where oscillations are observed, T_{c0} is comparable to the temperature at which $R(T)$ begins to decrease, strongly suggesting that pairing fluctuations begin at a relatively high temperature (*9*) to enhance the conductance. Subsequently, pairs form, becoming locally phase-coherent and spatially localized at low temperatures. We should add that localized Cooper pairs might also be present but not detectable in thinner films if their localization length is less than the interhole spacing.

The data indicate that Cooper pairs not only influence the transport process in the insulating films but, in fact, are the primary charge carriers. First, the continuous variation and size of T_0 near the IST tends to rule out a quasi-particle transport mechanism of the type exhibited in some granular films (*25*). The superconducting energy gap $\Delta_0 \cong 1.7\ k_B T_{c0}$ (*1*) is the expected activation energy for quasi-particle tunneling. Here Δ_0 is too large ($1.7\ k_B T_{c0} \gg T_0$) and varies too little over the d_{Bi} range of the oscillations to be associated with T_0. Second, the amplitude and phase of the magnetoresistance oscillations support a Cooper pair transport process. Oscillations with an $h/2eS$ period can also occur in both weakly and strongly localized normal metal systems. In both cases, their amplitude is very small (<1%) compared with those observed here (*26*). This difference reflects the much shorter phase-coherence length for single electrons as compared to that for Cooper pairs. Moreover, the phase of the oscillations in the strongly localized case is such that $R(H)$ first decreases (*26*), opposite to that in Fig. 2A. Instead, the phase here is consistent with field-induced screening currents reducing the effective Josephson coupling in the films (*27*) and thus decreasing the coherence of the Cooper pairs.

The activated resistances and $T_0(H)$ oscillations are reminiscent of those observed in lithographically defined Josephson junction arrays (JJAs) (*28*), where Cooper pair localization (CPL) naturally occurs if Coulomb interactions dominate Josephson coupling processes (*4*, *28*). This qualitative agreement suggests that a similar competition drives CPL in NHC films. In JJAs, well-defined inter-island capacitances control the repulsive charging energies, E_C, and inter-island tunneling rates control the Josephson coupling energy, E_J. Tuning $E_J < E_C$ creates a localized Cooper pair phase characterized by an activation energy that depends on E_C and oscillates with magnetic field. The field dependence suggests that an additional "phase" or E_J term also contributes to the activation energy (*27*). In NHC films, the links between nodes could dictate E_J. An estimate of E_C, however, indicates the necessity to consider more than a "lumped element" model to describe the NHC film CPL. Specifically, taking the nodal regions in the honeycomb array to be islands of diameter $L \approx 50$ nm, the estimated charging energy is $E_C = 4e^2/\varepsilon_0 \varepsilon L \approx 10^4\ \mathrm{K}/\varepsilon$, where ε is the dielectric constant and ε_0 is the vacuum permittivity. Even for ε as large as 100, E_C far exceeds all pairing-energy scales (for example, $T_{c0} \approx 2$ K) and thus cannot be directly relevant to this competition. Alternatively, this calculation implies that the pairs localize to islands that encompass a large number (thousands) of holes and thus are not associated with any obvious structure.

The data suggest that superconducting islands, without relation to any structure, may spontaneously form near the IST as experiments (*24*, *29*) and theory (*14*) suggest, through disorder-induced fluctuations in the amplitude of the order parameter (*14*). This tendency to form islands and their influence on the IST could be accentuated by the NHC substrate. The reduction in film area caused by the holes can inhibit "percolation," and the small thickness variations, $\delta d_{Bi}/d_{Bi} = 20\%$ due to the undulations in the substrate (*23*), may enhance order-parameter variations. Using $T_{c0}(d_{Bi})$ at 2 K (Fig. 3), we estimate this contribution to order-parameter variations, $\delta T_{c0}/T_{c0}$, to be as large as 40%.

The coincidence of the 2*e*-based oscillations with activated resistances and "quasi-reentrance" suggests the latter two observations as possible signatures of boson localization in unpatterned films. Interestingly, activated resistances (*7*) and quasi-reentrance (*6*) appear in the magnetic field–tuned IST of indium oxide, which those authors suggest is driven by CPL. These similarities across materials and ISTs hint that the NHC patterning and the application of magnetic fields induce similar fluctuations of the order-parameter amplitude. Moreover the present results both provide the clearest example of Cooper pair localization in an amorphous system to date and suggest a general approach to directly detecting their presence in other nonsuperconducting systems such as underdoped high-T_c superconductors above T_c (*18*).

References and Notes

1. J. Bardeen, L. N. Cooper, J. R. Schrieffer, *Phys. Rev.* **108**, 1175 (1957).
2. A. J. Leggett, *Rev. Mod. Phys.* **47**, 331 (1975).
3. M. W. Zwierlein, J. R. Abo-Shaeer, A. Schirotzek, C. H. Schunck, W. Ketterle, *Nature* **435**, 1047 (2005).
4. M. P. A. Fisher, *Phys. Rev. Lett.* **65**, 923 (1990).
5. V. V. Gantmakher, M. v. Golubkov, V. T. Dolgopolov, G. E. Tsydynzhaov, A. A. Shashkin, *J. Exp. Theor. Phys.* **68**, 363 (1998).
6. A. F. Hebard, M. A. Paalanen, *Phys. Rev. Lett.* **65**, 927 (1990).
7. G. Sambandamurthy, L. W. Engel, A. Johansson, D. Shahar, *Phys. Rev. Lett.* **92**, 107005 (2004).
8. M. A. Steiner, G. Boebinger, A. Kapitulnik, *Phys. Rev. Lett.* **94**, 107008 (2005).
9. C. Christiansen, L. M. Hernandez, A. M. Goldman, *Phys. Rev. Lett.* **88**, 037004 (2002).
10. D. Belitz, T. R. Kirkpatrick, *Rev. Mod. Phys.* **66**, 261 (1994).
11. D. B. Haviland, Y. Liu, A. M. Goldman, *Phys. Rev. Lett.* **62**, 2180 (1989).
12. A. Bezryadin, C. N. Lau, M. Tinkham, *Nature* **404**, 971 (2000).
13. J. S. Parker, D. E. Read, A. Kumar, P. Xiong, *Europhys. Lett.* **75**, 950 (2006).
14. A. Ghosal, M. Randeria, N. Trivedi, *Phys. Rev. B* **65**, 014501 (2001).
15. A. Yazdani, A. Kapitulnik, *Phys. Rev. Lett.* **74**, 3037 (1995).
16. J. M. Valles, R. C. Dynes, J. P. Garno, *Phys. Rev. Lett.* **69**, 3567 (1992).
17. N. Marković, A. M. Mack, G. Martinez-Arizala, C. Christiansen, A. M. Goldman, *Phys. Rev. Lett.* **81**, 701 (1998).
18. Z. A. Xu, N. P. Ong, Y. Wang, T. Kakeshita, S. Uchida, *Nature* **406**, 486 (2000).
19. R. Crane *et al.*, *Phys. Rev. B* **75**, 184530 (2007).
20. B. S. Deaver, W. M. Fairbank, *Phys. Rev. Lett.* **7**, 43 (1961).
21. R. Doll, M. Näbauer, *Phys. Rev. Lett.* **7**, 51 (1961).
22. W. A. Little, R. D. Parks, *Phys. Rev. Lett.* **9**, 9 (1962).
23. Materials and methods are available as supporting material on *Science* Online.
24. J. A. Chervenak, J. M. Valles, *Phys. Rev. B* **59**, 11209 (1999).
25. R. P. Barber Jr., S.-Y. Hsu, J. M. Valles Jr., R. C. Dynes, R. E. Glover III, *Phys. Rev. B* **73**, 134516 (2006).
26. A. G. Aronov, Y. V. Sharvin, *Rev. Mod. Phys.* **59**, 755 (1987).
27. P. Delsing, C. D. Chen, D. B. Haviland, Y. Harada, T. Claeson, *Phys. Rev. B* **50**, 3959 (1994).
28. L. J. Geerligs, M. Peters, L. E. M. de Groot, A. Verbruggen, J. E. Mooij, *Phys. Rev. Lett.* **63**, 326 (1989).
29. D. Kowal, Z. Ovadyahu, *Solid State Commun.* **90**, 783 (1994).

30. We are grateful to L. N. Cooper, D. Feldman, M. Feigelman, I. Beloborodov, and R. Barber for helpful discussions. This work has been supported by NSF through grants DMR-0203608 and DMR-0605797, by the Air Force Research Laboratory, and by the Office of Naval Research.

Supporting Online Material

www.sciencemag.org/cgi/content/full/318/5854/1273/DC1
Materials and Methods
Fig. S1
References

22 August 2007; accepted 16 October 2007
10.1126/science.1149587

End-to-End Stacking and Liquid Crystal Condensation of 6–to 20–Base Pair DNA Duplexes

Michi Nakata,[1]*† Giuliano Zanchetta,[2]* Brandon D. Chapman,[3] Christopher D. Jones,[1] Julie O. Cross,[4] Ronald Pindak,[3] Tommaso Bellini,[2]‡ Noel A. Clark[1]‡

Short complementary B-form DNA oligomers, 6 to 20 base pairs in length, are found to exhibit nematic and columnar liquid crystal phases, even though such duplexes lack the shape anisotropy required for liquid crystal ordering. Structural study shows that these phases are produced by the end-to-end adhesion and consequent stacking of the duplex oligomers into polydisperse anisotropic rod-shaped aggregates, which can order into liquid crystals. Upon cooling mixed solutions of short DNA oligomers, in which only a small fraction of the DNA present is complementary, the duplex-forming oligomers phase-separate into liquid crystal droplets, leaving the unpaired single strands in isotropic solution. In a chemical environment where oligomer ligation is possible, such ordering and condensation would provide an autocatalytic link whereby complementarity promotes the extended polymerization of complementary oligomers.

The ability of duplex DNA to form liquid crystal (LC) phases when hydrated has been known since the late 1940s and played a crucial role in deciphering its structure, enabling alignment of the DNA chains and measurement of the x-ray structure factor of a single chain uncomplicated by interchain correlations (*1*–*3*). Since that time, the LC phases of solutions of duplex B-form DNA (B-DNA) have been extensively characterized by optical (*4*–*9*), x-ray (*10*), and magnetic resonance (*11*, *12*) methods for chain lengths N, ranging from mega–base pair (bp) semiflexible polymers down to approximately 100 bp rigid rodlike segments, comparable in size to the B-DNA bend persistence length, $\Lambda_p \sim 50$ nm (*13*). These studies of long DNA (lDNA) have revealed an isotropic phase (I); chiral nematic (N), uniaxial columnar (C_U), and higher-ordered columnar (C_2) liquid crystal phases; and crystal (X) phases, with increasing DNA concentration.

The appearance of such LC phases has been accounted for theoretically by modeling B-DNA as a repulsive rigid or semiflexible rod-shaped solute. The basic model is Onsager's treatment of monodisperse repulsive hard rods (length L, diameter D) (*14*), which, if they are sufficiently anisotropic in shape, nematic order for volume fraction $\varphi > \varphi_{I\text{-}N} = 4D/L \approx 24/N$ ($D \sim 2$ nm, $L \sim N/3$ nm for B-DNA). The complete computer-simulated phase diagram for hard rods by Bolhuis and Frenkel (*15*) quantitatively confirms this prediction for $L/D > 4.7$ ($N > 28$ bp) and also shows that for $L/D < 4.7$ there should be no LC phases at any φ. We were therefore surprised to find nematic LC ordering in short B-DNA duplexes (sDNA) of length 6 bp $< N <$ 20 bp, with the nematic phase appearing for N values an order of magnitude smaller than those predicted from φ_{IN}, precluding ordering by the Onsager-Bolhuis-Frenkel (OBF) criterion. A similar conclusion was reached by Alam and Drobny in attempting to account for a magnetically reorientable, orientationally ordered phase in nuclear magnetic resonance studies of a B-DNA dodecamer (*12*). Additionally, we have observed columnar LC ordering for these oligomers, which is also notable, because in the hard-rod models (*15*), the only translationally ordered LC phase appearing is the lamellar smectic A (SmA). We show that the observation of the nematic and columnar LC phases provides clear evidence for end-to-end stacking of the sDNA into rod-shaped aggregates. The sensitivity of the aggregation to complementarity leads directly to a means of phase separation of complementary sDNA duplexes from a solution of complementary and noncomplementary oligomers.

We studied the series of self-complementary sDNA duplex-forming "palindromic" oligomers shown in Fig. 1, along with a variety of noncomplementary and partially complementary oligomers (*16*). sDNA solutions in gaps of thickness t between glass plates (4 μm $< t <$ 8 μm) were observed by (i) depolarized transmission light microscopy (DTLM) to probe optical textures, (ii)

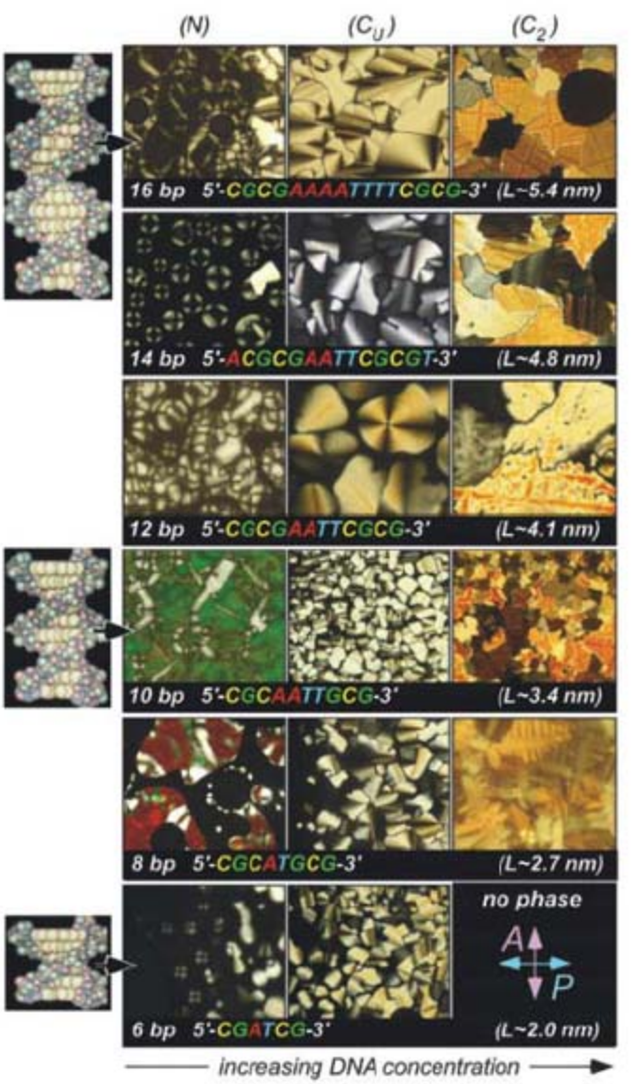

Fig. 1. Optical textures of the LC phases of a series of solutions of sDNA of increasing length obtained by depolarized light microscopy. Samples thickness is in the range 4 μm $< t <$ 8 μm, between glass plates. Isotropic (I) regions are black. The chiral nematic phase (N) appears as fluid birefringent domains when its helix pitch is a few microns or longer, or, when the pitch is shorter than ~400 nm, as a Grandjean texture with "oily streaks" exhibiting visible light selective reflection from the macroscopic optic axis helix (8 bp, 10 bp). The columnar C_U phase is identified by its smooth developable domains, a consequence of the uniaxial symmetry and splay expulsion of the columnar ordering. At yet higher DNA concentration, the C_2 phase exhibits dendritic growth forms, indicative of lower symmetry and more solidlike ordering. The width of each image is 120 μm.

[1]Department of Physics and Liquid Crystal Materials Research Center, University of Colorado, Boulder, CO 80309–0390, USA. [2]Dipartimento di Chimica, Biochimica e Biotecnologie per la Medicina, Università di Milano, Milano, Italy. [3]National Synchrotron Light Source, Brookhaven National Laboratory, Upton, NY 11973, USA. [4]Advanced Photon Source, Argonne National Laboratory, Argonne, IL 60439, USA.

*These authors contributed equally to this work.
†Deceased.
‡To whom correspondence should be addressed. E-mail: tommaso.bellini@unimi.it (T.B.); noel.clark@colorado.edu (N.A.C.)

optical reflection interferometry (ORI) to measure refractive indices and thus DNA concentration c (mg solute/ml solution), and (iii) synchrotron microbeam x-ray diffraction (XRD) to probe local molecular organization. Despite the challenges presented by the extremely small sDNA sample quantities available, these techniques provided unambiguous evidence for the N and C_U liquid crystal phases in the sDNA solutions. At higher concentration, more ordered C_2 and X-like phases, which are yet to be characterized, were also found. Figure 1 shows DTLM images of the typical textures. Observation of the local optical texture and ORI measurement of the local concentration of the palindromic oligomers enabled construction of the N-c phase diagrams of Fig. 2 and figs. S1 and S2 (*16*). Figure 2 combines the phase boundaries measured for sDNA with those obtained from the literature for lDNA (fig. S1A), along with the predictions from the Onsager and other models of interacting semiflexible rod-shaped particle and aggregate solutes (fig. S1B). The sDNA solutions exhibited thermotropic mesomorphism, melting at sufficiently high temperature, T, to the optically isotropic liquid (I) phase. This is shown in fig. S2, where we plot T_{LC}, the highest T at which the N and C_U phases are found. T_{LC} grows with N and, for each oligomer, is higher for the C_U phase (*16*).

Figure 2 shows that LC phases are found in the sub-Onsager region of the phase diagram of sDNA where they are not expected on the basis of duplex shape. When analyzed in the context of the extensive body of theory of the phase behavior of interacting rods, semiflexible polymers, and self-assembled linear aggregates, this phase diagram presents clear evidence that the origin of the LC phases in sDNA is the equilibrium end-to-end physical aggregation (living polymerization) of short duplexes into extended duplex units that are long and rigid enough to order. The key observations are as follows: (i) The sDNA LC phases have all the basic features of the LC ordering of lDNA: N phase, a state of negative optical anisotropy, miscible with the lDNA nematic and exhibiting a chiral helical precession of the director producing Bragg reflection (Fig. 1 and fig. S3); C_u phase, at higher concentration, an optically uniaxial phase exhibiting an XRD structure of hexagonally packed columns lacking positional correlation along their axes (fig. S4). (ii) Nematic and columnar LC ordering can be induced in weakly anisotropic solutes by equilibrium end-to-end self-assembly, that is, living polymerization of the oligomers into linear chains of particles (*17*–*19*). Computer simulations (*18*–*20*) show that for sufficiently rigid aggregate chains, the I-N transition occurs according to the OBF prediction if the average aggregate length $\langle L \rangle$ is used in the OBF model [green dots and construction in Fig. 2A (*18*)]. Rigidity is a key requirement, because even infinitely long flexible hard rods (*21*) must have a sufficiently long persistence length for a nematic phase to appear ($\Lambda_p > \sim 10\ D$). (iii) End-to-end adhesion suppresses the lamellar SmA phase predicted for monodisperse hard rods by favoring end-to-end rather than side-by-side positional correlations and by introducing unavoidable length polydispersity into the ordering units, both effects reducing the entropic free energy gain of lamellar ordering. (iv) Estimates of the stacking energy between duplexes are consistent with end-to-end attraction resulting from the hydrophobicity of the faces of their terminal base pairs (*16*, *22*). This sort of assembly is familiar in crystalline sDNA (*23*) and in sDNA/protein complexes (*24*, *25*), as well as in chromonic LCs (*26*), and has been extensively studied for particular DNA bases; for example, guanosine forms H-bonded tetramers, which aggregate into stacks (*27*). We show here that such aggregation, sketched in Fig. 3A, can have a substantial effect on the organization and phase behavior of B-form DNA. Although the duplexes individually are not anisotropic enough in steric shape to produce LC phases, the hydrophobic ends cause the formation of much more anisotropic assemblies that can orientationally and positionally order.

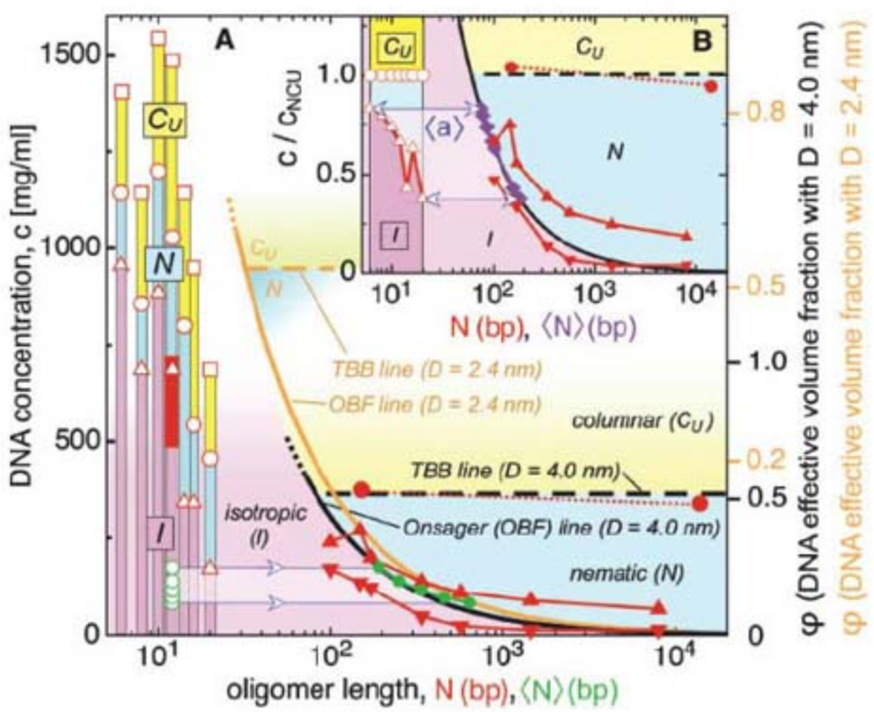

Fig. 2. Experimental c (DNA concentration, mg solute/ml solution) - N (oligomer length) phase behavior for short and long DNA (sDNA and lDNA, respectively) (fig. S1A), along with the theoretical behavior from several models of interacting rodlike particles (fig. S1B). **(A)** The solid red triangles and solid red curve bound the measured I-N phase coexistence for lDNA ($N > 100$) (*8*, *11*). The solid red circles and red dotted line give the measured N-C_U phase boundary of lDNA (*7*, *10*). For $N < 20$, phase transitions from our data are marked by red open symbols (I-N, triangles; N-C_U, circles; C_U-C_2, squares), and the range of each phase is indicated by colored columns (I, magenta; N, cyan, C_U, yellow), at $T = 20°C$ for $20 > N > 8$ and $T = 10°C$ for $N = 6$. The range of the $N = 12$ LC phase of (*12*) is given by the solid red rectangle. Theoretical phase boundaries for these transitions from model systems are shown for two choices of the volume fraction φ axis, one with the DNA effective electrostatic diameter $D = 4.0$ nm (heavy black lines/labels), applicable at low c, and the other with the DNA chemical diameter $D = 2.4$ nm (*21*) (heavy orange lines/labels), applicable at high c, i.e., small N. The $D = 4.0$ nm phase diagram [black OBF I-N line and dashed black TBB N-C_U line (fig S1) (*15*, *17*–*19*)] accounts well for the lDNA I-N and N-C_U data. The open and closed green dots represent, respectively, the spherical particles of the Lu and Kindt simulations [$L = D = 4.0$ nm (*18*)], and their effective aggregate lengths $\langle N \rangle$ at the I-N transition. **(B)** The c-N phase diagram of (A), but with c scaled with respect to $c_{N\text{-}CU}$, enabling an estimate of the length $\langle N \rangle$ (purple diamonds), and aggregation number $\langle a \rangle$ (blue arrows) in the sDNA aggregates.

Figure 2A shows that the lDNA I-N phase boundary measured for 100 bp < N < 8000 bp (*8*, *11*) is in reasonable agreement with the simple Onsager rigid-rod limit (OBF line, fig. S1) if the effective double-helix diameter is taken to be $D_{eff} = 4.0$ nm to account for the electrostatic repulsion between chains at low c (*8*). The choice $D_{eff} = 4.0$ nm also puts the lDNA experimental N-C_U phase boundary (*7*, *10*) at $\varphi_{N\text{-}CU} = 0.55$, in agreement with models of long polydisperse rods [Taylor, Bates, Bohle (TBB) line] (fig. S1) (*17*, *28*, *29*). However, as the oligomer length is decreased, the C_U phase and the nematic phase persist for duplexes as short as $N = 6$, although the c required to obtain these phases increases with decreasing N. For $N = 6$, the N-C_U transition is found at c = 1,200 mg/ml, about two-thirds that of neat duplex DNA $c_{DNA} = \rho_{DNA} = 1{,}800$ mg/ml (*30*). Thus, the LC phases of the oligomers of

smallest N may be better viewed as being like thermotropic LC phases, their interaxial distance approaching the chemical diameter (*10*, *31*) where steric repulsion dominates the interchain interactions. Hence, the increasing $\varphi_{N\text{-}CU}$ observed with decreasing N indicates that the effective chain diameter decreases, evolving from $D \sim 4.0$ nm to $D \sim 2.4$ nm. This change shifts the model phase boundaries in Fig. 2A to higher concentration (black φ scale → orange φ scale) to account for the increased concentration necessary for LC phase formation. The open green dots represent the spherical particles of Lu and Kindt (*18*) ($L = D = 4.0$ nm), and the construction with the closed green dots gives $\langle N \rangle$, the effective lengths in base pairs of the aggregates at which the N phase appears in their simulations. These lengths match the OBF line well, indicating that the model aggregates behave effectively as hard rods, justifying the similar construction in Fig. 2B.

This effective diameter variation is scaled out in Fig. 2B, where the c axis is normalized by $c_{N\text{-}CU}$, assuming the sDNA concentration at the N-C_U transition ($c_{N\text{-}CU}$) to correspond, for each oligomer, to an effective volume fraction $\varphi_{N\text{-}C} \sim 0.55$ (*17*–*19*). That is, we select the appropriate D for a given oligomer by requiring the N-C_U transition to occur at $\varphi \sim 0.55$. Figure 2B then enables analysis of the sDNA end-to-end stacking, because once the effective volume fraction is held by the strict requirement placed by the N-C_U transition, the amount of linear aggregation can be evaluated by horizontally projecting the I-N data points onto the black OBF line (blue arrows) for linear aggregation. The blue arrow construction thus gives an estimate of $\langle N \rangle$ (purple diamonds), and $\langle a \rangle$ (blue arrows), respectively the mean number of base pairs and the mean number of duplex oligomers in an aggregate necessary to generate an Onsager nematic. For $N = 6$, 8, 10, 12, 14, 16, and 20 bp, oligomers $\langle a \rangle$ and $\langle N \rangle$, obtained from Fig. 2B, are, respectively, $\langle a \rangle = 12$, 9, 9, 8, 11, 6, and 9 bp and $\langle N \rangle = 75$, 80, 87, 97, 100, 160, and 180 bp. The decreasing aggregate length needed for nematic order for shorter oligomers is a result of their higher concentration. The aggregation number does not depend strongly on N. Figure 2B also shows that the nematic range decreases, and thus that the flexibility of the aggregates increases with decreasing N (*20*, *21*).

From these lengths and the sDNA concentrations, it is possible to estimate the end-to-end stacking energy ΔE_S between the duplexes, where ΔE_S represents the difference between the energy of a stacked pair of duplexes relative to their mean status, which is strong repulsion, as shown by the substantial osmotic pressures in the N and C_U phases in the experiments of Podgornik *et al.* (*10*). Estimates for ΔE_S from expressions proposed to describe the living polymer mean aggregate length (*18*, *22*, *32*) lead to $4\ k_BT < \Delta E_S < 8\ k_BT$ per contact [equations S2 to S5 (*16*)], in addition to $T\Delta S_\theta$, $\sim 6\ k_BT$, the minimal orientational free energy cost of establishing common duplex axes in an aggregate (equation S1). None of the estimates show significant N dependence.

The requirement of developing sufficient shape anisotropy and rigidity in the aggregate units puts considerable constraints on the sDNA structure in order for LC phases to appear. Thus, sequence substitutions reducing the ability of the sDNA duplexes to form linear rigid aggregates will reduce the stability of the LC phases. For example, the addition of unpaired bases at the sDNA duplex ends, eliminates LC ordering by weakening end-to-end adhesion (*16*). This interplay of sequence and LC ordering leads to a remarkable means of condensation of complementary sDNA duplexes from mixed solutions of complementary and noncomplementary oligomers. This process is sketched in and demonstrated in Fig. 3C for a mixture of the mutually complementary, but not self-complementary, CCTCAAAACTCC (Z) + GGAGTTTTGAGG (Y) 12-nucleotide oligomers. In such a solution, at $T < T_m$, the DNA denaturation temperature, the complementary pairs form rigid duplexes that have a tendency to aggregate end-to-end, whereas the noncomplementary oligomers remain as flexible single strands. The LC ordering shows up via a first-order phase transition in which the appearance of the LC transition is accompanied by nearly complete phase separation of the duplexes into the LC domains, with the highly flexible (*33*) single strands left unbound in the isotropic phase. This phase separation can be understood on the basis of either the depletion interaction (*34*) or the immiscibility of rigid and flexible polymer solutes (*35*, *16*). If there is a large excess of noncomplementary oligomers, in this case $c_Y/c_Z = 10$, the LC phase appears as isolated drops (Fig. 3D). The dependence of the phase behavior on T and c, the area of the droplets, and the similarity of their birefringence to that of the C_U phase in complementary solutions indicate that the duplexes are essentially insoluble in the isotropic and that the single-stranded DNA is essentially insoluble in the LC, as expected from theory (*35*).

This LC ordering thus requires the end-to-end stacking of the duplex sDNA into semirigid linear aggregates, which in turn means that within the LC drops the terminal groups on neighboring oligomers are close to each other and thus that their effective concentration is much higher than in the surrounding isotropic (*16*). This observation has potential implications for the prebiotic chemical generation of complementarily H-bonded molecular assemblies. In the presence of appropriate ligation chemistry, inorganic catalysts, for example (*36*), this concentration enhancement should strongly pro-

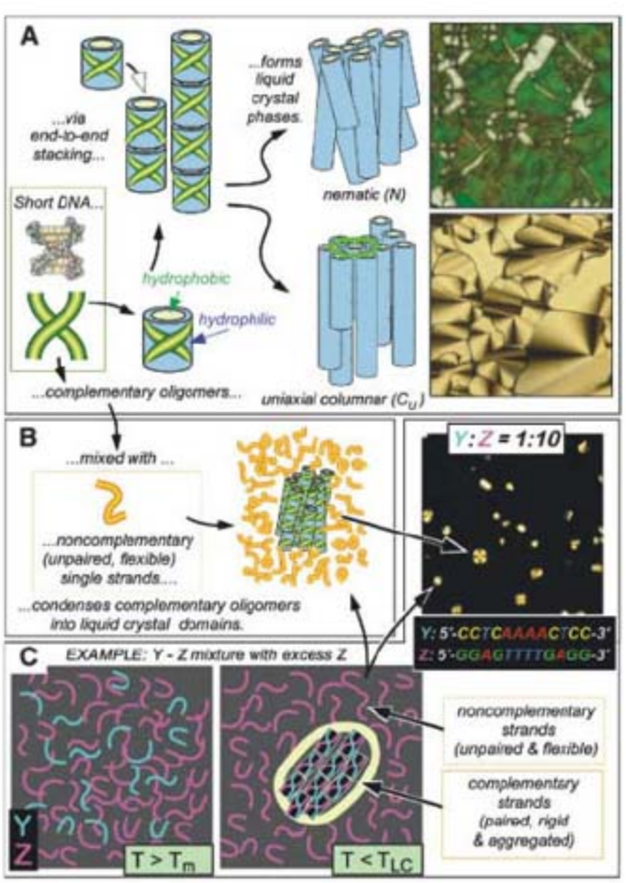

Fig. 3. **(A)** Nano-length B-DNA duplexes can be idealized as hydrophilic cylinders with hydrophobic ends capable of end-to-end adhesion and stacking into units sufficiently anisotropic to orientationally and positionally order into LC phases. The N phase is formed at lower concentration and the C_U phase at higher concentration. **(B)** Upon cooling a mixture of complementary (yellow/green) and noncomplementary (yellow/orange) single-stranded sDNAs, the complementary oligomers base pair to form duplexes, which then assemble as in (A) and phase-separate into LC domains. One way to achieve this is shown in **(C)**, a 1:10 [Y (cyan): Z (magenta)] mixture of mutually complementary, but not self complementary, 12-nucleotide oligomers. Duplexes form upon cooling below their denaturation temperature T_m, and the LC phase appears below T_{LC} through a first-order phase transition, in this case a C_U phase. With one of the oligomer species in excess, in this case Z, the transition to the LC phase is marked by the appearance of isolated LC (C_U) domains that sequester all of the other complementary oligomer, in this case Y, into LC droplets. (C) shows a resulting DTLM image of LC domains. In the 1:10 case, the LC birefringence (comparable to that of the C_U phase in a 1:1 mixture) and the ~7% area occupied by LC domains is consistent with an essentially complete condensation of Y oligomers into the LC phase.

mote ligation in the LC phase relative to that in the isotropic. Additionally, every ligation in the LC phase produces an extended complementary oligomer. In this case, the formation of the LC phase by the complementary duplexes has the autocatalytic effect of establishing conditions that would strongly promote their own growth into longer complementary chains relative to the non–LC-forming oligomers. The fact that the liquid crystal ordering is found to depend sensitively on complementarity introduces selectivity into this process and means that the overall structure of the complementary assemblies generated will actually be templated by the liquid crystal geometry. This appears to have been the case for the linear rodlike structure of base-paired polynucleotides.

References and Notes

1. R. E. Franklin, R. G. Gosling, *Nature* **171**, 740 (1953).
2. J. E. Lydon, *Liq. Cryst. Today* **12**, 1 (2003).
3. M. H. F. Wilkins, A. R. Stokes, H. R. Wilson, *Nature* **171**, 738 (1953).
4. V. Luzzati, V. A. Nicolaieff, *J. Mol. Biol.* **1**, 127 (1959).
5. C. Robinson, *Tetrahedron* **13**, 219 (1961).
6. F. Livolant, A. M. Levelut, J. Doucet, J. P. Benoit, *Nature* **339**, 724 (1989).
7. R. L. Rill, T. E. Strzelecka, M. W. Davidson, D. H. van Winkle, *Physica A* **176**, 87 (1991).
8. K. Merchant, R. L. Rill, *Biophys. J.* **73**, 3154 (1997).
9. F. Livolant, F. A. Leforestier, *Prog. Polym. Sci.* **21**, 1115 (1996).
10. R. Podgornik, H. H. Strey, V. A. Parsegian, *Curr. Opin. Colloid Interface Sci.* **3**, 534 (1998).
11. R. Brandes, D. R. Kearns, *Biochemistry* **25**, 5890 (1986).
12. T. M. Alam, G. Drobny, *J. Chem. Phys.* **92**, 6840 (1990).
13. P. J. Hagerman, *Annu. Rev. Biophys. Biophys. Chem.* **17**, 265 (1988).
14. L. Onsager, *Ann. N.Y. Acad. Sci.* **51**, 627 (1949).
15. P. Bolhuis, D. Frenkel, *J. Chem. Phys.* **106**, 666 (1997).
16. Materials and methods are available as supporting material on *Science* Online.
17. M. P. Taylor, J. Herzfeld, *Langmuir* **6**, 911 (1990).
18. X. Lu, J. T. Kindt, *J. Chem. Phys.* **120**, 10328 (2004).
19. P. Van der Schoot, M. E. Cates, *Langmuir* **10**, 670 (1994).
20. R. Hentschke, J. Herzfeld, *Phys. Rev. A* **44**, 1148 (1991).
21. J. V. Selinger, R. F. Bruinsma, *Phys. Rev. A* **43**, 2922 (1991).
22. V. R. Horowitz, L. A. Janowitz, A. L. Modic, P. A. Heiney, P. J. Collings, *Phys. Rev. E Stat. Nonlin. Soft Matter Phys.* **72**, 041710 (2005).
23. R. Wing *et al.*, *Nature* **287**, 755 (1980).
24. M. R. Redinbo, L. Stewart, P. Kuhn, J. J. Champoux, W. G. J. Hol, *Science* **279**, 1504 (1998).
25. C. A. Davey, D. F. Sargent, K. Luger, A. W. Maeder, T. J. Richmond, *J. Mol. Biol.* **319**, 1097 (2002).
26. J. E. Lydon, *Curr. Opin. Colloid Interface Sci.* **8**, 480 (2004).
27. J. T. Davis, *Angw. Chem. Int. Ed.* **43**, 668 (2004).
28. M. A. Bates, D. Frenkel, *J. Chem. Phys.* **109**, 6193 (1998).
29. A. M. Bohle, R. Holyst, T. Vilgis, *Phys. Rev. Lett.* **76**, 1396 (1996).
30. H. Durchschlag, in *Thermodynamic Data for Biochemistry and Biotechnology*, H. J. Hinz, Ed. (Springer-Verlag, New York, 1986), chap. 3.
31. M. Mandelkern, J. G. Elias, D. Eden, D. M. Crothers, *J. Mol. Biol.* **152**, 153 (1981).
32. P. L. C. Teixeira, J. M. Tavares, M. M. Telo da Gama, *J. Phys. Condens. Matter* **12**, R411 (2000).
33. B. Tinland, A. Pluen, J. Strum, G. Weill, *Macromolecules* **30**, 5763 (1997).
34. S. Asakura, F. Oosawa, *J. Chem. Phys.* **22**, 1255 (1954).
35. P. J. Flory, *Macromolecules* **11**, 1138 (1978).
36. J. P. Ferris, G. Ertem, *Science* **257**, 1387 (1992).

37. T.B., N.A.C., and M.N. conceived and initiated the study. M.N. and G.Z. designed and directed the experiments. M.N. fabricated the gradient cells and performed optical studies on them. G.Z. performed the interferometry to determine DNA concentration. G.Z. fabricated and performed optical studies on the complementary/noncomplementary mixture cells. M.N., G.Z., R.P., B.C., C.J., and J.C. performed the x-ray experiments. This work was supported by a Ministero dell' Università e della Ricerca grant COFIN-2004024508 (T.B. and G.Z), NSF grant DMR 0606528 (N.A.C. and M.N.), NSF Materials Research Science and Engineering Centers grant DMR 0213819 (N.A.C.), and DOE Nanoscale Science, Engineering, and Technology Grant 04SCPE389 (R.P. and B.D.C.). Use of the Advanced Photon Source was supported by the U.S. Department of Energy under contract DE-AC02-06CH11357.

Supporting Online Material

www.sciencemag.org/cgi/content/full/318/5854/1276/DC1
Materials and Methods
Figs. S1 to S5
References and Notes

16 April 2007; accepted 3 October 2007
10.1126/science.1143826

A High-Frequency Secondary Event During the 2004 Parkfield Earthquake

Bettina P. Allmann* and Peter M. Shearer

By using seismic records of the 2004 magnitude 6.0 Parkfield earthquake, we identified a burst of high-frequency seismic radiation that occurred about 13 kilometers northwest of the hypocenter and 5 seconds after rupture initiation. We imaged this event in three dimensions by using a waveform back-projection method, as well as by timing distinct arrivals visible on many of the seismograms. The high-frequency event is located near the south edge of a large slip patch seen in most seismic and geodetic inversions, indicating that slip may have grown abruptly at this point. The time history obtained from full-waveform back projection suggests a rupture velocity of 2.5 kilometers per second. Energy estimates for the subevent, together with long-period slip inversions, indicate a lower average stress drop for the northern part of the Parkfield earthquake compared with that for the region near its hypocenter, which is in agreement with stress-drop estimates obtained from small-magnitude aftershocks.

The 2004 magnitude (*M*) 6.0 Parkfield earthquake on the San Andreas Fault (SAF) in central California was well recorded by a dense network of seismic and geodetic sensors installed in anticipation of this event. The wealth of available data permits studying the rupture process of a moderate-sized crustal earthquake in detail. Results to date show that the earthquake ruptured about 20 km northward from the hypocenter over about 10 s. However, ground accelerations near the fault exhibit large variations, and the high-frequency (HF) waves radiated by the earthquake are not yet fully understood. We show that a large burst of HF energy occurred about 5 s into the earthquake, as seen both in full-waveform back projection of strong motion data and in the timing of a clear secondary arrival that is observed on many of the records.

We used acceleration data from the General Earth Observing System (GEOS) array, the California Geological Survey (CGS) array, and the U.S. Geological Survey (USGS) Parkfield dense seismograph array (UPSAR). These overlapping arrays were installed in the Parkfield region over the past 2 decades in order to record an expected *M* 6.0 earthquake (*1*). The CGS array consists mostly of analog stations that are triggered on the shear wave (*S*) arrival. These data are available in digital form with a 200-Hz sample rate (*2*). Altogether, there are 73 strong motion records from these networks in a 20-km radius around the Parkfield rupture area.

These data have been used to characterize strong ground motions from the mainshock and to invert for time-dependent slip models. These inversions are generally performed at relatively long periods because of the difficulty in fitting the more variable and incoherent HF part of the records. A different approach for imaging the earthquake rupture is by means of a back projection of the seismic waveforms into the volume surrounding the rupture (*3*). This method was first applied to rupture imaging of the 2004 Sumatra-Andaman earthquake with the use of teleseismic *P* records (*4*). For Parkfield, we stacked *S* waves on the north component from 68 out of 73 local strong-motion records along the travel-time operator obtained by ray tracing from each image point to each receiver through a reference one-dimensional (1D) velocity model. We forced the onset of waveforms to focus at the known hypocenter location of the mainshock by applying a static correction for each *S* arrival before stacking. This corrects for time shifts

Cecil H. and Ida M. Green Institute of Geophysics and Planetary Physics, Scripps Institution of Oceanography, University of California San Diego, 9500 Gilman Drive, La Jolla, CA 92093–0225, USA.

*To whom correspondence should be addressed. E-mail: ballmann@ucsd.edu

caused by 3D velocity structure along the ray paths. Assuming that the static shifts are time-invariant and dominated by near-surface velocity variations (*3*), the backstacked energy at times later than the onset of the *S* wave train will stack coherently and image the rupture process in space and time. Before back projection, we integrated the records to velocity, bandpass filtered the data between 2 to 8 Hz, and applied an automatic gain control (AGC) over a 10-s window in order to equalize the amplitudes of the records (*3*). We tapered the influence of stations near the perimeter of the aperture with a distance-dependent weight to reduce migration artifacts (*3*). The impulse response of our source-receiver geometry and the effect of artifacts are shown in more detail in the Supporting Online Material (SOM) text and in figs. S1 to S3.

A secondary event occurring 5 s after rupture initiation is the clearest signal seen in our back-projection results (Fig. 1) and is robust with respect to changes in the stacking method. Aside from the enforced maximum at the hypocenter (Fig. 1A), we observed a secondary maximum between 6- and 8-km depth at a distance of 12 to 14 km northwest of the hypocenter (Fig. 1B). Within the resolution constraints discussed in the SOM text, we observed the maximum focus of the subevent slightly to the southwest of the SAF, which is consistent with the fault geometry deduced from the aftershock distribution (*5*). Note that the amplitude of the peaks in these images is not necessarily proportional to the radiated energy of the events because of the AGC filtering as well as defocusing effects for the secondary event caused by uncertainties in the velocity model. Investigation of the time history (SOM text and fig. S4) suggests that any rupture in the area between the hypocenter and the subevent radiated much less seismic energy in the investigated frequency band. However, our results cannot resolve whether small amounts of HF radiation were emitted continuously as the rupture propagated from the hypocenter to this northern high-energy point or whether the rupture was discontinuous and the subevent was triggered by seismic waves from the hypocenter.

The secondary event can also be detected as a distinct HF arrival in the *S*-wave coda in records from many, but not all, stations in the area. The event is visible (Fig. 2) not only as an *S*-wave arrival on local strong-motion stations but also as a *P*-wave arrival on some stations of the Southern California Seismic Network (SCSN) at regional distances greater than 100 km (Fig. 2 inset). Notably, we observe that the event is best seen on stations to the south and east of the rupture zone. Moreover, compared with the *S* arrival from the hypocenter, the delay time of the secondary event is largest for stations south of the mainshock

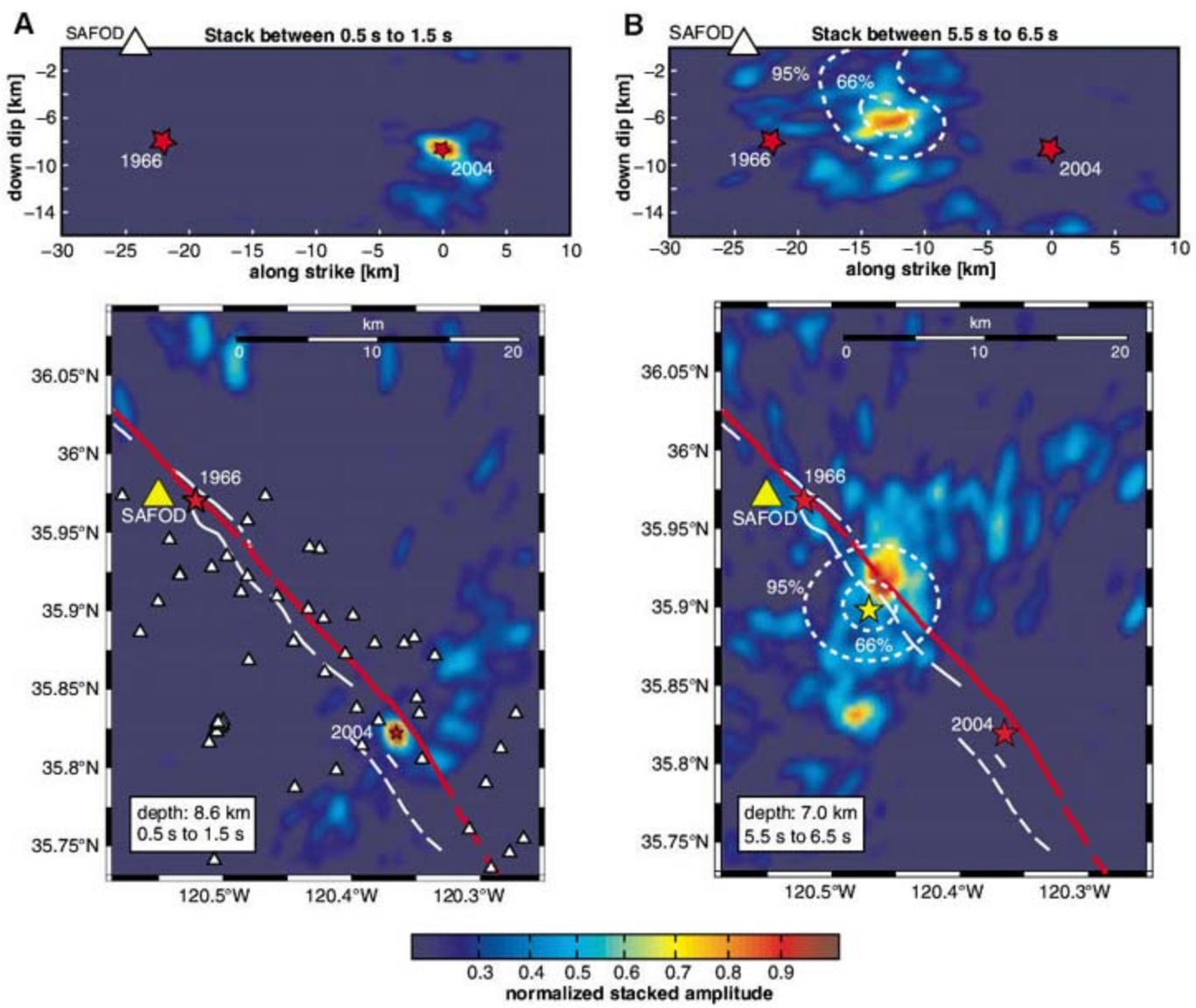

Fig. 1. Stack of backprojected amplitude for two 1-s time slices in comparison to the 66% and 95% confidence intervals (dashed) of the subevent location from travel time inversion (yellow star) for a cross section along the fault (top) and a mapview at the depth of the respective maximum (bottom). Red stars denote the hypocenters of the 1966 and the 2004 *M* 6 Parkfield earthquakes. Triangles denote strong-motion stations and the location of the San Andreas Fault Observatory at Depth (SAFOD). The surface trace of the SAF is shown as a red line. **(A)** Stack between 0.5 s to 1.5 s, where we obtain a focus at the hypocenter. **(B)** Stack between 5.5 s to 6.5 s, where we obtain a focus at the subevent. The normalized amplitude is increased by a factor of 1.6 for (B).

epicenter (Fig. 3). At local stations, the event is only visible in the *S* wave train on the horizontal components, whereas it is visible in the *P* wave train at regional distances, following the P_n phase from the hypocenter at an approximately constant delay time (Fig. 3, bottom).

We picked the differential arrival times between the mainshock and subevent *S* arrivals for 15 local stations, as well as between the mainshock and subevent P_n arrival for five regional stations that clearly show secondary arrivals. In order to locate the subevent, we performed a grid-search inversion of the differential travel times for the origin time and location of the secondary phase with respect to the known location and origin time of the hypocenter (*3*). We observed a best-fitting location for the nucleation zone of the subevent about 12.5 km along the fault plane to the northwest of the hypocenter at a depth of about 6.1 km (Fig. 4A). The subevent location is offset to the southwest of the fault, although the 95% confidence interval includes the main fault trace (Fig. 1B). The inverted origin time of this subevent is 4.95 s (± 0.1 s SD) with respect to the mainshock rupture initiation. The best-fitting subevent location resulting from this inversion agrees well with the back-projection image (Fig. 1B). To check our result, we forward-calculated travel times for the best-fitting subevent location (Fig. 3) and observed a generally good fit to the picks.

From our results, we can make a number of inferences about the secondary event. First, we can reject the possibility of this event being a reflected phase from the free surface or from the Mohorovičić discontinuity (Moho) because, in this case, the inversion result would have located the event in a mirror point either above the free surface or below the Moho. Second, it is reasonable to assume that the subevent is part of, or has been triggered by, the mainshock because dividing its distance from the mainshock hypocenter by the inverted origin time difference gives a reasonable value of 2.5 km/s as an estimate of the average rupture velocity. Third, due to the northward-propagating rupture of the mainshock, the travel times for stations to the north of the subevent are very close to the arrival times of the hypocenter. This explains why the subevent is not distinguishable on stations to the north: For these stations, the subevent is buried in the coda of the initial hypocenter pulse. However, it is not clear why the subevent is seen more distinctly on stations east of the fault compared with those to the west. Because of the lack of clear observations of the secondary arrival at stations to the north, the P_n observations to the south are critical for obtaining a reliable location for the subevent. With local *S* arrival times alone, there is a severe tradeoff between the event origin time and its location along the fault. In contrast to the travel time inversion, the back-projection method is able to clearly resolve the location of the secondary event with only *S* waveforms from local stations and does not require observations at regional distances. The close agreement seen in the location of the subevent between the two methods (Fig. 1) provides a good check on the internal consistency of the observations.

Sources of HF arrivals during the Parkfield *M* 6.0 rupture have also been identified by applying an array beam-forming technique on records of the small-aperture UPSAR (*6*). The northernmost inferred source (Fig. 4C), with the largest correlation and the largest acceleration pulse at the UPSAR array, likely is associated with our HF subevent (SOM text). The inferred average rupture velocity of about 2.4 km/s for this source is in good agreement with our observation of about 2.5 km/s.

Previous analyses of HF radiation from large earthquakes were often based on inversion of envelopes (*7*–*9*) and found sources of HF radiation located near the boundary of high slip zones. These inversions were limited to equal or lower resolution than slip inversions of low-frequency waveforms. Observations of HF radiation of great subduction earthquakes found

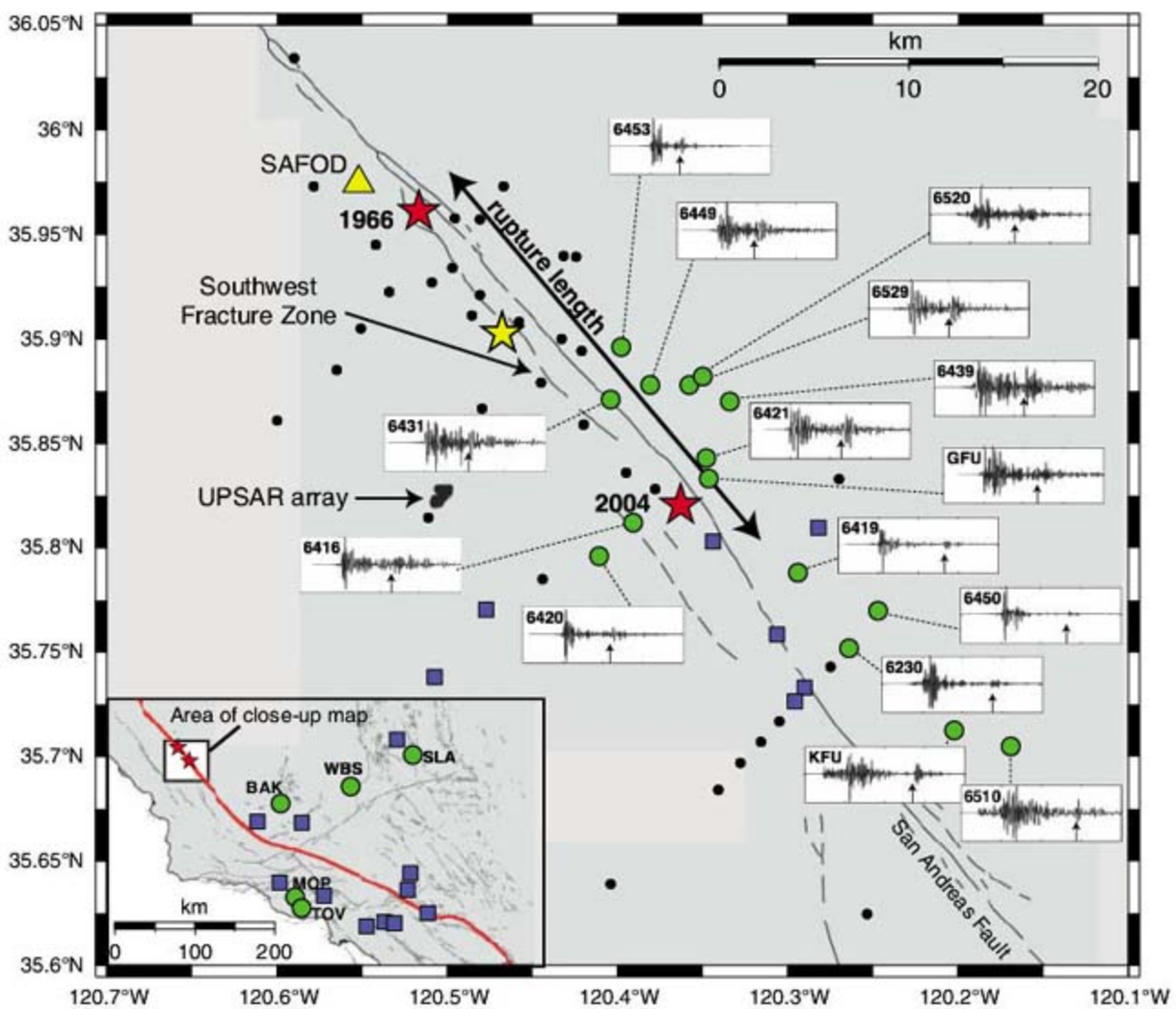

Fig. 2. Strong-motion stations in the Parkfield area and in southern California used in the investigation. Green dots denote stations where the secondary phase can be seen clearly (arrows in seismograms). Blue squares denote stations where the event is less prominent. Small black dots denote local stations where the event could not be visually detected. The displayed seismograms show 20 s of N-component acceleration data starting 5 s before the *S* first arrival, bandpass-filtered between 2 and 8 Hz. Red stars mark the epicenters of the 2004 and the 1966 *M* 6.0 Parkfield earthquakes, whereas the yellow star denotes the subevent location. The SAF surface trace and subsidiary faults are indicated by black lines.

sources of HF radiation near the end of the rupture but could not resolve whether the HF source was associated with the boundary of a slip patch or possibly with a stopping phase (*10*, *11*). Previous studies all have in common that a specific fault plane geometry, on which slip or HF radiation is to be inverted, is assumed a priori. The study presented here differs in two aspects: (i) We obtained increased resolution by direct back propagation of waveforms, thus omitting the step of forward-calculating and inverting individual waveforms, and (ii) we performed the back propagation in 3D, which allows a volumetric mapping of seismic radiation sources and does not require an assumption about any particular fault plane.

An important aspect of our result is the location of our subevent with respect to slip patches found in rupture models from long-period data. Compared to the slip model of (*12*), which had been derived from a subset of the strong motion data used in our study at lower frequencies between 0.16 and 1 Hz (Fig. 4B), our subevent is located at the southern edge of the northern high-slip patch. This observation is similar for a number of other slip models inverted by using various data and methods (*1*, *13*, *14*, *15*). Although these differ considerably in the details, they all have in common a broad region of high slip about 10 to 20 km north of the hypocenter (Fig. 4C). However, there are some fundamental differences between the data and methods used to locate the subevent and those used to invert for the slip models. Geodetic constraints on slip are based on the permanent coseismic displacement across the fault and say nothing about the dynamics of the rupture. Slip inversions from strong-motion data such as (*12*) (Fig. 4B) are typically based on filtered low-frequency waveforms below 1 Hz. On the other hand, we find the clearest observations of the subevent at frequencies higher than 1 to 2 Hz (fig. S5). Theoretical results show that enhanced HF radiation likely emanates from areas of changes in slip and/or rupture velocity or direction (*16*) and is therefore expected to occur at the edges of the slip areas inverted from low frequencies (*17*). Numerical simulations based on published slip models (*18*) or using complex fault geometries (*19*) indicate that HF energy radiation is concentrated near the initiation point of asperities or near changes in fault geometry. Comparison of our result with the slip model of (*12*) (Fig. 4B) reveals that our HF subevent is located in an area of high slip gradient, which is consistent with the numerical results and suggests that the rupture may have broken an asperity at this point, thus initiating the large moment release to the north seen in the long-period inversions. Geodetic slip models (Fig. 4C) are of lower resolution and may not be compared at this level of detail, even though we observed a consistent pattern among them. Both (*12*) and (*6*) report evidence for an increase in rupture velocity toward the north. We cannot resolve any changes in rupture velocity between the two events from the time history (fig. S4), mainly because we do not observe continuous HF radiation. The distribution of seismicity in the rupture area remains stationary before and after the 2004 *M* 6.0 Parkfield earthquake (*20*), with the bulk of the microseismicity distributed along a "streak" between 4- and 6-km depth, and a "hole" below (*21*) (Fig. 4A). We note that the slip area found by (*12*) largely coincides with the seismicity hole, except for an area between 5 and 12 km north of the hypocenter where little slip is observed. Our subevent is located within the seismicity hole, at the transition between this area of small slip and a large patch of high slip to the northwest, pointing to a change in slip amplitude as the main cause for the HF event.

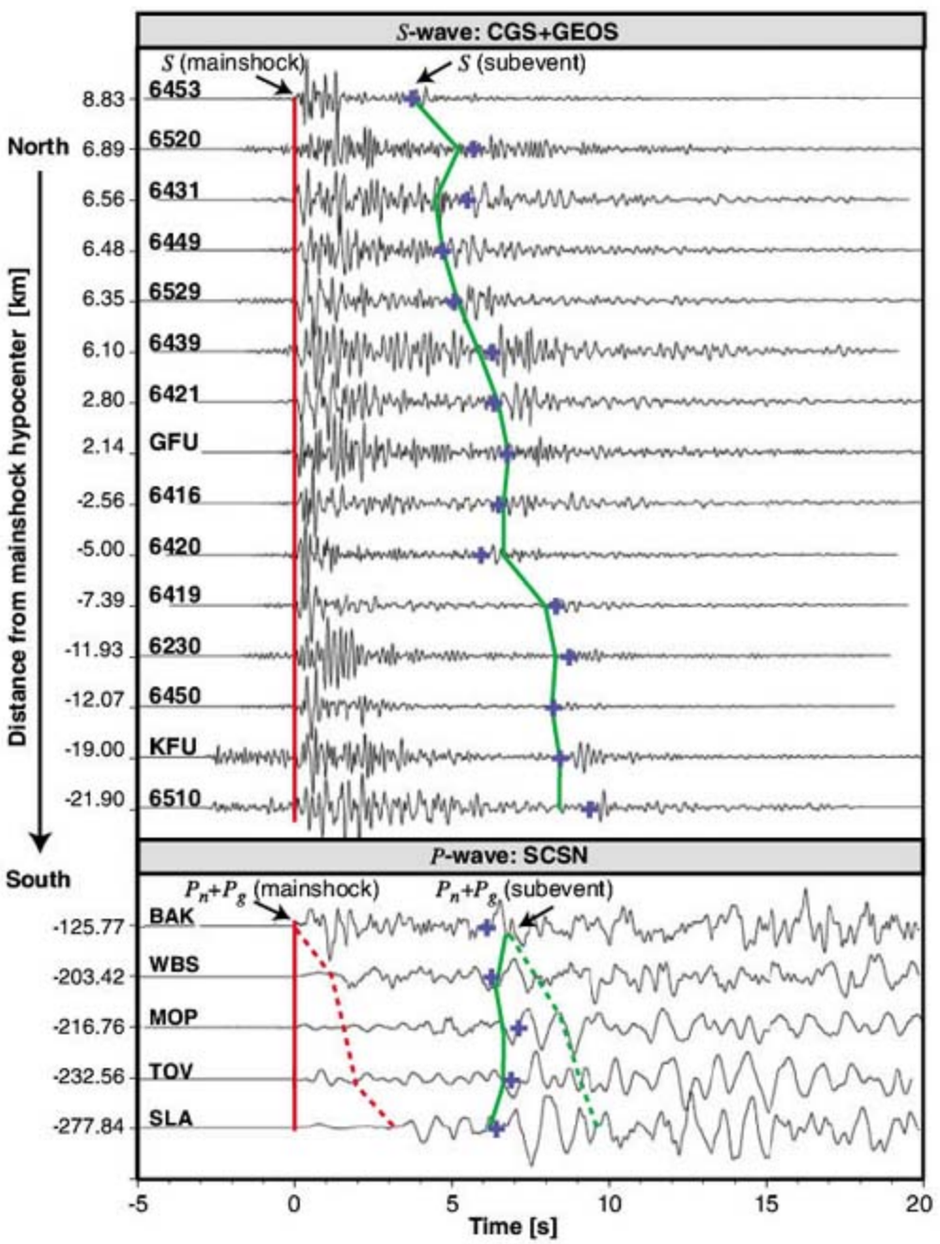

Fig. 3. Record section of the 2004 Parkfield mainshock for 15 local CGS and GEOS stations (**top**) and 5 regional SCSN stations (**bottom**) that clearly show secondary arrivals. The local data were bandpass-filtered between 2 and 8 Hz. The local stations are aligned along the *S*-wave arrival, and the regional stations are aligned along the P_n arrival from the hypocenter (red solid). The blue crosses denote the picked secondary phase arrivals for *S* and P_n. The solid green curve shows the theoretical arrival of the inverted best-fitting subevent location. Red and green dotted lines mark the theoretical P_g arrival of the hypocenter and the subevent, respectively. All stations are sorted with respect to distance from the hypocenter from north to south.

By estimating the average slip area and slip amplitude from the various slip models for the two slip patches near the hypocenter and to the north of the subevent, we can obtain an estimate of the seismic moment, M_0, associated with these slip patches. The models indicate that the bulk of the moment release occurred on the northern slip patch with a seismic moment about 2 to 20 times higher than the slip area near the hypocenter, with values of 6×10^{17} to 9×10^{17} Nm, which correspond to a magnitude of $M_w = 5.8$ to 5.9 for the northern subevent.

In comparison, assuming that the radiated seismic energy, E_R, is proportional to our

observed amplitudes (SOM text), we observe that the northern slip patch radiates one to five times less energy than the mainshock. From E_R and M_0 we can calculate the scaled energy (*22*), $\tilde{e} = E_R/M_0$, which is proportional to stress drop for a number of standard earthquake rupture models. The fact that the secondary event had a higher moment release than the initial event while radiating comparable or lesser amounts of seismic energy suggests that the northern slip event had a smaller average stress drop than that of the southern event. Our stress-drop results are consistent with the location of the subevent in a low stress-drop region computed from the background seismicity (*23*). On the other hand, the region around the mainshock hypocenter is dominated by relatively high stress-drop events in the background seismicity. These patterns of high and low stress-drop results were observed to be largely unchanged by the occurrence of the 2004 mainshock (*23*). These results suggest that at least some of the dynamic properties of large earthquake ruptures may be predictable from observations of small earthquakes near the fault. Strong heterogeneities in observed stress drops along a fault or changes in fault geometry may be an indication to expect heterogeneous slip behavior and associated HF radiation from a major or characteristic earthquake along the same fault segment.

These results indicate that waveform back projection can resolve changes in the rupture dynamics of crustal earthquakes in the M 6 range by imaging the source of HF seismic radiation. If adequate station coverage is available, this method is suited to be applied in an automated way to obtain near-real-time images of the rupture. Such images may help in the discrimination of the actual fault plane and may thus be useful for hazard assessment and guidance for emergency services.

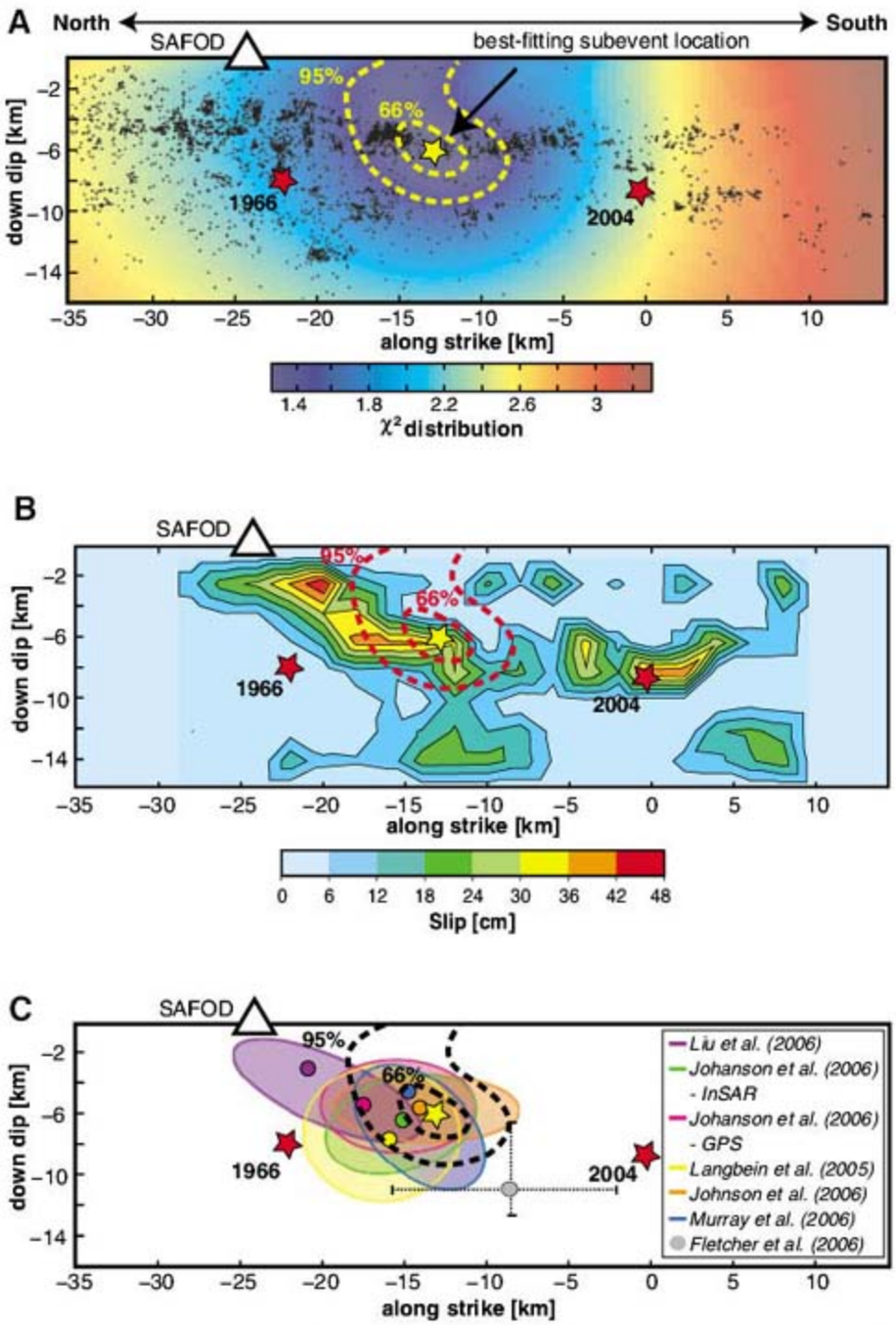

Fig. 4. Inversion result for locating the secondary event. The best-fitting location is shown as the yellow star including the 95% and 66% confidence intervals (dashed). The 1966 and 2004 hypocenters are shown as red stars. **(A)** The colors mark the logarithmic values of the χ^2 distribution. About 6000 relocated aftershocks of the 2004 mainshock are shown as black dots. **(B)** Comparison between the subevent location (yellow star) and the strong-motion slip inversion model obtained from (*12*). **(C)** Comparison between the subevent location and high-slip areas at the northern part of the mainshock rupture zone from various slip models (colored ellipses). The colored dots mark the observed maximum slip for the respective models. The location of a HF source during the mainshock rupture obtained from beamforming analysis at UPSAR (*6*) is also included as a gray dot, together with the location error bars (dotted lines).

References and Notes

1. J. Langbein *et al.*, *Seismol. Res. Lett.* **76**, 10 (2005).
2. A. F. Shakal, H. Haddadi, V. Graizer, K. Lin, M. Huang, *Bull. Seismol. Soc. Am.* **96**, S90 (2006).
3. Methods are available on *Science* Online.
4. M. Ishii, P. M. Shearer, H. Houston, J. E. Vidale, *Nature* **435**, 933 (2005).
5. R. W. Simpson, M. Barall, J. Langbein, J. R. Murray, M. J. Rymer, *Bull. Seismol. Soc. Am.* **96**, S28 (2006).
6. J. Fletcher, P. Spudich, L. Baker, *Bull. Seismol. Soc. Am.* **96**, S129 (2006).
7. Y. Zeng, K. Aki, T. Teng, *J. Geophys. Res.* **98**, 11981 (1993).
8. Y. Kakehi, K. Irikura, *Geophys. J. Int.* **125**, 892 (1996).
9. H. Nakahara, T. Nishimura, H. Sato, M. Ohtake, *J. Geophys. Res.* **103**, 855 (1998).
10. T. Sato, K. Imanishi, M. Kosuga, *Geophys. Res. Lett.* **23**, 33 (1996).
11. W. Nakayama, M. Takeo, *Bull. Seismol. Soc. Am.* **87**, 918 (1997).
12. P. Liu, S. Custódio, R. Archuleta, *Bull. Seismol. Soc. Am.* **96**, S143 (2006).
13. I. Johanson, E. Fielding, F. Rolandone, R. Bürgmann, *Bull. Seismol. Soc. Am.* **96**, S269 (2006).
14. K. Johnson, R. Bürgmann, K. Larson, *Bull. Seismol. Soc. Am.* **96**, S321 (2006).
15. J. Murray, J. Langbein, *Bull. Seismol. Soc. Am.* **96**, S283 (2006).
16. R. Madariaga, *Geophys. J. R. Astron. Soc.* **51**, 625 (1977).
17. P. Spudich, L. Frazer, *Bull. Seismol. Soc. Am.* **74**, 2061 (1984).
18. S. Ide, *Bull. Seismol. Soc. Am.* **92**, 2994 (2002).
19. R. Madariaga, J. Ampuero, M. Adda-Bedia, *Geophys. Monogr. Am. Geophys. Union* **170**, 223 (2006).
20. C. Thurber *et al.*, *Bull. Seismol. Soc. Am.* **96**, S38 (2006).
21. F. Waldhauser, W. Ellsworth, D. Schaff, A. Cole, *Geophys. Res. Lett.* **31**, L18608 (2004).
22. H. Kanamori, L. Rivera, *Geophys. Monogr. Ser.* **170**, 3 (2006).
23. B. Allmann, P. Shearer, *J. Geophys. Res.* **112**, B04305 (2007).

24. We are grateful to A. Goertz for valuable comments and suggestions. This research was funded by National Earthquake Hazards Reduction Program/USGS grant 03HQPA0001 and supported by the Southern California Earthquake Center (SCEC). SCEC is funded by NSF cooperative agreement EAR-0106924 and USGS cooperative agreement 02HQAG0008. The SCEC contribution number for this paper is 1121.

Supporting Online Material

www.sciencemag.org/cgi/content/full/318/5854/1279/DC1
Materials and Methods
SOM Text
Figs. S1 to S5

15 June 2007; accepted 15 October 2007
10.1126/science.1146537

Inconsistencies Between Pangean Reconstructions and Basic Climate Controls

Clinton M. Rowe,[1]* David B. Loope,[1] Robert J. Oglesby,[1]
Rob Van der Voo,[2] Charles E. Broadwater[1]

The supercontinent Pangea dominated our planet from the Permian into the Jurassic. Paleomagnetic reconstructions have been used to estimate the latitudinal position of Pangea during this 100-million-year period. Atmospheric circulation, recorded by eolian sandstones in the southwestern United States, shows a broad sweep of northeasterly winds over their northernmost extent, curving to become northwesterly in the south: This evidence is consistent with paleomagnetic reconstructions of the region straddling the equator in the Early Permian but is at odds with its northward movement to about 20°N by the Early Jurassic. At least one of the following scenarios must be true: The latitude based on paleomagnetism is incorrect; the interpretation of how winds shaped the dunes is mistaken; the basic climate controls in the Jurassic were different from those of today; or the paleogeographic reconstructions available are insufficient to adequately reproduce the wind fields responsible for dune formation.

From the Permian into the Jurassic—100 million years of Earth history—the supercontinent Pangea dominated our planet. Detailed maps of this pole-to-pole landmass, with paleomagnetic data from each continental block, were published in the 1980s, establishing paleomagnetism as the method par excellence of estimating paleolatitude (*1*). Geologic work delineating the extent of climate-sensitive sedimentary rocks (e.g., coal, glacial till, evaporites, and carbonate sediments) has often helped to reduce uncertainties in the quality of paleomagnetic data and has sometimes led the way to important reinterpretations (*2*, *3*).

Atmospheric circulation is driven by the latitudinal distribution of solar heating, which is modified by the rotation of the planet and the distribution of landmasses. Eolian dunes conclusively provide direct evidence of atmospheric circulation (*4*, *5*). Opdyke and Runcorn (*6*) were the first to recognize the planetary-scale winds that deposited the Late Paleozoic eolian cross-strata of Wyoming and northern Utah. The markedly consistent dip directions of Early Permian through Early Jurassic cross-strata in the western United States (*7*, *8*) are accurate indicators of paleowind direction (Fig. 1), because they were deposited by transverse dunes that migrated downwind by repeated avalanching (*9*). We have extended the trade-wind explanation for the Wyoming rocks southward by interpreting eolian strata of the Colorado Plateau (southern Utah and Arizona) as records of northwesterly winds lying south of the trades in Pangea's monsoonal wind regime (*10*) (Fig. 2).

[1]Department of Geosciences, University of Nebraska, Lincoln, NE 68588–0340, USA. [2]Department of Geological Sciences, University of Michigan, Ann Arbor, MI 48109–1005, USA.

*To whom correspondence should be addressed. E-mail: crowe1@unl.edu

The Paleozoic formations that contain the most abundant evidence of life in the ancient dunefields (Cedar Mesa and Esplanade sandstones) were deposited by the northwesterly winds; the formations deposited farther north in the trade-wind belt (i.e., Tensleep, Weber, Casper, and DeChelly) contain comparatively fewer signs of life. These wind and biotic patterns persisted through the Early Jurassic (*11*). During the entire interval, the dominant winds in the north came from the northeast, curving to become northwesterly over the southern portion of the outcrops. Jurassic dunes in the south were seasonally drenched with rain, whereas weaker southeasterly winds reversed the dry-season slip faces (*12*).

Conventional wisdom, largely based on paleomagnetic evidence, places the plateau along or just north of the equator during the Early Permian and then moves the plateau north through the Triassic to lie near 20°N by the Early Jurassic, as calculated from published mean poles. Best estimates for the global mean poles for ~200 million years ago vary between 70°N, 96°E and 66°N, 91°E (in North American coordinates), with the variations being minor and depending on methodology (*13*). These mean poles yield paleolatitudes for a location in southeast Utah (40°N, 110°W) ranging between 17°N and 28°N. We do not know of any published paleomagnetic syntheses that placed the area south of the equator during the Early Jurassic. Yet the constancy of the wind regime indicated by the dip directions of the cross-strata suggests that the sand dunes and the plateau stayed within the same climatic zone during the entire time span. Furthermore, the inferred northward migration appears to be inconsistent with basic qualitative concepts of climate: Northeasterly winds changing southward to northwesterlies would be out of place near 20°N but would fit well near and just south of the equator, where northwesterly winds represent cross-equatorial flow induced by a strong summer monsoonal circulation in the southern hemisphere (SH). The wind regimes recorded by the rocks are consistent with paleogeographic reconstructions and climate simulations (*14*) of the Late Permian, with the Colorado Plateau straddling the equator, but are very much at odds with a northward movement to about 20°N by the Early Jurassic. Given our understanding of basic climate controls, as supported by climate model results, the wind regime that formed the eolian sandstones of the Colorado Plateau must have occurred on or south of the equator rather than at the generally accepted paleomagnetic latitude of about 20°N (*15*).

An earlier attempt at paleogeographic interpretation (*10*) was partially based on the wind regime simulated by a Jurassic climate model (*16*) and on paleomagnetic data collected from Colorado Plateau strata (*17*–*19*). The climate model showed trade winds during December, January, and February turning to become westerly a few degrees north of the equator. This corresponded reasonably well to estimates of paleolatitude for the Colorado Plateau (*17*, *20*) but did not fit well with paleomagnetic data from the eastern United States (which placed the center of the plateau at about 18°N) nor with the Pangean reconstruction shown by the Paleomap Project (*21*). Moreover, the Jurassic climate model had extremely low resolution (8° in latitude by 10° in longitude) and was simplistic by current standards. More recently, geophysicists have called attention to the importance of sediment compaction to paleomagnetic interpretations, especially for rocks in which the paleomagnetic signal is carried by detrital hematite. Comparisons of paleomagnetic data from such sedimentary rocks with those from igneous rocks (which do not compact) indicate that sedimentary rocks are likely to yield paleolatitudes that are too low (*22*, *23*). Because the sedimentary rocks from the plateau that provided the evidence for a low-latitude position contain detrital hematite, most paleomagneticists would now favor the higher-latitude interpretation for the plateau, thereby aggravating the discrepancy with our earlier climate-based interpretation.

In an attempt to resolve the discrepancy between winds that appear to have been constant over 100 My and the paleomagnetic evidence for northward movement of the Colorado Plateau, we made a series of climate simulations for the Early Jurassic using the latest version of the Community Climate System Model (*24*, *25*) from the National Center for Atmospheric Research. We made four model simulations with atmospheric CO_2 at present-day levels; two of these runs used "conventional wisdom" for Early Jurassic paleogeography based on Paleomap (*21*), and two were made with Paleomap-derived paleogeography shifted 30° southward along the nominal 150°E meridian to put the Colorado Plateau under a favorable SH wind regime. For each pair of runs with a given paleogeography, one was made with prescribed sea surface temperatures (SSTs) for the Early Jurassic

derived from Chandler *et al.* (*16*) and the other was made with SST computed via a slab ocean model component. We conducted additional model runs using the unshifted paleogeography with constant 100-m topography and with uniform vegetation to exclude these factors as major influences on atmospheric circulation. Finally, to investigate the impact of increased CO_2, we conducted two additional model runs using the shifted paleogeography, the slab ocean model, and, respectively, four times and eight times present-day CO_2 levels. All model runs were at T31 (3.75° in latitude by 3.75° in longitude) resolution, and the last 10 model years were averaged to produce climatologies for analysis.

Every model configuration yielded a strong monsoon that is hemispherically symmetric [that is, with strong low pressure in the summer hemisphere and strong high pressure in the winter hemisphere (Fig. 3)]. Low-latitude winds over western Pangea during SH summer curve from northeasterly trades in the northern hemisphere (NH) to northwesterlies after crossing the equator. These simulated winds are physically reasonable and consistent with trade-wind flow in the winter hemisphere and strong monsoonal heating in the summer hemisphere. This is the only wind regime with the large, concave-to-the-east, north-to-south sweep in agreement with the winds recorded by the eolian sandstones of the western United States. This is also consistent with current concepts of the atmospheric general circulation and would indicate a low-latitude SH location for the Colorado Plateau during the Jurassic. Furthermore, every model configuration yielded the necessary countervailing southeasterly winds during SH winter, which are consistent with the key characteristics of the southernmost paleodunes. In addition, every simulation exhibits seasonally dry periods for the region of the Colorado Plateau, which is consistent with the rock record (*12*). Finally, although the atmospheric concentration of CO_2 for the Early Jurassic is uncertain, the model results obtained to date show that the winds are insensitive to a range of CO_2 values from the present-day concentration (355 parts per million) to eight times that amount. However, increased atmospheric CO_2 does change modeled precipitation, with possible impacts on the migration of the dunes (fig. S1).

Results from our simulations (Fig. 3), like those of the low-resolution model (*16*), show that although the trade winds turned while north of the equator in eastern Pangea, these winds turned 5° to 10° south of the equator in western Pangea. Thus, we could infer that this was the position occupied by the Colorado Plateau (1 or 2 grid points south of the placement in the earlier study). Our model would then indicate that the Jurassic sandstones were deposited between 10°S and 20°S, not 10°N to 20°N as suggested by paleomagnetism-based reconstructions. Assuming that winds inferred from the sandstones should correspond to the winds shown by the model, either the climate model is incorrect or the northward movement of the Colorado Plateau occurred much later than suggested by current paleogeographic reconstructions. This result is independent of whether topography representative of the Jurassic is imposed or if the geography is shifted such that the Colorado Plateau is centered at 10°S. Furthermore, the simulations are robust regardless of whether SSTs are prescribed or calculated via a slab ocean model.

If we assume that the winds inferred from the paleodunes are correct, the climate model results and the paleomagnetism-based paleogeographic reconstructions cannot both be correct, though both can be wrong. We are left with the following possibilities: (i) The paleomagnetism-based paleogeographic reconstructions are incorrect in moving the Colorado Plateau from around the equator to about 20°N between the Early Permian and the Early Jurassic; (ii) the Early Jurassic climate model results are incorrect in simulating a pattern of northeasterly trade winds north of the equator, arcing just south of the equator into monsoonal-driven northwesterlies; or (iii) the circulation patterns inferred for the dunes represent an extreme climate state that is far removed from the mean state that we have simulated thus far.

The paleomagnetic reconstructions appear to be tightly constrained by data (*23*); so, if paleomagnetic interpretations are indeed the cause of

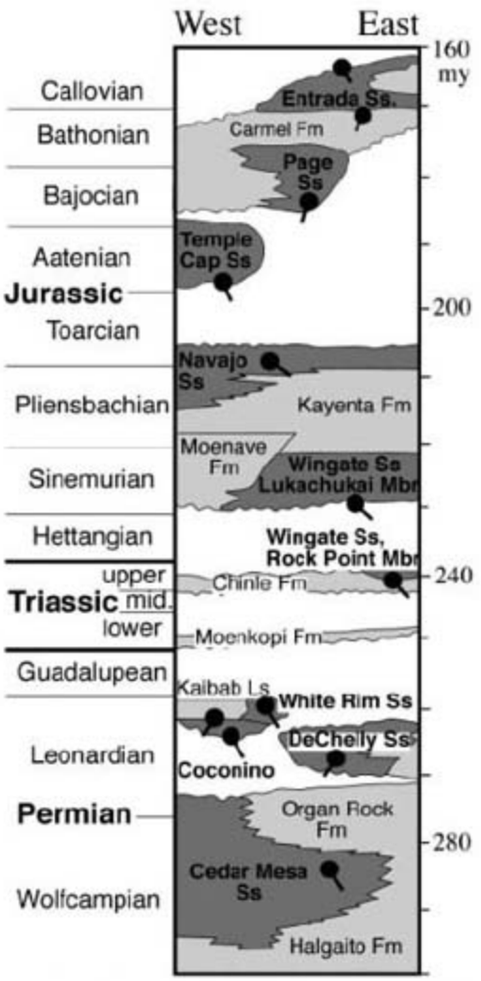

Fig. 1. The eolian sandstones of the Colorado Plateau (dark shading) reach an aggregate of 2500 m in thickness and span about 140 My of Earth history. The tails of the black "tadpoles" (circles with extending lines) point in the mean dip direction of dune cross-strata and, therefore, point in the downwind direction of the paleowinds that drove the dunes. From the base of the Cedar Mesa Sandstone (Ss) (bottom) to the top of the Temple Cap Ss, the rocks show northwesterly winds (interpreted as the belt of tropical westerlies situated south of the trade winds). The DeChelly Ss is somewhat anomalous, showing northeasterly winds. Northern exposures of the Coconino Ss, however, record northeasterly winds (interpreted as trade winds); to the south, it records winds from the northwest. West-to-east variations in rock strata are depicted across the diagram; unshaded areas show major unconformities (gaps in the rock record). Fm, formation; Mbr, member; Ls, limestone. [Modified from Blakey *et al.* (*26*) and Peterson (*7*)]

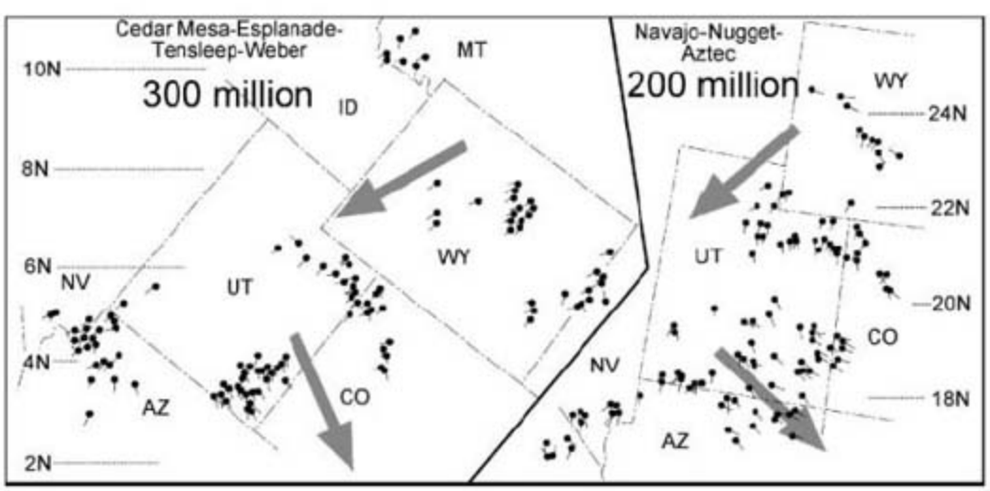

Fig. 2. Dip directions of cross-strata of Late Paleozoic (left) and Early Jurassic (right) eolian sandstones. Tails of "tadpoles" point downwind; each represents scores of measurements. Large gray arrows show the flow of trade winds (top arrows) and tropical westerlies (bottom arrows). Paleomagnetic data indicate that, during the Permian, Utah was near the equator but that, by the Jurassic, it had drifted to 20°N. [Modified from Peterson (*7*)]

this conundrum, a basic assumption of the paleomagnetism model would have to be questioned; given the consistency of Early Jurassic paleomagnetic poles from the Atlantic Ocean–bordering continents (*13*) and the convincing paleolatitude determinations from the Newark sediments (*23*), we are not ready to argue that the paleomagnetic field model must be wrong. However, the climate model results appear to be very robust based on our understanding of fundamental climatic controls. Indeed, the basic qualitative nature of these results could have been inferred just from this understanding, without the use of a climate model. Our modeling work to date suggests that atmospheric CO_2 is not likely to have a substantial impact on the orientation and migration of paleodunes, in large part because of the spatial and seasonal homogeneity of this gas (which means that it warms or cools more-or-less uniformly around the globe). The most relevant potential climate control that we have not yet considered is changing orbital states. Orbital cyclicity is known to strongly affect both the latitudinal and seasonal distribution of solar radiation and could therefore affect the monsoonal circulations that prevailed over Pangea. Furthermore, the amplitudes and periodicities of obliquity, precession, and eccentricity cycles in the past could have differed from those at present.

During the past two decades, climate models have been increasingly used to simulate atmospheric circulations of the past. Slipface orientations of modern dunes coincide well with the pattern of modern circulation (*4*), and we have shown that the dip directions of avalanche-dominated eolian cross-strata can, in conjunction with model simulations, be used to accurately delineate ancient atmospheric circulation. Past climate reconstructions are important in their own right, and they have previously provided strong constraints on paleogeographic reconstructions based on paleomagnetic data. Although proxy records such as coal and evaporite deposits are subject to uncertain interpretation of paleoclimatic conditions (e.g., temperature, precipitation, and evaporation), wind directions preserved in eolian sediments relate directly to the atmospheric circulation. Furthermore, atmospheric circulation patterns can be a more profound indicator of a given climatic state than temperature and precipitation alone. Because the atmospheric general circulation is strongly linked to latitude, this information has great value as an independent check on magnetism-based paleogeographies.

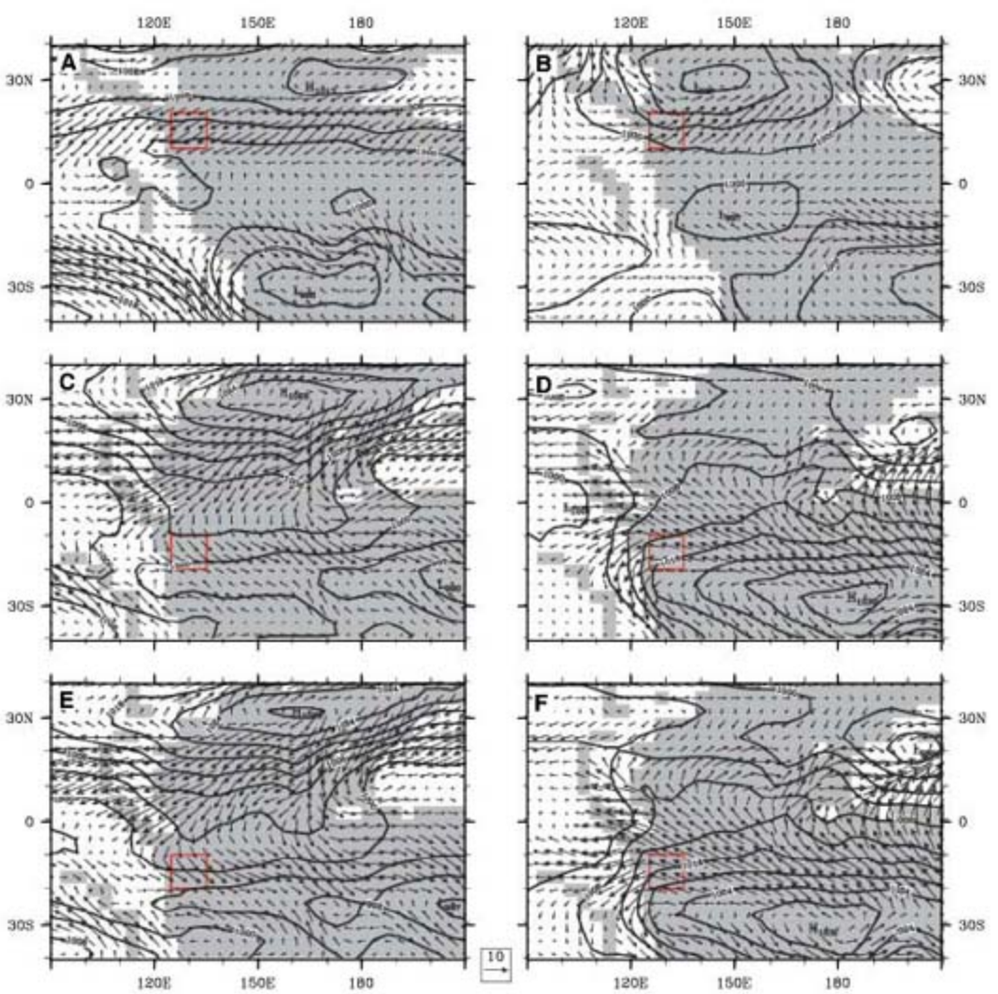

Fig. 3. Simulation results for NH winter [December, January, February (DJF), left column] and NH summer [June, July, August (JJA), right column] for unshifted paleogeography with prescribed SST (**A** and **B**), shifted paleogeography with prescribed SST (**C** and **D**), and shifted paleogeography with slab ocean (**E** and **F**). Sea-level pressure (hPa) is contoured at 4-hPa intervals, and winds at the lowest model level are given as vectors, with a 10 m s^{-1} reference vector shown at bottom. The Colorado Plateau is outlined in red.

References and Notes

1. E. Irving, *Proc. Natl. Acad. Sci. U.S.A.* **102**, 1821 (2005).
2. R. Van der Voo, *Paleomagnetism of the Atlantic, Tethys, and Iapetus Oceans* (Cambridge Univ. Press, Cambridge, 1993).
3. P. H. Heckel, B. J. Witzke, in *The Devonian System: A Palaeontological Association International Symposium*, M. R. House, C. T. Scrutton, M. G. Bassett, Eds. (Palaeontological Association, London, 1979), vol. 23, pp. 99–123.
4. D. G. Blumberg, R. Greeley, *J. Clim.* **9**, 3248 (1996).
5. R. Sridhar *et al.*, *Science* **313**, 345 (2006).
6. N. D. Opdyke, S. K. Runcorn, *Bull. Geol. Soc. Am.* **71**, 959 (1960).
7. F. Peterson, *Sediment. Geol.* **56**, 207 (1988).
8. Peterson (*7*) reports consistency values (vector mean strength) for the dip directions of eolian sandstones from western United States paleowind indicators. These factors are high (above 0.80) for nearly all of the Pennsylvanian through Early Jurassic sandstones and many are well above 0.90. The lowest factors (0.67 and 0.75) are for the most areally extensive unit (the Navajo Sandstone) and, based on the location of this sandstone formation, likely reflect key geographic differences in the ancient wind field (that is, the arc connecting the trades and tropical westerlies) that are fundamental to our results.
9. G. Kocurek, *Annu. Rev. Earth Planet. Sci.* **19**, 43 (1991).
10. D. B. Loope, M. B. Steiner, C. M. Rowe, N. Lancaster, *Sedimentology* **51**, 315 (2004).
11. D. B. Loope, C. M. Rowe, *J. Geol.* **111**, 223 (2003).
12. D. B. Loope, C. M. Rowe, R. M. Joeckel, *Nature* **412**, 64 (2001).
13. J. Besse, V. Courtillot, *J. Geophys. Res.* **107**, 10.1029/2000JB000050 (2002).
14. F. Fluteau, J. Besse, J. Broutin, G. Ramstein, *Palaeogeogr. Palaeoclimatol. Palaeoecol.* **167**, 39 (2001).
15. Paleomagnetic evidence indicates that (relative to the North American craton) the Colorado Plateau has been structurally rotated clockwise about 6° since the Late Carboniferous (*20*). Counterclockwise rotation of the paleowind vectors (derived from Permian through Early Jurassic rocks) to correct for this deformation would make the wind vectors in the southern Colorado Plateau even more westerly and makes placement of Jurassic strata in the subtropical trade-wind belt even more anomalous.
16. M. Chandler, D. Rind, R. Ruedy, *Bull. Geol. Soc. Am.* **104**, 543 (1992).
17. M. B. Steiner, in *Mesozoic Paleogeography of the West-Central United States*, M. W. Reynolds, E. D. Dolly, Eds. (The Rocky Mountain Section, Society of Economic Paleontologists and Mineralogists, Denver, CO, 1983), pp. 1–11.
18. S. R. May, R. F. Butler, *J. Geophys. Res.* **91**, 11519 (1986).
19. D. R. Bazard, R. F. Butler, *J. Geophys. Res.* **96**, 9847 (1991).
20. M. B. Steiner, *Tectonics* **22**, 1020 (2003).
21. C. R. Scotese, PALEOMAP; www.scotese.com/jurassic.htm.
22. L. Tauxe, *Earth Planet. Sci. Lett.* **233**, 247 (2005).
23. D. V. Kent, L. Tauxe, *Science* **307**, 240 (2005).
24. W. D. Collins *et al.*, *J. Clim.* **19**, 2122 (2006).
25. B. L. Otto-Bliesner *et al.*, *J. Clim.* **19**, 2526 (2006).
26. R. C. Blakey, F. Peterson, G. Kocurek, *Sediment. Geol.* **56**, 3 (1988).

27. This work was supported by a grant from NSF to D.B.L. and C.M.R. The authors thank C. R. Scotese for providing topographic data for his Jurassic paleogeography reconstruction. Computing support was provided by the National Center for Atmospheric Research and the University of Nebraska Research Computing Facility.

Supporting Online Material

www.sciencemag.org/cgi/content/full/318/5854/1284/DC1
Fig. S1

18 June 2007; accepted 12 October 2007
10.1126/science.1146639

Time-Resolved Investigation of Coherently Controlled Electric Currents at a Metal Surface

J. Güdde, M. Rohleder, T. Meier,* S. W. Koch, U. Höfer†

Studies of current dynamics in solids have been hindered by insufficiently brief trigger signals and electronic detection speeds. By combining a coherent control scheme with photoelectron spectroscopy, we generated and detected lateral electron currents at a metal surface on a femtosecond time scale with a contact-free experimental setup. We used coherent optical excitation at the light frequencies ω_a and $\omega_a/2$ to induce the current, whose direction was controlled by the relative phase between the phase-locked laser excitation pulses. Time- and angle-resolved photoelectron spectroscopy afforded a direct image of the momentum distribution of the excited electrons as a function of time. For the first ($n = 1$) image-potential state of Cu(100), we found a decay time of 10 femtoseconds, attributable to electron scattering with steps and surface defects.

The electric conductivity of most materials is limited by fast scattering processes of electrons. In the case of metals, the time scale between the individual scattering events is typically in the range of femtoseconds (*1*). Usual conductivity measurements cannot access this time scale because available electronic equipment can neither produce trigger signals nor detect transients that are shorter than tens of picoseconds. Here, we introduce an experimental technique to measure the dynamics of electrical currents on the femtosecond time scale. The technique combines methods of coherent control with time- and angle-resolved photoelectron spectroscopy. Our setup is contact-free. It involves the all-optical generation of electric current pulses and the time-resolved measurement of the momentum distribution of the electrons that carry the current.

The basic optical excitation scheme that we apply has been used to induce electric currents in semiconductors (*2*, *3*) and to generate terahertz radiation (*4*). It is a variant of the Brumer-Shapiro scheme of coherent control (*5*). Two phase-locked laser fields with frequencies ω_a and $\omega_a/2$ coherently excite electrons from an occupied into an unoccupied state—for example, from the valence band into the conduction band of a semiconductor. The quantum mechanical interference of the two different excitation pathways (i.e., the one- and the two-photon transitions) allows control of the excitation of electrons at different points in momentum space (k-space). In this way, variation of the relative phase between the two laser fields can set the direction as well as the magnitude of an induced current density. In the present experiment, the current is not induced in the volume of a semiconductor but at the surface of a metal. There, strong electron-electron interaction may severely limit the attainable degree of quantum coherence. However, previous work clearly demonstrated that a fixed phase relationship between an excited electron and the corresponding photohole can persist considerably longer than an optical cycle and that coherent control in metals is possible (*6*–*8*). As shown below, models developed for photocurrents in semiconductors, if appropriately modified, are indeed able to describe the current generation at a metal surface.

The detection of current pulses is just as important as their generation. Commonly this is accomplished by measuring a voltage drop between two contacts. Whereas this straightforward method clearly showed that the optical excitation scheme resulted in macroscopic electrical currents in semiconductors (*2*, *3*), it is not suitable for detailed studies with ultrafast time resolution. Instead, a contact-free laser-based method is also required for the detection of currents. With time- and angle-resolved photoelectron spectroscopy, we can achieve femtosecond time resolution. Moreover, as this technique directly maps out the excited electrons in k-space, it has the capability to provide information on the generation and decay of currents in unprecedented detail. The macroscopic current density is given by the sum over the microscopic contributions of the individual carriers with charge $\pm e$ and moving with velocities v; in the case of a surface electron current,

$$j_{\parallel} = -e\int n_e v_{\parallel}\, dv_{\parallel} = -e\int_0^{k_{max}} \left[n_e(+k_{\parallel}) - n_e(-k_{\parallel})\right]\frac{\hbar k_{\parallel}}{m_e}dk_{\parallel} \quad (1)$$

where $j_{\parallel}$ is the total lateral current density, $\hbar$ is Planck's constant divided by 2π, n_e is the density of excited electrons, $k_{\parallel}$ is the electron momentum parallel to the surface divided by $\hbar$, k_{max} is the maximum value of $k_{\parallel}$, and m_e is the electron mass. At the surface of a well-ordered solid, $k_{\parallel}$ of a photoemitted electron is conserved (*9*). By measuring the kinetic energy E_{kin} and the emission angle θ normal to the surface, the parallel momentum of the emitted electrons can be determined from the relation

$$k_{\parallel} = \hbar^{-1}\sqrt{2m_e E_{kin}}\,\sin\theta \quad (2)$$

Because $n_e(k_{\parallel})$ is proportional to the angle-resolved photoemission yield, the method can be used to determine not only $j_{\parallel}$ but also the individual contributions of electrons of different momenta to this current.

We have applied this optical current generation and detection scheme to image-potential states on the (100) surface of a copper single crystal (*10*). Electrons excited to image-potential states are bound perpendicular to the metal surface by the Coulombic image potential, whereas they can move almost freely parallel to the surface (*11*, *12*). In order to investigate these states with photoelectron spectroscopy, a short ultraviolet laser pulse with frequency ω_a is normally used to populate them via optical interband transitions from occupied bulk states below the Fermi level E_F (Fig. 1B). The temporal evolution of the population of the states is then probed by photoemitting the excited electrons with a second laser pulse at variable time delay and frequency ω_b (*13*–*16*). A typical angle-resolved spectrum of such a two-photon photoemission experiment (2PPE) showing the first ($n = 1$) image-potential state of Cu(100) is depicted in Fig. 1A. The imaging photoelectron analyzer of our experimental setup makes it possible to measure the photoemission intensity within a continuous range of emission angles and energies simultaneously (*17*). The data clearly reveal the free electron–like parabolic energy dispersion $E(k_{\parallel})$ of the state parallel to the surface. The distribution of the 2PPE intensity is symmetric with respect to the surface normal, as neither the pump nor the probe process is able to alter the symmetry of the system with respect to the surface normal.

The situation changes when the phase-locked $\omega_a/2$ pump pulse is used for excitation in addition to the ω_a pulse. The coherent excitation of the image-potential state with the pulse pair produces an asymmetric distribution (Fig. 1C). In this particular case, the photoemission intensity is enhanced for positive values of $k_{\parallel}$. The asymmetric population of the image-potential states in momentum space corresponds to a ballistic electron current flowing within a sheet 4 Å thick in front of the surface. Before discussing this current in more detail, we first show that the coherent optical excitation scheme allows control over its magnitude and direction in a manner similar to that previously shown in bulk GaAs (*3*, *4*).

For reasons described below, the coherent excitation process at the metal surface does not allow for full control over the sign of the parallel momentum of the excited electrons. Only a portion of the excited electrons contributes to

Fachbereich Physik und Zentrum für Materialwissenschaften, Philipps-Universität, Renthof 5, D-35032 Marburg, Germany.

*Present address: Department Physik, Universität Paderborn, Warburger Str. 100, D-33098 Paderborn, Germany.

†To whom correspondence should be addressed. E-mail: hoefer@physik.uni-marburg.de

the net current (Fig. 1C). This fraction can be visualized very clearly by subtracting a symmetric distribution from the measured asymmetric spectra. Figure 2 displays such photoemission difference spectra for various values of the phase difference $\Delta\phi = \phi(\omega_a) - 2\phi(\omega_a/2) + \phi_0$ between the two pump pulses (*18*). The data for $\Delta\phi = 90°$ correspond to the difference of the spectra plotted in Fig. 1, A and C. They show the momentum distribution for the maximum current flowing in the $+k_{||}$ direction. Changing $\Delta\phi$ from 90° to 270° clearly reverses the direction of the current. For $\Delta\phi = 180°$, no net current is generated but the overall excited population is enhanced. $\Delta\phi = 120°$ and $\Delta\phi = 240°$ represent intermediate cases with a weak current flowing in positive and negative directions, respectively (*19*).

For a better understanding of the coherent excitation process, we now inspect the phase dependence of the photoemission intensity for specific emission angles in more detail and compare it with the results of model calculations. The red and green data points in Fig. 3A depict the photoemission intensity integrated over the corresponding red and green rectangular areas in Fig. 1C, which are centered at $k_{||} = +0.224$ Å^{-1} and $k_{||} = -0.224$ Å^{-1}, respectively. The photoemission intensity varies sinusoidally with the phase difference $\Delta\phi$, as expected for a process that is proportional to the product $\mathcal{E}(\omega_a)\mathcal{E}^2(\omega_a/2)$, where $\mathcal{E}(\omega_a)$ and $\mathcal{E}(\omega_a/2)$ are the electric field strengths of the two pump laser pulses. The data for opposite $k_{||}$ are phase-shifted by about 30°, resulting in an asymmetry of the photoemission intensity.

Because only a fraction of the excited electrons contribute to the net current, the observed phase shift between opposite values of $k_{||}$ is less than 180°. As a quantitative measure of the net current carried by electrons at a given magnitude of $k_{||}$, we introduce the asymmetry parameter $A_{\text{current}} = (I_{+k||} - I_{-k||})/(I_{+k||} + I_{-k||})$. A_{current} represents the relative contribution of the coherently controlled current to the total photoemission intensity for a given parallel momentum. It has a sinusoidal dependence on $\Delta\phi$ and is symmetric around $A_{\text{current}} = 0$ (Fig. 3B). This again shows that the magnitude as well as the direction of the current can be controlled by varying the relative phase between the excitation pulses. For the larger values of $k_{||}$, about 5% of all excited electrons contribute to the optically induced current. A_{current} has been found to increase linearly with parallel momentum. Because the total population in the image-state band decreases with increasing $k_{||}$ (Fig. 1), the absolute number of electrons that carry a net current is roughly independent of $k_{||}$ (Fig. 2).

The solid lines in Fig. 3, A and B, depict the results of model calculations where we have numerically solved the optical Bloch equations for a multiband model. The optical generation of currents is described by considering not only resonant optical interband transitions between initially occupied and unoccupied bands, but also the field-induced intraband accelerations (*20*, *21*). Intraband accelerations are the standard components for the description of the electronic response of solids to static and low-frequency electric fields (*1*). This process, however, is often neglected when light-matter interaction is analyzed because optical frequencies cannot resonantly generate such excitations. Compared to previous theoretical treatments of current generation in GaAs, the situation at the Cu(100) surface requires two modifications. Whereas the initial state in a bulk system with three-dimensional translation symmetry is given by a single or few discrete valence bands, the projection of the bulk copper s/p band onto the surface results in a continuum of initial states for the photoexcitation (*16*, *22*). This continuum is approximated by a set of narrowly spaced dispersionless bands below the Fermi level E_F. In addition, the break of inversion symmetry at the surface opens up additional excitation pathways because nonresonant transitions are allowed between all bands, even in dipole approximation. The inclusion of resonant and nonresonant interband as well as nonresonant intraband transitions results in three qualitatively different excitation processes that contribute to the population of the excited surface state (Fig. 3C).

The first such process is the interaction of laser field $\mathcal{E}(\omega_a)$ with the polarization that is induced by the same field between the occupied bulk bands and the image-potential state. This process [(i) in Fig. 3C] can be described by pure resonant interband transitions between occupied and unoccupied bands ($a_i \rightarrow b$). It depends only on the pump field $\mathcal{E}(\omega_a)$ and is responsible for the phase-independent offset of the photoemission intensity.

The laser field $\mathcal{E}(\omega_a)$ also interacts with the two-photon polarization $\mathcal{P}^{(2)}(\omega_a) = \chi^{(2)}\mathcal{E}^2(\omega_a/2)$ generated by the laser field $\mathcal{E}(\omega_a/2)$. This process (ii) becomes possible because of the broken inversion symmetry of the copper crystal at the surface, and it is described here by inclusion of nonresonant interband transitions between different bands below E_F ($a_i \rightarrow a_{j\neq i}$). The nonvanishing $\mathcal{P}^{(2)}(\omega_a)$ alone gives rise to the well-known phenomenon of surface second-harmonic generation (*23*). Here, the interaction with the laser field $\mathcal{E}(\omega_a)$ leads to a population of the image-potential state that varies sinusoidally with $\Delta\phi$ but is symmetric in $k_{||}$ and therefore is without a phase shift for $\pm k_{||}$ (*24*).

Finally, the interaction with both laser fields can generate an optically induced current that corresponds to the population of an excited state asymmetric with respect to $k_{||}$. One of several excitation pathways for this process (iii) is illustrated in Fig. 3C. It includes the excitation of a nonresonant intraband polarization within

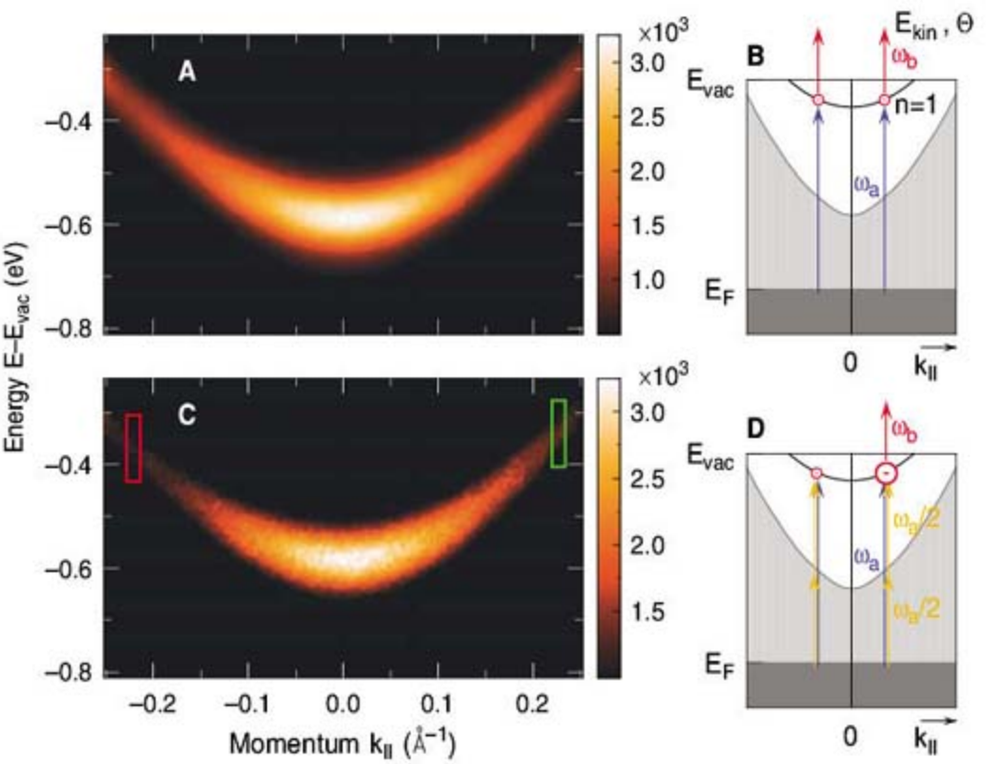

Fig. 1. (**A**) $E(k_{||})$ 2PPE spectrum of the $n = 1$ image-potential state on the Cu(100) surface. Energies are referred to the vacuum level E_{vac}. The color scale indicates the photoemission intensity. (**B**) Energy diagram of the corresponding excitation and photoemission scheme together with the surface-projected bulk band structure of Cu(100), where $E_{vac} - E_F = 4.64$ eV. Filled and empty projected bulk bands are marked by dark and light shades. The solid curve depicts the $n = 1$ image-potential band. (**C**) $E(k_{||})$ spectrum of the $n = 1$ state for excitation with two phase-locked laser pulses at frequencies ω_a and $\omega_a/2$ as depicted in (**D**). The 2PPE spectra in (A) and (C) have been recorded with zero time delay of the photoemission pulse ω_b. The red and green rectangles in (C) mark the two regions evaluated in Fig. 3.

an occupied band ($a_i \rightarrow a_{j=i}$), which is responsible for the acceleration of the excited electrons. The population is proportional to $\mathcal{E}(\omega_a)\mathcal{E}^2(\omega_a/2)$ as in process (ii) but has a phase shift of 180° for $\pm k_{||}$. However, the superposition with process (ii) leads to a reduced total phase shift, the magnitude of which depends on the ratio between the third- and second-order nonlinear susceptibilities (i.e., on the strength of specific optical transition matrix elements), but not on the relative field strengths. By adjusting the transition dipoles and the amplitudes of the two incident pulses in our model calculation, we can achieve very good agreement with the experimental data (Fig. 3, A and B).

We now turn to the decay dynamics of the generated current pulses. Electric currents in metals usually decay by means of quasi-elastic collision processes of the electrons with phonons and defects. In k-space these scattering processes lead to a fast randomization of any asymmetry of the electron population generated by the applied electric field. In our system, because the electrons are excited several electron volts above the Fermi level, an additional decay channel, ultimately limiting the time duration of the current pulses, is the inelastic electron-hole pair decay of the population of the image-potential states due to Coulomb interaction with electrons of the bulk metal (*25*). Our experimental technique is able to monitor both decay channels directly. For this purpose we detect the photoemission intensity from a 800-nm probe pulse at different time delays Δt with respect to the pump-pulse pair.

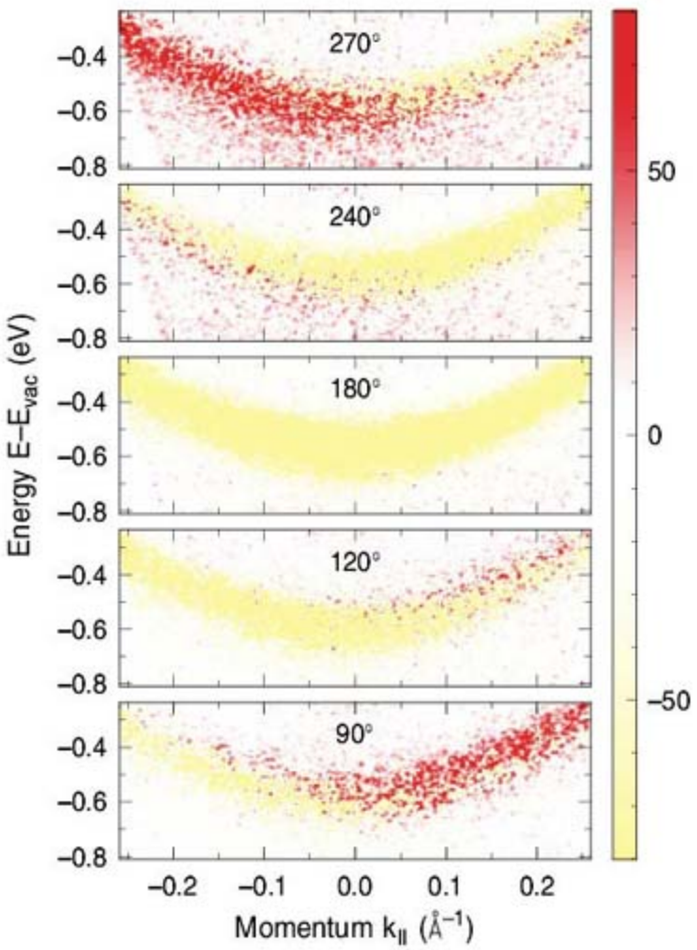

Fig. 2. Contribution of the coherently controlled surface current to the total photoemission intensity for various relative phases $\Delta\Phi$ between the ω_a and $\omega_a/2$ excitation pulses. Plotted are the differences between two-dimensional $E(k_{||})$ spectra recorded for the indicated $\Delta\phi$ and a phase-averaged spectrum. Red colors indicate an excess of electrons, yellow colors a deficiency. For 90° and 270° the maximum current is generated in directions $+k_{||}$ and $-k_{||}$, respectively.

Corresponding raw two-dimensional difference spectra together with phase-averaged intensity spectra are displayed in Fig. 4, A to D. The difference spectra correspond to the respective maxima of the coherently excited current, which have been determined by varying the relative phase between the two pump pulses for each delay (Fig. 3). The phase-averaged spectra correspond to the data observed in a conventional time-resolved 2PPE experiment. They represent the total excited-state population. Comparison of both data sets clearly shows that the asymmetry of the excited-state population levels off considerably faster than the overall population decays. At $\Delta t = 150$ fs, for example, there is still considerable population left in the image-potential band (~20%), whereas the asymmetry between positive and negative values of $k_{||}$ has vanished below the detection limit.

To quantify the decay time of the current, we evaluated the already defined asymmetry $A_{current}$ at $k_{||} = \pm 0.15$ Å^{-1} as a function of delay Δt (Fig. 4E). $A_{current}(\Delta t)$ would have a constant value if quasi-elastic scattering processes were negligible for the current decay ($\tau \rightarrow \infty$). In the limit of a very fast scattering time ($\tau \rightarrow 0$), the asymmetry would be maximum for negative Δt and would decay while electron population still built up within the finite excited-state lifetime (dashed line in Fig. 4E). The experimentally observed decrease of $A_{current}$ from its initial value of 5% corresponds to a scattering time of $\tau = 10$ fs.

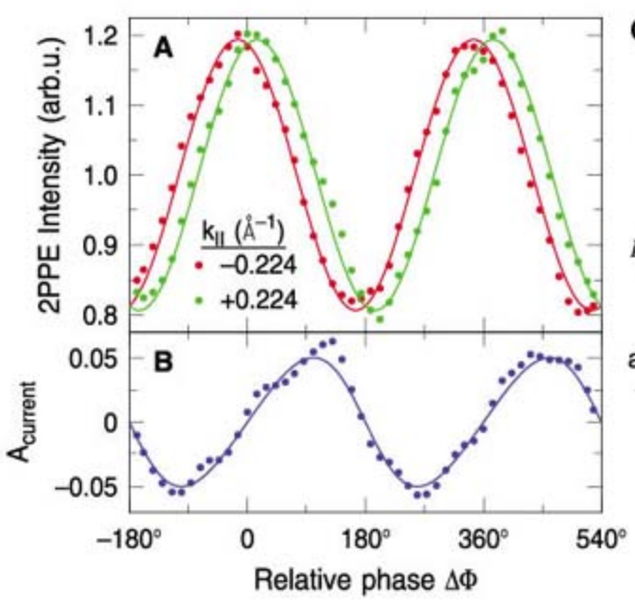

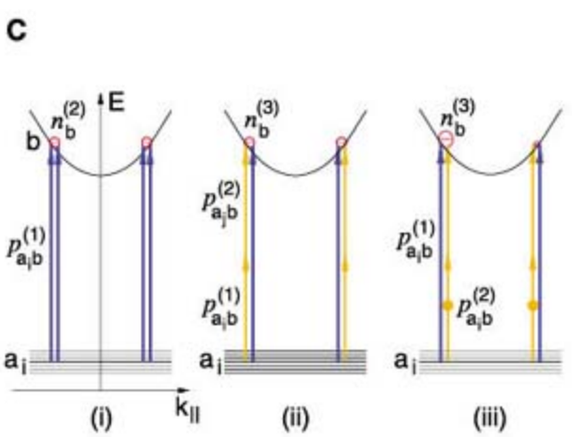

Fig. 3. (**A**) Photoemission intensity as a function of relative phase $\Delta\Phi$ for opposite parallel momentum $k_{||} = \pm 0.224$ Å^{-1}. Red and green data points, normalized experimental photoemission intensity integrated over the red and green rectangles in Fig. 1C; solid lines, model calculations. (**B**) Relative intensity contrast $A_{current}$ for opposite parallel momenta corresponding to the relative contribution of the coherently excited current to the total photoemission signal. (**C**) Illustration of the multiband model and three excitation pathways that lead to (i) an incoherent background, (ii) a phase-dependent population that is symmetric in $k_{||}$, and (iii) the coherent current generation (i.e., a phase-dependent population that is asymmetric in $k_{||}$). Interband transitions are depicted as simple arrows; intraband transitions are denoted by an additional dot.

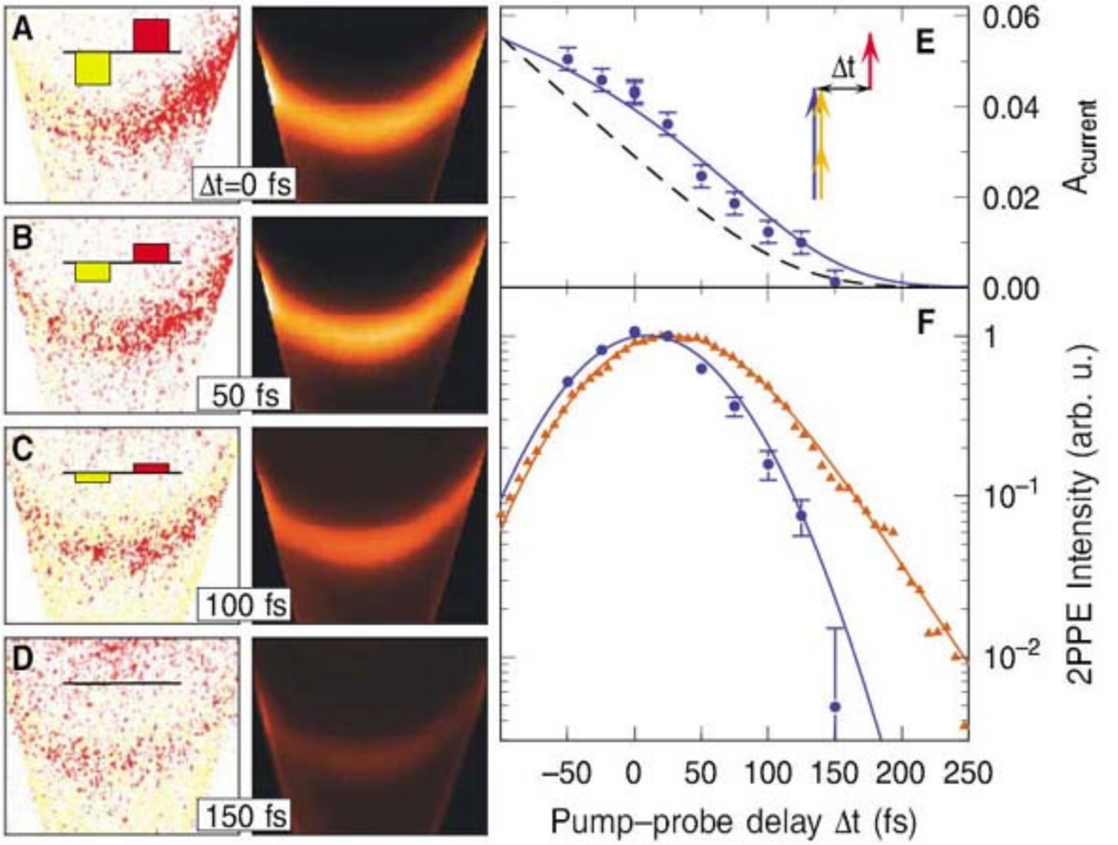

Fig. 4. (**A** to **D**) Two-dimensional difference spectra (left) and phase-averaged photoemission intensity spectra (right) for different delays Δt between the two simultaneously arriving ω_a and $\omega_a/2$ excitation pulses and the ω_b probe pulses. The color coding is the same as in Figs. 1 and 2. The red and yellow bars illustrate the corresponding asymmetries $A_{current}$ evaluated at $k_{||} = \pm 0.15$ Å^{-1}. (**E**) Asymmetry $A_{current}$ as a function of delay Δt. Dots, experimental data; solid line, model calculation for a current decay time of $\tau = 10$ fs, taking into account the finite laser pulse duration and the population decay time of 35 fs; dashed line, same calculation for an instantaneous decay ($\tau \to 0$). (**F**) Temporal evolution of the population of the $n = 1$ image-potential state at the band bottom, as given by the 2PPE intensity (orange), and the current (blue), as determined by multiplying the asymmetry $A_{current}$ with this intensity. Error bars indicate uncertainty arising from intensity fluctuations in the difference spectra.

The current thus decays much faster than the total excited-state population, which has a lifetime of 35 fs at the band bottom (Fig. 4F).

The short decay time of the current induced in the image-potential states clearly indicates that it does not predominantly decay as a result of scattering processes of electrons with bulk phonons, but decays mainly by scattering with surface imperfections (*26*). Steps, adsorbed CO molecules, or Cu adatoms were shown to have a strong influence on linewidths of 2PPE spectra as well as on the decay of quantum beats in earlier investigations of Cu(100) image-potential states (*27*–*30*). In these previous experiments, however, quasi-elastic momentum scattering processes were just one of many possible contributions to the measurement, whereas they are singled out in the present work. Other factors that may enter the 2PPE linewidth are instrumental broadening effects, surface inhomogeneities, or the temporal shape of short laser pulses. Moreover, intraband electron-scattering processes that conserve energy and momentum contribute to dephasing and line broadening but do not lead to current decay. Under the assumption that these factors were negligible in the previous studies, the current decay time of $\tau = 10$ fs measured here corresponds to a defect concentration of 1 to 2% of a monolayer (*26*).

Note that our method for the investigation of ultrafast current dynamics uses a coherent optical excitation scheme only for the creation of an initially asymmetric population distribution in momentum space. Unlike in interferometric 2PPE (*6*, *31*), there is no fixed phase relationship between the excitation pulses and the time-delayed photoemission probe pulse used for band mapping. The scattering processes leading to current decay are thus observed directly in terms of an incoherent population dynamics in momentum space. This stands in contrast to methods that deduce quasi-elastic scattering times from phase decay rates in various ways. These include previous 2PPE experiments (*6*, *14*, *27*, *29*) as well as most all-optical spectroscopies (*32*). For this reason, we believe that the microscopic understanding of carrier transport, not only in metallic systems but also in well-studied semiconductors, could benefit from a combination of coherent current generation with time-resolved photoelectron spectroscopy. Because the escape depth of low–kinetic energy photoelectrons from solids amounts to several tens of atomic layers (*9*), the detection method is certainly not restricted to surfaces.

References and Notes

1. N. W. Ashcroft, N. D. Mermin, *Solid State Physics* (Holt, Rinehart & Winston, New York, 1976).
2. E. Dupont, P. B. Corkum, H. C. Liu, M. Buchanan, Z. R. Wasilewski, *Phys. Rev. Lett.* **74**, 3596 (1995).
3. A. Haché *et al.*, *Phys. Rev. Lett.* **78**, 306 (1997).
4. D. Cote, J. M. Fraser, M. DeCamp, P. H. Bucksbaum, H. M. van Driel, *Appl. Phys. Lett.* **75**, 3959 (1999).
5. P. Brumer, M. Shapiro, *Chem. Phys. Lett.* **126**, 541 (1986).
6. S. Ogawa, H. Nagano, H. Petek, A. P. Heberle, *Phys. Rev. Lett.* **78**, 1339 (1997).
7. H. Petek *et al.*, *Phys. Rev. Lett.* **79**, 4649 (1997).
8. U. Höfer *et al.*, *Science* **277**, 1480 (1997).
9. S. Hüfner, *Photoelectron Spectroscopy—Principles and Applications* (Springer, Berlin, 2003).
10. The experiments were performed at room temperature in an ultrahigh-vacuum chamber with a base pressure of 6×10^{-11} mbar. The Cu(100) sample was prepared by standard sputtering and annealing procedures. Surface cleanliness and order were verified by x-ray photoemission spectroscopy and low-energy electron diffraction. The optical setup to generate phase-locked ultrashort pump laser pulses at frequencies ω_a and $\omega_a/2$ is described in detail in (*31*). Their wavelength varied between 270 and 285 nm (540 and 570 nm); the pulse durations were 90 and 60 fs. The time-delayed probe pulse for photoemission (ω_b) had a wavelength of 800 nm and a pulse duration of 70 fs. For the measurements that did not require a time delay between pump and probe pulses (Figs. 1 to 3), the photoelectrons emitted by the half-gap pulses were recorded (i.e., $\omega_b = \omega_a/2$). A hemispherical electron analyzer equipped with an angle-resolved lens mode and a two-dimensional image-type detector (Specs Phoibos-150) served as the electron spectrometer (*17*).
11. P. M. Echenique, J. B. Pendry, *J. Phys. C* **11**, 2065 (1978).
12. K. Giesen *et al.*, *Phys. Rev. B* **35**, 975 (1987).
13. R. W. Schoenlein, J. G. Fujimoto, G. L. Eesley, T. W. Capehart, *Phys. Rev. Lett.* **61**, 2596 (1988).
14. E. Knoesel, A. Hotzel, M. Wolf, *J. Electron Spectrosc. Relat. Phenom.* **88–91**, 577 (1998).
15. N. H. Ge *et al.*, *Science* **279**, 202 (1998).
16. I. L. Shumay *et al.*, *Phys. Rev. B* **58**, 13974 (1998).
17. M. Rohleder, K. Duncker, W. Berthold, J. Güdde, U. Höfer, *N. J. Phys.* **7**, 103 (2005).
18. The constant offset ϕ_0 is unknown for the position of the sample surface. It is fixed here by setting $\Delta\phi = 0$ for a maximum of the total photoemission intensity.
19. The total value of generated current density $j_{||}$ may be estimated from the photoemission intensity of the difference spectra, which corresponds to $n_e \approx 10^{-6}$ per surface atom, and by considering that the electrons with a mean $k_{||} = 0.1$ Å^{-1} have velocities of $v_{||} \approx 1$ Å/fs. We arrive at $j_{||} \approx 1$ nA per surface atom.
20. T. Meier, F. Rossi, P. Thomas, S. W. Koch, *Phys. Rev. Lett.* **75**, 2558 (1995).
21. H. T. Duc, T. Meier, S. W. Koch, *Phys. Rev. Lett.* **95**, 086606 (2005).
22. M. J. Weida, S. Ogawa, H. Nagano, H. Petek, *J. Opt. Soc. Am. B* **17**, 1443 (2000).

23. T. F. Heinz, in *Nonlinear Surface Electromagnetic Phenomena*, H.-E. Ponath, G. I. Stegeman, Eds. (Elsevier, Amsterdam, 1991), pp. 353–416.
24. J. M. Fraser, A. I. Shkrebtii, J. E. Sipe, H. M. van Driel, *Phys. Rev. Lett.* **83**, 4192 (1999).
25. P. M. Echenique *et al.*, *Surf. Sci. Rep.* **52**, 219 (2004).
26. See supporting material on *Science* Online.
27. C. Reuß *et al.*, *Phys. Rev. Lett.* **82**, 153 (1999).
28. M. Roth, M. T. Pickel, J. X. Wang, M. Weinelt, T. Fauster, *Phys. Rev. Lett.* **88**, 096802 (2002).
29. K. Boger, M. Weinelt, T. Fauster, *Phys. Rev. Lett.* **92**, 126803 (2004).
30. F. E. Olsson *et al.*, *Phys. Rev. B* **70**, 205417 (2004).
31. J. Güdde, M. Rohleder, U. Höfer, *Appl. Phys. A* **85**, 345 (2006).
32. J. Shah, *Ultrafast Spectroscopy of Semiconductors and Semiconductor Nanostructures* (Springer-Verlag, Berlin, 1996).

33. Supported by Deutsche Forschungsgemeinschaft grant HO 2295/3 and by the Center for Optodynamics, Marburg, Germany.

Supporting Online Material

www.sciencemag.org/cgi/content/full/318/5854/1287/DC1
SOM Text
References

20 June 2007; accepted 3 October 2007
10.1126/science.1146764

Emission of Coherent THz Radiation from Superconductors

L. Ozyuzer,[1,2] A. E. Koshelev,[2] C. Kurter,[2,3] N. Gopalsami,[4] Q. Li,[2] M. Tachiki,[5] K. Kadowaki,[6] T. Yamamoto,[6] H. Minami,[6] H. Yamaguchi,[6] T. Tachiki,[7] K. E. Gray,[2] W.-K. Kwok,[2] U. Welp[2]*

Compact solid-state sources of terahertz (THz) radiation are being sought for sensing, imaging, and spectroscopy applications across the physical and biological sciences. We demonstrate that coherent continuous-wave THz radiation of sizable power can be extracted from intrinsic Josephson junctions in the layered high-temperature superconductor $Bi_2Sr_2CaCu_2O_8$. In analogy to a laser cavity, the excitation of an electromagnetic cavity resonance inside the sample generates a macroscopic coherent state in which a large number of junctions are synchronized to oscillate in phase. The emission power is found to increase as the square of the number of junctions reaching values of 0.5 microwatt at frequencies up to 0.85 THz, and persists up to ~50 kelvin. These results should stimulate the development of superconducting compact sources of THz radiation.

The observed gap in the generation of electromagnetic radiation, extending approximately from 0.5 THz to 2 THz, stems from the separation of the two general paradigms for generating electromagnetic waves (*1*–*3*): alternating currents in semiconductor-based electronics and electronic transitions between quantized electronic states in lasers, respectively. The frequency of semiconductor devices is bounded from above by limits of the electron velocities, whereas the frequency of solid-state lasers is bounded from below by thermal energies that limit the smallest electronic transitions useful for lasing. Josephson junctions—two superconducting electrodes separated by a thin insulating layer—naturally convert dc voltages into high-frequency electromagnetic radiation spanning the THz gap, with 1 mV corresponding to 0.483 THz. Although the emission from a single junction is weak, many such junctions emitting in phase at the same frequency can produce useful emission power (*4*–*6*). Stacks of junctions with unsurpassed packing density occur naturally in the layered high-temperature superconductor $Bi_2Sr_2CaCu_2O_8$ (BSCCO). This material, composed of superconducting CuO_2-layers that are coupled through the intrinsic Josephson effect (*7*), can sustain high voltages across the junctions and holds the potential for very intense, coherent radiation (*8*–*10*) that covers the THz gap. However, the key requirement for producing useful radiation from BSCCO, namely achieving synchronization of the high-frequency oscillations of all the junctions in the stack, has so far been a major challenge preventing the realization of this potential. Various approaches for synchronizing the junctions have been considered, such as applying a magnetic field to induce coherent Josephson vortex flow (*11*–*16*) or inserting the BSCCO crystal into a microwave cavity (*17*). However, the far-field radiation power obtained from BSCCO is limited to the pW range (*18*).

We show that THz radiation power in the μW range can be produced using a method by which the phase of the emission from the atomic scale Josephson junctions in BSSCO is synchronized by a standing electromagnetic wave that is formed by multiple reflections in the cavity formed by the side surfaces of the crystal, exactly as in a laser. Electromagnetic waves inside a BSCCO crystal propagate as Josephson plasma modes (*19*–*21*), which resemble the guided modes in an optical waveguide. The average electric field on the side surfaces cancels in all but the in-phase mode, so only this mode produces noticeable emission (Fig. 1, C and D). Resonances that occur on the long dimension of the mesa incur sign changes of the electric field on the long side faces and do not contribute to the emission in a substantial way. In the in-phase mode, the coherent superposition of the electromagnetic waves from each junction creates a macroscopic coherent state in which the radiation power increases as the square of the number of junctions. We report that more than 500 junctions can be made to oscillate in phase, producing continuous wave coherent radiation power up to ~0.5 μW at frequencies up to 0.85 THz. The available power is potentially much larger, because there is evidence that 20 μW of power are pumped into the observed THz cavity resonance. The emission persists up to temperatures of ~50 K. In contrast to previous studies (*11*–*16*), emission does not require the application of a magnetic field, considerably simplifying the design of superconducting THz sources. In fact, a single applied dc current leads to the efficient excitation of continuous coherent THz radiation.

We report results on a series of BSCCO samples in the form of mesas (Fig. 1, A and B) with widths varying from 40 μm to 100 μm, a length of 300 μm, and a height of about 1 μm. The mesas and the electrical contacts are fabricated in a series of thermal evaporation, photolithography, and Ar ion milling steps (*22*).

Figure 2 shows the current-voltage-characteristics (IV-c) and the radiation power detected by the bolometer. Both quantities are recorded simultaneously as a function of decreasing bias voltage for the parallel and perpendicular settings of a parallel-plate cut-off filter (*22*). The data reveal peaks of radiation near 0.37 V and 0.71 V that are polarized with their E-field perpendicular to the CuO_2-planes, and unpolarized radiation at high current and voltage bias. The former is identified as Josephson radiation, whereas the latter is thermal radiation. Upon rotating the cut-off filter, both peaks decrease in the same proportion, indicating the same radiation frequency. The peak power in Fig. 2 is around 11 nW, and we recorded up to 50 nW when no filters are inserted into the beam path (fig. S4). Correcting for the collection angle of the bolometer yields a total radiation power of the sample of ~0.5 μW. These values are more than 10^4 times as large as previous reports on far-field radiation from BSCCO mesas (*18*). The back-bending of the IV-c and the unpolarized thermal radiation indicate heating of the mesa at the highest currents. The effective mesa temperatures along the IV-c, shown in Fig. 2, are estimated by

[1]Department of Physics, Izmir Institute of Technology, TR-35430 Izmir, Turkey. [2]Materials Science Division, Argonne National Laboratory, Argonne, IL 60439, USA. [3]Physics Division, Illinois Institute of Technology, Chicago, IL 60616, USA. [4]Nuclear Engineering Division, Argonne National Laboratory, Argonne, IL 60439, USA. [5]Graduate School of Frontier Sciences, The University of Tokyo, 5-1-5 Kashiwanoha, Kashiwa 277-8568, Japan. [6]Institute of Materials Science, University of Tsukuba, 1-1-1 Tennodai, Tsukuba-shi, Ibaraki-ken 305-8577, Japan. [7]Department of Electrical and Electronic Engineering, National Defence Academy, Hashirimizu 1-10-20, Yokosuka, Kanagawa 239-8686, Japan.

*To whom correspondence should be addressed. E-mail: welp@anl.gov

equating (*23*) the mesa resistivity to the quasiparticle resistivity, $\rho_c(T)$, of BSCCO (fig. S5). Also included in Fig. 2 is a simulation of the thermal radiation obtained with the help of the Stefan-Boltzmann law and a numerical solution of the heat-diffusion equation (*22*). The agreement of the simulation with the data shows that our thermal model is accurate and that thermal management in such large mesas can be achieved.

An estimation of the radiation frequency is given by the filter cut-off frequency at which the polarization ratio levels off (Fig. 3 A) and by far-infrared spectra (Fig. 3B). Both methods yield consistent results, i.e., 0.36, 0.48, 0.59, and 0.85 THz for the 100-μm, 80-μm, 60-μm and 40-μm wide mesas, respectively. The value of 0.85 THz is the highest frequency of far-field radiation from a superconducting source yet observed (fig. S8). These frequency values are in good agreement with the fundamental cavity resonance, $f = c_0/2nw$, where w is the width of the mesa and $n \approx 3.5$ is the c-axis far-infrared refractive index of BSCCO (*24*), which for $w = 80$ μm yields $f = 0.52$ THz. Furthermore, the observed radiation frequencies increase approximately proportionally to $1/w$ (see inset of Fig. 3 B), demonstrating that they correspond to a cavity resonance. To excite this resonance, the Josephson frequency, $f = V_{jct}/\Phi_0$ should match the resonance frequency, where Φ_0 is the flux quantum and V_{jct} the voltage per junction. Using the mesa height of 1.1 μm as determined from atomic force microscopy, and 1.56 nm spacing of the CuO_2-double layers, the voltage shown in Fig. 2 for the large radiation peak of the 80-μm mesa corresponds to 0.49 THz, consistent with the spectroscopic data. Thus, upon decreasing the bias from the fully resistive state, the emission power builds up as the Josephson frequency comes into resonance with the cavity. With decreasing voltage, some junctions may switch back from the resistive into the superconducting state (*25*). During such a jump the voltage per remaining resistive junction and the Josephson frequency increase. Consequently, the system falls out of resonance with the cavity mode, and emission ceases. With further decreasing bias, the resonance is again approached from above, and the behavior repeats itself, yielding a second emission peak involving a smaller number of active junctions.

Radiation from the same sample containing a varying number of emitting junctions allows for a direct test of coherency. Figure 4A displays a sequence of emission peaks for positive and negative bias voltages on the 80-μm mesa. The fraction of active junctions, n_{rel}, relative to the highest emission peak, can be determined directly from the resistances corresponding to the various branches in the IV-c (fig. S7). An analysis (*10*, *26*) of the loss mechanisms shows that for mesas with height less than 1.0 to 1.5 μm, quasiparticle losses are larger than losses due to radiation. In this limit, the emitted power increases like the square of the number of coherently oscillating junctions. The experimentally observed peak powers are proportional to n_{rel}^2, demonstrating directly that the junctions in the stack emit coherently. Figure 4C shows a close-up of the return branch of IV-c and of the radiation power of the third peak in Fig. 4A. The absence of a jump in the IV-c allows us to establish a baseline of the current and to determine the excess current that supplies the energy for the excitation of the cavity resonance. The height of the resonance in the IV-c depends on the quality factor of the cavity resonance (*26*). These data suggest that about 20 μW—about 2.5% of the total dc power dissipated in the mesa—are pumped into the in-phase resonance, implying that considerably enhanced radiation powers could be obtained with this mesa, for example, through improved impedance matching with the help of antennas, gratings, or dielectric coatings.

In a homogeneous mesa in zero magnetic field, the Josephson oscillations do not couple directly to the cavity resonances. However, when the Josephson frequency is twice as large as the cavity frequency, the resonance may be excited as a result of a parametric instability leading to so-called zero field steps in the IV-c, which were observed in conventional Josephson junctions (*27*). Our frequency analysis rules out this excitation mechanism. A plausible mechanism of coupling can arise from an asymmetric modulation of the Josephson critical current

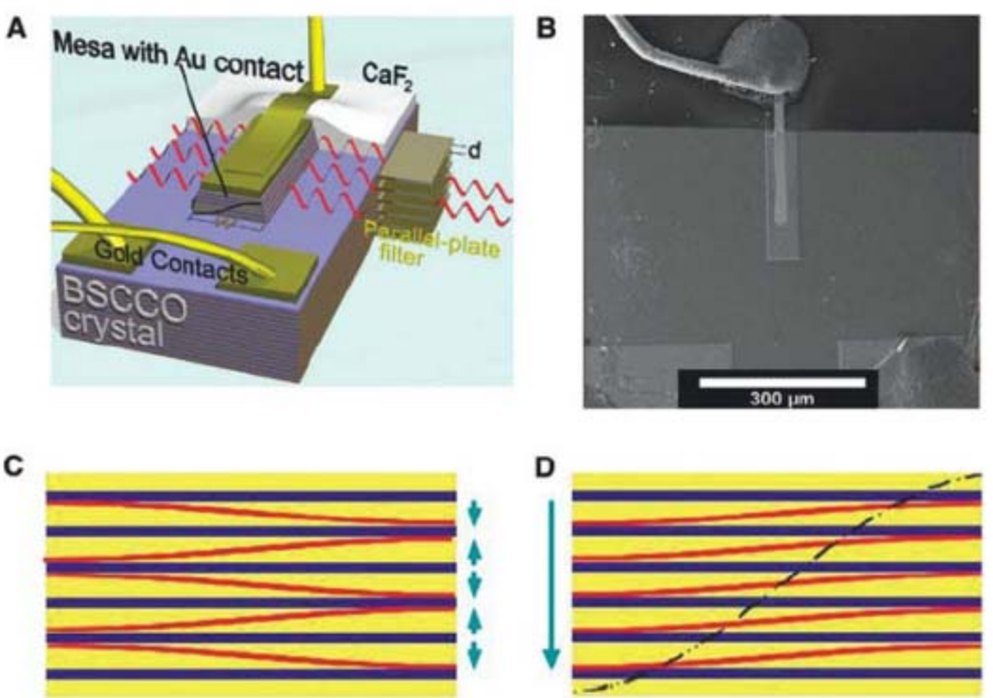

Fig. 1. (**A**) Schematic of the BSCCO mesas. The applied c-axis current excites the fundamental cavity mode (solid half-wave) on the width w of the mesa, and high-frequency electromagnetic radiation is emitted from the side faces (red waves), whose polarization and frequency are analyzed with parallel-plate filters (*22*). (**B**) Scanning electron microscopy image of the mesa. Schematics of the anti-phase (**C**) and of the in-phase (**D**) mode. The blue and yellow layers are the CuO_2 layers and Bi-Sr-O layers. The red waves represent the alternating electric field. In the anti-phase mode the electric field on the long side face largely cancels, resulting in negligible emission. For the in-phase mode, the electric fields from each junction add to create an intense standing wave (black dashed line) and strong emission.

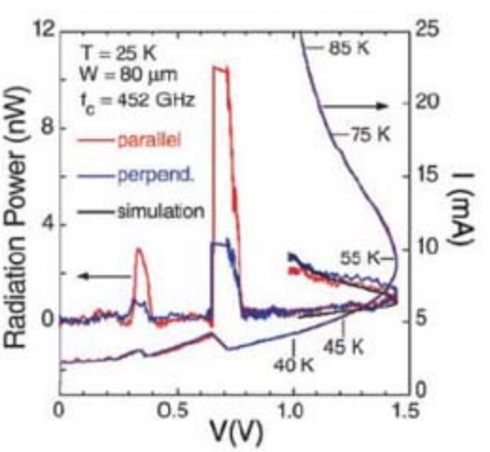

Fig. 2. Current-voltage characteristics and radiation power of the 80-μm mesa. The voltage dependence of the current (right y-axis) and of the radiation power (left y-axis) at 25 K for parallel and perpendicular settings of the filter with 0.452 THz cut-off frequency are shown for decreasing bias in zero applied magnetic field. Polarized Josephson emission occurs near 0.71 and 0.37 V, and unpolarized thermal radiation occurs at higher bias. The black solid line is a simulation of the thermal radiation (*22*).

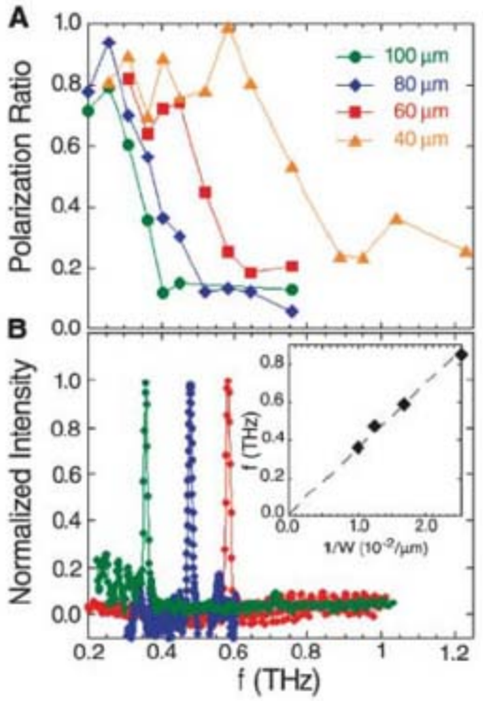

Fig. 3. Spectral characterization of the emission. **(A)** The polarization ratio—defined as the ratio the radiation power measured at perpendicular and at parallel filter settings—of the emission peaks is shown for four mesas as a function of cut-off frequency of the filters. The radiation frequency is estimated from the filter cut-off frequency at which the polarization ratio levels off at high frequencies (*22*). **(B)** Far-infrared spectra of the Josephson radiation. Sharp emission lines are clearly resolved. The observed line width of ~9 GHz (FWHM) is instrument-resolution limited. The scaling of the emission frequency with the inverse mesa width, shown in the inset, demonstrates that a cavity resonance on the width is excited.

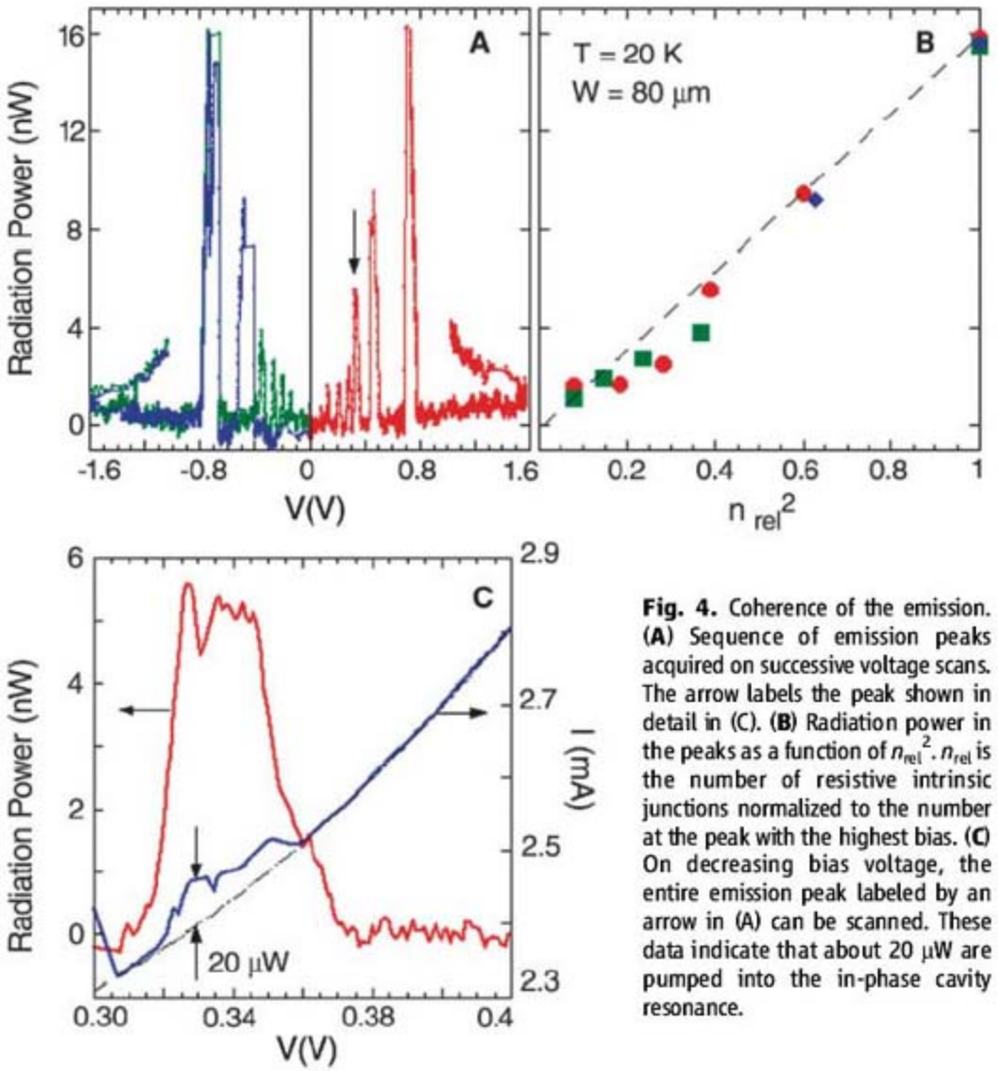

Fig. 4. Coherence of the emission. **(A)** Sequence of emission peaks acquired on successive voltage scans. The arrow labels the peak shown in detail in (C). **(B)** Radiation power in the peaks as a function of n_{rel}^2. n_{rel} is the number of resistive intrinsic junctions normalized to the number at the peak with the highest bias. **(C)** On decreasing bias voltage, the entire emission peak labeled by an arrow in (A) can be scanned. These data indicate that about 20 μW are pumped into the in-phase cavity resonance.

along the width of the mesa, due to, for example, an inhomogeneous oxygen concentration or defects induced during fabrication processes. For single junctions, the coupling of a modulated critical current distribution to cavity resonances has been observed (*28*). A recent quantitative analysis of radiation and transport properties of mesas with such modulation (*26*) suggests that the radiation power from the mesas described here can be as high as 1 mW under optimized conditions. Therefore, we anticipate that the observed radiation power can be significantly increased by enhancing the coupling to the internal cavity mode by deliberately introduced strong modulations of the Josephson critical current. There is a large effort to develop quantum cascade lasers as sources of THz radiation (*1*). Presently, their lowest emission frequency is ~1.6 THz, with a continuous wave emission power of ~0.5 mW (*1*, *29*). The superconducting sources described here are a competitive technology for the frequency range of 0.5 THz to 1.5 THz, which is also the range where compact solid-state sources are most lacking.

References and Notes

1. M. Tonouchi, *Nat. Photon.* **1**, 97 (2007).
2. M. Lee, M. C. Wanke, *Science* **316**, 64 (2007).
3. A. Borak, *Science* **308**, 638 (2005).
4. M. Darula, T. Doderer, S. Beuven, *Supercond. Sci. Technol.* **12**, R1 (1999).
5. A. K. Jain, K. K. Likharev, J. E. Lukens, J. E. Sauvageau, *Phys. Rep.* **109**, 309 (1984).
6. P. Barbara, A. B. Cawthorne, S. V. Shitov, C. J. Lobb, *Phys. Rev. Lett.* **82**, 1963 (1999).
7. R. Kleiner, F. Steinmeyer, G. Kunkel, P. Müller, *Phys. Rev. Lett.* **68**, 2394 (1992).
8. T. Koyama, M. Tachiki, *Solid State Commun.* **96**, 367 (1995).
9. M. Tachiki, M. Iizuka, K. Minami, S. Tejima, H. Nakamura, *Phys. Rev. B* **71**, 134515 (2005).
10. L. N. Bulaevskii, A. E. Koshelev, *J. Superconduct. Novel Magnetism* **19**, 349 (2006).
11. H. B. Wang *et al.*, *Appl. Phys. Lett.* **89**, 252506 (2006).
12. M.-H. Bae, H.-J. Lee, J.-H. Choi, *Phys. Rev. Lett.* **98**, 027002 (2007).
13. K. Kadowaki *et al.*, *Physica C* **437-438**, 111 (2006).
14. A. Irie, Y. Hirai, G. Oya, *Appl. Phys. Lett.* **72**, 2159 (1998).
15. V. M. Krasnov, N. Mros, A. Yurgens, D. Winkler, *Phys. Rev. B* **59**, 8463 (1999).
16. S. M. Kim *et al.*, *Phys. Rev. B* **72**, 140504 (2005).
17. S. Madsen, G. Fillatrella, N. F. Pedersen, *Eur. Phys. J. B* **40**, 209 (2004).
18. I. E. Batov *et al.*, *Appl. Phys. Lett.* **88**, 262504 (2006).
19. R. Kleiner, *Phys. Rev. B* **50**, 6919 (1994).
20. L. N. Bulaevskii, M. Zamora, D. Baeriswyl, H. Beck, J. R. Clem, *Phys. Rev. B* **50**, 12831 (1994).
21. N. F. Pedersen, S. Sakai, *Phys. Rev. B* **58**, 2820 (1998).
22. Materials and methods are available as supporting material on *Science* Online.
23. A. Yurgens, D. Winkler, N. V. Zavaritsky, T. Claeson, *Phys. Rev. Lett.* **79**, 5122 (1997).
24. M. B. Gaifullin, M. Matsuda, N. Chikumoto, J. Shimoyama, K. Kishio, *Phys. Rev. Lett.* **84**, 2945 (2000).
25. M. Machida, T. Koyama, M. Tachiki, *Phys. Rev. Lett.* **83**, 4618 (1999).
26. A. E. Koshelev, L. N. Bulaevskii, cond-mat/0708.3269.
27. T. A. Fulton, R. C. Dynes, *Solid State Commun.* **12**, 57 (1973).
28. M. Russo, R. Vaglio, *Phys. Rev. B* **17**, 2171 (1978).
29. C. Walther, G. Scalari, J. Faist, H. Beere, D. Ritchie, *Appl. Phys. Lett.* **89**, 231121 (2006).

30. We thank L. Bulaevskii for many illuminating discussions; A. Imre for assistance with the microscopy performed at the Electron Microscopy Center and at the Center for Nanoscale Materials, both at Argonne National Laboratory; and R. Eyes for quantitative analysis of the transmission through parallel-plate filters. This work was supported by the U.S. Department of Energy–Basic Energy Sciences under contract DE-AC02-06CH11357; the Japanese Ministry of Education, Culture, Sports, Science, and Technology; and the Turkish TUBITAK under project 106T053. We thank the Institute for Theoretical Sciences, a joint institute of Argonne National Laboratory and the University of Notre Dame, for program coordination support.

Supporting Online Material

www.sciencemag.org/cgi/content/full/318/5854/1291/DC1
Materials and Methods
Figs. S1 to S8
References

28 August 2007; accepted 2 October 2007
10.1126/science.1149802

Shape and Temperature Memory of Nanocomposites with Broadened Glass Transition

Pierre Miaudet,[1] Alain Derré,[1] Maryse Maugey,[1] Cécile Zakri,[1] Patrick M. Piccione,[2] Rabi Inoubli,[2] Philippe Poulin[1]*

Shape-memory polymers can revert to their original shape when they are reheated. The stress generated by shape recovery is a growing function of the energy absorbed during deformation at a high temperature; thus, high energy to failure is a necessary condition for strong shape-memory materials. We report on the properties of composite nanotube fibers that exhibit this particular feature. We observed that these composites can generate a stress upon shape recovery up to two orders of magnitude greater than that generated by conventional polymers. In addition, the nanoparticles induce a broadening of the glass transition and a temperature memory with a peak of recovery stress at the temperature of their initial deformation.

Shape-memory materials (*1*) are usually made of lightweight polymers (*2*) or metallic alloys (*3*). They have been investigated for more than 30 years and have applications in packaging, biomedical devices, heat-shrink tubing, deployable structures, microdevices, etc. Shape-memory polymers are deformed at a high temperature (T_d) and then cooled down under fixed strain to trap the deformed polymer chains, thus storing mechanical energy. Upon reheating, typically in the vicinity of the glass transition temperature (T_g), the polymer chains become mobile, and the material can relax by reverting toward its original and more stable shape. The efficiency of a shape-memory polymer is empirically controlled by its composition, as defined by the polymer's chemical structure, molecular weight, degree of cross-linking, and fraction of amorphous and crystalline domains (*2*, *4*–*7*). The energy that is restored with shape recovery is a growing function of the energy supplied during the deformation at a high temperature (*4*, *8*). Shape-memory polymers can exhibit large strain when they revert toward their initial shape. Unfortunately, this large strain is usually associated with a low stress recovery from a few tenths of a megapascal to a few tens of megapascals (*2*, *8*–*11*). Consequently, the energy density, which results from a combination of stress and strain, is rather low and not among the best as compared with other actuator technologies (*9*). For example, the recovery stress of shape-memory metallic alloys can reach 800 MPa for the best materials (*3*). Shape-memory effects of alloys are based on a temperature-induced martensitic phase transformation from a low- to a high-symmetry crystallographic structure (*3*, *12*, *13*). In spite of their large stress recovery, shape-memory alloys have several drawbacks when compared to polymers. They are six times heavier than polymers, and their recovery strain does not exceed 8%. Combining large stress and large strain recovery, as well as finding more controlled programming procedures, remain critical challenges for the development of smarter and stronger shape-memory materials.

The inclusion of nanoparticles has been shown to improve the behavior of shape-memory polymers. These efforts include an increase in their mechanical properties (*14*–*17*), the addition of conductive nanoparticles to achieve shape-memory effects, which can be triggered by Joule's heating (*18*), or the inclusion of magnetic nanoparticles, which can cause heating in the presence of an alternating magnetic field (*19*). Other smart nanocomposites have been made by adding carbon nanotubes (CNTs) to conductive polymers (*20*) or elastomers (*21*).

We studied fibers that contain a large fraction of CNTs embedded in polyvinyl alcohol (PVA). They are obtained by a particular coagulation spinning process that allows a homogeneous distribution of the CNTs within the fibers. Those fibers are investigated because they are known to exhibit an exceptional energy to failure (*22*, *23*), which is a necessary condition to store a large amount of mechanical energy. Elicarb CNTs (single walled nanotubes from Thomas Swan, County Durham, United Kingdom) were used (see section 1 in *24*). The spinning process (*25*) consists of injecting a dispersion of surfactant-stabilized CNTs in the co-flowing stream of a coagulating polymer solution. PVA (molecular weight 195,000 provided by Seppic, Paris, France) was used as coagulating agent. This method leads to nanotube-PVA composite fibers with a fraction of nanotubes of ~20 weight percent. PVA was chosen because it exhibits strong interactions with CNTs. This is reflected in the effective coagulation spinning and high toughness of the composite fibers.

The obtained fibers are stretched at a deformation temperature T_d and then cooled down to room temperature under fixed strain. Their length does not change when the load is released at room temperature, thus showing good "shape fixity." The fibers, however, shrink substantially when they are reheated (*24*). Quantitative characterizations are obtained by performing thermomechanical measurements in a temperature-controlled chamber (see section 3 in *24*). Figure 1 shows the stress needed to stretch the fibers up to 800% at different temperatures. A greater stress is needed to deform the fibers at low T_d. At higher T_d, the fibers become softer and can be more easily deformed; this softness is associated with a lower supply of mechanical energy. This can be estimated from Fig. 1, where the area under each curve corresponds to the energy supplied to the fibers at different T_d, from 70° to 180°C, and upon mechanical stretching.

As shown in Fig. 2, when reheated at fixed strain the fibers generate a strong stress with a maximum at a well-defined temperature (T_s). The occurrence of a peak recovery stress in conditions of fixed strain has already been observed for other shape-memory polymers and nanocomposites (*8*, *26*), but with no direct link between T_s and T_d. In conventional materials, the peak of recovery stress occurs in the vicinity of the glass transition of the neat polymer. In fact, this is interpreted in the literature as a direct manifestation of the glass transition of the pure polymer (*26*). When the

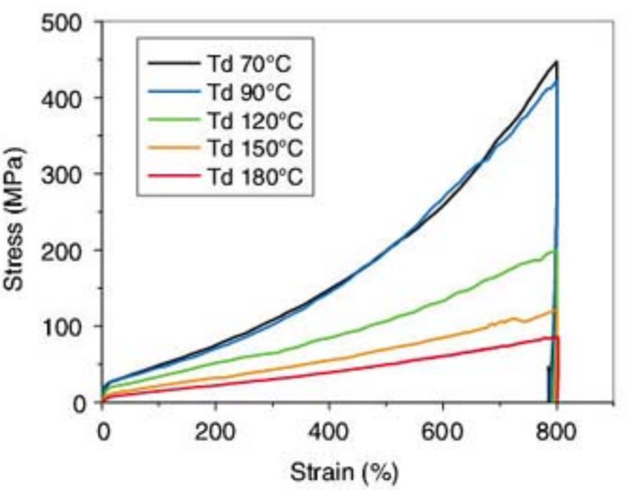

Fig. 1. Stress versus strain curves of nanotube-composite fibers. The fibers are stretched up to 800% at different temperatures (T_d). The area under the curves corresponds to the mechanical energy supplied to the fibers.

[1]Centre de Recherche Paul Pascal–CNRS, Université Bordeaux I, 115 Avenue Schweitzer, F-33600 Pessac, France. [2]Arkema, Groupement de Recherches de Lacq, RN 117, F-64170 Lacq, France.

*To whom correspondence should be addressed. E-mail: poulin@crpp-bordeaux.cnrs.fr

materials are initially deformed above the glass temperature transition, the peak disappears and the stress generated by shape recovery substantially decreases. This occurs because polymer chains can relax when deformed at temperatures well above T_g, thus decreasing the potential for stored mechanical energy.

In this case, the peak is preserved well above the T_g of the neat PVA and, more strikingly, T_s and T_d are roughly equal. This near-equality means that the fibers memorize the temperature at which they have been deformed. The peak of stress generated can be observed up to 180°C, which is ~100°C above the T_g of the neat PVA (see section 4 in *24*). This distinctive feature provides an opportunity to rationally control T_s without varying the chemical structure of the material. In addition, it is observed that the maximal stress generated by the fiber is close to 150 MPa. This value is from one to two orders of magnitude greater than the stress generated by conventional shape-memory polymers. It is obtained for fibers that have been deformed at 70° and 90°C, temperatures that are in the vicinity of the T_g of the neat PVA. These temperatures correspond to the conditions for which the greatest energy is supplied during the initial deformation. The stress recovery is closer to the stress generated by shape-memory metallic alloys, which ranges between 200 and 800 MPa for NiTi alloys (*3*, *9*, *12*, *13*). However, nanotube fibers, like other polymeric materials, are much lighter (1.4 versus 6.5 g/cm^3 for NiTi) and exhibit strain recovery greater than that of the best metallic alloys (several tens of a percent versus 8% for NiTi).

The strain recovery rate under conditions of free load is shown in Fig. 3. The strain recovery rate is taken as $\frac{l_d - l(T)}{l_d}$, where l_d is the length of the fiber after deformation at T_d and cooling at room temperature, and $l(T)$ is the length of the fiber upon reheating at a given temperature T. Other practical examples of large strain recovery are shown in Movies S1 and S2 (*24*). The curves in Fig. 3 are shifted to the right with increasing T_d. This is again a consequence of the temperature memory, and fibers that have been stretched at greater T_d recover their shape at higher temperatures. An inflexion region can be seen in the curves of Fig. 3. The temperature of this inflexion is close to T_d. Although the temperature memory is more clearly observed through peaks of recovery stress, it is still apparent in strain recovery experiments.

Additionally, because CNT fibers are electrically conductive, the thermal shape-memory effects can be triggered by Joule's heating when an electrical current is passed through the fiber (*24*). This can be beneficial for the direct use in microdevices where heating by an external source can be difficult.

The present results can be understood on the basis of previous knowledge of the structure of CNT-PVA fibers and on the main known features of nanocomposites and shape-memory polymers. Shape-memory polymers usually involve two phases (*2*, *4*, *5*, *17*): (i) a fixed one, which can be made of crystallites, rigid segments, or chemical cross-links, and (ii) a mobile one, which is made of amorphous polymer. The latter drives shape-memory effects through elongation and contraction of the polymer chains during programming and shape recovery, respectively, but the fixed phase is necessary to lock deformations in the material. Shape-memory effects are more pronounced in the vicinity of T_g, because this temperature corresponds to the relaxation of the amorphous fractions of the polymer. CNTs substantially alter the thermomechanical properties of the composite fibers in several ways. First, and as shown in Fig. 4, they act as reinforcements characterized by an increase of one order of magnitude of the storage modulus. Second and as already reported (*23*, *27*), they favor the stabilization of crystalline domains. This can contribute to the locking of mechanical constraints. In a similar way, Meng *et al.* reported that CNTs can interact with the rigid segments of block copolymers to improve shape-memory phenomena (*17*). However, the most distinctive feature arises from the alteration of the relaxations of the polymer.

Neat PVA can exhibit several thermomechanical relaxations, depending on its degree of cross-linking and humidity (*28*). The T_g of the material presently used is about 80°C in its dry state (*24*).

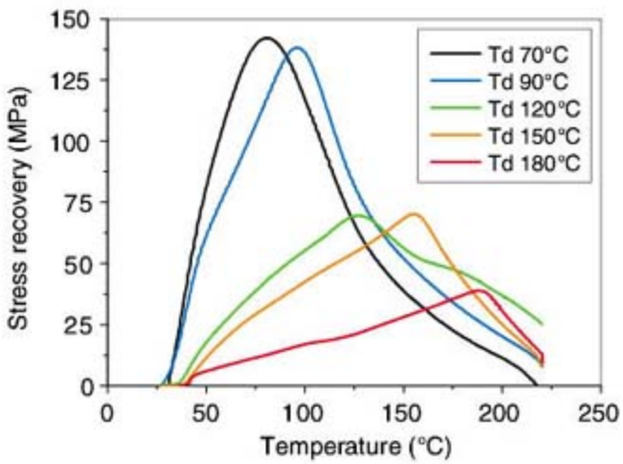

Fig. 2. Stress generated by a nanocomposite fiber when it is reheated. The strain is fixed and the temperature is increased from room temperature to 230°C at a rate of 5°C/min. The different colors correspond to the temperatures T_d at which the fibers have been initially deformed. A peak is observed in each case for a temperature T_s roughly equal to T_d.

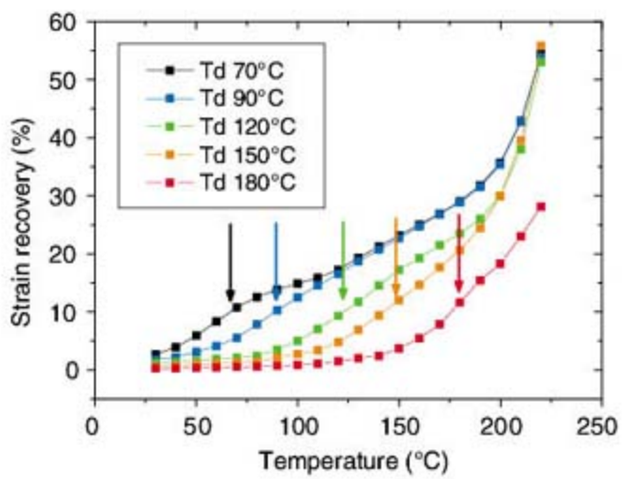

Fig. 3. Strain recovery upon reheating in conditions of free load for nanotube fibers that have been deformed at different T_d. The recovery strain is taken as $\frac{l_d - l(T)}{l_d}$. The arrows indicate an inflexion region that can be noticed in the increase of strain recovery.

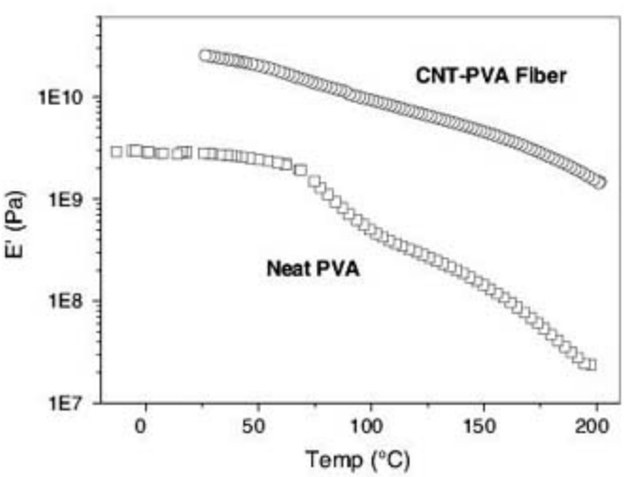

Fig. 4. Storage modulus E' as a function of temperature for neat and dried PVA (squares) and for dried CNT-PVA fibers (circles). The T_g of the neat PVA is about 80°C. The presence of the CNTs substantially alters the thermomechanical properties of the polymer: (i) The storage modulus is greater, (ii) the relaxation at T_g is not observed anymore, and (iii) the storage modulus is much less temperature-dependent; indicating thereby a broadening of the glass transition.

The relaxation at T_g is characterized by a large decrease of the storage modulus (*28*). The main relaxation in the vicinity of T_g is not seen in the presence of CNTs. The storage modulus is less temperature-dependent and reflects a broadening of the glass transition. It has been shown that large gradients of T_g can develop at the interface of nanoparticles (*29*). The transition can be shifted up by more than 100°C when the polymer is confined at 1 nm from the interface and by only a few degrees Celsius at 10 nm (*29*). The effect becomes negligible at greater distances. The average diameter of the polymer layers around the CNTs is $D = r/\sqrt{\phi}$, where r is the average diameter of the CNT bundles, and ϕ is the CNT volume fraction. This yields $D = 11$ nm by assuming $r \sim 5$ nm and an equal density for the CNTs and the polymer (*24*). The polymer shells around the CNTs largely overlap and percolate, such as the CNTs themselves, meaning that there is a distribution of polymer-to-CNT distances that ranges from molecular contact to several nanometers. This distribution of confinement results in a wide broadening of the relaxation-time spectrum and specifically the glass transition through a distribution of polymer fractions that exhibit different T_g. This property is responsible for peaks of stress recovery well above the T_g of the neat polymer. Indeed, when the material is stretched at T_d, the polymer fractions that have lower T_g (far from the interface) can quickly relax and do not efficiently participate in the storage of mechanical energy. In contrast, polymer fractions with T_g close to T_d dominate the behavior by storing and restoring mechanical energy. Composites treated in the vicinity of T_g of the neat polymer still exhibit higher toughness and generate greater stress recovery than those treated at temperatures well above T_g of the neat polymer. This indicates that the fractions of amorphous polymer with unshifted or slightly shifted T_g remain the major components of the composite. Polymer fractions with strongly shifted glass transition are confined in smaller volumes closer to the interface of the nanotubes. The effect of the polymer fractions with high T_g is thus less pronounced. The lower volume of more confined polymer results in lower recovery stress at high temperatures, as experimentally observed. The decreasing volume of polymer fractions closer to the CNT interfaces can also contribute in sharpening memory effects. Polymer fractions with T_g above T_d can participate in the shape-memory behavior, but their volume becomes smaller as we consider higher T_d. This lowers the recovery stress above T_d and contributes in defining more precisely the temperature of maximal recovery stress.

The phenomena investigated herein, and shape-memory properties in general, are expected to depend on kinetics, such as the glass transition of conventional polymers. But relaxations in glasses become exponentially slow or fast when the temperature is shifted, respectively, below or above temperatures of the glass transition region. The present effects have been observed from 70° to 180°C in the same conditions, meaning that temperature memorization is not incidentally due to the heating rate. Preliminary experiments with a heating rate of 1°C/min confirmed this feature and yielded the same temperature-memory behavior. Furthermore, the intrinsic mechanical properties of the CNTs are not expected to play a critical role in the investigated phenomena because the levels of mechanical stresses are too low to achieve large deformations of the CNTs. The Young's modulus of CNTs is several hundred gigapascals (*30*), whereas the maximal stress of the composite fibers during deformation does not exceed 0.5 GPa. However, polymer nanoconfinement and the high fraction of CNTs are essential features to achieve temperature-memory and strong shape-memory effects through alterations of the thermomechanical properties of the polymer.

References and Notes

1. E. Hornbogen, *Adv. Eng. Mater.* **8**, 101 (2006).
2. A. Lendlein, S. Kelch, *Angew. Chem. Int. Ed.* **41**, 2034 (2002).
3. J. Van Humbeeck, *Adv. Eng. Mater.* **3**, 837 (2001).
4. B. K. Kim, S. Y. Lee, M. Xu, *Polymer* **37**, 5781 (1996).
5. T. Ohki, Q.-Q. Ni, N. Ohsako, M. Iwamoto, *Compos. Part A Appl. Sci. Manuf.* **35**, 1065 (2004).
6. J. Hu, Z. Yang, L. Yeung, F. Ji, Y. Liu, *Polym. Int.* **54**, 854 (2005).
7. J. Morshedian, H. A. Khonakdar, M. Mehrabzadeh, H. Eslami, *Adv. Polym. Technol.* **22**, 112 (2003).
8. K. Gall *et al.*, *J. Biomed. Mater. Res. Part A* **73a**, 339 (2005).
9. R. D. Kornbluh *et al.*, *Proc. SPIE*, **4698**, 254 (2002).
10. A. Lendlein, R. Langer, *Science* **296**, 1673 (2002); published online 25 April 2002 (10.1126/science.1066102).
11. V. B. Gupta, J. Radhakrishnan, S. K. Sett, *Polymer* **35**, 2560 (1994).
12. E. Patoor, D. C. Lagoudas, P. B. Entchev, L. C. Brinson, X. Gao, *Mech. Mater.* **38**, 391 (2006).
13. D. C. Lagoudas *et al.*, *Mech. Mater.* **38**, 430 (2006).
14. K. Gall, M. L. Dunn, Y. Liu, G. Stefanic, D. Balzar, *Appl. Phys. Lett.* **85**, 290 (2004).
15. Y. Liu, K. Gall, M. L. Dunn, P. McCluskey, *Mech. Mater.* **36**, 929 (2004).
16. K. Gall *et al.*, *Acta Mater.* **50**, 5115 (2002).
17. Q. Meng, J. Hu, Y. Zhu, *J. Appl. Polym. Sci.* **106**, 837 (2007).
18. H. Koerner, G. Price, N. A. Pearce, M. Alexander, R. A. Vaia, *Nat. Mater.* **3**, 115 (2004).
19. R. Mohr *et al.*, *Proc. Natl. Acad. Sci. U.S.A.* **103**, 3540 (2006).
20. G. M. Spinks, V. Mottaghitalab, M. Bahrami-Saniani, P. G. Whitten, G. G. Wallace, *Adv. Mater.* **18**, 637 (2006).
21. S. V. Ahir, E. M. Terentjev, *Nat. Mater.* **4**, 491 (2005).
22. A. B. Dalton *et al.*, *Nature* **423**, 703 (2003).
23. P. Miaudet *et al.*, *Nano Lett.* **5**, 2212 (2005).
24. See supporting materials available on *Science* Online.
25. B. Vigolo *et al.*, *Science* **290**, 1331 (2000).
26. Y. Miyamoto, K. Fukao, H. Yamao, K. Sekimoto, *Phys. Rev. Lett.* **88**, 225504 (2002).
27. M. Cadek *et al.*, *Nano Lett.* **4**, 353 (2004).
28. J.-S. Park, J.-W. Park, E. Ruckenstein, *J. Appl. Polym. Sci.* **82**, 1816 (2001).
29. J. Berriot, H. Montes, F. Lequeux, D. Long, P. Sotta, *Europhys. Lett.* **64**, 50 (2003).
30. B. I. Yakobson, L. S. Couchman, in *Dekker Encyclopedia of Nanoscience and Nanotechnology* (Taylor & Francis Group, New York, 2004), pp. 587–601.

31. We thank J. L. Barrat for fruitful discussions about gradients of T_g in nanocomposites. This work was financially supported by the Délégation Générale pour l'Armement and the Conseil Régional d'Aquitaine.

Supporting Online Material

www.sciencemag.org/cgi/content/full/318/5854/1294/DC1
Materials and Methods
SOM Text
Figs. S1 to S5
References
Movies S1 and S2

23 May 2007; accepted 3 October 2007
10.1126/science.1145593

Efficient Transplantation via Antibody-Based Clearance of Hematopoietic Stem Cell Niches

Agnieszka Czechowicz, Daniel Kraft, Irving L. Weissman,*† Deepta Bhattacharya†

Upon intravenous transplantation, hematopoietic stem cells (HSCs) can home to specialized niches, yet most HSCs fail to engraft unless recipients are subjected to toxic preconditioning. We provide evidence that, aside from immune barriers, donor HSC engraftment is restricted by occupancy of appropriate niches by host HSCs. Administration of ACK2, an antibody that blocks c-kit function, led to the transient removal of >98% of endogenous HSCs in immunodeficient mice. Subsequent transplantation of these mice with donor HSCs led to chimerism levels of up to 90%. Extrapolation of these methods to humans may enable mild but effective conditioning regimens for transplantation.

Allogeneic bone marrow transplantation (BMT) generally requires conditioning of the recipient through cytoreductive treatments to prevent immunological rejection of the graft. Because these regimens can be associated with serious side effects (*1*), such preparative treatments are often omitted for patients with diseases such as severe combined immunodeficiency (SCID), as these patients are incapable of rejecting donor grafts (*2*). Nonetheless, although large numbers of B and T lymphocytes are at least transiently generated, the levels of donor HSC engraftment are usually less than 1% after transplantation into unconditioned SCID recipients (*3*–*6*). Although several studies have concluded that transplanted HSCs can easily replace

endogenous HSCs without conditioning (*7*, *8*), earlier studies suggested that the availability of niches is a limiting factor to transplantation (*9*). Thus, we reasoned that donor HSC engraftment might be limited by the occupancy of appropriate niches by endogenous HSCs, and that the development of reagents that specifically remove host HSCs could lead to safer transplantation-based therapies for hematological and nonhematological disorders than those currently in use.

To address whether endogenous HSCs could be replaced by transplanted HSCs in a linear dose-dependent manner, we transplanted unconditioned Rag2$^{-/-}$ γc$^{-/-}$ mice (*10*, *11*) with varying numbers of c-kit^{+} lineage^{-} Sca-1^{+} (KLS) CD34^{-} CD150^{+} HSCs from mice expressing green fluorescent protein (GFP) driven by the β-actin promoter (*12*–*16*). Peripheral blood granulocyte chimerism was measured at 16 weeks after transplant; this method has been shown to accurately reflect donor HSC chimerism in this system (*3*, *15*). Donor granulocyte chimerism increased measurably in doses of 10 to 250 transplanted HSCs, but transplantation of more than 250 cells led to at most modest increases in chimerism (Fig. 1). Transplantation of 18,000 HSCs, representing ~70% of the total number of HSCs in an adult mouse (*17*, *18*), led to a mean chimerism of only 3% (Fig. 1, top panel). Similar results were obtained through transplantation of unfractionated bone marrow (*12*) (fig. S1). These data suggest that without conditioning, HSC engraftment is limited by the number of saturable niches that are empty at the time of transplant or become empty as the transplanted cells still survive.

To determine the specificity of these niches, we competitively transplanted unconditioned Rag2$^{-/-}$ γc$^{-/-}$ (CD45.2) mice with 1000 CD45.1 HSCs along with 100,000 GFP^{+} KLS CD34^{+} progenitor cells, which are the immediate progeny of HSCs (*16*, *19*). No significant difference in donor HSC chimerism was observed in these mice relative to recipients that received 1000 HSCs alone ($P = 0.77$) (Fig. 1, lower right panel), which suggests that HSCs and their immediate progeny use distinct niches to maintain function.

To determine whether the specific elimination of host HSCs would allow for high levels of donor HSC engraftment, we compared a number of different candidate HSC-depleting monoclonal antibodies, including α-Sca1 (*13*), α-integrin α4 (*20*), and α-ESAM1 (*21*), but ultimately selected ACK2, an antibody known to recognize and antagonize c-kit (*22*), the receptor for stem cell factor (SCF) (*23*). We reasoned that if the ACK2 antibody were capable of depleting endogenous HSCs, residual antibody in the serum of mice would also deplete transplanted donor HSCs. To determine the kinetics of antibody clearance in vivo, we administered ACK2 intravenously to Rag2$^{-/-}$ γc$^{-/-}$ mice and tested the serum for the presence of antibody (*12*). ACK2 remained in the serum until 5 days after injection; however, no ACK2 was detected by 7 or 8 days after injection (Fig. 2A). All mice survived the ACK2 treatment with no obvious signs of distress (*12*) (table S1 and fig. S2). At this time point, a ~99% decrease in the number of HSCs (Fig. 2B) was observed, and comparable levels of depletion were observed in B cell–deficient and wild-type mice (*12*) (fig. S3). To further confirm HSC depletion, we transplanted 200,000 bone marrow cells into lethally irradiated recipients 9 days after ACK2 treatment (*12*). Transplantation of bone marrow from ACK2-

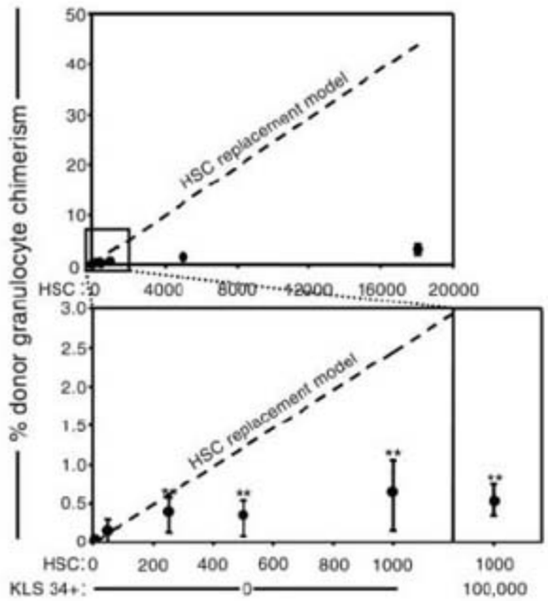

Fig. 1. Available HSC niches can be saturated with donor HSCs. Peripheral blood of transplanted unconditioned RAG2$^{-/-}$ γc$^{-/-}$ mice was analyzed 16 weeks after HSC transplantation for GFP^{+} granulocytes. The lower panel represents an expanded view of results from transplantation of 10 to 1000 HSCs. In the lower right panel, mice were cotransplanted with 1000 CD45.1 HSCs and 100,000 GFP^{+} KLS CD34^{+} cells. Mean values ± SEM are shown ($n = 4$ or 5 for each dose); $^{**}P < 0.05$ relative to the chimerism arising from the 10 HSC–transplanted group. The dashed line represents the theoretical HSC chimerism if engraftment were to increase linearly with transplanted cell dose from the observed chimerism at the 50 HSC–dose group.

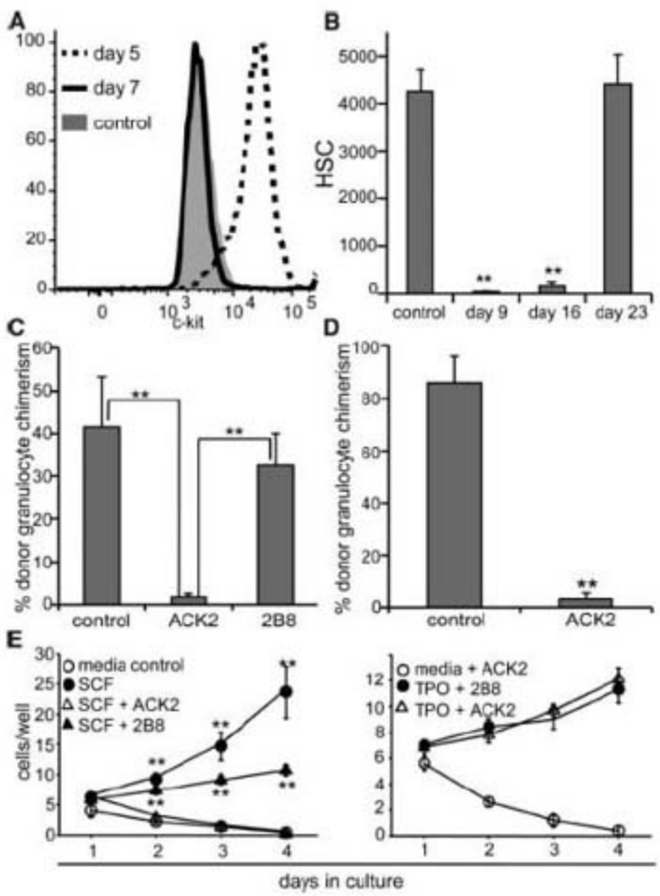

Fig. 2. ACK2 treatment depletes HSCs in vivo. (**A**) ACK2 is cleared from serum of RAG2$^{-/-}$ γc$^{-/-}$ mice 7 days after injection. Serum of mice receiving 500 μg of ACK2 was analyzed every 2 days for ACK2 antibody by staining c-kit^{+} mast cells (*31*). (**B**) ACK2 administration leads to depletion of bone marrow HSCs. Numbers of KLS CD135^{-} CD150^{+} HSCs were determined in femurs and tibia of ACK2-treated and control mice. Mean values ± SEM are shown ($n = 3$ for each time point); $^{**}P < 0.001$. (**C**) ACK2 treatment, but not 2B8 treatment, depletes functional HSCs from bone marrow. We transplanted 200,000 unfractionated bone marrow cells from RAG2$^{-/-}$ γc$^{-/-}$ mice, treated with 500 μg of ACK2 or 2B8 9 days earlier, into wild-type irradiated recipients alongside 200,000 untreated competitor wild-type bone marrow cells. Mean values ± SEM are shown ($n = 5$ to 8); $^{**}P < 0.01$. (**D**) ACK2 treatment does not directly cause HSC mobilization to the spleen. Entire splenocyte populations from mice treated with 500 μg of ACK2 9 days earlier were transplanted alongside 200,000 competitor bone marrow cells from wild-type mice. Mean values ± SEM are shown ($n = 3$ to 9); $^{**}P < 0.001$. (**E**) ACK2 inhibits SCF-mediated HSC proliferation. HSCs were isolated from wild-type mice, plated at 10 cells per well cultured in the presence of SCF or TPO and ACK2 or 2B8. Proliferation was observed by light microscopy. $^{**}P < 0.05$ as compared to ACK2-treated samples.

Institute of Stem Cell Biology and Regenerative Medicine, Departments of Pathology and Developmental Biology, Stanford University School of Medicine, Stanford, CA 94305, USA.

*To whom correspondence should be addressed. E-mail: irv@stanford.edu

†These authors contributed equally to this work.

treated animals led to >90% lower engraftment relative to controls (Fig. 2C), thus confirming that ACK2 depletes functional HSCs from the bone marrow.

To determine the mobilizing effects of ACK2 treatment, we transplanted the entire splenocyte populations of ACK2-conditioned animals into lethally irradiated recipients (*12*). The donor chimerism resulting from ACK2-treated splenocytes was reduced by >95% relative to controls (Fig. 2D). These data indicate that ACK2 treatment does not induce HSC depletion from the bone marrow by mobilizing HSCs to the spleen. Moreover, we were unable to detect HSCs in the spleen, liver, or blood after ACK2 treatment by flow cytometry (fig. S4). Mobilization was only observed during the recovery phase, well after ACK2 had already cleared from the serum (fig. S5).

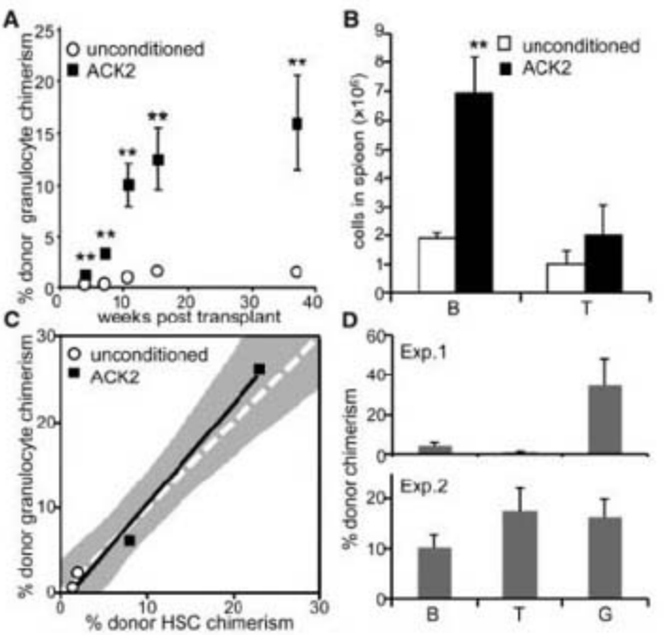

Fig. 3. ACK2 treatment enhances HSC engraftment. **(A)** ACK2 conditioning leads to higher donor myeloid chimerism. Donor granulocyte chimerism was measured after transplantation of 5000 HSCs in RAG2$^{-/-}$ mice conditioned with ACK2 7 days before transplant and compared to that of unconditioned mice. Mean values ± SEM are shown (n = 4); $^{**}P < 0.01$. **(B)** HSC transplantation of ACK2-treated animals leads to lymphocyte reconstitution. We enumerated splenic donor-derived B and T cells from ACK2-treated and unconditioned RAG2$^{-/-}$ mice 39 weeks after transplantation with wild-type HSCs. Mean values ± SEM are shown (n = 3 to 5); $^{**}P < 0.01$. **(C)** Granulocyte chimerism accurately measures bone marrow HSC chimerism. Peripheral blood granulocyte (Ter119$^-$ CD3$^-$ B220$^-$ Mac-1^{high} side scatter^{high}) chimerism at 37 weeks after transplantation was correlated with HSC (c-kit$^+$ lineage$^-$ Sca-1$^+$ CD34$^-$ CD150$^+$) chimerism in the bone marrow at 39 weeks after transplantation upon killing. Solid line illustrates linear regression, with 95% confidence interval shaded in gray. Dashed line represents theoretical values if donor granulocyte chimerism were identical to donor HSC chimerism. **(D)** Secondarily transplanted donor HSCs from ACK2-treated mice give rise to long-term multilineage engraftment. Peripheral blood chimerism of B cells (B), T cells (T), and granulocytes (G) is shown 16 weeks after secondary transplant for two independent experiments. Mean values ± SEM are shown (n = 7 or 8 in each experiment).

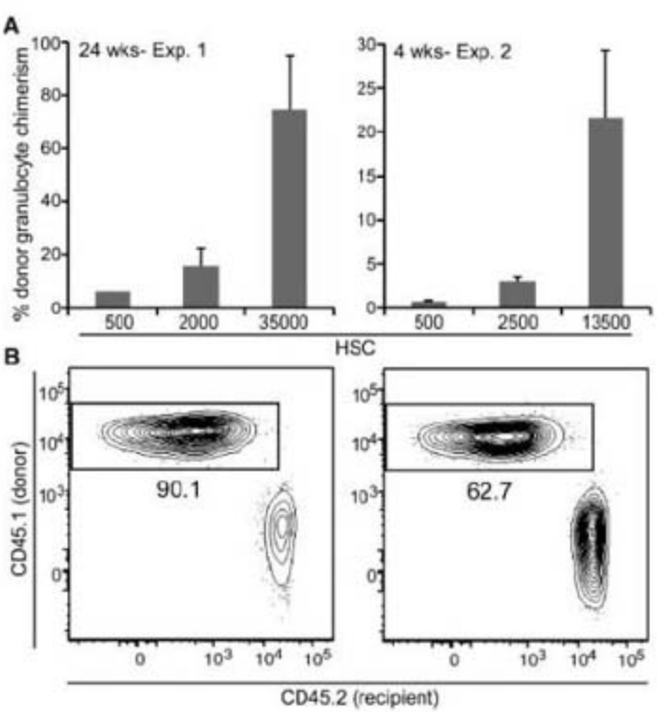

Fig. 4. Donor chimerism increases with transplanted HSC cell number in ACK2-treated mice. **(A)** ACK2 treatment increases available HSC niche space. In two separate experiments, RAG2$^{-/-}$ γc$^{-/-}$ mice were treated with ACK2 and transplanted 9 days later with varying doses of HSCs (CD45.1). Donor granulocyte chimerism was measured as above 24 weeks after transplantation for the first experiment, and 4 weeks after transplantation for the second experiment. Mean values ± SEM are shown. **(B)** Flow cytometry profiles of mice transplanted with 35,000 HSCs. Chimerism of CD3$^-$ B220$^-$ Mac1^{high} side scatter^{high} peripheral blood granulocytes is shown. Numerical values represent percent donor chimerism.

To determine the mechanism by which ACK2 depletes HSCs, we compared the effects of ACK2 treatment to that of 2B8, another c-kit monoclonal antibody of the same IgG2b isotype. 2B8 treatment did not decrease functional HSC numbers in vivo, as transplantation of bone marrow cells from mice treated with 2B8 resulted in levels of engraftment similar to those of controls (Fig. 2C). Next, we cultured purified HSCs in the presence of ACK2 and found that it completely inhibited SCF-dependent proliferation, but not thrombopoietin (TPO)–mediated proliferation (Fig. 2E) (*12*). These data, along with data showing that distinct c-kit–expressing progenitors are depleted at differential rates (*12*) (fig. S6), suggest that ACK2 does not deplete through Fc-mediated functions. Rather, consistent with studies using c-kit mutant mice (*12*, *24*, *25*), the complete inhibition of c-kit signaling by ACK2 (Fig. 2E) can deplete HSCs, whereas the partial inhibition by 2B8 cannot.

By 23 days after treatment, HSC cell surface profiles (fig. S5) and numbers (Fig. 2B) had returned to near normal levels. These data indicate that ACK2 causes a marked but transient depletion of host HSCs and results in a short window during which ACK2-treated animals might be receptive to donor HSC transplantation. To test whether the ablation of host HSCs could improve the efficiency of donor HSC engraftment, we conditioned RAG2$^{-/-}$ (CD45.1) mice with ACK2 and transplanted them with 5000 wild-type CD45.2 HSCs after serum clearance of ACK2. The mean donor granulocyte chimerism at 37 weeks after transplant was 16.1%, reflecting a factor of >10 increase over control recipients (Fig. 3A). These engrafted HSCs also gave rise to peripheral B and T cells (Fig. 3B).

We also analyzed bone marrow HSC chimerism directly at this late time point to confirm the increase in engraftment, and found that it correlated well with peripheral blood granulocyte chimerism (Fig. 3C). Secondary transplants of donor HSCs re-isolated from primary recipients led to multilineage engraftment for at least 16 weeks after transplant (Fig. 3D), confirming that transplanted HSCs regain their normal cell surface phenotype and cell cycle status (fig. S7) by at least 7 to 9 months after transplant in ACK2-treated animals (*12*).

These data did not distinguish whether ACK2 treatment increased niche space or whether, as in unconditioned animals, only a small fraction of transplanted HSCs initially engrafted but then competitively expanded. If niche space had truly been freed, HSC chimerism would be expected to increase linearly with transplanted cell dose. To distinguish between these alternatives, we transplanted ACK2-conditioned RAG2$^{-/-}$ γc$^{-/-}$ (CD45.2) recipient mice with varying doses of CD45.1 HSCs. Donor engraftment increased linearly with transplanted HSC dose in two independent experiments at both early and late time points (Fig. 4A),

consistent with the emptying of HSC niches by ACK2 treatment. Strikingly, donor chimerism values of up to 90% were achieved at the 35,000 HSC dose (Fig. 4B) and upon repetitive rounds of ACK2 treatment and transplantation of a total of 15,000 HSCs (fig.S8), which, upon extrapolation to humans, is a clinically obtainable number (*12*).

Allogeneic BMT is used routinely for a number of clinical purposes, such as for the treatment of SCID (*26*, *27*). Our results provide evidence that in the absence of conditioning, donor HSC engraftment is limited by the occupancy of appropriate niches by host HSCs. These data offer an explanation for the poor donor HSC engraftment observed in unconditioned SCID patients (*4*, *5*), which in turn may be responsible for the low levels of donor B lymphopoiesis and the finite duration of T cell production (*6*, *28*).

We have shown that administration of ACK2 in vivo leads to the rapid but transient depletion of host HSCs, and that subsequent transplantation of highly purified HSCs leads to donor chimerism levels of up to 90%. When coupled with highly specific immunosuppressive depleting antibodies, shown to be effective in both mice (*29*) and humans (*30*) as transplantation conditioners, the use of HSC-specific depleting antibodies may be an attractive alternative to conventional methods of conditioning [which carry serious health risks (*1*)] and may thus increase the utility of allogeneic BMT for both hematological and nonhematological disorders.

References and Notes

1. C. Ferry, G. Socie, *Exp. Hematol.* **31**, 1182 (2003).
2. R. H. Buckley *et al.*, *J. Med.* **340**, 508 (1999).
3. D. Bhattacharya, D. J. Rossi, D. Bryder, I. L. Weissman, *J. Exp. Med.* **203**, 73 (2006).
4. G. E. Tjonnfjord, R. Steen, O. P. Veiby, W. Friedrich, T. Egeland, *Blood* **84**, 3584 (1994).
5. S. M. Muller, T. Kohn, A. S. Schulz, K. M. Debatin, W. Friedrich, *Blood* **96**, 4344 (2000).
6. M. Cavazzana-Calvo *et al.*, *Blood* **109**, 4575 (2007).
7. G. Brecher, J. D. Ansell, H. S. Micklem, J. H. Tjio, E. P. Cronkite, *Proc. Natl. Acad. Sci. U.S.A.* **79**, 5085 (1982).
8. F. M. Stewart, R. B. Crittenden, P. A. Lowry, S. Pearson-White, P. J. Quesenberry, *Blood* **81**, 2566 (1993).
9. H. S. Micklem, C. M. Clarke, E. P. Evans, C. E. Ford, *Transplantation* **6**, 299 (1968).
10. Y. Shinkai *et al.*, *Cell* **68**, 855 (1992).
11. J. P. Goldman *et al.*, *Br. J. Haematol.* **103**, 335 (1998).
12. See supporting material on *Science* Online.
13. G. J. Spangrude, S. Heimfeld, I. L. Weissman, *Science* **241**, 58 (1988).
14. M. J. Kiel, O. H. Yilmaz, T. Iwashita, C. Terhorst, S. J. Morrison, *Cell* **121**, 1109 (2005).
15. D. E. Wright, A. J. Wagers, A. P. Gulati, F. L. Johnson, I. L. Weissman, *Science* **294**, 1933 (2001).
16. M. Osawa, K. Hanada, H. Hamada, H. Nakauchi, *Science* **273**, 242 (1996).
17. G. A. Colvin *et al.*, *Leukemia* **18**, 575 (2004).
18. K. Sudo, H. Ema, Y. Morita, H. Nakauchi, *J. Exp. Med.* **192**, 1273 (2000).
19. D. J. Rossi *et al.*, *Proc. Natl. Acad. Sci. U.S.A.* **102**, 9194 (2005).
20. D. A. Williams, M. Rios, C. Stephens, V. P. Patel, *Nature* **352**, 438 (1991).
21. E. C. Forsberg *et al.*, *PLoS Genet.* **1**, e28 (2005).
22. M. Ogawa *et al.*, *J. Exp. Med.* **174**, 63 (1991).
23. O. N. Witte, *Cell* **63**, 5 (1990).
24. R. A. Fleischman, B. Mintz, *Proc. Natl. Acad. Sci. U.S.A.* **76**, 5736 (1979).
25. C. L. Miller *et al.*, *Exp. Hematol.* **24**, 185 (1996).
26. F. H. Bach, R. J. Albertini, P. Joo, J. L. Anderson, M. M. Bortin, *Lancet* **ii**, 1364 (1968).
27. R. A. Gatti, H. J. Meuwissen, H. D. Allen, R. Hong, R. A. Good, *Lancet* **ii**, 1366 (1968).
28. M. Sarzotti *et al.*, *J. Immunol.* **170**, 2711 (2003).
29. P. Gambel, L. H. Francescutti, T. G. Wegmann, *Transplantation* **38**, 152 (1984).
30. A. B. Cosimi *et al.*, *J. Med.* **305**, 308 (1981).
31. T. Nakano *et al.*, *J. Exp. Med.* **162**, 1025 (1985).

32. We thank D. Bryder for helpful discussions and technical assistance; L. Jerabek for laboratory management; C. Richter for antibody production; L. Hidalgo, D. Escoto, and J. Dollaga for animal care; C. Park for histological expertise; and M. Longaker and D. Rossi for critical reading of the manuscript. Supported by NIH grants 5R01HL058770 and 5R01CA086065 (I.L.W.), a fellowship from the Medical Scholars Program at Stanford University School of Medicine (A.C.), a fellowship from the Cancer Research Institute and NIH grants T32AI0729022 and 5K01DK078318 (D.B.), and Hope Street Kids Award and NIH grant 5K08HL076335 (D.K.). I.L.W. owns Amgen stock, cofounded and consulted for Systemix, is a cofounder and director of Stem Cells Inc., and cofounded and is a director of Cellerant Inc.

Supporting Online Material

www.sciencemag.org/cgi/content/full/318/5854/1296/DC1
Materials and Methods
SOM Text
Figs. S1 to S7
Table S1
References

27 August 2007; accepted 19 October 2007
10.1126/science.1149726

Requirement of Inositol Pyrophosphates for Full Exocytotic Capacity in Pancreatic β Cells

Christopher Illies,[1] Jesper Gromada,[2] Roberta Fiume,[1] Barbara Leibiger,[1] Jia Yu,[1] Kirstine Juhl,[3] Shao-Nian Yang,[1] Deb K. Barma,[4] John R. Falck,[4] Adolfo Saiardi,[5] Christopher J. Barker,[1]* Per-Olof Berggren[1]

Inositol pyrophosphates are recognized components of cellular processes that regulate vesicle trafficking, telomere length, and apoptosis. We observed that pancreatic β cells maintain high basal concentrations of the pyrophosphate diphosphoinositol pentakisphosphate ($InsP_7$ or IP_7). Inositol hexakisphosphate kinases (IP6Ks) that can generate IP_7 were overexpressed. This overexpression stimulated exocytosis of insulin-containing granules from the readily releasable pool. Exogenously applied IP_7 dose-dependently enhanced exocytosis at physiological concentrations. We determined that IP6K1 and IP6K2 were present in β cells. RNA silencing of IP6K1, but not IP6K2, inhibited exocytosis, which suggests that IP6K1 is the critical endogenous kinase. Maintenance of high concentrations of IP_7 in the pancreatic β cell may enhance the immediate exocytotic capacity and consequently allow rapid adjustment of insulin secretion in response to increased demand.

Phosphoinositides have a prominent role in cellular signal-transduction events (*1*–*3*). Highly phosphorylated inositol polyphosphates, distant derivatives of the inositol 1,4,5-trisphosphate (IP_3) second messenger, function in signal-transduction and cellular regulation (*4*–*6*). The pyrophosphate derivatives of IP_6 diphosphoinositol pentakisphosphate, and bis-(diphospho)inositol tetrakisphosphate are commonly referred to as IP_7 and IP_8 (also, $InsP_7$ and $InsP_8$, respectively). These inositol pyrophosphate derivatives rapidly turnover and are estimated to have similar free energy of hydrolysis to that of adenosine 5′-triphosphate (ATP) (*4*). A striking consequence of this high-energy phosphate group is the ability of IP_7 to phosphorylate a subset of proteins directly in an ATP- and enzyme-independent manner (*7*). The variety of cellular responses that are apparently controlled by inositol pyrophosphates (*4*, *8*) may be facilitated by the differential intracellular distribution of the kinases that make them (*9*). The concentrations of inositol pyrophosphates can be dynamically regulated during key cellular events. For example, IP_7 concentrations change during cell cycle progression (*10*), and IP_7 regulates cyclin–cyclin-dependent kinase complexes (*11*), whereas IP_8 increases acutely in response to cellular stress (*8*). IP_6 also functions as an enzymatic cofactor (*4*), and so, by analogy, it is possible that even at concentrations found in unstimulated cells, IP_7 could be an important regulatory molecule.

[1]The Rolf Luft Research Center for Diabetes and Endocrinology, Karolinska Institutet, SE-171 76, Stockholm, Sweden. [2]Diabetes and Metabolism Disease Area, Novartis Institutes for BioMedical Research, Cambridge, MA 02139, USA. [3]Joslin Diabetes Center, Harvard Medical School, Boston, MA 02215, USA. [4]Department of Biochemistry, University of Texas Southwestern Medical Center, Dallas, TX 75390, USA. [5]U.K. Medical Research Council (MRC) Cell Biology Unit and Laboratory for Molecular Cell Biology, Department of Biochemistry and Molecular Biology, University College London, Gower Street, London WC1E 6BT, UK.

*To whom correspondence should be addressed. E-mail: chris.barker@ki.se

Phosphoinositides are key regulators of the insulin-secreting pancreatic β cell (*12*). These cells influence blood glucose homeostasis by coupling increases in the concentration of glucose and other circulatory or neuronal-derived regulators to the exocytosis of insulin. IP_6 activates voltage-dependent L-type Ca^{2+} channels (*13*), exocytosis (*14*, *15*), and dynamin-mediated endocytosis (*16*), all key processes in insulin secretion. A role for IP_7 in the β cell has not yet been determined. However, given the suggested involvement of inositol pyrophosphates in vesicle trafficking (*4*), the critical nature of such trafficking events for the process of insulin exocytosis and the high β cell concentration of IP_6 (*13*), the immediate precursor of IP_7, we explored a possible role for IP_7 in the regulation of insulin exocytosis.

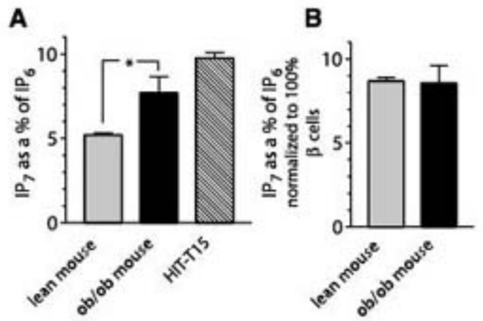

Fig. 1. Concentrations of IP_7 in pancreatic β cells. **(A)** Comparison of ^{3}H-labeled IP_7 as a percentage of ^{3}H-labeled IP_6 in pancreatic islets or insulin-secreting HIT-T15 cells. Data are from three or four separate experiments. *$P < 0.05$, two-tailed *t* test. **(B)** The islet data from (A) were transformed to take into account the different β cell composition of lean mouse (60%) versus *ob/ob* mouse (90%) islets.

We used [^{3}H]*myo*-inositol labeling to examine insulin-secreting cells and pancreatic islets for the presence of various inositol pyrophosphate species. IP_7 was identified by its coelution with a bona fide IP_7 standard (fig. S1) (*17*). Very little IP_8 was detectable. In normal mouse pancreatic islets (60% β cells), the relative concentration of IP_7 was 5.21 ± 0.12% (± SEM, $n = 3$) of IP_6. In contrast, the percentage of IP_7 in islets from *ob/ob* mice, which have more than 90% β cells, was significantly greater, i.e., 7.71 ± 0.93% of IP_6 (± SEM, $n = 4$; $P < 0.05$; unpaired, two-tailed *t* test). This suggests that the increased IP_7 concentrations might be restricted primarily to the β cells. When we normalized the primary mouse data, on the assumption that only β cells make IP_7 (Fig. 1B), they suggested that the β cells maintain IP_7 levels at about 9% of those of IP_6. Of the insulin-secreting cell lines, only hamster HIT-T15 cells have a considerable amount of IP_7 (10% of that of IP_6) (Fig. 1A). We used equilibrium labeling techniques (*13*) to estimate that the basal concentration of IP_7 in HIT-T15 cells was 5.8 ± 0.14 μM (± SEM, $n = 3$), which reflects a concentration at the top end of the range that has been estimated in other mammalian cells or yeast (1 to 5 μM) (*4*). Because IP_7 is in a state of rapid exchange with the cellular IP_6 pool in mammalian cells (*4*) and because the cellular concentration of IP_6 in β cells is also high (*13*), it is perhaps not surprising that IP_7 in these cells is at high concentrations.

To investigate whether high IP_7 concentrations keep β cells in a responsive state, we overexpressed all three reported mammalian IP6Ks in primary β cells and examined whether stimulated exocytosis was enhanced. We used cell capacitance as a measure of exocytosis, detecting the increase in β cell surface area that occurs when the insulin-containing granules fuse with the plasma membrane (*18*). The perforated patch

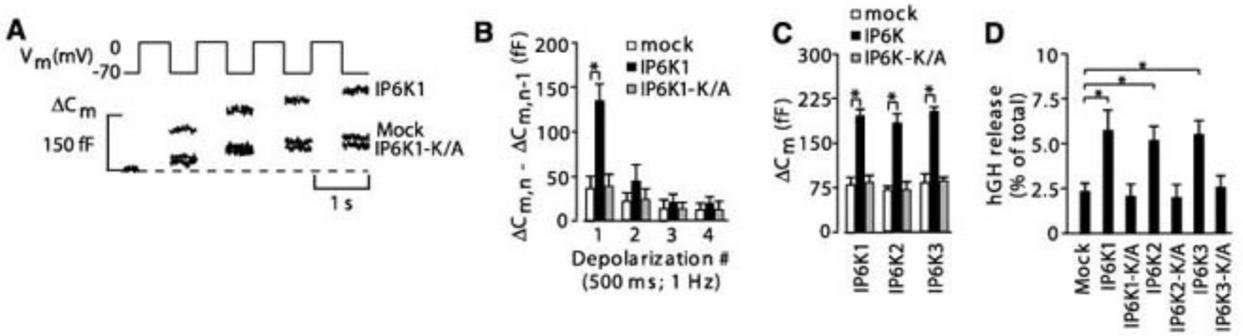

Fig. 2. Increased exocytosis in pancreatic β cells after expression of IP6Ks. **(A)** Individual mouse β cells were transfected with enhanced green fluorescent protein (EGFP) (mock) or a combination of EGFP and either wild-type (IP6K1) or a catalytically inactive (IP6K1-K/A) variant of IP6K. Increases in cell capacitance (ΔC_m) were elicited by a train of four 500-ms depolarizations (1 Hz) by using the perforated patch configuration. The extracellular medium contained 3 mM glucose. Recordings are representative of 8 to 12 different experiments. **(B)** Histogram summarizing the average increment in cell capacitance per pulse ($\Delta C_{m,n} - \Delta C_{m,n-1}$) during the train in cells mock-transfected or overexpressing either IP6K1 or IP6K1-K/A. Values ± SEM are from 8 to 12 experiments. *$P < 0.05$ from Dunnett's test for multiple comparisons. **(C)** Average total increase in cell capacitance at the end of the train in mock-transfected cells or cells overexpressing either IP6Kn or IP6Kn-K/A type 1, 2, and 3 kinase, respectively. Values ± SEM are from 7 to 12 experiments. *$P < 0.05$ from Dunnett's test for multiple comparisons. **(D)** INS-1E cells cotransfected with pCMV5-hGH and empty vector (pcDNA3) (mock-transfected) or with pCMV5-hGH and IP6Kn or IP6Kn-K/A types 1, 2, and 3 kinase, respectively. hGH secretion was measured in Krebs-Ringer bicarbonate Hepes buffer with 3 mM glucose. The amount of secreted hGH is expressed as a percentage of total hGH in the cells. Values ± SEM are from three experiments (each in triplicate). *$P < 0.05$ from Dunnett's test for multiple comparisons.

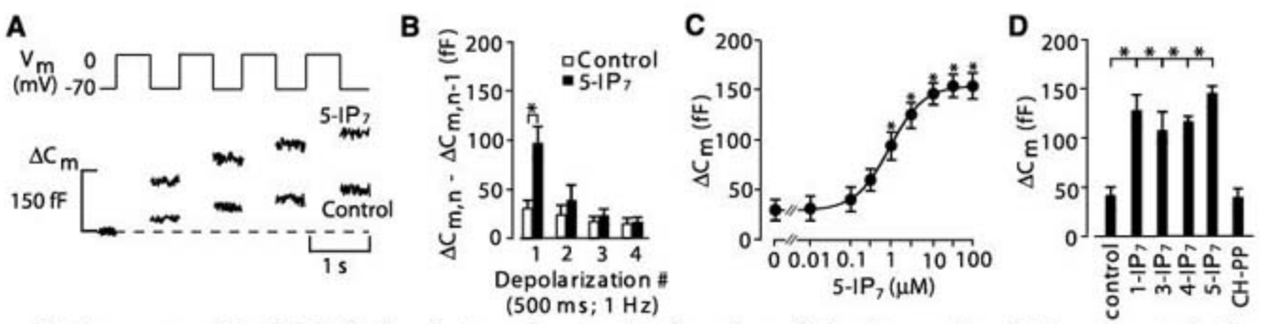

Fig. 3. Promotion of Ca^{2+}-dependent exocytosis by 5-IP_7. Individual mouse β cells were subjected to a train of four 500-ms depolarizations (1 Hz) by using the standard whole-cell patch-clamp configuration. **(A)** Exocytosis was observed under control conditions and in the presence of 3 μM 5-IP_7 in the pipette-filling solution. 5-IP_7 was allowed to diffuse into the cell for 2 min before initiation of the experiment. Recordings are representative of six experiments for both conditions. **(B)** Histogram summarizing the average increment in cell capacitance per pulse ($\Delta C_{m,n} - \Delta C_{m,n-1}$) during the train in the absence or presence of 3 μM 5-IP_7 in the pipette-filling solution. Values ± SEM are from six experiments. *$P < 0.05$ from Dunnett's test for multiple comparisons. **(C)** Concentration dependence of stimulatory action of 5-IP_7 on exocytosis. The curve represents a least-squares fit of the mean data points to the Hill equation. Values ± SEM are from five to seven experiments. *$P < 0.05$ from Dunnett's test for multiple comparisons. **(D)** A comparison of several isomers of IP_7 at a 10 μM concentration on total increase in exocytosis with the same protocols as in (A). Values ± SEM are from five to eight experiments. *$P < 0.05$ from Dunnett's test for multiple comparisons.

whole-cell technique was used to allow measurements in metabolically intact cells, and exocytosis was elicited by groups of four 500-ms depolarizing pulses from –70 to 0 mV. In mock-transfected cells, capacitance increased by 79 ± 11 fF (n = 8) (Fig. 2, A and B). In cells overexpressing IP6K1, the amplitude of the capacitance increase averaged 198 ± 12 fF (n = 10; P < 0.05), whereas no effect on exocytosis was observed in cells overexpressing a catalytically inactive version of IP6K1 (Fig. 2, A and B). The capacitance increase evoked by the first depolarization was augmented by 293% in cells overexpressing wild-type IP6K1. Exocytosis during the first depolarization is thought to largely represent the content of the readily releasable pool (RRP) of exocytotic granules (*19*). The size of the RRP (in femtofarads) can be estimated by using the equation: RRP = $S/(1 - R^2)$, where S is the sum of the responses to the first (ΔC_1) pulse and the second (ΔC_2) pulse, and R is the ratio $\Delta C_2/\Delta C_1$ (*19*). We estimate that the RRP averaged 96 ± 9 fF (n = 8) and 225 ± 21 fF (n = 10) in mock-transfected and wild-type IP6K1 transfected cells, respectively. Thus, IP6K1 increased the size of the RRP by 134%. Using a conversion factor of 3 fF per granule (*20*), we estimated that the RRP contained 30 granules in mock-transfected and 75 granules in wild-type IP6K1 transfected cells. The stimulatory action of IP6K1 was restricted to the first depolarization, and little enhancement was seen over that observed in mock-transfected cells during the final three pulses (Fig. 2A). This became obvious when the net increase per pulse was plotted (Fig. 2B). The exhaustion of the exocytotic response during the train appeared not to reflect inactivation of the depolarization-induced Ca^{2+} current, because the change in the integrated Ca^{2+} current (Q_{Ca}) was much smaller (20%) than the decrease in exocytosis (fig. S2), but also see (*21*).

As did IP6K1, IP6K2 and IP6K3 also stimulated exocytosis (Fig. 2C). Overexpression of a catalytically inactive version of IP6K2 and IP6K3 did not affect the exocytotic capacity (Fig. 2C). We also overexpressed IP6K1-3 in rat insulinoma INS-1E cells in a human growth hormone (hGH) transient cotransfection assay, in which hGH acted as a reporter of exocytosis from transfected cells. Total increases in cell capacitance in INS-1E cells overexpressing IP6K1 (212 ± 28 fF; n = 5) were comparable to those observed in primary mouse β cells (201 ± 16 fF; n = 12). Overexpression of each IP6K-stimulated hGH secretion was 150% above basal (n = 9 to 12; P < 0.05), an effect that was not shared by their catalytically inactive mutants (Fig. 2D).

IP6Ks can also use IP5 as a substrate, generating a different subset of inositol pyrophosphates (*4*). Therefore, we verified that 5-IP_7 (mammalian IP_7 with pyrophosphate in the 5 position) directly promoted exocytosis (Fig. 3, A to C). We also assessed other isomers of IP_7 (Fig. 3D). To measure the effects of 5-IP_7 on exocytosis, we applied trains of depolarizations in standard whole-cell patch-clamp experiments in which the β cell was dialyzed for 2 min with a solution containing 3 μM 5-IP_7. A group consisting of four 500-ms depolarizations was then applied to evoke exocytosis. In a series of six experiments, the total increase in cell capacitance amounted to 231 ± 12 fF (P < 0.01) in the presence of 3 μM 5-IP_7 in the pipette-filling solution and 77 ± 11 fF under control conditions, respectively (Fig. 3A). As was the case for cells overexpressing the IP6Ks, the capacitance was primarily increased by the first depolarization in the presence of 5-IP_7, with little effect of the subsequent three depolarizations (Fig. 3B). The ability of 5-IP_7 to stimulate exocytosis was not associated with a change in the whole-cell Ca^{2+} current (fig. S3). The stimulatory action of 5-IP_7 on exocytosis was concentration-dependent (Fig. 3C), with a half-maximal stimulatory effect at 1.02 μM, and a cooperativity factor of 1.5. Thus, 5-IP_7 enhanced exocytosis within the physiological range of IP_7 concentrations (1 to 10 μM). Other isomers of IP_7 also stimulated exocytosis at 10 μM. CH-PP (monocyclohexyl trisodium diphosphate), a simple pyrophosphate based on cyclohexane, was ineffective (Fig. 4E). Under the conditions used to examine 5-IP_7's effect on exocytosis, the net effect of IP_6 appeared to promote endocytosis not exocytosis (fig. S4), because the effect of IP_6 on exocytosis could only be discerned under conditions in which endocytosis was inhibited (*15*). This was not the case for 5-IP_7. Furthermore, the effect of IP_6 on exocytosis, when endocytosis was inhibited, did not selectively promote secretion from the RRP (fig. S4). Our experiments do not preclude a role for a more phosphorylated pyrophosphate.

To test whether endogenous IP_7 contributed to the exocytotic capacity in a physiologically relevant manner, we first examined the mRNA encoding IP6Ks from β cells or islet lysates by quantitative polymerase chain reaction (PCR). Message encoding IP6K1 and IP6K2 but not IP6K3 was detected (Fig. 4A). We then decreased expression of IP6K1 and IP6K2 in β cells with small interfering RNA (siRNA). Mouse-specific siRNAs were screened by using the mouse β cell line MIN6m9 and TaqMan real-time PCR gene expression assays (fig. S5). Elimination of either IP6K1 or IP6K2 reduced cellular IP_7 levels (fig. S6). In order to be able to select primary β cells transfected with siRNA for further electrophysiological studies, suitable

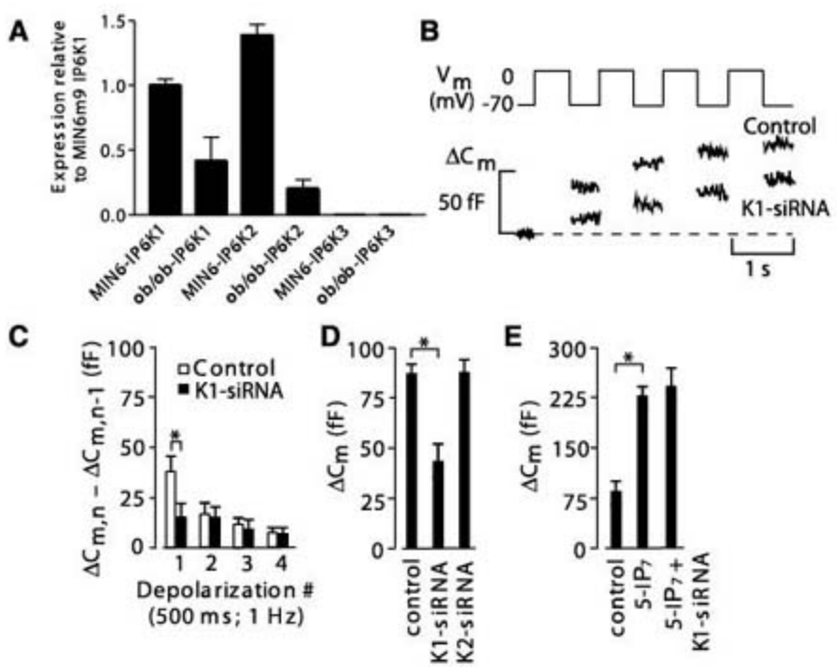

Fig. 4. **(A)** RNA silencing of IP6K1, but not IP6K2, inhibits release of granules from the RRP. Total RNA was extracted from islets and MIN6m9 cells and reverse-transcribed. Relative expression of mRNA was measured by quantitative real-time PCR with the use of appropriate primers and probes. Primers and probe for 18S ribosomal RNA were used as endogenous control. **(B)** Mouse β cells were transfected with fluorescently tagged siRNA to IP6K1 or a negative control at 25 nM and were subjected to a train of four 500-ms depolarizations (1 Hz) with the perforated patch configuration. Increases in cell capacitance (ΔC_m) were measured in fluorescent cells at 3 mM glucose in the extracellular medium. Recordings are representative of six (control) and eight (siRNA-treated cells) experiments. **(C)** Histogram summarizing the average increment in cell capacitance per pulse ($\Delta C_{m,n} - \Delta C_{m,n-1}$) during the train in cells mock-transfected or overexpressing either siRNA to IP6K1 or negative control. Values ± SEM are from six and eight experiments. *P < 0.05 from Dunnett's test for multiple comparisons. **(D)** Effect of siRNA to IP6K1 and IP6K2 on total capacitance increase. Values ± SEM are from five to eight experiments. *P < 0.05 from Dunnett's test for multiple comparisons. **(E)** Effect of 5-IP_7 on exocytosis under control conditions and in cells with reduced expression levels of IP6K1 (whole-cell patch, see Fig. 3). Values ± SEM are from five or six experiments. *P < 0.05 from Dunnett's test for multiple comparisons.

siRNA candidates were fluorescently tagged at the 5′ end of sense and antisense strands and transfected. Cell-capacitance measurements on mouse β cells transfected with fluorescently tagged siRNA were recorded by using the perforated patch-clamp technique. Inhibition of IP6K1, but not of IP6K2, reduced the exocytotic capacity (Fig. 4D), and the effect of silencing was again most pronounced on the first pulse, reflecting depletion of the RRP of granules (Fig. 4, B and C). Furthermore, addition of 5-IP_7 in the presence of siRNA to IP6K1 restored a normal exocytotic response (Fig. 4E). Thus, endogenous IP_7 generated by IP6K1, but not IP6K2, appears to account for the enhanced exocytotic capacity in β cells. The discrepancy between our exogenous versus endogenous systems may reflect a differential distribution or cellular associations of the two kinases in vivo. IP6K1 associates with proteins involved in exocytosis but IP6K2 does not (*22*). Studies on IP6K2 have also revealed a discrepancy between overexpression studies and gene silencing (*23*).

IP6K1 siRNA did not alter number of L-type Ca^{2+} channels per patch or channel open probability, mean closed time, or mean open time (fig. S7). Hence, in contrast to IP_6, IP_7 appears not to affect L-type Ca^{2+} channel activity (*13*).

We find that the pancreatic β cell maintains high concentrations of IP_7. This apparently functions in the insulin secretory process by regulating the RRP of insulin-containing granules, thereby maintaining the immediate exocytotic capacity of the β cell. It is noteworthy that a putative disruption of the IP6K1 gene in a family with type 2 diabetes (*24*) and reduced plasma insulin levels in mice in which the IP6K1 gene has been deleted (*25*). This may be of interest in the context of understanding the molecular mechanisms underlying the development of diabetes.

References and Notes

1. M. J. Berridge, *Ann. N.Y. Acad. Sci.* **766**, 31 (1995).
2. B. Vanhaesebroeck *et al.*, *Annu. Rev. Biochem.* **70**, 535 (2001).
3. T. Takenawa, T. Itoh, *Biochim. Biophys. Acta* **1533**, 190 (2001).
4. M. Bennett, S. M. Onnebo, C. Azevedo, A. Saiardi, *Cell. Mol. Life Sci.* **63**, 552 (2006).
5. R. F. Irvine, M. J. Schell, *Nat. Rev. Mol. Cell Biol.* **2**, 327 (2001).
6. S. B. Shears, *Biochem. J.* **377**, 265 (2004).
7. A. Saiardi, R. Bhandari, A. C. Resnick, A. M. Snowman, S. H. Snyder, *Science* **306**, 2101 (2004).
8. X. Pesesse, K. Choi, T. Zhang, S. B. Shears, *J. Biol. Chem.* **279**, 43378 (2004).
9. A. Saiardi, E. Nagata, H. R. Luo, A. M. Snowman, S. H. Snyder, *J. Biol. Chem.* **276**, 39179 (2001).
10. C. J. Barker, J. Wright, P. J. Hughes, C. J. Kirk, R. H. Michell, *Biochem. J.* **380**, 465 (2004).
11. Y. S. Lee, S. Mulugu, J. D. York, E. K. O'Shea, *Science* **316**, 109 (2007).
12. C. J. Barker, I. B. Leibiger, B. Leibiger, P.-O. Berggren, *Am. J. Physiol. Endocrinol. Metab.* **283**, E1113 (2002).
13. O. Larsson *et al.*, *Science* **278**, 471 (1997).
14. A. M. Efanov, S. V. Zaitsev, P.-O. Berggren, *Proc. Natl. Acad. Sci. U.S.A.* **94**, 4435 (1997).
15. M. Høy, P.-O. Berggren, J. Gromada, *J. Biol. Chem.* **278**, 35168 (2003).
16. M. Høy *et al.*, *Proc. Natl. Acad. Sci. U.S.A.* **99**, 6773 (2002).
17. Materials and methods are available as supporting material on *Science* Online.
18. P. Rorsman, E. Renström, *Diabetologia* **46**, 1029 (2003).
19. K. D. Gillis, R. Mossner, E. Neher, *Neuron* **16**, 1209 (1996).
20. C. S. Olofsson *et al.*, *Pfluegers Arch.* **444**, 43 (2002).
21. E. Renström, L. Eliasson, K. Bokvist, P. Rorsman, *J. Physiol.* **494**, 41 (1996).
22. H. R. Luo *et al.*, *Neuron* **31**, 439 (2001).
23. E. Nagata *et al.*, *J. Biol. Chem.* **280**, 1634 (2005).
24. J. Kamimura *et al.*, *J. Hum. Genet.* **49**, 360 (2004).
25. Lexicon knockout mouse NIH-0750, Mouse Genome Database (MGD), Mouse Genome Informatics Web Site, www.informatics.jax.org/external/ko/lexicon/1223.html (18 July 2006).

26. We thank S. H. Snyder for constructs, C. B. Wollheim for both INS-1E cells and hGH constructs, S. Seino for MIN6m9 cells and I. B. Leibiger for discussion. This work was supported by grants from Karolinska Institutet, Novo Nordisk Foundation, the Swedish Research Council, the Swedish Diabetes Association, EFSD, The Family Erling-Persson Foundation, Berth von Kantzow's Foundation, Robert A. Welch Foundation, NIH (GM31278), EuroDia (LSHM-CT-2006-518153), and the U.K. Medical Research Council.

Supporting Online Material

www.sciencemag.org/cgi/content/full/318/5854/1299/DC1
Materials and Methods
Figs. S1 to S7
References

21 June 2007; accepted 5 September 2007
10.1126/science.1146824

Transposase-Derived Transcription Factors Regulate Light Signaling in *Arabidopsis*

Rongcheng Lin,[1] Lei Ding,[1] Claudio Casola,[2] Daniel R. Ripoll,[3] Cédric Feschotte,[2] Haiyang Wang[1]*

Plants use light to optimize growth and development. The photoreceptor phytochrome A (phyA) mediates various far-red light–induced responses. We show that *Arabidopsis FHY3* and *FAR1*, which encode two proteins related to *Mutator*-like transposases, act together to modulate phyA signaling by directly activating the transcription of *FHY1* and *FHL*, whose products are essential for light-induced phyA nuclear accumulation and subsequent light responses. FHY3 and FAR1 have separable DNA binding and transcriptional activation domains that are highly conserved in *Mutator*-like transposases. Further, expression of *FHY3* and *FAR1* is negatively regulated by phyA signaling. We propose that FHY3 and FAR1 represent transcription factors that have been co-opted from an ancient *Mutator*-like transposase(s) to modulate phyA-signaling homeostasis in higher plants.

Plants constantly monitor their light environment in order to grow and develop optimally, using a battery of photoreceptors. Phytochromes are a family of photoreceptors that monitors the incident red [(R), 600 to 700 nm] and far-red [(FR), 700 to 750 nm] light wavelengths by switching reversibly between the R light–absorbing, biologically inactive Pr form and the FR light–absorbing, biologically active Pfr form (*1*, *2*). Upon photoactivation, phyA, the primary photoreceptor for FR light, is translocated from the cytoplasm into the nucleus to induce FR light–responsive gene expression that is required for various photoresponses, such as seed germination, seedling de-etiolation, FR light–preconditioned blocking of greening, and flowering (*3*). Genetic studies have identified two pairs of homologous genes essential for phyA signaling: (i) *FAR1* (far-red–impaired response 1) and *FHY3* (far-red–elongated hypocotyl 3) and (ii) *FHY1* (far-red–elongated hypocotyl 1) and *FHL* (*FHY1*-like) (*4*–*7*). FHY1 and FHL have been implicated in mediating the light-dependent nuclear accumulation of phyA (*8*, *9*). However, the biochemical function of FHY3 and FAR1 remains to be elucidated.

FHY3 and FAR1 share extensive sequence homology with MURA, the transposase encoded by the maize *Mutator* element, and with the predicted transposase of the maize mobile element *Jittery* (*10*, *11*). Both of these transposons are members of the superfamily of *Mutator*-like elements (MULEs) (*12*). Database mining and phylogenetic analysis revealed that FHY3/FAR1-like sequences are present in various angiosperms and fall into several phylogenetic clusters intermingled with MULE transposases (*13*) (table S1 and fig. S1). These proteins share an N-terminal C2H2-type zinc-

[1]Boyce Thompson Institute for Plant Research (BTI), Cornell University, Ithaca, NY 14853, USA. [2]Department of Biology, University of Texas, Arlington, TX 76019, USA. [3]Computational Biology Service Unit (CBSU), Cornell University, Ithaca, NY 14853, USA.

*To whom correspondence should be addressed. E-mail: hw75@cornell.edu

chelating motif of the WRKY-GCM1 family, a central putative core transposase domain, and a C-terminal SWIM motif (*14*, *15*), with highly conserved predicted secondary and tertiary structures (figs. S2 and S3). To investigate the molecular function of FHY3 and FAR1, we generated transgenic plants expressing FHY3 and FAR1 proteins fused with a glucocorticoid receptor (GR) to control their nuclear localization (*16*). Both the *FHY3p::FHY3-GR* and *FAR1p::FAR1-GR* transgenes conferred a dexamethasone (DEX)–dependent rescue of the respective mutant phenotype (fig. S4), indicating that FHY3 and FAR1 act in the nucleus.

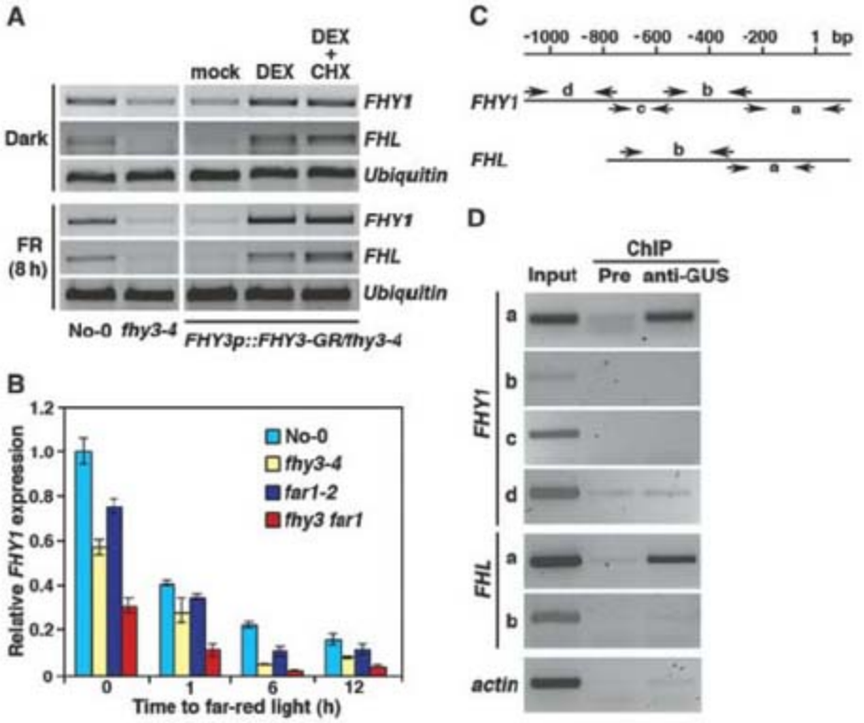

Fig. 1. FHY3 and FAR1 directly up-regulate *FHY1* and *FHL* expression. (**A**) Both *FHY1* and *FHL* are up-regulated by DEX or DEX plus CHX treatment in the *FHY3p::FHY3-GR/fhy3-4* transgenic plants. Seedlings were grown in darkness for 4 days and were then kept in darkness or transferred to FR light for 8 hours (h) before analysis. Expression of a *Ubiquitin* gene was shown as a control. No-0, wild-type No-0 ecotype. (**B**) Reduced expression of *FHY1* in the *fhy3-4*, *far1-2*, and *fhy3 far1* double mutants, as compared with that in the wild-type No-0 plants. Error bars represent SDs of triplicate experiments. (**C**) Diagram of the promoter fragments of *FHY1* and *FHL*. The locations of PCR primers used for the enrichment test are indicated (arrows). "1" indicates the putative transcription initiation site. (**D**) Enrichment of the "a" fragments of the *FHY1* and *FHL* promoters from the anti-GUS ChIP samples. Pre, preimmune.

Previous studies suggested that FHY3 is required for maintaining proper expression levels of *FHY1* and *FHL* in a light-independent manner (*7*, *10*). Semiquantitative reverse transcription polymerase chain reaction (RT-PCR) analysis showed that DEX or DEX plus cycloheximide [(CHX), a protein synthesis inhibitor (*17*) (fig. S5)] treatment, but not mock treatment, restored the expression levels of *FHY1* and *FHL* in both dark-grown and FR light–grown *FHY3p::FHY3-GR/fhy3-4* transgenic seedlings (Fig. 1A). This observation suggests that FHY3 activates *FHY1* and *FHL* expression. In addition, quantitative RT-PCR showed that *FHY1* expression was also reduced in the *far1-2* mutant and was much further reduced in the *fhy3 far1* double mutant, as compared with that in the wild-type seedlings (Fig. 1B). This result suggests that FHY3 and FAR1 act together to up-regulate *FHY1* expression.

We next performed a chromatin immunoprecipitation (ChIP) assay to test for a direct interaction of FHY3 with the *FHY1* and *FHL* promoters in vivo, using the *35S::GUS-FHY3/fhy3-4* transgenic plants (*5*). Multiplex PCR revealed enrichment for the "a" fragments [365 and 353 base pairs (bp), respectively] of the *FHY1* and *FHL* promoters in the anti-GUS ChIP samples, as compared with that in the ChIP samples prepared with preimmune antisera and the *Actin* gene control (Fig. 1, C and D). This

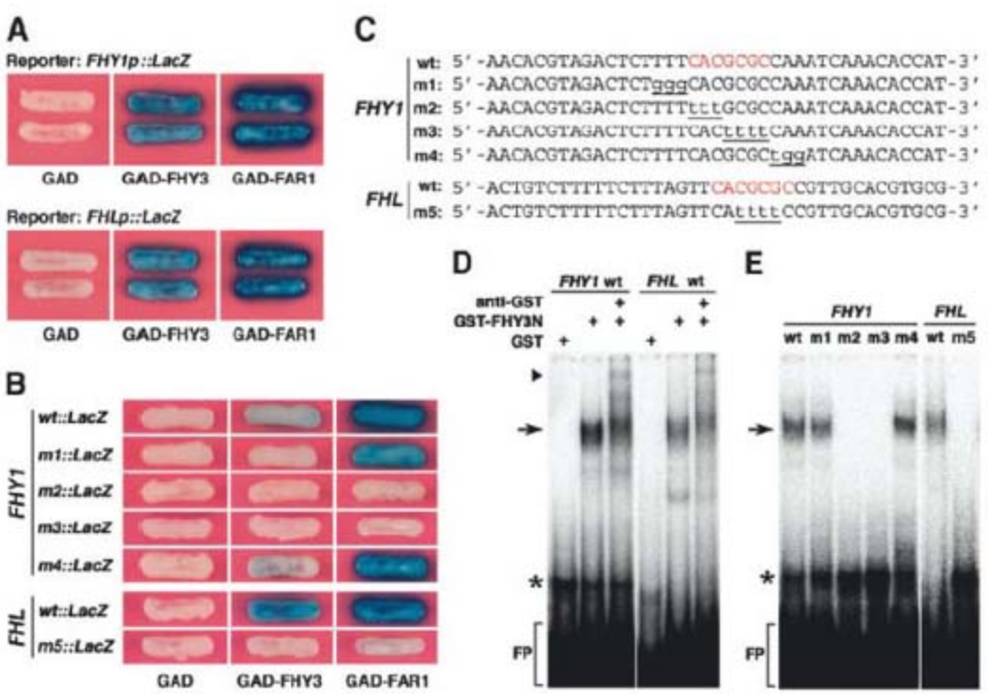

Fig. 2. FHY3 and FAR1 directly bind to the *FBS* motif present in the *FHY1* and *FHL* promoters via the N-terminal zinc finger motif. (**A**) GAD-FHY3 and GAD-FAR1, but not GAD itself, strongly activate expression of the *LacZ* reporter genes driven by the *FHY1* and *FHL* promoters in yeast. (**B**) GAD-FHY3 and GAD-FAR1 activate the *LacZ* reporter genes driven by the wild-type 39-bp subfragments of *FHY1* and *FHL* promoters (*wt::LacZ*) in yeast. Mutations in the *FBS* motif (m2, m3, and m5) abolish activation of the *LacZ* reporter gene expression. (**C**) Diagram of the wild-type and mutant *FHY1* and *FHL* subfragments used to drive the *LacZ* reporter gene expression and as probes in EMSA. The wild-type *FBS* motif is shown in red. Nucleotide substitutions in the mutant fragments are underlined. (**D** and **E**) EMSA assay showing that GST-FHY3N protein, but not GST by itself, specifically binds to the *FHY1* and *FHL* wild-type probes (D) but not to the m2, m3, and m5 mutant probes (E). Arrows indicate the up-shifted bands. The triangle indicates the supershifted DNA-protein-antibody complex when incubated with antibodies to GST. Asterisks indicate nonspecific binding. FP, free probe.

result indicates that FHY3 directly occupies the *FHY1* and *FHL* promoters in vivo. Moreover, constitutive overexpression of *FHY1* suppressed the phenotypes of the *fhy3-4*, *far1-2*, and *fhy3 far1* double mutants (fig. S6). Further, in response to FR light treatment, the nuclear accumulation of phyA–green fluorescent protein (phyA-GFP) is modestly reduced in the *fhy3-4* mutant (reduced to about 60% of the wild-type levels) but is essentially abolished in the *fhy3 far1* double mutant (fig. S7). Together, these findings suggest that FHY3 and FAR1 act together to regulate phyA nuclear accumulation through direct activation of *FHY1* and *FHL* expression.

We next used a yeast one-hybrid assay to delineate the DNA sequences to which FHY3 and FAR1 bind. GAL4 transcriptional activation domain–FHY3 (GAD-FHY3) or GAD-FAR1 fusion proteins, but not GAD alone, activated the *LacZ* reporter genes driven by the *FHY1* and *FHL* promoters (Fig. 2A). Deletion analysis narrowed down the FHY3/FAR1 binding site to a 39-bp promoter subfragment located on the "a" fragment for both *FHY1* and *FHL* (Fig. 2B). Notably, these subfragments share a stretch of consensus sequence: 5′-TTCACGCGCC-3′ (Fig. 2C). Mutating the core sequence "CACGCGC" of this motif (m2 and m3 for *FHY1* and m5 for *FHL*) abolished the reporter gene activation by both GAD-FHY3 and GAD-FAR1. Mutating the flanking sequences (m1 and m4) did not obviously affect the reporter gene activation by GAD-FAR1 but clearly reduced activation by GAD-FHY3 (Fig. 2B). Thus, "CACGCGC" likely defines a cis-element that confers specific binding for FHY3 and FAR1 and is named *FBS* for FHY3/FAR1 binding site.

Domain deletion analysis revealed that the N-terminal fragments of FHY3 and FAR1 are necessary and sufficient for activating the *LacZ* reporter genes driven by the *FHY1* and *FHL* promoters (fig. S8). Consistent with this finding, electrophoretic mobility shift assay (EMSA) showed that recombinant GST-FHY3N fusion protein (glutathione *S*-transferase fused with the first 200 amino acids of FHY3, including the zinc finger motif) caused an up-shift of the radiolabeled wild-type *FHY1* and *FHL* probes (Fig. 2D) but not of the m2, m3, and m5 mutant probes (Fig. 2E). Moreover, the addition of antibodies to GST caused a supershift of the wild-type probes (Fig. 2D). Further, preincubation of the GST-FHY3N fusion proteins with two metal chelators, 1,10-*o*-phenanthroline or EDTA, effectively reduced DNA binding activity (fig. S9). Thus, we conclude that FHY3 binds directly to the *FBS* motif by the N-terminal zinc finger motif. Genome-wide analysis by means of the PatMatch program (*18*) against an *Arabidopsis* promoter database (http://stan.cropsci.uiuc.edu/sift/index.php) revealed that the *FBS* motif is also present in the promoters of hundreds of other genes, including the R light photoreceptor *PHYTOCHROME B* (*PHYB*), *CIRCADIAN CLOCK–ASSOCIATED 1* (*CCA1*), and *EARLY FLOWERING 4* (*ELF4*). Yeast one-hybrid assay showed that GAD-FHY3 and GAD-FAR1 are capable of activating the *LacZ* reporter genes driven by *PHYB*, *ELF4*, and *CCA1* promoter fragments containing the wild-type *FBS* motif but not a mutated *FBS* motif (fig. S10). This observation is consistent with a reported role of FHY3 in gating R light signaling to the circadian clock (*19*).

To test whether FHY3 has an intrinsic transcriptional regulatory activity, we fused a full-length FHY3 with the LexA DNA binding domain. The LexA-FHY3 fusion protein, but not

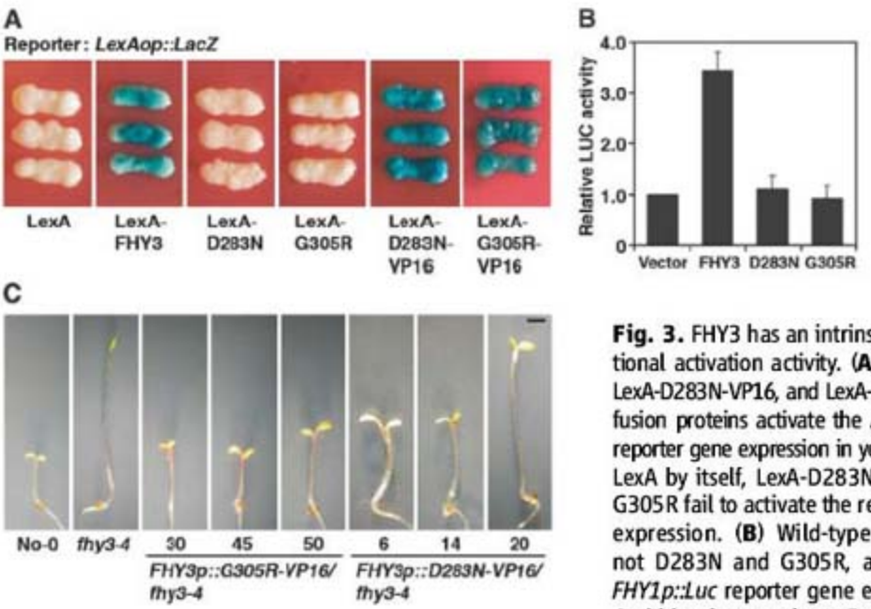

Fig. 3. FHY3 has an intrinsic transcriptional activation activity. (**A**) LexA-FHY3, LexA-D283N-VP16, and LexA-G305R-VP16 fusion proteins activate the *LexAop::LacZ* reporter gene expression in yeast, whereas LexA by itself, LexA-D283N, and LexA-G305R fail to activate the reporter gene expression. (**B**) Wild-type FHY3, but not D283N and G305R, activates the *FHY1p::Luc* reporter gene expression in *Arabidopsis* protoplasts. Error bars represent SDs of triplicate experiments. LUC, luciferase. (**C**) Images of 4-day-old FR light–grown seedlings of multiple independent lines, showing that the *FHY3p::D283N-VP16* and *FHY3p::G305R-VP16* fusion genes confer complete or partial rescue of the *fhy3-4* mutant phenotype. Scale bar, 2 mm.

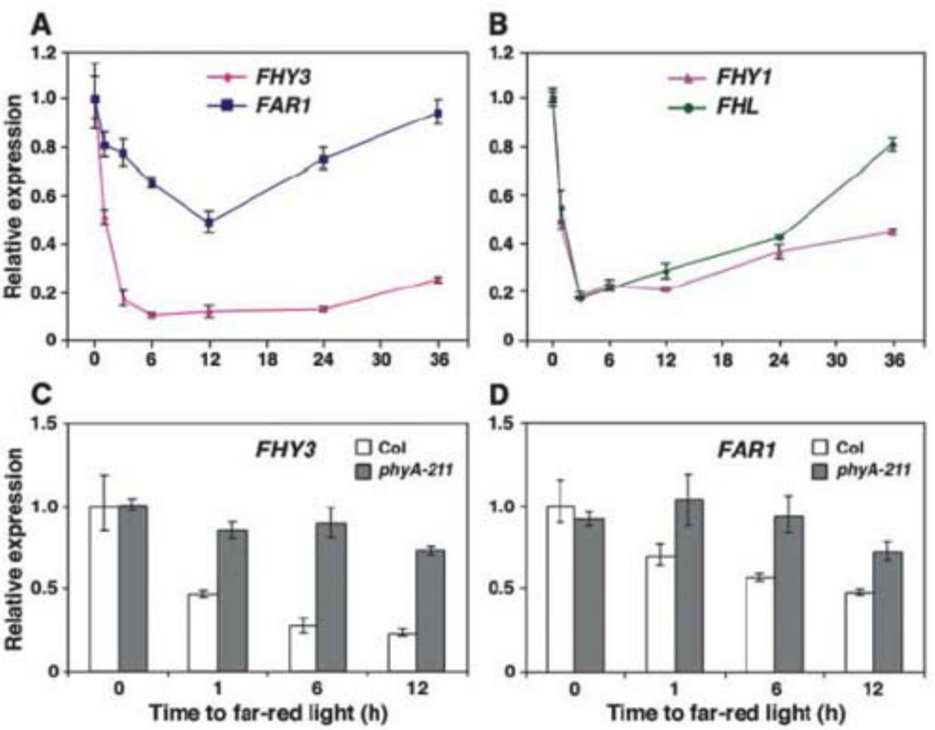

Fig. 4. Down-regulation of *FHY3*, *FAR1*, *FHY1*, and *FHL* by phyA signaling. (**A** and **B**) The transcript levels of *FHY3* and *FAR1* (A) and *FHY1* and *FHL* (B) are down-regulated by FR light. (**C** and **D**) The transcript levels of *FHY3* (C) and *FAR1* (D) remain relatively stable in the *phyA-211* mutant, as compared with levels in the Columbia wild-type (Col) background. The expression levels in dark-grown wild-type plants were set as 1. Error bars in (A) to (D) represent SDs of triplicate experiments.

LexA alone, activated a *LacZ* reporter gene driven by the *LexA* operator (Fig. 3A). Two amino acid–substituted FHY3 proteins corresponding to the *fhy3-9* Gly^{305}→Arg^{305} (G305R) and *fhy3-10* Asp^{283}→Asn^{283} (D283N) mutant alleles (*5*) failed to activate the *LacZ* reporter gene (Fig. 3A), despite comparable levels of expression for the wild-type and mutant FHY3 fusion proteins. In addition, wild-type FHY3 protein, but not the G305R or D283N mutant proteins, activated a luciferase reporter gene driven by the *FHY1* promoter in *Arabidopsis* protoplasts (Fig. 3B). Further, fusion with the VP16 activation domain of herpes simplex virus restored the transcriptional activation activity of G305R and D283N (Fig. 3A), and the fusion proteins conferred a complete or partial rescue of the *fhy3-4* mutant phenotype (Fig. 3C). These results suggest that the intrinsic transcriptional activation activity of FHY3 is essential for its biological function. Domain deletion analysis revealed that the C-terminal region of FHY3 and FAR1 that lacks the N-terminal zinc finger motif is necessary and fully capable of activating the reporter gene expression in yeast, whereas their N-terminal DNA binding domains are unable to activate the reporter gene (fig. S11). These observations suggest that FHY3 and FAR1 have separable DNA binding and transcriptional activation domains.

Finally, we examined how FR light regulates the expression of *FHY3* and *FAR1* using quantitative RT-PCR. In a wild-type background, the transcript levels of *FHY3* declined rapidly after exposure to FR light. Expression of *FAR1* was also down-regulated by FR light, although with slower kinetics and to a lesser degree (Fig. 4A). Expression of *FHY1* and *FHL* displayed a pattern similar to that of *FHY3* (Fig. 4B), which is consistent with their being the direct target genes of *FHY3* and *FAR1*. In contrast, expression of *FHY3* and *FAR1* remained high in the *phyA-211* mutant under FR light (Fig. 4, C and D). These results indicate that expression of *FHY3* and *FAR1* is subject to a negative feedback regulation by phyA signaling and suggest that FHY3 and FAR1 act at a focal point of a feedback loop that maintains the homeostasis of phyA signaling (fig. S12).

Our phylogenetic and functional analyses support a scenario whereby one or several related MULE transposases gave rise to the *FHY3/FAR1*-related genes during the evolution of angiosperms through a process termed "molecular domestication" (*20*), with concomitant loss of the ability to transpose (*21*) (fig. S13). Similar to this, DAYSLEEPER, an *Arabidopsis hAT*-like transposase, has been shown to act as a DNA binding protein and is essential for plant development (*22*). However, it is not known whether this protein can directly regulate gene expression. Our results demonstrate that a transposase-derived protein can bind to a promoter region and directly stimulate the transcription of that gene. Innovation of phyA, which occurred before the origin of angiosperms, has been hypothesized to confer an adaptive advantage to the successful colonization of the first angiosperms on Earth (*23*). The domestication of FHY3 and FAR1 from an ancient transposase(s) might mark an event in the evolution of angiosperms serving to meet the challenges of changing light environments. Our results also provide functional evidence to support the proposition that transposable elements, which are prevalent throughout the genomes of many plants and animals, can serve as a source of new transcription factors that allow populations to adapt and species to evolve (*24*).

References and Notes

1. M. M. Neff, C. Fankhauser, J. Chory, *Genes Dev.* **14**, 257 (2000).
2. P. H. Quail, *Nat. Rev. Mol. Cell Biol.* **3**, 85 (2002).
3. F. Nagy, S. Kircher, E. Schäfer, *Semin. Cell Dev. Biol.* **11**, 505 (2000).
4. M. Hudson, C. Ringli, M. T. Boylan, P. H. Quail, *Genes Dev.* **13**, 2017 (1999).
5. H. Wang, X. W. Deng, *EMBO J.* **21**, 1339 (2002).
6. T. Desnos, P. Puente, G. C. Whitelam, N. P. Harberd, *Genes Dev.* **15**, 2980 (2001).
7. Q. Zhou *et al.*, *Plant J.* **43**, 356 (2005).
8. A. Hiltbrunner *et al.*, *Curr. Biol.* **15**, 2125 (2005).
9. A. Hiltbrunner *et al.*, *Plant Cell Physiol.* **47**, 1023 (2006).
10. M. E. Hudson, D. R. Lisch, P. H. Quail, *Plant J.* **34**, 453 (2003).
11. R. Lin, H. Wang, *Plant Physiol.* **136**, 4010 (2004).
12. D. Lisch, *Trends Plant Sci.* **7**, 498 (2002).
13. The accession numbers for *Arabidopsis* PHYA, FHY3, FAR1, FHY1, FHL, and the maize MURA and the predicted transposase of *Jittery* are NP_172428, NP_188856, NP_567455, NP_181304, AAC23638, AAA21566, and AAF66982, respectively.
14. M. M. Babu, L. M. Iyer, S. Balaji, L. Aravind, *Nucleic Acids Res.* **34**, 6505 (2006).
15. K. S. Makarova, L. Aravind, E. V. Koonin, *Trends Biochem. Sci.* **27**, 384 (2002).
16. D. Wagner, R. W. M. Sablowski, E. M. Meyerowitz, *Science* **285**, 582 (1999).
17. The effectiveness of CHX treatment in inhibiting protein synthesis was shown by blocking HY5 protein accumulation in FR light–treated *Arabidopsis* seedlings (fig. S5). A full description of the materials and methods are available as supporting material on *Science* Online.
18. T. Yan *et al.*, *Nucleic Acids Res.* **33**, W262 (2005).
19. T. Allen *et al.*, *Plant Cell* **18**, 2506 (2006).
20. W. J. Miller, J. F. McDonald, D. Nouaud, D. Anxolabéhère, *Genetica* **107**, 197 (1999).
21. We observed partial synteny conservation of *Arabidopsis FHY3* and *FAR1* with their orthologs in *Brassica* and *Populus*, suggesting that the genomic locations of these genes have been fixed in the eudicots (fig. S13).
22. P. Bundock, P. Hooykaas, *Nature* **436**, 282 (2005).
23. S. Mathews, *J. Hered.* **96**, 197 (2005).
24. C. Biémont, C. Vieira, *Nature* **443**, 521 (2006).

25. We thank F. Nagy, X. Dong, and P. Fobert for sharing the *PHYAp::AtphyA-GFP4* transgenic line, a GR construct, and a VP16 template, respectively; X. W. Deng, G. Martin, J. Nasrallah, D. Stern, and S. Mathews for commenting on the manuscript; and Z. Fei for helping promoter analysis. This work was supported by funds from BTI, Triad Foundation, and NSF (IOS-0641639 to H.W. and DBI-0618969 for microscopy facilities at BTI), (to H.W.), University of Texas at Arlington and NIH (R01 GM77582-01 to C.F.), and Microsoft Corporation to CBSU (to D.R.R.).

Supporting Online Material

www.sciencemag.org/cgi/content/full/318/5854/1302/DC1
Materials and Methods
Figs. S1 to S13
Tables S1 and S2
References

11 June 2007; accepted 17 October 2007
10.1126/science.1146281

Social Comparison Affects Reward-Related Brain Activity in the Human Ventral Striatum

K. Fliessbach,[1] B. Weber,[1] P. Trautner,[1] T. Dohmen,[2] U. Sunde,[2] C. E. Elger,[1] A. Falk[3]*

Whether social comparison affects individual well-being is of central importance for understanding behavior in any social environment. Traditional economic theories focus on the role of absolute rewards, whereas behavioral evidence suggests that social comparisons influence well-being and decisions. We investigated the impact of social comparisons on reward-related brain activity using functional magnetic resonance imaging (fMRI). While being scanned in two adjacent MRI scanners, pairs of subjects had to simultaneously perform a simple estimation task that entailed monetary rewards for correct answers. We show that a variation in the comparison subject's payment affects blood oxygenation level–dependent responses in the ventral striatum. Our results provide neurophysiological evidence for the importance of social comparison on reward processing in the human brain.

The absolute consumption level, or alternatively the absolute level of income, is the most important determinant of individual well-being in traditional economic models of decision-making. These models typically assume that social comparisons, and therefore relative income, play no role. This view has long been challenged by social psychologists and anthropologists, who have argued that comparison with other individuals

is a central phenomenon within human societies (*1*, *2*). The question of whether social comparison affects individuals' subjective well-being, and thus behavior, is of fundamental importance, with far-reaching implications for the positive and normative predictions of economic theories. Examples include patterns of consumption and savings, the design of optimal taxation and redistribution schemes, labor supply, and the optimal provision of incentives in firms (*3*–*6*). Social comparison is also a premise of any model of social preferences, because these theories model fairness judgments and resulting reciprocal responses based on an individual's outcomes relative to the outcomes of relevant others (*7*, *8*).

Despite the importance of distinguishing the roles of absolute and relative income levels for subjective well-being, and thus for human decision-making, the underlying neurobiological basis of social comparison is not well understood. One of the reasons is that the role of relative comparison for subjective well-being has mainly been investigated using predicted comparison income from self-reported survey data or actual outcomes of a priori defined reference groups (*9*). Several methodological problems plague research in this area, including the measurement of relevant incomes and reference groups, the measurement of subjective well-being, and the potential endogeneity of income (*10*, *11*). Combining functional magnetic resonance imaging (fMRI) and behavioral experiments allows us to circumvent most of these empirical problems by measuring neurophysiological responses to absolute and relative incomes in the human brain. Brain regions that are engaged in the prediction and registration of rewards include midbrain-striatal and midbrain-prefrontal dopaminergic projections (*12*). Activity in these brain regions is influenced both by primary rewards such as food delivery (*13*) and by more abstract forms of rewards such as monetary incentives (*14*, *15*). We tested the hypothesis that activity in these brain areas increases with higher relative payments. This hypothesis is in contrast to the traditional economic paradigm, which predicts differential activation only in response to changes in one's own rewards but not to changes in others' rewards. In the experiment, two subjects simultaneously and repeatedly performed a simple work task in two adjacent MRI scanners (Fig. 1). Nineteen subject pairs were included, and data from 33 subjects could be analyzed (*16*). The task involved estimating the number of dots on a screen. At the end of each of 300 trials, both subjects received a feedback. This feedback provided information about both subjects' performance (whether the estimates were correct or incorrect), as well as about both subjects' payments in a given trial. Payment conditions are illustrated in Table 1. Conditions C1 to C5 applied when the estimate of at least one subject was incorrect. These conditions were used to identify reward-sensitive brain regions independently of the conditions of interest, C6 to C11. The latter applied if both subjects solved the task correctly. For these trials, rewards were chosen from a 2 by 3 factorial design in which we varied the absolute level of payment (high versus low) (factor 1) and the relation of a subject's payment to that of the other subject (1:2, 1:1, or 2:1) (factor 2). Our set-up allows us to study the impact of relative payments on reward processing in a clean and controlled way: In each trial the task was exactly the same for both subjects, and the subjects knew that. Moreover, because both subjects were scanned, they were performing under the same circumstances. Thus, the experimental environment provides no basis or justification for differential payment and is therefore well suited to study the consequences of relative income differences for the same performance under identical conditions.

Subjects solved the estimation task correctly in 81 percent of the trials (SD 0.07), matching almost exactly the intended probability of correct task performance of 0.8. Conditions C1 to C5 of our design allow for a functional definition of reward-related structures in our group of subjects independent of a priori information. For this purpose,

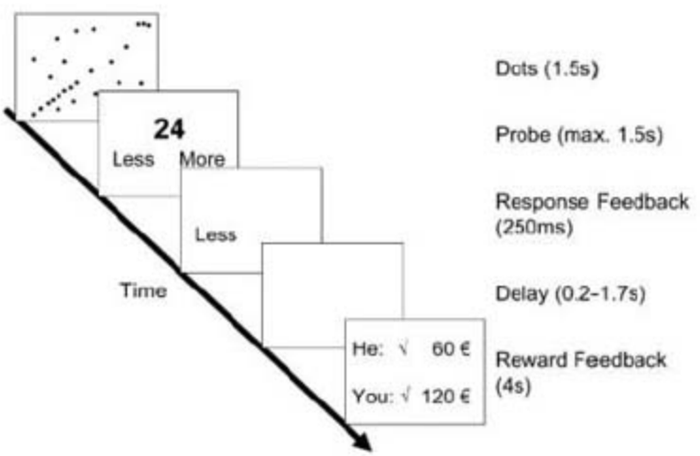

Fig. 1. Single-trial settings. Subjects saw a number of blue dots for 1500 ms (screen 1). Immediately afterward, a number was presented and subjects had to decide by button press whether the number of dots on the first screen had been lower or higher within a time limit of 1500 ms (screen 2). After a response feedback (250 ms, screen 3) and a short delay (blank screen 4), a feedback screen informed subjects about their and the other subject's performance (correct or incorrect), together with the respective monetary rewards (screen 5).

Table 1. Payoff conditions. Subjects received a payment only if they solved the estimation task correctly. When both subjects' estimates were incorrect, both received nothing (experimental condition C1). When only one of the subjects solved the estimation task correctly, he received either about 30 € (low level) or about 60 € (high level) while the other received no payment (see conditions C2 to C5). The conditions of interest (bold) were those in which both subjects solved the estimation task correctly and received payments according to one of the six conditions C6 to C11. These conditions were randomly drawn, and thus occurred with approximately equal frequency. Note that frequencies in conditions C2,3 and C4,5 are not identical because five subjects were dropped from the analysis.

Accuracy	Relative reward level (A:B)	Absolute reward level	Payoffs in Euros (subject A–subject B)	Condition	Percentage of occurrence
Both subjects incorrect			0 – 0	C1	6.5
Subject A correct		High	60 – 0	C2	14.3
		Low	30 – 0	C3	
Subject B correct		High	0 – 60	C4	13.3
		Low	0 – 30	C5	
Both subjects correct (conditions of interest)	**1:2**	**High**	**60 – 120**	**C6**	**65.9**
		Low	**30 – 60**	**C7**	
	1:1	**High**	**60 – 60**	**C8**	
		Low	**30 – 30**	**C9**	
	2:1	**High**	**120 – 60**	**C10**	
		Low	**60 – 30**	**C11**	

[1]Life and Brain Center Bonn, Department of NeuroCognition and Clinic of Epileptology, Bonn, Germany. [2]Institute for the Study of Labor, Bonn, Germany. [3]University of Bonn, Department of Economics, Bonn, Germany.

*To whom correspondence should be addressed. E-mail: armin.falk@uni-bonn.de

conditions in which a subject solved the task correctly and received a payment while the other subject did not (C2 and C3) were contrasted with conditions in which a subject received no payment (C1, C4, and C5). This contrast yielded significant activation in three bilateral and three medial regions, which defined our regions of interest: left and right occipital cortex, left and right angular gyrus, left and right ventral striatum, precuneus, and medial orbitofrontal cortex (two distinct activations) (Fig. 2), thus including the regions known to be critically involved in the processing of reward (*12*). The opposite contrast (C1,4,5 > C2,3) yielded right and left insular activation, but only when using a less strict threshold (*16*). Time-course analyses of the blood oxygen level–dependent (BOLD) response showed a strong positive response to the onset of the task (fig. S1). This is consistent with temporal difference models of ventral striatal function, given that the task served as a cue for a possible upcoming reward, thus inducing reward expectation (*17*). To appropriately model the response to the reward feedback, we therefore controlled for task-related activity by including task-onset times as an additional regressor in our analysis. The resulting time courses for the reward feedback are shown in Fig. 3C. There is a positive hemodynamic response in conditions C2 and C3 (subject receives payment, the other does not) and a decrease of the BOLD signal for conditions C1, C4, and C5 (subject receives no payment). Intermediate response levels were observed in the conditions of interest in which both subjects received money (C6 to C11). In these conditions, the BOLD signal was strongest when a subject received more than the other subject (2:1), followed by equal payments (1:1) and trials in which a subject received less than the other subject (1:2).

In the following, we exclusively analyze the conditions of interest, that is, conditions C6 to C11. For these conditions, we extracted mean parameter estimates for the above-mentioned regions of interest. They were subjected to a 2 by 3 repeated-measurements analysis of variance (ANOVA) with different absolute payment levels (low or high) and relative payments (1:2, 1:1, or 2:1) as factors. In case of bilateral activations, we included the side of the brain as a cofactor. In the ventral striatum, the BOLD response strongly depended on relative payment. The main effect for this factor is: $F_{2,31} = 8.0$, $P < 0.001$. According to our hypothesis, the parameter estimates increased with the ratio between a subject's reward and the other subject's reward: They were lowest for the conditions in which less

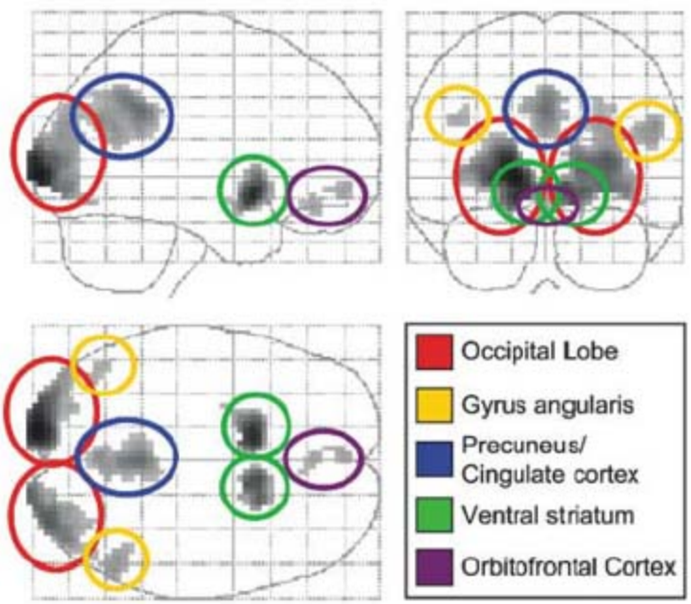

Fig. 2. Glassbrain projection of brain regions showing stronger BOLD responses in conditions in which a subject received a reward while the other did not (C2 and C3) compared with conditions in which a subject did not receive a reward at all (C1, C4, and C5).

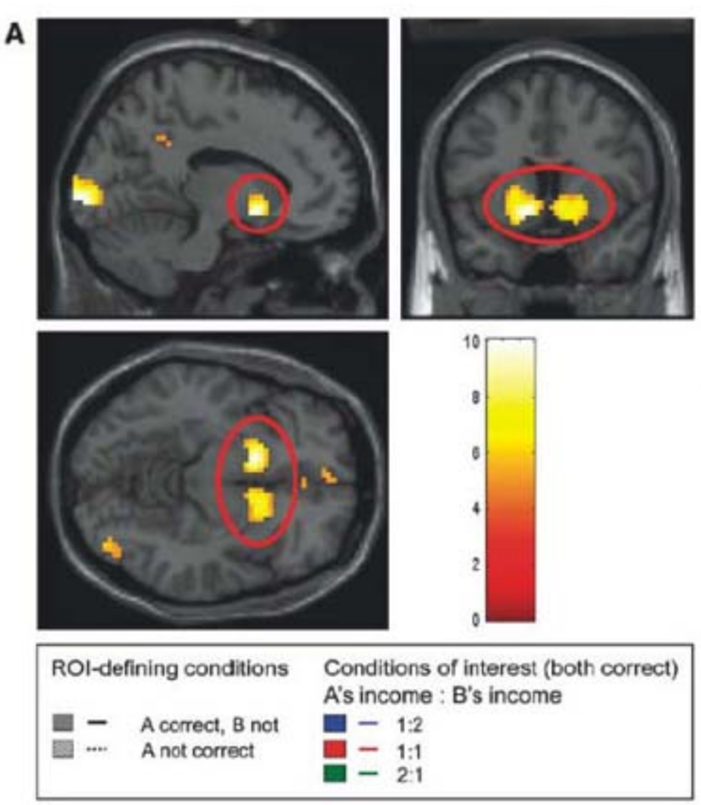

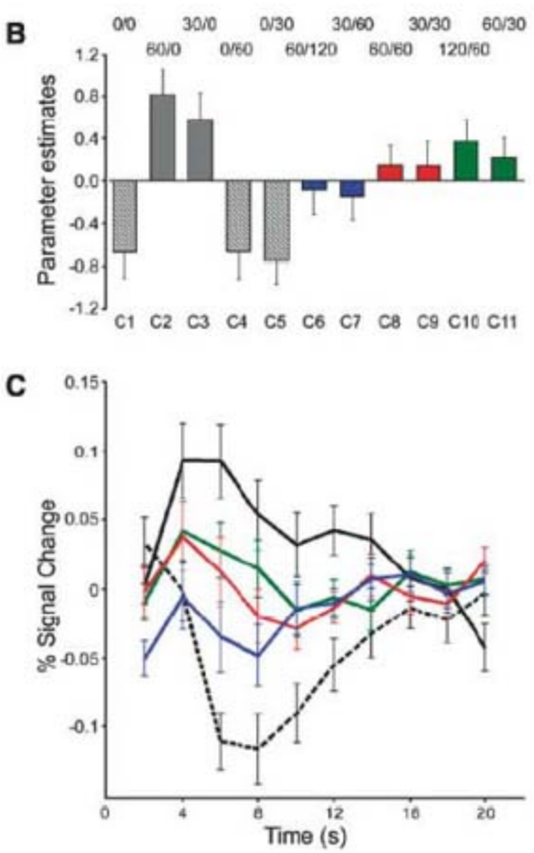

Fig. 3. (**A**) T-Map projected on a single-subject template for the contrast between C2, C3 > C1, C4, C5 with focus on the activation maximum in the left ventral striatum (TAL: X, −12; Y, 8; Z, 8). (**B**) Parameter estimates for suprathreshold voxels from this contrast show a dependency of the activation on the relative reward level. (**C**) Event-related signal changes after the reward feedback collapsed over trials in which a subject received a reward while the other did not (+SEM) (C2, C3, black line), trials where a subject received no reward (C1, C4, C5, black dashed line), and different relative reward levels (1:2, blue line; 1:1, red line; 2:1, green line).

money was earned, followed by the conditions with equal payment, and were highest in the conditions in which a subject earned more money (Fig. 3B) (see table S2 for means and standard errors). All other main effects and interactions of the ANOVA analysis turn out to be insignificant. This holds for the main effect of high versus low payment condition as well as its interaction with relative payment. The latter result suggests that the importance of relative comparison is independent of the level of payment. In addition, there was no significant impact of the side of the activation or the scanner type. All posterior regions (occipital lobe, angular gyrus, and precuneus/cingulate cortex) showed a different pattern, with response intensity significantly varying with both absolute and relative payment. In these regions, responses were highest for the high-payment condition in the 1:2 and the 2:1 conditions, that is, in situations when high amounts of money were unequally paid regardless of which of the subjects received more. A similar pattern was found in the two orbitofrontal regions. The posterior of the two orbitofrontal regions additionally showed a significant interaction between absolute and relative payment (table S3 and fig. S2). In the insular regions identified by the contrast C1,4,5 > C2,3, activation intensity did not depend on relative or absolute rewards level or an interaction between the two factors (all $P > 0.5$). To test whether, in addition to the regions of interest, other regions were affected by relative comparison, the same ANOVA as described above was run in a whole-brain analysis. The strongest main effect of relative reward level was found in the left and right ventral striatum. The left activation cluster extended into the left amygdala and putamen (fig. S3). In addition, significant activations were found in several bilateral parietal and occipital regions and in the right middle lateral prefrontal cortex (Brodmann areas 8 and 9) (table S4). In contrast to the striatal activations, none of these regions showed a systematic increase of activation with increasing relative income.

Right after the experiment, subjects completed a short questionnaire, which contained questions about willingness to reciprocate kind or unkind actions as well as personality measures (*16*). Reciprocity is a particularly important type of social preference and is based on the comparison of outcomes relative to those of relevant others (*8*). In this sense, social comparison is a prerequisite of reciprocal behavior, and we would expect that the more a person is concerned with relative outcomes the more he should be willing to reciprocate. To explore this, we regressed the variability of ventral striatal responses to relative reward differences on the willingness to reciprocate, controlling for personality traits (table S5). This variability turned out to be stronger for subjects who report stronger overall reciprocal inclinations ($t = 2.10$, $P = 0.048$).

This study shows a relationship between relative income and hemodynamic responses in the ventral striatum. Receiving less than another subject was associated with a reduced BOLD signal in this area. Relative reward processing has previously been demonstrated in the striatum (*18*) and orbitofrontal cortex (*19*) of primates, where neuronal responses to a given reward depend on alternative reward outcomes. Similarly, context dependency of ventral striatal responses in humans has been demonstrated with fMRI. Responses to the same rewards differ depending on the sequence of previous rewards and losses (*20*, *21*) and on the set of possible outcomes from which the actual reward is chosen (*14*, *22*). Our study introduces two critical new aspects of relative reward processing in the ventral striatum. First, it shows that social context is an important factor for reward processing. Second, in contrast to previous studies, the differences in reward activation cannot be explained by a mismatch between expected and received reward.

Whereas in previous studies reward expectation has been manipulated, in our study reward expectation in the conditions of interest should be the same. The differential activation in response to these conditions shows an immediate impact of contextual social information on ventral striatal responses. Although null results in fMRI studies must be interpreted with caution, the fact that no other brain area showed a similar response pattern suggests that this impact is not mediated by brain areas known to be involved in social cognition.

The temporal difference model of ventral striatal function assumes that this brain region is involved in the comparison of predicted and actually received rewards (i.e., reward prediction error) (*23*). In our study, we find a strong positive response to the onset of the task. We assume that the task serves as a cue for a possible upcoming reward and thus induces reward expectation. Consistent with the temporal difference model, we observed a decrease in the BOLD signal if a subject did not receive a payment and thus reward expectations were not met. Likewise, the BOLD signal increased when a subject was the only one to receive a payment. We hypothesize that outperforming someone else or the "joy of winning" contributes to this response in addition to the monetary reward. For the conditions of interest in which both subjects are correct, the response increases with increasing relative reward. These trials are not confounded with the aspect of winning and losing, because both subjects have solved the same task correctly.

By showing that social comparisons affect activation levels in the ventral striatum, our findings complement recent work on other-regarding preferences such as reciprocity or empathy (*24*). It has been shown, for example, that reciprocal action in the form of punishing norm violations is associated with ventral striatal activation (*25*). Similarly, a recent hyperscanning fMRI experiment revealed specific brain activations for benevolent versus malevolent decisions in the dorsal striatum, highlighting the role of this part of the basal ganglia for reciprocal interactions (*26*). Subjects in these studies made decisions that revealed their preferences. In our study, in contrast, we show that social comparison affects ventral striatal activity even if subjects are not actively engaged in decision-making. In this sense, our study shows that mere contextual information about another person has an immediate impact on motivation-related brain processes.

References and Notes

1. L. Festinger, *Hum. Rel.* **7**, 117 (1954).
2. J. M. Olson, C. P. Herman, M. P. Zannan (Eds.), *Relative Deprivation and Social Comparison* (Lawrence Erlbaum, Hillsdale, NJ, 1986).
3. C. D. Carroll, in *Does Atlas Shrug? The Economic Consequences of Taxing the Rich*, J. Slemrod, Ed. (Harvard Univ. Press, Cambridge, 2000).
4. R. Frank, *Am. Econ. Rev.* **95**, 137 (2005).
5. M. J. Boskin, E. Sheshinski, *Q. J. Econ.* **92**, 589 (1978).
6. D. Neumark, A. Postlewaite, *J. Pub. Econ* **70**, 157 (1998).
7. E. Fehr, K. Schmidt, *Q. J. Econ.* **114**, 817 (1999).
8. E. Fehr, S. Gächter, *J. Econ. Perspect.* **14**, 159 (2000).
9. A. Clark, A. Oswald, *J. Pub. Econ.* **61**, 359 (1996).
10. A. Ferrer-i-Carbonell, *J. Pub. Econ.* **89**, 997 (2005).
11. A. Clark, P. Frijters, M. Shields, *J. Econ. Lit.*, in press.
12. J. P. O'Doherty, *Curr. Opin. Neurobiol.* **14**, 769 (2004).
13. J. P. O'Doherty, R. Deichmann, H. D. Critchley, R. J. Dolan, *Neuron* **33**, 815 (2002).
14. H. C. Breiter, I. Aharon, D. Kahneman, A. Dale, P. Shizgal, *Neuron* **30**, 619 (2001).
15. B. Seymour, N. Daw, P. Dayan, T. Singer, R. Dolan, *J. Neurosci.* **27**, 4826 (2007).
16. Materials and methods are available as supporting material on *Science* Online.
17. M. Haruno, M. Kawato, *J. Neurophysiol.* **95**, 948 (2006).
18. H. Cromwell, O. Hassani, W. Schultz, *Exp. Brain Res.* **162**, 520 (2005).
19. T. Tremblay, W. Schultz, *Nature* **398**, 704 (1999).
20. R. Elliot, K. J. Friston, R. J. Dolan, *J. Neurosci.* **20**, 6159 (2000).
21. Y. Akitsuki *et al.*, *Neuroimage* **19**, 1674 (2003).
22. S. Niewenhuis *et al.*, *Neuroimage* **25**, 1302 (2005).
23. J. P. O'Doherty, P. Dayan, K. Friston, H. Critchley, R. J. Dolan, *Neuron* **38**, 329 (2003).
24. T. Singer *et al.*, *Science* **303**, 1157 (2004).
25. D. J. F. de Quervain *et al.*, *Science* **305**, 1254 (2004).
26. B. King-Casas *et al.*, *Science* **308**, 78 (2005).

Supporting Online Material

www.sciencemag.org/cgi/content/full/318/5854/1305/DC1
Materials and Methods
SOM Text
Figs. S1 to S3
Tables S1 to S5
References

30 May 2007; accepted 18 October 2007
10.1126/science.1145876

Hold Your Horses: Impulsivity, Deep Brain Stimulation, and Medication in Parkinsonism

Michael J. Frank,[1]* Johan Samanta,[2,3] Ahmed A. Moustafa,[1] Scott J. Sherman[3]

Deep brain stimulation (DBS) of the subthalamic nucleus markedly improves the motor symptoms of Parkinson's disease, but causes cognitive side effects such as impulsivity. We showed that DBS selectively interferes with the normal ability to slow down when faced with decision conflict. While on DBS, patients actually sped up their decisions under high-conflict conditions. This form of impulsivity was not affected by dopaminergic medication status. Instead, medication impaired patients' ability to learn from negative decision outcomes. These findings implicate independent mechanisms leading to impulsivity in treated Parkinson's patients and were predicted by a single neurocomputational model of the basal ganglia.

Should you vacation in Montreal or Rome, eat chocolate fondue or tiramisu, go skiing, or visit world-class museums? Such win/win decisions are notoriously difficult to make, often leading to seemingly counterproductive deliberation and hesitation. Intuitively, either option should produce satisfactory results, so why wait? Mathematical models of decision-making suggest that individuals only execute a choice once the "evidence" in its favor crosses a critical decision threshold (*1*, *2*). But the notion of decision threshold need not imply some fixed value. Indeed, individuals can optimally adjust decision thresholds to meet current task demands (*3*–*5*). At the neurobiological level, one model posits that the subthalamic nucleus (STN) dynamically modulates decision thresholds in proportion to reinforcement and decision conflict (*6*). In essence, this model predicts that when faced with multiple seemingly good options, the STN enables you to adaptively "hold your horses," buying more time to settle on the best one. Supporting this account, STN dysfunction in rats causes premature responding in choice paradigms (*7*, *8*). Here we provide direct evidence in humans and show that STN disruption causes impulsive responding during high-conflict win/win decisions.

We administered computerized decision-making tasks to two groups of patients with Parkinson's disease (PD), and age-matched control participants (table S1). One group of patients ($n = 17$) was tested in different sessions on and off deep brain stimulation (DBS) of the STN, an increasingly common surgical procedure to treat motor symptoms of the disease (*9*). [See (*10*) for DBS surgical procedures, stimulation parameters (table S2), and confirmation of electrode implants in the STN (fig S1).] DBS patients were on relatively low doses of medication in both sessions (*9*, *10*). The second patient group ($n = 15$) was tested on and off dopaminergic medication. The purpose of the medication manipulation was twofold: (i) to test whether any effects of DBS on conflict-based decisions were selective to that treatment; and (ii) to replicate findings that dopaminergic medication impairs patients' ability to learn from the negative outcomes of their decisions (*11*–*13*), which could account for pathological gambling behavior (*14*). Thus, we tested two potentially distinct mechanisms by which Parkinsonian treatments can cause impulsive behavior (*14*, *15*).

Participants were tested with a probabilistic selection task (*12*, *16*). Three different stimulus pairs (AB, CD, EF) were presented in random order, and participants had to choose one of the two stimuli (Fig. 1A). Feedback followed the choice to indicate whether it was correct or incorrect, but this feedback was probabilistic. In the most reliable AB pair, a choice of stimulus A led to positive feedback in 80% of trials, whereas a choice of stimulus B led to negative feedback in these trials. In a subsequent "test phase," participants chose between novel combinations of all stimuli. Positive-feedback learning was indicated by reliable choice of the most positive stimulus A in these novel test pairs, whereas negative-feedback learning was indicated by reliable avoidance of stimulus B (*12*, *16*). To examine conflict effects, we measured reaction times for test pairs having similar reinforcement values (e.g., 80 versus 70%; high conflict) compared with low-conflict pairs having more easily discriminable values (*6*, *16*) (Fig. 1A).

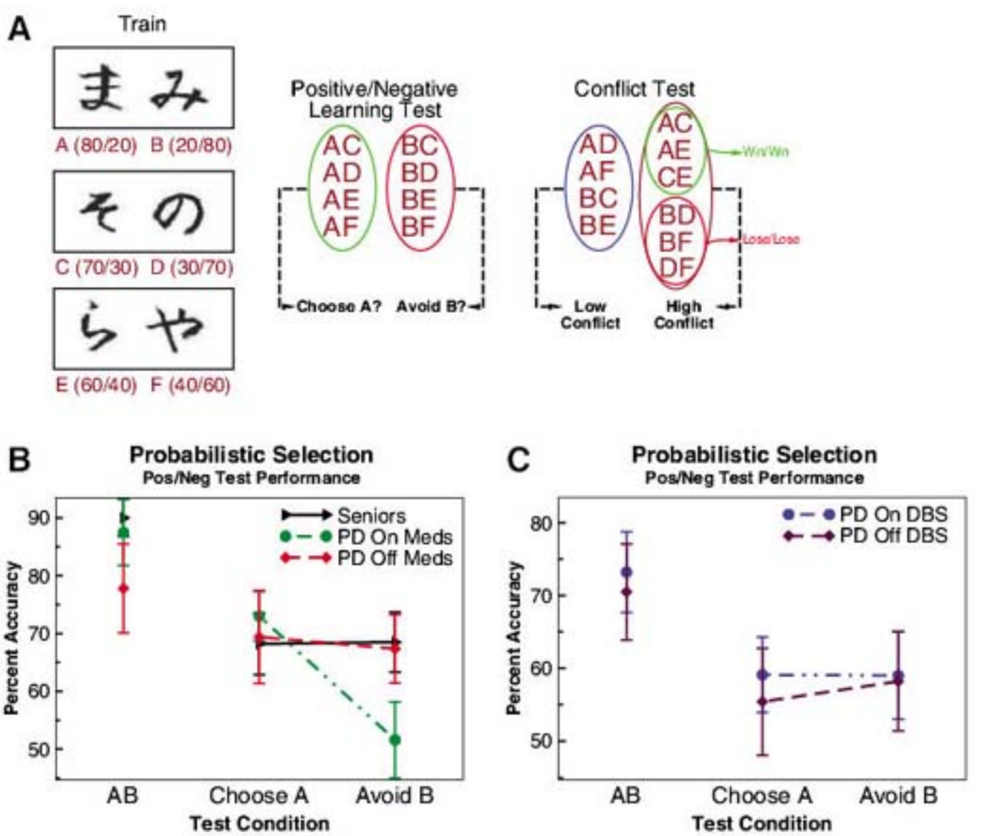

Fig. 1. (**A**) Probabilistic selection task. Each stimulus pair is presented separately in different trials, in random order. Correct choices are determined probabilistically (percent positive/negative feedback is shown in parentheses for each stimulus). A test phase ensues that presents all novel recombinations to assess positive/negative learning biases and conflict (*12*, *16*). (**B**) PD and medication effects, showing selectively impaired avoid-B performance in medicated patients. Nonmedicated patients performed similarly to controls, but were slower to acquire probabilistic contingencies in the learning phase (*10*). (**C**) DBS effects. DBS patients were more advanced in their disease progression than the medication group (table S1); within-patient treatment effects are therefore more interpretable than between-group effects. Error bars are SEs.

[1]Department of Psychology and Program in Neuroscience, University of Arizona, Tucson, AZ 85721, USA. [2]Banner Good Samaritan Medical Center, Phoenix, AZ 85004, USA. [3]Department of Neurology, University of Arizona, Tucson, AZ 85724, USA.

*To whom correspondence should be addressed. E-mail: mfrank@u.arizona.edu

It is precisely in these high-conflict choices that it may be adaptive to "hold your horses," increasing the likelihood of settling on the more optimal choice (*6*). We predicted that compared with controls, PD patients (regardless of treatment) would show reinforcement learning deficits (*11*). We further predicted that dopaminergic medication would impair negative-feedback learning (*12*, *13*), whereas DBS would cause impulsive responding in the face of conflict (*6*).

Patients were slower than controls to learn probabilistic reinforcement contingencies (*10*). As shown previously (*12*), patients on medication were selectively impaired at learning from negative decision outcomes [Fig. 1B; see (*10*) for detailed analysis]. Notably, DBS status (on versus off) did not affect positive- or negative-feedback learning (Fig. 1C). Rather, DBS induced impulsive responding under high-conflict conditions. Overall, participants significantly slowed responses for correct high- relative to low-conflict decisions ($F[1,51] = 13.5$, $P < 0.001$; Fig. 2, A and C). This conflict-induced slowing is reminiscent of the deferred decisions under conflict observed in other contexts, including economic decisions (*17*). In contrast, patients on DBS failed to slow down with increased decision conflict (group by conflict interaction, $F[4,51] = 4.9$, $P = 0.002$). The within-subject effect of DBS (on versus off) on conflict-induced slowing was significant ($F[1,51] = 4.6$, $P = 0.036$). Patients on DBS even responded marginally faster under high- than under low-conflict conditions ($F[1,51] = 3.6$, $P = 0.06$). Finally, dopaminergic medication had no effect on conflict-induced slowing ($F[1,51] = 0.5$), and there were no other group/conflict differences.

In models and animals with STN dysfunction, premature responding is associated with suboptimal choices (*6*–*8*). Notably, the tendency for DBS patients to show speeded high-conflict responses was especially pronounced when choosing the less optimal stimulus ("error trials"; $F[1,51] = 16.1$, $P = 0.0002$; Fig. 2, B and D). Further, the more DBS patients exhibited high-conflict premature responding (as defined by faster error than correct choices), the more errors they made in high- than in low-conflict conditions [$r(13) = 0.53$, $P = 0.05$; P's > 0.3 for all other groups]. Thus, high-conflict premature responding led to suboptimal choices under DBS.

Why should DBS patients respond even faster to high- than to low-conflict choices? We posited that the presence of two positive stimuli in high-conflict "win/win" choices could lead to such impulsive responding. Indeed, patients on DBS responded significantly faster during high-conflict win/win conditions (Fig. 3A; $F[1,51] = 5.2$, $P = 0.027$); this faster responding was not observed for lose/lose decisions (fig. S2).

Finally, to control for a possible confounding effect of DBS during the learning phase, we also used a "retrograde DBS" procedure. All patients who had learned the task off DBS were subsequently tested again in a second test phase, identical to the first, after having their stimulators turned on (and a 10-min delay). If DBS genuinely and primarily interferes with the ability to modulate decision times as a function of conflict, these patients should no longer show a conflict-induced slowing effect in the second test phase.

Indeed, the conflict-induced slowing effect was reversed in the second test phase, with DBS patients responding significantly faster to win/win decisions (Fig. 3B; $F[1,51] = 4.7$, $P = 0.03$). These same patients had exhibited the opposite pattern—slowing responses for win/win conditions—just minutes before in the off-DBS state (Fig. 3A). A subset of senior controls ($n = 14$) who were also tested in a second test phase, with the same temporal delay between phases, continued to show conflict-induced slowing ($F[1,51] = 4.3$, $P = 0.04$). Furthermore, to provide a treatment control, patients who learned off medication were also tested in a second test phase after taking their regular dose of levodopa medication [but with a longer delay to allow medication to be absorbed (*10*)]. Critically, there was a significant treatment by conflict interaction ($F[1,51] = 6.0$, $P = 0.017$], such that DBS reversed conflict-induced slowing but medication did not.

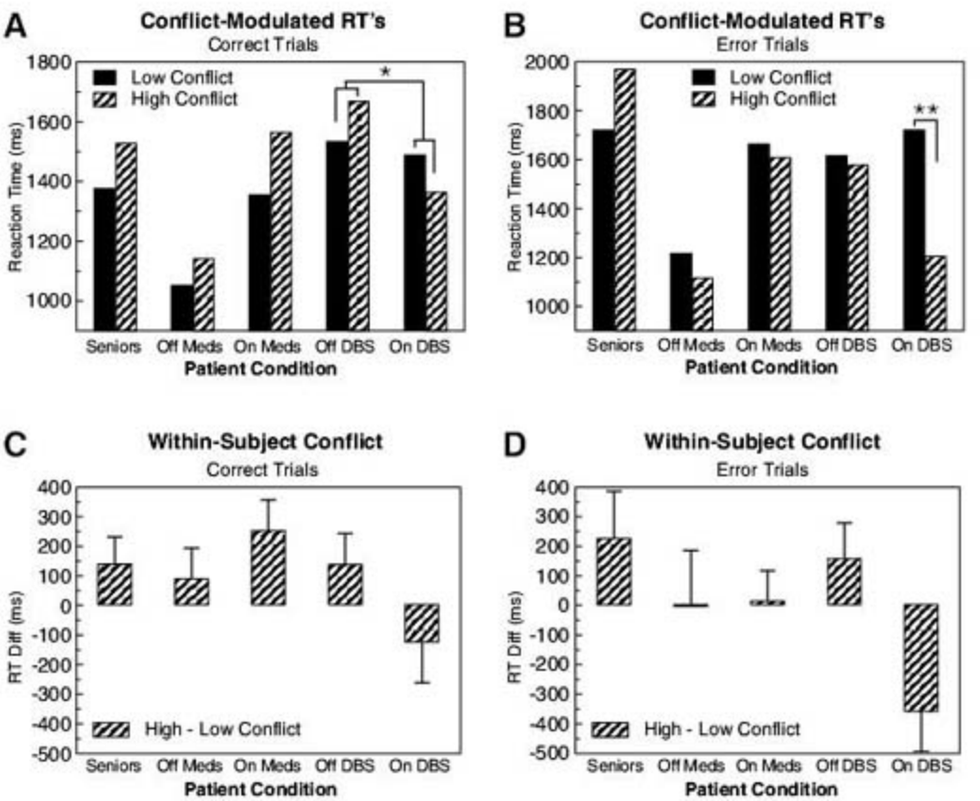

Fig. 2. Conflict effects on decision times. Mean of median reaction times (RTs) are shown for low- and high-conflict conditions in **(A)** correct and **(B)** error trials. Within-subject RT differences (high–low conflict) are also shown in **(C)** correct and **(D)** error trials. The DBS (on versus off) effect on conflict-induced slowing was significant (*$P < 0.05$). Patients on DBS actually responded more rapidly to high-conflict choices, particularly in error trials (**$P < 0.001$).

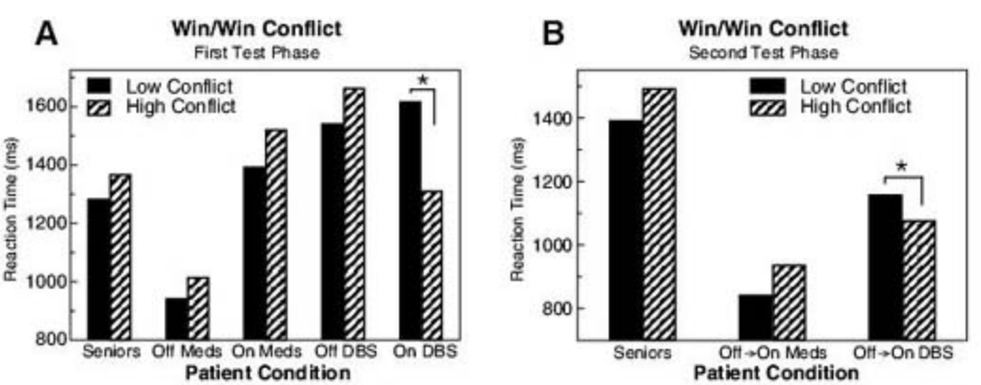

Fig. 3. High-conflict win/win decisions (correct trials; similar results in error trials, not shown). **(A)** Patients on DBS responded significantly faster during high-conflict win/win decisions. **(B)** "Retrograde DBS." Patients who acquired the reinforcement contingencies off DBS were then tested again in a second test phase, after their DBS units were turned back on (*$P < 0.05$).

Taken together, our findings provide evidence for two distinct computational roles of the basal ganglia in decision-making. Dopaminergic medication altered patients' relative tendency to learn from positive versus negative outcomes (*12*, *13*, *18*), without affecting conflict-induced slowing. In contrast, DBS induced speeded high-conflict choices, without affecting learning biases. Both of these findings are captured by a single a priori computational model of the basal ganglia in learning and decision-making (*6*).

As in other models, the basal ganglia in our model supports adaptive decision-making by modulating the selection of frontal cortical action plans (*5*, *6*, *11*, *19*–*21*). In brief, two main neuronal populations in the striatum have opposing effects on action selection via output projections through the globus pallidus, thalamus, and back to the cortex (Fig. 4A). Activity in "Go" neurons facilitates the execution of a cortical response, whereas "NoGo" activity suppresses competing responses. Dopamine bursts and dips that occur during positive and negative outcomes (*22*) drive Go learning (via D1 receptors) to seek rewarding actions, and NoGo learning (via D2 receptors) to avoid actions that are nonrewarding (*11*). Complementing this functionality, the STN provides a self-adaptive dynamic control signal that temporarily prevents the execution of any response, depending on decision conflict (*6*). Notably, the STN receives direct projections from the presupplementary motor area (preSMA) and cingulate cortex regions that detect and integrate response conflict (*23*–*25*). In turn, the STN sends a "Global NoGo" signal via diffuse excitatory projections to basal ganglia output nuclei (*19*, *26*) with consequent inhibition of thalamocortical activity. This STN mechanism provides a means to implement cognitive control, by effectively raising decision thresholds in the face of conflict (*6*). Supporting this notion, neuroimaging studies have found that preSMA and STN coactivation is associated with slowed response times under decision conflict (*25*), and STN-DBS reduces coupling between cingulate and basal ganglia output (*27*).

This single model captures both medication and DBS effects, as revealed in computational simulations of these dynamics [Fig. 4, B to D; see (*6*, *10*) for detailed modeling methods]. To simulate PD, we decreased dopamine levels. To simulate medication, we maintained relatively elevated dopamine levels but prevented them from sufficiently decreasing during negative feedback, due to tonic D2 stimulation (*11*, *12*). The resulting Go/NoGo learning and medication effects replicate those reported with an earlier basal ganglia model that did not include the STN (*12*) and show that these learning biases are insensitive to STN manipulation. Here, we focus on DBS simulations in high-conflict decision-making.

The mechanisms underlying the therapeutic effects of DBS are controversial (*28*). One dominant theory is that high-frequency DBS paradoxically acts like a lesion [e.g., via "depolarization block" (*29*)]. Indeed, like DBS, both real and simulated STN lesions ameliorate abnormal network oscillations and motor symptoms of PD (*6*, *30*). To simulate STN lesions, we simply removed STN from processing altogether (*6*). A second theory is that DBS induces regular high-frequency STN firing patterns (*31*) and actually enhances STN output (*28*). To simulate this version, we externally applied high-frequency excitatory input to the STN [see (*10*) for details]. We posited that either DBS mechanism would prevent the STN from naturally and dynamically responding to its cortical inputs and would therefore disrupt conflict-induced slowing.

After training networks with probabilistic reinforcement, we tested them with low- and high-conflict trials, in which two responses were associated with competing reinforcement probabilities (*6*, *10*). Whereas intact networks showed substantial conflict-induced slowing, those with either STN lesions or external stimulation exhibited the same speeded win/win responding observed in DBS patients (Fig. 4C). This "impulsive" speeding resulted from the presence of two striatal "Go" unit populations (one for each rewarding response), which enhanced the probability that one of them surpassed threshold (*6*). Counteracting this factor, in intact networks, cortical response conflict led to an initial STN surge, postponing responding until this STN activity subsided (Fig. 4D). In STN-lesioned networks, there was no such mechanism to allow this slowing to occur. In networks with external stimulation, the idiosyncratic, non–task-related STN firing prevented it from responding naturally and adaptively to conflict signals. Accordingly, the network could select a response earlier in time (Fig. 4D). In sum, our model captures the main observed effects of different PD treatments and in so doing may reveal different computational functions of the basal ganglia in decision-making.

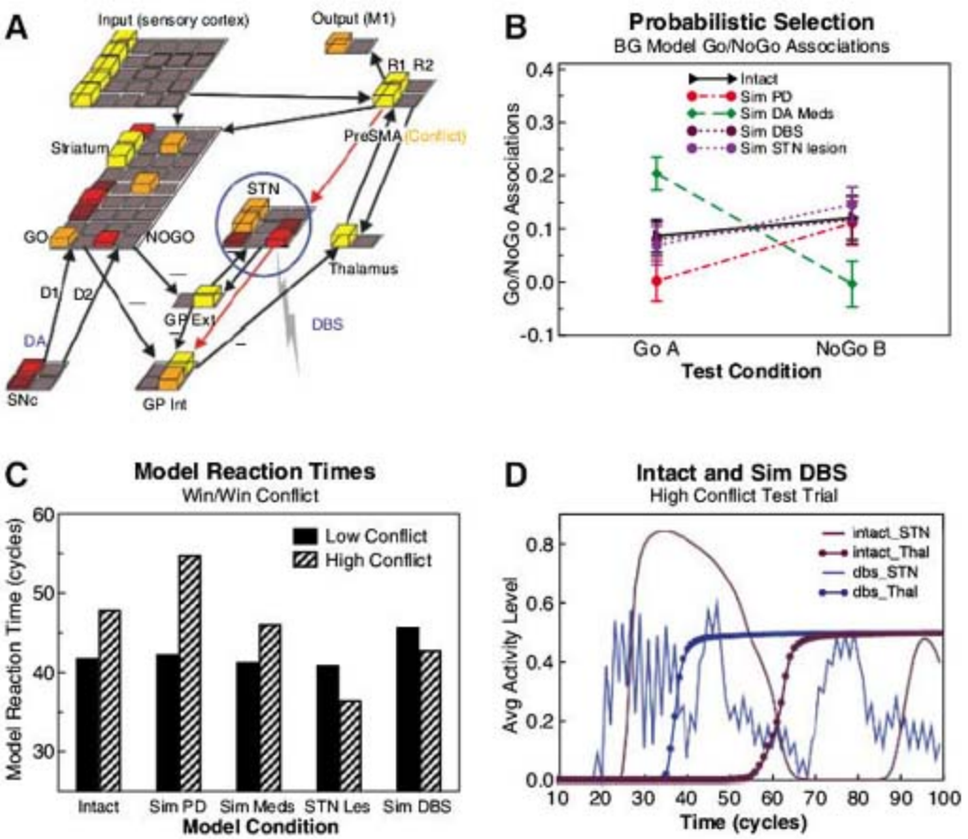

Fig. 4. **(A)** Neural network model of the basal ganglia (squares represent units, with height and color reflecting neural activity). The preSMA selects a response (R1 or R2) via direct projections from the sensory input and is modulated by basal ganglia (BG) output via the thalamus. Go and NoGo units are, respectively, in the left and right halves of the striatum, with separate columns for each response, and receive dopaminergic (DA) learning signals from the substantia nigra pars compacta (SNc). The STN sends a Global NoGo signal by exciting globus pallidus, internal segment (GP Int) in proportion to response conflict in preSMA (these projections shown in red). In the case shown, conflict is low because only a single response (R1) is active. **(B)** Model predictions for reinforcement learning. Plots show striatal activation-based receptive fields indicating summed Go-A and NoGo-B associations (*10*, *12*). **(C)** The same model's predictions for conflict-induced slowing. Reaction times are indexed by the number of processing cycles before a given response is selected (*10*). Simulation results reflect mean values across 25 network runs with random initial synaptic weights. **(D)** Normalized activity in the model STN and thalamus, in a representative high-conflict win/win trial. The model selects a response when thalamus activity rises. The model selects a response when thalamus activity rises and subsequently facilitates the associated preSMA units.

Hybridization Oven

The Big Shot III Hybridization Oven is suitable for all types of hybridization and incubation applications, including northern blots, Southern blots, and microarrays. The Big Shot III features a proportional integral derivative (PID) controller that provides rapid heating and temperature stability from 10°C to 100°C. A fully programmable digital timer and an adjustable safety over-temperature cutout allows unattended operation for almost 100 hours. The device offers carousel speed control up to 60 rpm in 1 rpm increments. In addition to the standard 35-mm bottle carousel supplied with each unit, accessory carousels are available for 55-mm and 70-mm bottles for processing larger membranes, for conical and round bottom sample tubes, and for standard and deep-well microplates. The Big Shot III is stackable and comes with a reversible door.

Boekel Scientific For information 800-336-6929. www.boekelsci.com

Temperature Control Unit

Available in three models, the Ministat thermoregulator range is built for the crowded laboratory workbench or for use in fume hoods where space is at a premium. The instruments offer precise temperature control from –40°C to 200°C. All-stainless-steel construction eliminates the need for a gasket between the outer case and the bath, improving insulation and enhancing long-term durability and chemical resistance. Ministat units also feature variable pump control, which allows faster heating and cooling for demanding applications. The units feature a choice of interchangeable controllers and a backlit LCD display designed for simple and intuitive operation. All units in the family also feature over-temperature protection and bath-fluid level monitoring devices.

Radleys For information +44 1799 513320 www.radleys.co.uk

Cell Cycle Assay

The Guava Cell Cycle Assay, when used in conjunction with a Guava PCA or EasyCyte platform, offers cell cycle phase analysis at your benchtop without the use of complicated flow cytometric methods. The cell cycle phase percentages and counts are displayed on the same screen as acquisition, without the need for involved software set-up, making it easy to visualize the results in both histogram and statistical formats. Unlike traditional methods, the cell counts for each sample are direct and absolute, without the use of reference beads.

Guava Technologies For information +44 1780 764390 wwww.guavatechnologies.com

Freeze Dryers

Featuring the latest advancements in benchtop freeze drying, the AdVantage Plus Series is available with up to three fluid-cooled shelves that maintain a level of precision in temperature control previously available only in production-scale units. As with the previous generation AdVantage model, a choice of condenser temperatures at –53°C, –75°C, and –85°C enables processing of a wide range of samples in stoppered vials or bulk drying in freeze-dry flasks or trays. These compact, affordable units are loaded with functions that enable materials to be processed quickly, efficiently, and conveniently. An optional workstation enables all aspects of the lyophilization cycle to be precisely controlled, monitored, recorded, and presented in graphic format.

Genevac +44 1473 240000 www.genevac.co.uk

Cytotoxicity Assay

The CytoScan-Fluoro Cytotoxicity Assay measures the release of lactate dehydrogenase (LDH) from cells with damaged membranes. Released LDH is measured directly in the cell culture wells with a coupled enzymatic assay that results in the conversion of a nonfluorescent compound to a fluorescent compound, which can be detected with a fluorometer.

G-Biosciences/Genotech For information 314-991-6034 www.GBiosciences.com

RNAi Screening

The LentiExpress small-hairpin RNA (shRNA) based system is for rapid high-throughput RNA interference (RNAi) screening with minimal reagent preparation or optimization required. The addition of this technology to the Mission shRNA platform pairs the benefits of lentiviral-based shRNA with a simple streamlined protocol. The bottleneck for researchers is the time and expense required to generate viral particles and devise a robust screening strategy. With the Mission LentiExpress technology, researchers can eliminate reagent preparation with a sophisticated yet simple method to perform complex screens. An optimization plate enables researchers to quickly optimize the system for their particular cell line. This optimization process is simple compared with other transfection methods. A researcher simply adds the desired number of cells to each well, continues with optional selection and/or addition of small molecules (for example, pharmaceutical compounds), and then proceeds directly to the desired assay for gene silencing or loss of function.

Sigma-Aldrich For information 800-521-8956 www.sigma-aldrich.com

RNA Purification Kit

The SurePrep RNA Purification Kits enable the capture of all sizes of RNA molecules from biological samples. This technology provides purified full-length large RNAs as well as small RNAs such as microRNA (miRNA) and small-interfering RNA. SurePrep kits are versatile, isolating RNA from a wide variety of tissues and cell types, and they save time in the lab by reducing the number of steps involved in RNA purification. The SurePrep line makes use of spin-column chromatography with a proprietary resin for capturing RNA molecules from plant and animal tissues, cultured cells, fungi, blood, bacteria, and yeast. The product line includes the TrueTotal Kit, which enables the extraction of all sizes of RNA, including large messenger RNA, ribosomal RNA, and small RNA species (less than 200 nucleotides) such as transfer RNA and miRNA.

Thermo Fisher For information 973-889-6365 www.fishersci.com/RNA111M

Newly offered instrumentation, apparatus, and laboratory materials of interest to researchers in all disciplines in academic, industrial, and government organizations are featured in this space. Emphasis is given to purpose, chief characteristics, and availability of products and materials. Endorsement by *Science* or AAAS of any products or materials mentioned is not implied. Additional information may be obtained from the manufacturer or supplier.

BUILDING BRIDGES, FINDING SOLUTIONS

Complex scientific problems and socially relevant issues are challenging scientists to find new ways to integrate knowledge from multiple and disparate fields. Increasingly, collaborative approaches are changing the way science is done.

By Jill U. Adams

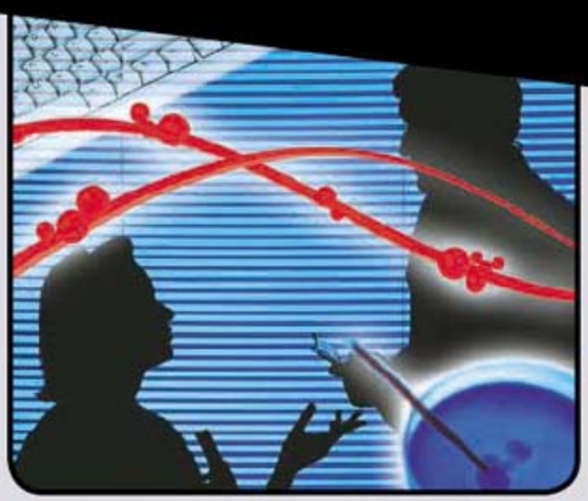

Consider obesity. It's a complex problem with no easy solution. Risk factors reside in your genes, the microflora in your gut, the food you ate as a child, the people who share your home, and the physical environment of your town. But how do the genetics interact with the availability of sidewalks in your neighborhood? How do the foods you eat affect the microbial population in your intestines?

These multifaceted questions are answerable if geneticists and urban planners—or economists and immunologists—sit down in a room together and share their ideas. They may speak different dialects, use dissimilar methods, and experience personality clashes, but to succeed, scientists from diverse fields must find a way to shed preconceptions and make the effort to understand a foreign discipline.

"Interdisciplinary research is when you get people to work together enough that you go beyond disciplines working separately on the same issue," says **Barry Popkin,** director of the University of North Carolina's Interdisciplinary Obesity Program. To get people out of their comfort zone, he says, it takes time and inducement. "Sometimes it takes money."

Incentives might bring scientists to the interdisciplinary table, but they won't keep them there. To bridge disciplines takes "an extra effort," says **Carol Van Hartesveldt,** program director for IGERT at the National Science Foundation (NSF). IGERT stands for Integrative Graduate Education and Research Traineeship program and is the mechanism by which NSF encourages training in interdisciplinary research. "The focus is on funding projects with excellent, significant, timely, cutting-edge research. That's why people take the trouble to do this."

For administrators who want to encourage interdisciplinary research, it's important to define a central focus, to give it adequate time, and to keep people talking. Established researchers who enter the fray should work well with others, ask "dumb" questions, and stay open to possibilities. For postdoctoral and graduate students, it's essential to get comfortable exposing yourself to outside influences and alternative research fields.

> "Interdisciplinary research is when you get people to work together enough that you go beyond disciplines working separately on the same issue."

Barry Popkin

Finding Focus

In industry, the focus is the product or unmet need. Teams work toward the company goal of getting a worthy creation on the market.

"I think it is part and parcel of the way biotech companies function and have to function, frankly, in order to do excellent and relevant work," says **Douglas Williams,** executive vice president and chief scientific officer of ZymoGenetics in Seattle, Washington. The market is so competitive, he says, that companies do whatever they can to keep ahead of the curve.

In addition to mixing scientific disciplines, companies also blend expertise at different stages of the product pipeline. "We're bringing together skill sets that are necessary for taking an idea all the way to a product," says Williams. "Project teams form, but the team structure tends to morph over time," he says, as the focus shifts from research to development and eventually to marketing and sales, as the product gets closer to the marketplace.

continued »

UPCOMING FEATURES

Faculty Positions — January 25

Diversity: Women in Science — February 8

Postdoctoral Scientists — February 22

"You rally people around a societal problem that transcends a particular discipline."
—Bruce Wilcox

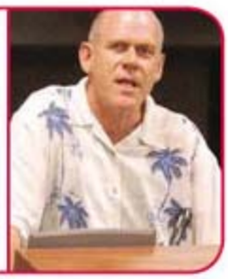

CREDIT: RON PAIK

Because companies by definition have a strong product focus, one might think that they've got the interdisciplinary approach down pat. But that's not necessarily the case, says **John Tallarico,** group leader of chemogenetics at the Novartis Institutes for BioMedical Research in Cambridge, Massachusetts. A company has to be specifically structured for true cross-fertilization to occur. At Novartis, this means different categories of groups, some oriented by disease area, some specializing in methods, and some specifically created to build bridges among other groups.

"If things are classically broken down, the pharmacologists only care about pharmacology, the chemists only care about medicinal chemistry, the cell biologists only care about their bioassays," says Tallarico. "When there's a real silo effect, it's hard to be one of the groups who bridges those things, because people will always question you. What are you actually good at? What do you do?"

Many companies now boast about doing interdisciplinary work—a sign that things are changing. But change takes time, even at a company like Novartis where the push for collaboration comes from the top, says Tallarico. Flexibility in thinking and a willingness to take risks—those are traits that Tallarico wants in his team members. And yet he acknowledges, "It's nontrivial to convince colleagues that these are the best people out there."

Staying Flexible

"What's exciting about Novartis is that you're going to have many different flavors of scientists at the table," says Tallarico. When interviewing, he wants to know if a candidate is intimidated or excited by that prospect. "Some people have a passion for learning new things—that's huge," he says. "If I had to phenotype my group, I'd say that they like to push the envelope. And if they're not being pushed themselves, they kind of get bored."

Some themes carry over to the academic side, including the truism that only some people are comfortable bridging disciplines. "You can't make everybody be an interdisciplinarian," says **Bruce Wilcox,** director of an NSF-funded IGERT in ecology, conservation, and pathogen biology at the University of Hawaii in Manoa. "You have to cultivate and develop those people with that inclination."

In Wilcox's training program, bridging disciplines begins with a student's application. "They have to find a mentor/sponsor who must then interact with two or three other faculty—at least one of whom is in a different department," he says. The mentor team must then convince the selection committee that they will collaborate.

As for a defining focus, Wilcox says, "You rally people around a societal problem that transcends a particular discipline." In his case, the theme is understanding how biodiversity relates to human health, specifically with regard to emerging infectious disease. "We try to inculcate in the students that the research they're doing—in minute detail—also needs to be placed in a larger context." For instance, can they scale it up from a coral polyp to a coastal ecosystem, and relate it to the health of society?

Even when the motivation is there, scientists trained in different fields have different cultures, different jargon, and different ways of thinking. One goal of the IGERT program, says NSF's Van Hartesveldt, "is that students learn how to talk, discuss, and approach problems with people from other disciplines."

Institutionalized Roadblocks

In addition to disciplinary barriers, there are organizational sticking points that can hinder team research. In a university setting, faculty members face bureaucratic issues concerning money and recognition, says Van Hartesveldt. "When there are multiple authors on a publication or co-principal investigators on a grant, who gets credit? When there is overhead income [for indirect costs], which department gets it?"

The National Institutes of Health (NIH) is promoting interdisciplinary research as part of the NIH Roadmap and has addressed institutional obstacles directly. "Heretofore, if you were a co-principal investigator, it was tantamount to being partially pregnant. It had no meaning," says **Lawrence Tabak,** who is the director of the National Institute of Dental and Craniofacial Research and co-chair of the interdisciplinary research implementation group. "But now NIH has come up with a way of formally recognizing multiple PIs. We think that this is a big deal and will help universities recognize contributions related to team science."

The more the implementation group tackled institutional barriers, says Tabak, the more they realized that NIH itself had its own impediments. First and foremost was that interdisciplinary research requires interdisciplinary review, he says. "When I've sat on study sections, anything that was interdisciplinary was met with one of two characterizations: overly ambitious or unfocused."

In order to review proposals and evaluate programs, you have to define your goals, says **Elizabeth Wilder,** another implementation group member who is now acting associate director of NIH's Office of Portfolio Analysis and Strategic Initiatives. "The group spent a fair amount of time establishing the goals, both big and small." Training an interdisciplinary work force and continued »

Fuel Cell IGERT at Rensselaer Polytechnic Institute
fuelcell-igert.rpi.edu

Igert at University of Hawaii at Manoa
www.jabsom.hawaii.edu/igert

International Institute for Applied Systems Analysis
www.iiasa.ac.at

National Science Foundation
www.nsf.gov

NIH Roadmap for Interdisciplinary Research
www.nihroadmap.nih.gov/interdisciplinary

Novartis Institutes for BioMedical Research
www.nibr.novartis.com

University of North Carolina Interdisciplinary Obesity Program
www.cpc.unc.edu/idoc

ZymoGenetics
www.zymogenetics.com

ADDITIONAL RESOURCES:

Merck/AAAS Undergraduate Science Research Program
www.merckaaasusrp.org

Interdisciplinary Research

"Science is the foundation and the tool, but it is talented people who discover drugs."
—John Primeau

CREDIT: LORI PERRIN

making it easier for academic researchers to traverse departmental boundaries are overarching objectives.

Short-term goals are ones that can be measured—like publications. "You've got to do a cluster analysis," says Tabak. "If only biochemists, or only physicists, are citing a paper, maybe it's not truly interdisciplinary. But if you have social scientists citing it along with physicists ... now maybe you've got something cooking."

New ways to measure graduate student training are also needed. In the same way that a discipline-bridging project may get accused of lacking rigor, a lab-hopping graduate student may suffer some dilution of primary training.

Michael Jensen, who directs an IGERT on fuel cells at Rensselaer Polytechnic Institute in Troy, New York, admits that the time students need to work with different faculty is debited from any single effort. "But if we're looking at the professional growth of the individuals, then we should be encouraging them to take a broader approach," he says. "I think we turn out a much better prepared student."

Jensen has participated in many interdisciplinary projects over the years. "I know that it's these intersections of fields that can be the most productive areas for advancement," he says. "Even though people pay it lip service by saying that it's a great place to be, it's sometimes a very difficult place to work."

Entrepreneurship and Public Policy

Jensen's IGERT includes faculty and students from six different academic units, the most unusual of which is management. All the typical careers for Ph.D. scientists—academia, industry, or startup companies—require some aspect of entrepreneurship, says Jensen. "A faculty member has to come with an idea and sell it to get funding. Industry often wants a researcher to be the champion for a technology. And if you're starting you own company, you're definitely an entrepreneur."

With multiple skills, individuals can function as more than cogs in a machine. "Science is the foundation and the tool, but it's talented people who discover drugs," says **John Primeau,** executive director of infection chemistry at AstraZeneca in Waltham, Massachusetts. "In the past you'd have a smaller number of very smart people calling all the shots and directing the groups," he says. Primeau says his company lets the people with the expertise—the scientists doing the work—influence strategy. By empowering project teams, progress is faster and more efficient "because the people who have seen the data are also the people who are making decisions on the data."

Many proponents believe that interdisciplinary research is a must to address complex problems in society. At the International Institute for Applied Systems Analysis (IIASA) in Laxenburg, Austria, "The goal is to do research in global change relevant to policy," says **Leen Hordijk,** IIASA's director. An international research organization with scientists from 38 different countries, IIASA was founded as an east-west think tank at the height of the Cold War.

It's the societal aspect of research done at the institute that makes it a draw to many researchers, says Hordijk. "People want to contribute to that. It's the excitement of having real influence."

The scientific staff reflects IIASA's broad goals. Forty percent are social scientists, 20 percent are mathematicians, and another 40 percent come from engineering and the natural sciences. "The natural sciences covers a very broad range," says Hordijk, including atmospheric scientists, ecologists, evolutionary scientists, meteorologists, and limnologists, to name a few. "Most of the groups at the institute have a tool in development: a database or a model," says Hordijk. "These common tasks bring different disciplines together on major environmental, social, and energy problems facing our planet—work that is well beyond any one discipline."

Keys to Success

To get started, leaders have to get people talking. "You find targets of opportunity and you find ways to help people work together," says UNC's Popkin, who describes a retreat attended by 50 faculty members. "Three days produced a number of projects—people talking at lunches, breaks, and walking. It doesn't happen in any systematic way."

And they have to keep them talking, says AstraZeneca's Primeau. "The whole idea is to share," he says. "We're spread across the globe, so we're trying to put together the infrastructure—in terms of information technology systems—to allow people to share data freely. That's the biggest challenge because we move so much information now."

Institutions must provide "a long-term setting with long-term goals," says IIASA's Hordijk. "In universities, you seldom have enough time to build a relationship," due to short-term funding and staff turnover, both of which can "break a growing collaboration."

As a director of an academic interdisciplinary center, Popkin agrees. "It takes time to truly build teams. Not one or two years, it takes five years—for people to truly start talking to and understanding each other. And for the methods to start melding together—the measurement concerns, the statistical concerns, and the theoretical concerns."

With regard to individual team members, it takes time to internalize unfamiliar perspectives and to get educated beyond one's training. Maybe it just takes time for scientists to move beyond the indoctrination that comes with training in a particular field of study. NIH's Tabak calls it "checking your hat at the door."

To ZymoGenetics' Williams it's the play-well-with-others approach. "It's recognizing that you don't have all of the answers. The interdisciplinary teams that do it well are the ones that have no preconceived notions about where the next great idea is going to come from."

And the learning curve that comes from crossing disciplines can reinvigorate a passion for science.

Jill U. Adams is an interdisciplinary freelance writer living in upstate New York.

DOI: 10.1126/science.opms.r0700032

Takeda Cambridge Limited

www.takedacam.com

Principal Scientist – Metabolism

Takeda Cambridge is a drug discovery company specialising in identifying and validating novel drug targets derived from the human genome. Worldwide, Takeda develops, manufactures and markets a broad range of superior pharmaceutical products to strive toward better health for individuals and progress in medicine. We are currently seeking to recruit a Principal Scientist based in our Cambridge facility to lead our metabolic disease programme. This role will be responsible for developing a mechanistic understanding of new drug targets in key metabolic pathophysiological pathways of obesity and diabetes.

Applicants must have sound knowledge of the pathophysiology of metabolic diseases and their translation from transgenic models to humans. In addition, significant technical skills in advanced metabolic experimental design and implementation are required. This expertise will have been acquired in an industrial or academic setting.

The successful applicant will have a publication track record in the field of diabetes and obesity and will be a highly motivated, committed scientist able to drive projects forward independently. Good interpersonal skills and an emphasis on teamwork are essential. This position reports to the Head of Discovery Biology and is closely integrated within the Biology department.

The company offers a competitive salary and attractive benefits package.

Closing date for applications: 31 December 2007

Please send a covering letter, your c.v. and the names of two referees to:
Human Resources, Takeda Cambridge Ltd, 418 Cambridge Science Park, Cambridge, CB4 0PA, UK. Please indicate where you saw this advertisement.
Tel: +44 (0)1223 477910 Fax: +44 (0)1223 477911 email: hr@takedacam.com

Takeda Cambridge is an equal opportunities employer

INTERDISCIPLINARY RESEARCH

Opportunities

Gundersen Lutheran
HEALTH SYSTEM

Hematology/Oncology Research Scientist

Gundersen Lutheran Medical Center, the western academic campus of the University of Wisconsin medical school, seeks an outstanding scientist to spearhead the development of a basic science cancer research program at the Center for Cancer and Blood Disorders. Candidates must have a PhD or MD/PhD, with previous research experience in tumor biology, oncogenesis, cancer genetics, or angiogenesis. Consideration will be given to individuals with experience limited to post-doctoral fellowships, but preference will be given to individuals with proven experience developing an independent research program, obtaining extramural funding, and publication in peer-reviewed journals. Position includes generous start-up funds and state-of-the-art laboratory space at the La Crosse Health Science Consortium Center. A joint faculty appointment with the University of Wisconsin Medical School and/or University of Wisconsin-La Crosse is also expected.

Gundersen Lutheran Health System is a large, multi-specialty group practice with more than 600 medical and mid-level providers. It is consistently designated as a Top 100 Integrated Healthcare Network. The Center for Cancer and Blood Disorders, consisting of 6 medical oncologists, 4 hematologists, 2 pediatric hematologist/oncologists, and 2 radiation oncologists, sees over 1,400 new patients each year and has a strong clinical research program. Currently, there are over 150 active clinical trials through participation in ECOG, COG, RTOG, GOG, ACOSOG, CTSU, Wisconsin Oncology Network, Phase 2 Consortium, and Transfusion Medicine/Hemostasis Clinical Trials Network.

La Crosse is a city of 50,000+ (with a regional population of over 500,000), on the banks of the upper Mississippi River. Safe neighborhoods, excellent schools, affordable housing, remarkable natural beauty and extensive recreational/cultural choices converge for a great lifestyle in this family-friendly region. All of this, coupled with a competitive compensation and benefit package, makes this a premier opportunity.

We invite you to contact Kalah Haug, Medical Staff Development, 608-775-1005 or 800-362-9567 ext. 51005, kjhaug@gundluth.org. Please also visit us at: www.gundluth.org

We support a safe, healthy and drug-free work environment through background checks and controlled substance screening. EOE/AA/TTD/LEP

RUTGERS

NEW BRUNSWICK

Founding Director

Rutgers, the State University of New Jersey, is searching for an outstanding NIH-funded scholar to be the Founding Director of the New Jersey Institute of Food, Nutrition, and Health, a newly constituted center with faculty drawn from the Departments of Nutritional Sciences, Food Science, Animal Science, Chemical Biology, Plant Science, and Family and Community Health Sciences. The Directorship provides a unique opportunity to build and lead the Institute from conception to fruition. The Institute is one of three primary life science initiatives of the university's President and Executive Vice President for Academic Affairs. The Director will report to the Executive Dean of the School of Environmental and Biological Sciences. A doctorate in nutrition, medicine, public health, or related scientific discipline is required.

The Institute will be a key player among the vibrant biomedical, biological, and behavioral science communities on the New Brunswick/ Piscataway campuses. The Founding Director will be expected to attract extramural funding and to build academic linkages between existing program areas which include the Rutgers Institute of Human Genetics, Food Policy Institute, and Center for Lipid Research; the Rutgers-UMDNJ/Robert Wood Johnson Medical School joint initiatives which include the Center for Advanced Biotechnology and Medicine, Stem Cell Institute, and School of Public Health; and the UMDNJ Cancer Institute of New Jersey, Child Health Institute, and Cardiovascular Institute.

The commitment of Rutgers University to the new Institute is outstanding and includes significant resources for start-up costs, new faculty and staff, and foundation support for continued growth, along with new and renovated laboratory space dedicated to the initiative.

A letter of application, curriculum vitae, names of four professional references, and a statement of leadership objectives should be sent by electronic or regular mail to the: **Office of the Executive Dean, School of Environmental and Biological Sciences, 88 Lipman Drive, Rutgers, The State University of New Jersey, New Brunswick, NJ 08901 (execdean@AESOP.Rutgers.edu)**. Inquiries can be made to **Dr. Michael A. Gallo**, Search Committee Chair (**magallo@eohsi.rutgers.edu**). Review of applicants will begin **January 2, 2008**, and continue until a suitable candidate is identified. Starting date is negotiable, on or after July 1, 2008.

Rutgers, The State University of New Jersey, is an Affirmative Action/Equal Opportunity Employer and seeks to employ the best qualified individual without regard to race, religion, color, national origin, ancestry, age, sex, sexual orientation, physical or mental handicap or disability, or marital, military, or veteran's status. Individuals covered by Section 503 of the Vocational Rehabilitation Act of 1973 or Section 402 of the Veteran's Readjustment Assistance Act of 1974 may self identify. If you wish to self identify, please do so in the cover letter transmitting your curriculum vitae/ resume. Employment eligibility verification required.

Science
AAAS

Editor in Earth and Space Sciences

Join the editorial team at *Science*. We are seeking a new Associate Editor in the physical sciences. Applicants should have a broad range of interests and research experience in astronomy and astrophysics and/or the Earth and planetary sciences. Applicants should have post-doctoral experience, multiple publications, and a breadth of knowledge of cutting-edge research in these fields. Responsibilities include managing the review, selection, and editing of manuscripts, working with authors on revisions, solicitation of Reviews and special issues, and fostering contacts and communication with the scientific community. The position is for either our Washington, DC, or Cambridge, UK, offices.

For consideration, send a resume and cover letter along with salary requirements to:

AAAS
Human Resources Department, Suite #101
1200 New York Avenue
Washington, DC 20005

Applications can also be sent by e-mail to **hrtemp@aaas.org** or Fax to **202-682-1630**. Visit us at **http://www.aaas.org**.

EOE. Nonsmoking work environment.

Huazhong Agricultural University (HZAU), a national key university founded in 1898, As an university of 211 Project, she is under the administration of Ministry of Education of China, featuring superior with agriculture and life science.The beautiful campus, located at Lion Hill by South Lake in the city of Wuhan, covers an area of about 5 square kilometers.

HZAU comprises 13 colleges and 2 independent departments, with over 1200 faculty members. HZAU is armed with 48 undergraduate programs, 87 master programs, 54 PhD programs, 10 PhD disciplines, 10 post-doctoral research centers, 8 national key specialties and 1 national key discipline. In the new century, HZAU will further speed up her progress and strive to become a distinctive research university.

Now we are inviting applications for **FACULTY POSITIONS** of the Chang Jiang Scholars Distinguished Professor Programme in the following 8 research fields: crop breeding and genetics, microbiology, pomology, biochemistry and molecular biology, aquiculture, animal genetics breeding and reproduction, production and cultivation, agricultural and forestry economics and management. Furthermore, all the disciplines are inviting applications for excellent researchers with doctor's degree.

Details are available at **http://www.hzau.edu.cn**, or direct inquiries to Department of Personnel of the university **rcjlzx@mail.hzau.edu.cn** (e-mail) or **+86-27-87280957** or **+86-27-87281533** (telephone)

UNIVERSITY OF CALIFORNIA
UCMERCED

Senior Faculty Positions in Ecology (Deadline Extended)

Applicants are invited for two senior faculty positions in Ecology at UC Merced, the new 10th campus in the University of California system. Appointments will be made at Associate or Full Professor. Outstanding individuals with research interests in any area of ecology using experimental, field, computational, and/or theoretical approaches and working at population to ecosystem scales are encouraged to apply. We seek distinguished scholars who will provide leadership in establishing an internationally recognized program in ecology, and who will participate in developing innovative, interdisciplinary curricula and in teaching and mentoring of a diverse undergraduate and graduate student population.

Applications from interdisciplinary teams of ecologists offering an integrated research approach will be considered. For more information and to apply, visit:

http://jobs.ucmerced.edu/n/academic/position.jsf?positionId=1221

Application deadline is extended to **December 15, 2007**.

AA/EOE

THE UNIVERSITY OF KANSAS
KU

Faculty Position in Bioinformatics/Computational Biology

The Center for Bioinformatics (**www.bioinformatics.ku.edu**) and the Department of Electrical Engineering and Computer Science (**http://www.eecs.ku.edu**) at The University of Kansas invite applications for a tenure-track assistant professor position expected to begin August 18, 2008. The Bioinformatics initiative is part of a major expansion in Life Sciences and complements existing strengths in information technology, structural biology, computational chemistry, biophysics, proteomics, developmental and molecular genetics, and drug design. **Duties:** to establish and maintain an externally-funded research program, to participate in teaching, and to provide service. **Required Qualifications:** Ph.D. in a discipline related to Bioinformatics or Computer Science expected by start date of appointment; potential for excellence in research in Bioinformatics; and commitment to teaching bioinformatics and computer science courses; strong record of research accomplishments in at least one of the following areas: biomolecular networks modeling, bioinformatics databases, and computational modeling of biomolecular systems. For the full position announcement, refer to: **http://www2.ku.edu/~clas/employment/FY09_Index.htm** and click the Bioinformatics/EECS download button. E-mail application as a single file, including CV, letter of application, statement of past and future research and teaching interests and philosophy to: **asawyer@ku.edu**. Have at least three letters of reference sent separately to: **Dr. Robert F. Weaver, Professor and Associate Dean, College of Liberal Arts and Sciences, c/o Anne Sawyer, The University of Kansas, 1450 Jayhawk Blvd, 200 Strong Hall, Lawrence, KS 66045-7535**. Initial review of applications begins January 15, 2008 and will continue until the position is filled.

EO/AA Employer.

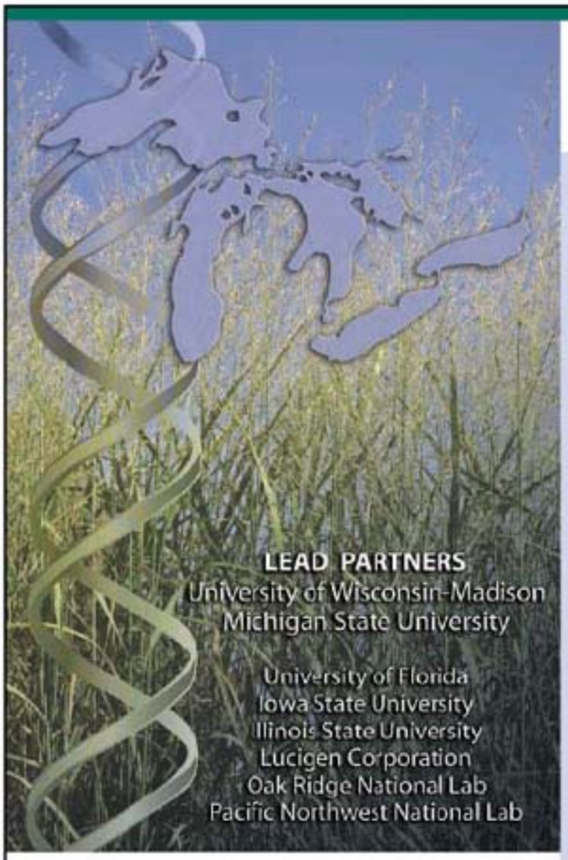

DOE Bioenergy Research Centers

Great Lakes Bioenergy Research Center (GLBRC)

BIOENERGY RESEARCH POSITIONS AVAILABLE

The DOE's Great Lakes Bioenergy Research Center is an emerging worldwide center of excellence for research and development of cellulosic biofuels and other bioenergy products. The GLBRC is initiating integrated research to remove existing bottlenecks in the bioenergy pipeline, while developing technologies and practices that are economically and environmentally sustainable.

Post-doctoral, research, and graduate student positions are available in plant and microbial bioenergy programs

Areas of Research Focus:

- Improving Plant Biomass for Biofuels
- Biomass Engineering and Processing
- Microbial and Chemical Conversion of Biomass to Fuels
- Environmental and Economic Sustainability of Biofuel Systems
- Genomics, Modeling and Enabling Bioenergy Technologies

To learn more about this center and employment opportunities please visit "Jobs" at
www.greatlakesbioenergy.org

DIRECTOR, OFFICE OF SCIENCE OUTREACH
University of Missouri-Columbia (MU)

We seek a Director for the Office of Science Outreach in the MU Science Education Center (**www.musec.missouri.edu**). This individual will hold the title of Assistant/Associate Professor of Professional Practice (full-time, non-tenure) in the Department of Learning, Teaching, and Curriculum and the Division of Biological Sciences. This individual will provide intellectual and creative leadership for a coordinated Science Outreach Program at MU in which scientists and science educators interact with K-12 students and their teachers. The Director will collaborate with scientists to integrate K-12 outreach components into their research proposals and to design effective assessments of those components; initiate grant proposals for professional development projects for K-12 science teachers; and provide intellectual support for a "Scientists in the Schools" program staffed by graduate students. Applicants must have a PhD in Science Education, Biological Sciences, or in a related area and experience in science outreach K-12.

Applicants should submit a letter of interest and outreach vision, c.v., and 3 letters of reference to: **Prof. Sandra Abell, Director, MU Science Education Center, 303 Townsend Hall, University of Missouri-Columbia, Columbia, MO 65211** or **AbellS@missouri.edu**. Review of applications will begin **November 30, 2007** and will continue until the position is filled.

MU is an Equal Opportunity/Affirmative Action Employer. We specifically encourage applications from women and minorities.

---

3 Global Change Biology Tenure Track Positions

The Department of Biology at the University of Massachusetts at Amherst is seeking to fill three tenure-track faculty positions at the Assistant professor level:

One position is broadly defined as the area of **Ecological Physiology**. We are looking for a researcher whose work is field-based and integrative, and are particularly interested in researchers using genetic and hormonal approaches within an ecological context. Organismal focus (animal or plant) is open.

The second position is in the area of **Endocrine Disruption**. We are seeking a researcher whose interest is in effects of environmental contaminants on endocrine physiology. We are particularly interested in researchers examining the physiological mechanisms underlying endocrine disruption.

The third position is in the area of **Plant Metabolism**. We are seeking a researcher who uses systems biology and/or functional genomic approaches to understanding plant metabolism. The area of research should be relevant to the use of plants for bioenergy, for example, carbon metabolism or biopolymer production by plants.

The researchers would be expected to participate in a broad multi-disciplinary initiative in Global Change Biology within the Department of Biology. This initiative bridges a group of faculty who use multiple levels of analysis to understand how rapid environmental changes are impacting populations and individual organisms, including: loss of biodiversity, rapid evolution, disruption of physiology, reduced agricultural outputs, and evolution of new pathogens. Postdoctoral experience required.

Applications, which should include CV, statements of research interest and teaching philosophy, and the names, addresses and e-mails of at least 3 references, should be sent to: **Biology Search c/o Ms. Karen Nelson, Biology Department, University of Massachusetts, Amherst, MA 01003**. It is very important that you reference the position number to which you are applying. Positions to be filled contingent upon funding. The position numbers are as follows: • **Ecological Physiology R32351** • **Endocrine Disruption R32352** • **Plant Metabolism R32353**. Evaluation of applications will begin on **December 10, 2007** and continue until the positions are filled.

The University of Massachusetts is an Affirmative Action Equal Opportunity Employer. Women and members of minority groups are encouraged to apply. The Biology Department is aggressive in its efforts to hire candidates who will enhance the diversity and general balance of the faculty and the sciences.

University of Pittsburgh

Professor Position

Department Environmental and Occupational Health Graduate School of Public Health

The Department of Environmental and Occupational Health, Graduate School Public Health invites applications for a tenure/tenure track position at the rank of Professor. We are seeking qualified Ph.D. and/or M.D. candidates with a demonstrated record of excellence in research in environmental genetics and molecular and cell biology in environmental health sciences. Applicants are expected to have history of leadership in environmental health science with a strong and current track record of research funding and involvement in graduate education. Opportunities exist for collaborative interactions within Graduate School of Public Health and School of Medicine including programs with extensive recent growth such as pulmonary and cardiovascular biology, stem cell and developmental biology, neuroscience, cancer biology and free radical biology. Further collaborations and support are available from outstanding resources in genomics, structural and computational biology and toxicology, imaging, gene therapy and drug discovery programs.

The successful candidate will be expected to develop outstanding independent research programs and participate in graduate teaching and advising. Attractive start-up packages and competitive salaries have been committed.

Applications will be received until the position is filled. Interested applicants should provide a one-page statement of proposed research, a curriculum vitae and names and contact information of three references to: **Valerian Kagan, Ph.D., Sc.D., Department Environmental and Occupational Health, Graduate School of Public Health, University of Pittsburgh, Bridgeside Point, 328 CLMCS, 100 Technology Drive, Pittsburgh, PA 15219; Recruitment@eoh.pitt.edu.**

The University of Pittsburgh is an Affirmative Action, Equal Opportunity Employer.

MICHIGAN STATE UNIVERSITY

EVOLUTIONARY ECOLOGIST

The Department of Zoology at Michigan State University invites applications for an academic year (AY), tenure-track position at the Assistant Professor level. We seek an individual with excellent quantitative skills to address cutting-edge questions about the evolutionary ecology of animals using field, experimental, and/or theoretical approaches.

The successful candidate will contribute to undergraduate and graduate teaching and research training, participate in MSU's interdepartmental graduate program in Ecology, Evolutionary Biology, and Behavior (**http://www.msu.edu/~eebb**), and maintain a successful, externally funded research program. Information about the Department of Zoology can be found at **http://www.zoology.msu.edu/**.

Applicants should have a PhD; postdoctoral experience is desirable. Application via email is preferred; materials should be sent to **zoology@msu.edu**. We would prefer to receive the cover letter, curriculum vitae, a summary of research accomplishments and future objectives, and a description of teaching philosophy and goals as a single PDF file. Up to three reprints or preprints may be submitted. Please have three letters of reference sent via email, with signed paper copies sent in parallel to **The Evolutionary Ecology Search Committee, Department of Zoology, Michigan State University, Natural Science Building, East Lansing, MI, 48824-1115**. The review of applications will begin **December 17, 2007** and will continue until a suitable candidate is identified. Questions regarding this position may be sent to **Tom Getty (getty@msu.edu)**, Chair of the Search Committee.

MSU is an Affirmative Action, Equal Opportunity Employer, committed to achieving excellence through cultural diversity. The University actively encourages applications and/or nominations of women, persons of color, veterans and persons with disabilities.

MEMORIAL UNIVERSITY

Tenure-Track position in Behavioural Ecology/ Animal Behaviour

The Department of Psychology at Memorial University of Newfoundland (**www.mun.ca/psychology**) invites applications for a tenure-track position in Behavioural Ecology/Animal Behaviour at the rank of Assistant Professor (VPA-PSYC-2007-004). Preference will be given to applicants whose research has a strong field component and focuses on local marine and/or terrestrial species. The successful candidate will have a Ph.D. in Psychology or a closely related discipline and is expected to contribute to the interdisciplinary Cognitive and Behavioural Ecology graduate programme.

Applicants should send (1) a curriculum vitae; (2) a statement of research interests, including selected reprints; (3) a statement of their teaching interests and evidence of effective teaching; and (4) the names and contact information of three referees to: **Dr. Ian Neath, Head, Department of Psychology, Memorial University of Newfoundland, St. John's, NL, A1B 3X9**. Electronic submissions may be sent via e-mail to **ineath@mun.ca**. The appointment will begin on July 1, 2008, or as soon as possible thereafter. The closing date for the position is **January 25, 2008**.

Memorial University is the largest university in Atlantic Canada. As the province's only university, Memorial plays an integral role in the education and cultural life of Newfoundland and Labrador. Offering diverse undergraduate and graduate programmes to almost 18,000 students, Memorial provides a distinctive and stimulating environment for learning in St. John's, a very safe, friendly city with great historic charm, a vibrant cultural life, and easy access to a wide range of outdoor activities.

Memorial University is part of a lively and engaging scientific, arts, and engineering community which maintains an inventory of available positions for qualified partners. Partners of candidates for this position are invited to include their resume for possible matching with other job opportunities.

All qualified candidates are encouraged to apply; however, Canadians and permanent residents will be given priority. Memorial University is committed to employment equity and encourages applications from qualified women and men, visible minorities, aboriginal people and persons with disabilities. Informal inquiries are welcomed.

Faculty Position
UNMC Eppley Institute for Research in Cancer and Allied Diseases

The **Eppley Institute for Research in Cancer and Allied Diseases**, a multi-disciplinary cancer research institute at the **University of Nebraska Medical Center (UNMC)**, invites applications for tenure-leading positions at all levels. We seek candidates with outstanding records of cancer research achievement focusing on basic molecular and cellular mechanisms, molecular therapeutics, or specific disease models. Researchers with expertise using chemical genetic or chemical genomic approaches, including, but not limited to state-of-the-art techniques for identifying small molecules directed at cancer targets, *in vitro* and *in vivo* methods to enhance molecular target validation, and techniques for identifying and validating cancer biomarkers are encouraged to apply.

The Eppley Institute for Research in Cancer and Allied Diseases, an integral part of both the University of Nebraska Medical Center and the UNMC Cancer Center (NCI-designated Cancer Center), continues aggressive recruitment of outstanding scientists in several areas of scientific priority. The Institute provides a supportive environment that fosters creative, multidisciplinary research with world-class laboratory facilities, state of the art core facilities, and outstanding institutional and state support. New faculty will find a collaborative scientific environment coupled with very competitive start-up packages. Both pre- and post-doctoral fellowships are available for support of trainees. Omaha, the nation's 42nd largest city, offers an outstanding school system, low cost of living, and numerous recreational activities.

Candidates should have a Ph.D. and/or M.D. degree and postdoctoral research experience. Applicants can apply online to position **#2468** at **https://jobs.unmc.edu**. Additional information can be found at **http://www.unmc.edu/cancercenter/**. Candidates should also forward a minimum of 3 letters of reference to: **Search Committee, Eppley Institute for Research in Cancer and Allied Diseases, Attn: Matt Winfrey, University of Nebraska Medical Center, 986805 Nebraska Medical Center, Omaha, Nebraska, 68198-6805.**

The University of Nebraska Medical Center is an Equal Opportunity Employer.

DIRECTOR, THE EDWARDS LIFESCIENCES CENTER FOR ADVANCED CARDIOVASCULAR TECHNOLOGY

THE HENRY SAMUELI SCHOOL OF ENGINEERING AT THE UNIVERSITY OF CALIFORNIA, IRVINE invites qualified applicants for the founding *Director* position of the newly established *Edwards Lifesciences Center for Advanced Cardiovascular Technology*. The faculty appointment will be at the rank of Professor in the DEPARTMENT OF BIOMEDICAL ENGINEERING, beginning July 1, 2008. We seek a visionary leader in the field of cardiovascular technology who will develop the new center to be an academic center of excellence in the design and translation of new cardiovascular technology. The Edwards Lifesciences Center has an initial naming endowment from Edwards Lifesciences, a global leader in devices to treat cardiovascular disease, located just ten minutes from campus. Additional resources for the Center will be new faculty positions in biomedical engineering dedicated to cardiovascular research, and approximately 13,000 assignable square feet of new research and administrative space in Engineering Unit 3 slated to open in the summer, 2009.

The successful applicant will:

- **have a distinguished and scholarly background in high impact cardiovascular research, with evidence of translating this technology to the private sector.**
- **show evidence or potential to provide strong leadership.**
- **be expected to leverage the resources from the endowment to significantly enhance the research and training environment of the Center.**
- **hold an M.D. or Ph.D. degree in biomedical engineering or related field.**
- **will be expected to advise students, and contribute to the teaching and training programs in biomedical engineering.**
- **enhance collaborative opportunities between the Center and other faculty members within the Department of Biomedical Engineering, the Henry Samueli School of Engineering, and the College of Health Sciences.**

The University of California, Irvine is situated in Orange County's rapidly growing high technology sector that includes more than 150 biomedical companies which are actively involved in our program.

For full consideration, candidates should upload applications electronically, please refer to the following website for instructions: **http://www.eng.uci.edu/** - click on the Employment side bar. Applications should include a curriculum vitae, a brief (no more than 2 pages) description of a vision for the Edwards Lifesciences Center, and names of at least three references. Questions regarding these positions may be addressed to **Ms. Ruth M. Gratzer, rmgratze@uci.edu**. For more information about the Department of Biomedical Engineering please visit our website at **http://www.bme.uci.edu**. Applications will be accepted until the position is filled, although maximum consideration will be given to applications received by **February 1, 2008**.

UCI is an Equal Opportunity Employer committed to excellence through diversity and strongly encourages applications from all qualified applicants, including women and minorities. UCI is responsive to the needs of dual career couples, is dedicated to work-life balance through an array of family-friendly policies, and is the recipient of an NSF ADVANCE Award for gender equity.

THE UNIVERSITY OF CHICAGO CANCER RESEARCH CENTER TRANSLATIONAL CANCER IMMUNOLOGY/IMMUNOTHERAPY

The University of Chicago Cancer Research Center, together with the Section of Hematology/Oncology, the Section of Pediatric Hematology/Oncology, and the Department of Pathology is seeking faculty with translational research interests in cancer immunology. The preferred candidates will be an MD, PhD, or MD/PhD with expertise in clinical and/or laboratory-based cancer immunology research. Excellent teaching skills are also required. Clinical candidates must be BC/BE in the relevant specialty and must be eligible for medical licensure in the State of Illinois. Successful candidates will become integrated members of the Immunology and Cancer research communities at the University of Chicago, with laboratory space available in the new Knapp Center for Biomedical Discovery building. Translational research efforts are supported by outstanding infrastructure components, including a cGMP facility, Human Immunologic Monitoring Facility, and core facilities for gene expression profiling, flow cytometry, monoclonal antibody production, tissue banking, clinical trial data management, and others. Academic rank and salary commensurate with background and experience. Send curriculum vitae including a brief description of research interests and references to: **Thomas F. Gajewski, MD, PhD, in care of Patricia Geiger, The University of Chicago, 5841 South Maryland Avenue, MC1140, Chicago, IL 60637** or via email to **pgeiger@medicine.bsd.uchicago.edu**. *The University of Chicago is an Affirmative Action/Equal Opportunity Employer.*

EXECUTIVE DIRECTOR / CEO WOMEN'S & CHILDREN'S HEALTH RESEARCH INSTITUTE SOUTH AUSTRALIA www.wchri.com.au

Due to the retirement of the current Executive Director, the Women's & Children's Health Research Institute (WCHRI) is seeking a new Executive Director. The successful candidate will drive the implementation of a recently signed research partnership with the Children, Youth and Women's Health Service, and will build partnerships with other research organisations and universities to achieve critical mass.

WCHRI is an independent medical research institute committed to improving the health of women and children. Established in 1989 as the Child Health Research Institute, WCHRI currently has around seventy staff and students located in seven research groups: Basic Nutrition, Applied Nutrition, Epithelial Biology, Skin Biology, Leukaemia, Leucocyte Biology and Molecular Immunology. The research groups are located in three hospitals in Adelaide in keeping with our commitment to clinically relevant research.

WCHRI is well positioned for growth and provides exciting possibilities for the right applicant. The Institute has an excellent track record in attracting funding from national and international funding agencies and industry and is equipped with state of the art facilities. Our scientists are highly collaborative, both within and outside the Institute, and most are Affiliates of the University of Adelaide.

The Executive Director will bring to this role excellent leadership, communication, negotiation, planning and interpersonal skills, as well as an outstanding international track record of basic and/or clinical research relevant to WCHRI's vision. The successful candidate will be expected to enhance WCHRI's profile both in the international research community and with Government and the local community. The Executive Director will also be expected to attract peer reviewed research funds to continue internationally recognised research.

Terms, conditions and salary will be competitive and commensurate with the qualities sought in a successful applicant.

More information is available on our website **http://www.wchri.com.au** or contact the current Executive Director, Professor Heddy Zola Tel: 61 8 8161 7015, email: **heddy.zola@adelaide.edu.au**

Resumes including covering letter and the names of three referees to:
The Business Manager,
Women's & Children's Health Research Institute,
72 King William Rd,
North Adelaide,
South Australia, 5006

Or may be submitted electronically to:
kathy.kingston@adelaide.edu.au

Closing Date: 18 January 2008

Penn
University of Pennsylvania

ASSISTANT or ASSOCIATE PROFESSOR
Stem Cell Biology

The Department of Animal Biology and the newly established Institute for Regenerative Medicine at the University of Pennsylvania are soliciting applications for a TENURE-TRACK faculty position at the ASSISTANT or ASSOCIATE PROFESSOR level. Animal Biology has a strong commitment to basic biomedical research and is located at the heart of Penn's Philadelphia campus in an interactive scientific environment. Candidates with research interests in the broad areas of basic and translational research in stem cell biology, using various model systems, are encouraged to apply. Applicants must have a PhD, MD, VMD/DVM or equivalent degree along with postdoctoral training, and should be prepared to establish an independent extramurally funded research program. Applicants are expected to interact with multiple existing Research Centers at Penn, such as the Center for Animal Transgenesis and Germ Cell Research, and to teach in the Department and in University-wide graduate programs.

Candidates should apply online by **February 1, 2008** at **https://facultysearches.provost.upenn.edu/**, and attach PDF files containing a curriculum vitae, a statement of research interests, as well as three reference letters to: **Dr. O. Jacenko, University of Pennsylvania School of Veterinary Medicine, 3800 Spruce Street, Philadelphia, PA 19104-6046; FAX: 215-573-5189.**

The University of Pennsylvania is an Equal Opportunity/Affirmative Action Employer. Minorities/Females/Individuals with Disabilities/Veterans encouraged to apply.

Penn
University of Pennsylvania

ASSISTANT or ASSOCIATE PROFESSOR
Mitochondrial Biology and Metabolism

The Department of Animal Biology at the University of Pennsylvania is soliciting applications for a TENURE-TRACK faculty position at the ASSISTANT or ASSOCIATE PROFESSOR level. Candidates with research interests in the broad areas of basic and translational research that pertains to mitochondrial biology/genetics, bioenergetics, and cell metabolism as well as their functions in stem cell biology and/or dysfunction in cancer and other disorders are encouraged to apply. This position is for interfacing with existing strengths of the School- and University-wide programs in obesity/diabetes, oncology, neurodegeneration, stem cell biology, and infectious diseases.

Animal Biology has a strong commitment to basic biomedical research and is located in the heart of Penn's Philadelphia campus in an interactive scientific environment. Applicants must have a PhD, MD, VMD/DVM or equivalent degree along with postdoctoral training, and should be prepared to establish an independent extramurally funded research program. Applicants are expected to interact with multiple existing Research Centers at Penn, such as the Mari Lowe Comparative Oncology Center, and to teach in the Department and in University-wide graduate programs.

Candidates should apply online at **https://facultysearches.provost.upenn.edu/** by **February 1, 2008** and attach PDF files containing a curriculum vitae, a statement of research interests, and three reference letters addressed to: **Dr. S. Fuchs, University of Pennsylvania School of Veterinary Medicine, 3800 Spruce Street, Philadelphia, PA 19104-6046; FAX: 215-573-5189.**

The University of Pennsylvania is an Equal Opportunity/Affirmative Action Employer. Minorities/Females/Individuals with Disabilities/Veterans encouraged to apply.

Head, Department of Biology
Texas A&M University
College Station, Texas

A national search is underway to identify outstanding candidates for Head of Biology at Texas A&M University, one of the largest universities in the nation with an enrollment of over 46,000 students and recently rated #1 in serving the needs of the nation by Washington Monthly. Our thematically diverse department is at the research and teaching core of the basic life sciences at Texas A&M University. The department seeks an individual with a vibrant and internationally recognized research program, a sincere commitment to undergraduate and graduate education, and proven leadership skills.

The Biology Department has nearly 1800 undergraduate majors, 90 graduate students, 44 full-time faculty members, 6 joint appointments, and 7 lecturers. The university is committed to increasing the number of full-time tenured and tenure-track faculty to at least 50, including expansion of research space. Department facilities support a wide range of molecular biological, imaging, and computational technologies. Complementary expertise and specialized research facilities are available on campus. Further information about the department, its faculty, and its facilities can be found at our website: **www.bio.tamu.edu.**

Applicants should send by email a CV and a statement of research accomplishments, teaching perspective and administrative philosophy to: **Headsearch@mail.bio.tamu.edu**. Review of applications will begin **January 15, 2008**, and continue until the position is filled.

Texas A&M University is an Equal Opportunity/Affirmative Action Employer that is dedicated to the goal of building a culturally diverse and pluralistic faculty and staff who are committed to teaching and working in a multicultural environment. We strongly encourage applications from women, minorities, veterans, and individuals with disabilities. The university is particularly responsive to the needs of dual-career couples.

Department Head, Environmental and Radiological Health Sciences
Colorado State University

This is (**www.cvmbs.colostate.edu/erhs/**) an opportunity for an individual with bold vision to lead a vigorous, diverse group of scholar/entrepreneurs. Sections of Cancer Biology, Epidemiology, Occupational Health, Radiation Protection, Toxicology, and Diagnostic Imaging, all have internationally recognized research and programs in human/animal health. Strength lies in affiliation/administration of super clusters – joining of academia and business to move discovery to practice (**http://superclusters.colostate.edu/**). The Department is key to the Cancer Research super cluster; NIOSH Center for Agricultural Health/Safety; NIOSH MAP Education Research Center; and is a key to the Colorado School of Public Health initiative. The department affiliates with another super cluster and 3 programs of excellence (**http://vpr.colostate.edu/index.asp?url=prse**). The Department Head will provide academic/scientific leadership, strategic vision development, business/facilities management, development/mentoring of faculty and have a commitment to diversity as demonstrated by persistent effort, active planning, and allocation of resources or accountability for diversity.

Applicants must have a Ph.D., D.V.M., M.D., or equivalent; demonstrate achievement in scholarly activity, teaching/mentoring, strategic planning; plus meet requirements for a full, tenured professor. A letter of application, curriculum vitae, and list of three references, who may be contacted when appropriate, should be sent electronically or by post to:

Dr. Kenneth Blehm
CSU, Campus 1601
Fort Collins, CO 80523-1601

Ken.Blehm@ColoState.EDU

Review begins **February 1, 2008** until successful.

CSU is an EO/AA Employer.

TEXAS A&M UNIVERSITY

Associate Dean for Research and Graduate Studies
College of Veterinary Medicine & Biomedical Sciences
Texas A&M University

Position Description: The College of Veterinary Medicine & Biomedical Sciences at Texas A&M University invites applications and nominations for the position of Associate Dean for Research and Graduate Studies.

Qualifications: The successful candidate must hold a Ph.D. and qualify for tenure within one of the departments of the College of Veterinary Medicine & Biomedical Sciences. It is envisioned that a person who has enjoyed success in graduate education and research would achieve satisfaction from facilitating the success of others in their academic endeavors. Excellent interpersonal communication skills, substantial experience in graduate education, demonstrated leadership and organizational abilities, and firsthand experience with a variety of funding sources, which support veterinary or biomedical research and education, are required.

Responsibilities: The Associate Dean for Research and Graduate Studies reports directly to the Dean of the College, is a member of the College's Executive Committee, and is responsible for managing the administrative aspects of the research and graduate studies programs in the college. This is a full time administrative/service position. A more detailed description of the position may be found at **www.cvm.tamu.edu**.

Position Posting Date: November 1, 2007

Application Review: Review of applications and nominations will begin immediately and will continue until the position is filled.

Application Procedure: Applicants should submit a letter of intent, *Curriculum vitae*, and reference list. References will not be contacted until the advanced stages of screening, and candidates will receive prior notification. Inquiries, nominations, and applications should be submitted to: **Drs. Duane C. Kraemer or Timothy D. Phillips, Co-Chairs of the Search Committee, College of Veterinary Medicine & Biomedical Sciences, 4461 TAMU, Texas A&M University, College Station, Texas 77843-4461; Telephone: 979-845-5761; email: dkraemer@cvm.tamu.edu or tphillips@cvm.tamu.edu.**

Texas A&M University is an Equal Opportunity Employer. Ethnic minorities and women are encouraged to apply. The candidate selected for this position must be able to meet eligibility requirements to work in the United States at the time of appointment and must be able to communicate effectively in the English language.

MEDICAL COLLEGE OF GEORGIA SCHOOL OF MEDICINE NEUROSCIENCE FACULTY POSITION

The new Brain and Behavior Discovery Institute at the Medical College of Georgia is part of a university-wide brain discovery initiative that brings together scientists to map neural circuits and decipher neural dynamics underlying various cognitive behaviors. We are seeking four (4) faculty members on the tenure track level who will be appointed as faculty at the Assistant Professor, Associate Professor and Full Professor levels in the relevant neurosciences department of the School of Medicine and Institute of Molecular Medicine and Genetics. We are particularly interested in candidates who study neural network mechanisms using *in vivo* electrode arrays or optical imaging techniques in awake rodents, non-human primates, and humans. We are also seeking a faculty member in the area of monkey brain fMRI, brain-machine-interface research, or computational neuroscience. Candidates using mathematical and computational, i.e. (systems neurobiology) approaches should have experiences in large database construction, statistical pattern recognition, or intelligent computing such as the hierarchical temporal memory (HTM) algorithm and Bayesian network computation.

Consideration of candidates will begin **January 15, 2008** and will continue until the search has been successfully concluded. Letters nominating qualified candidates are requested and may be sent to: **Joe Z. Tsien, Ph.D., Neuroscience Faculty Search Committee, The Brain and Behavior Discovery Institute, Medical College of Georgia, Augusta, GA 30912-4750, ATTN: Ann Gambill; agambill@mcg.edu.** Interested individuals should submit a cover letter, current resume/*Curriculum Vitae*, along with a 2 to 4 page research plan, and arrange for submission of 3 letters of recommendation.

EEO/AA/Equal Access Employer.

ACH #'s 55479, 55480, 55481 & 55482

Faculty Positions
Department of Pharmacology
The University of Michigan

The University of Michigan, Department of Pharmacology is seeking outstanding scientists for a tenure-track **ASSISTANT PROFESSOR** position. We are especially looking for an outstanding scholar with exceptional potential to develop a vibrant research program that augments current department initiatives in *Pharmacogenetics/genomics*, *Drug Metabolism*, or *Signal Transduction* (see **http://sitemaker.umich.edu/pharmacology/faculty_listing** for faculty interests). Qualifications include a Ph.D. in Pharmacology or a related discipline and/or M.D. degree, 3-5 years of postdoctoral experience, and research accomplishments as evidenced by scholarly contributions to the literature.

The successful candidate will join a dynamic, diverse, and collaborative department in a Top 10 Medical School in a university setting with superb opportunities for career development. The quality of life in Ann Arbor is outstanding. The combination of a large, major research university and a small, safe, family-oriented community make Ann Arbor an ideal environment to develop an academic and research career. Ann Arbor also offers an outstanding combination of sports, recreation, and cultural events.

Faculty members are expected to establish a highly visible externally funded research program and to excel in teaching medical students and other health professionals, as well as graduate and postdoctoral students. An attractive startup package including excellent laboratory facilities and generous startup funds will be available.

Send your CV, a two- to four-page summary of your research and future plans, and details of your teaching experience. Three letters of recommendation should also be sent. Address all correspondence to: **Chair, Pharmacology Search Committee, Department of Pharmacology, University of Michigan Medical School, 2301 MSRB III, 1150 West Medical Center Dr., Ann Arbor, MI 48109-5632**. Application materials may also be sent electronically to: **pharmsearch@umich.edu**.

The University of Michigan is an Affirmative Action/Equal Opportunity Employer. Applications from qualified women, minorities and/or disabled individuals are encouraged.

POSITIONS OPEN

FACULTY POSITION in INFECTIOUS DISEASES
Fred Hutchinson Cancer Research Center and the University of Washington

The Fred Hutchinson Cancer Research Center (FHCRC) and the University of Washington (UW) are jointly recruiting a full-time faculty position at the **ASSISTANT or ASSOCIATE MEMBER/PROFESSOR** level for a faculty position in the Program in Infectious Diseases in the Clinical Research Division of the FHCRC and the Division of Allergy and Infectious Disease at the UW, with preference being given to those who study fungal diseases. A Doctorate degree is required. The individual will be expected to develop independent research programs. University of Washington faculty engage in teaching, research, and service. Excellent collaborations are available with scientists in clinical, molecular medicine, and basic sciences at the FHCRC and the UW. Salary depends on experience and excellent benefits. Interested candidates may submit curriculum vitae, a concise statement of their research plan, and three reference letters to:

Lawrence Corey, M.D.
Head, Program in Infectious Diseases
Fred Hutchinson Cancer Research Center
1100 Fairview Avenue N., LE-500
P.O. Box 19024
Seattle, WA 98109

Application review will continue until the position is filled.

The University of Washington and the Fred Hutchinson Cancer Research Center are Affirmative Action, Equal Opportunity Employers, dedicated to the goal of building a culturally diverse and pluralistic faculty and staff committed to teaching and working in a multicultural environment, and strongly encourage applications from women, minorities, individuals with disabilities, and covered veterans.

ASSISTANT PROFESSOR (TENURE TRACK)
Behavioral Neuroscience
Morehouse College

The Division of Science and Mathematics at Morehouse College seeks candidates for a tenure-track Assistant Professor position in behavioral neuroscience. This appointment will be in the Biology, Chemistry, Computer Science, Mathematics, Physics, or Psychology Department depending on the neuroscience interests and expertise of the successful candidate. We seek an individual possessing a Ph.D., postdoctoral experience, and a commitment to undergraduate teaching. The successful candidate is expected to establish a strong research program that involves undergraduates. Submit curriculum vitae, description of teaching experience and philosophy, description of research interests and career goals, and the names and contact information for three references to: **Dr. J.K. Haynes, Dean, Division of Science and Mathematics, Morehouse College, 830 Westview Drive, S.W., Atlanta, GA 30314,** or by **e-mail: jhaynes@morehouse.edu.** Deadline: February 16, 2008. *Morehouse College is an Equal Opportunity/Affirmative Action Employer.*

ASSOCIATE PROFESSOR of CANCER BIOLOGY

Associate Professor position available immediately at the Laboratory of Molecular Oncology, Institute for Nutritional Sciences, Chinese Academy of Sciences, Shanghai, China. Our research focus on the molecular mechanisms of oncogenes and tumor suppressors in cancers. Interested candidates who have previous experience in cancer biology, signal transduction, immunology, and/or animal model should send their curriculum vitae and the names of three references to: **Dong Xie, Ph.D., telephone: 01186-21-5492-0918; e-mail: dxie@sibs.ac.cn.** Successful applicants will be provided with a generous package and an interactive research environment.

POSITIONS OPEN

The University of Connecticut invites applications to fill the **NORTHEAST UTILITIES (NU) FOUNDATION CHAIR of ENVIRONMENTAL ENGINEERING** within the Civil and Environmental Engineering Department of the School of Engineering and the Center for Environmental Sciences and Engineering. **DISTINGUISHED SCHOLARS and FULL PROFESSORS** with a record of excellence in multidisciplinary collaborative research and teaching, especially in the following environmental areas are encouraged to apply: sustainable engineering; environmental biotechnology; geoenvironmental remediation; pollution prevention; biofuels; climate change impacts on environmental processes; and soil and water quality in natural and engineered systems. It is expected that the Chair will assume a significant leadership role in catalyzing collaborative environmental research and forming partnerships with governmental agencies and industry, thereby enhancing the University's growing international reputation in environmental sustainability. The Chair will control the revenue from the NU Foundation Chair of Environmental Engineering endowment consistent with University policies and the conditions of the endowment. Salary, benefits, and a competitive startup package will be commensurate with the record of the applicant. A more detailed description of the position and expected qualifications can be found in the following **websites: http://www.engr.uconn.edu/cee, www.engr.uconn.edu/environ** and **www.cese.uconn.edu.** Confidential review of applications will begin immediately and continue until the position is filled. Candidates should submit the following, preferably as one PDF file: a letter of interest, current curriculum vitae, a statement of interdisciplinary research vision, and contact information for at least four references to: **Chair, Northeast Utilities Foundation Search Committee, e-mail: nusearch@engr.uconn.edu** (search #2008203). *We encourage applications from underrepresented groups, including minorities, women, and people with disabilities.*

QUANTITATIVE BIOLOGY

The National Institute of Standards and Technology (NIST)'s Biochemical Science Division is encouraging **RESEARCH SCIENTISTS** with expertise in the tools of modern quantitative biology to consider employment at NIST. We are seeking researchers to join interdisciplinary teams in the following areas: quantitative high content cell imaging and image processing; image analysis, image informatics, and image databases; gene expression array validation; and application of neutrons to the study of biomolecular structure and function.

The successful applicant has a Ph.D. or equivalent experience in relevant specialties of physics, engineering, chemistry, or biology, and can demonstrate success as an independent and team researcher by a record of high-quality publications. Candidates with multidisciplinary expertise are preferred. Home to three recent Nobel laureates, NIST is known for its high impact basic research and its contribution to commercially important innovation and technical development. The Biochemical Science Division is located on the 500-acre NIST campus in Gaithersburg, Maryland, nine miles north of Bethesda and 20 miles north of Washington, D.C.

Positions are available at a salary range of $55,706 to $121,967, based on qualifications. Candidates should send curriculum vitae and a description of research interests and expertise to: **Ms. Lisa Marth, Biochemical Science Division Administrative Assistant, 100 Bureau Drive Stop 8310, Gaithersburg, MD 20899,** and apply as one the following series: Physicist (1310), Chemist (1320), Engineer (0801) or Biologist (0401) to the NIST Applicant Supply File at **website: https://rproxy.nist.gov/asf.**

U.S. citizenship is required for permanent NIST positions. NIST is an Equal Opportunity Employer.

POSITIONS OPEN

FULL-TIME FACULTY MEMBER with an INTEREST in STEM CELL RESEARCH RELATED to DIABETES

The Division of Metabolism, Endocrinology, and Nutrition at the University of Washington is recruiting a full-time faculty member at the **ASSISTANT, ASSOCIATE, or FULL PROFESSOR** level or the **RESEARCH ASSISTANT, RESEARCH ASSOCIATE, or RESEARCH PROFESSOR** level, without tenure for reasons of funding. The appointment requires a doctoral degree. The successful applicant should have demonstrated experience/interest in developmental aspects of the pancreatic beta cell and/or use of stem cells for the treatment of diabetes. Interested applicants should submit a letter of interest, detailed curriculum vitae, and a brief summary of research interests and funding to:

Michael W. Schwartz, M.D.
Search Committee Chair
Harborview Medical Center
P.O. Box 359675
325 Ninth Avenue
Seattle, WA 98104-2499

Review of applications will begin November 2007, and continue until the position is filled. The University of Washington faculty engage in teaching, research, and service. *The University of Washington is an Affirmative Action, Equal Opportunity Employer. Women and minorities are encouraged to apply.*

ASSISTANT/ASSOCIATE PROFESSOR
Dairy Technology

The Department of Food Science and Nutrition at the University of Minnesota seeks applicants for this nine-month, tenure-track position. Search and apply for requisition number 151791 at **website: http://www1.umn.edu/ohr/employment/index.html.** *The University of Minnesota is an Equal Opportunity Educator and Employer.*

The Department of Biochemistry and Molecular Biology at the University of Chicago invites applications for a tenure track appointment as Assistant Professor. We seek individuals with outstanding records in the area of membrane protein biophysics and dynamics who value teaching and aim to develop independent and creative research programs. We anticipate a minimum of two years of postdoctoral experience and a mastery of structural biology (e.g., X-ray crystallography and NMR spectroscopy). Modern laboratory facilities and generous support will help this individual establish a highly productive, externally funded research program. The Department is linked to sister programs in physical sciences, bioinformatics and computation, cell biology, basic medical science, the Institute for Biophysical Dynamics and the Argonne National Laboratory.

Applications must include a curriculum vitae, a summary of past accomplishments and a plan for future research and arrive before **January 1, 2008**. Applicants must also arrange for three letters of reference to be mailed to us. Address: **Chair, Membrane Protein Search Committee, Department of Biochemistry and Molecular Biology, 929 E. 57th Street, Chicago IL 60637.**

The University of Chicago is an Affirmative Action/ Equal Opportunity Employer.

Center for AIDS Prevention Studies University of California, San Francisco

Search for Academic Specialists: Social Behavioral HIV Prevention Research

The mission of the Center for AIDS Prevention Studies (CAPS) is to conduct domestic and international research to prevent the acquisition of HIV and to optimize health outcomes among HIV-infected individuals. CAPS, based in the Department of Medicine, Division of Prevention Science, at the University of California, San Francisco (UCSF), is recruiting one or more academic Specialists in the area of HIV/AIDS or social behavioral research applied to prevention science and the development of effective HIV prevention interventions. The Specialist series is used for academic appointees who are engaged in research in specialized areas and who do not have any teaching responsibilities.

UCSF seeks candidates whose experience, teaching, research, or community service has prepared them to contribute to our mission. Strong NIH funding track record and experience directing federally funded research studies required. Research expertise in the following areas sought: social psychology, sociology, epidemiology, clinical psychology, anthropology, community psychology, medical sociology, and statistics. Populations and areas of special interest include: ethnic and minority populations, incarcerated populations and their families, optimizing health outcomes, MSM, IDU, and biological approaches.

Interested candidates should submit a detailed cover letter describing their interests and experience as well as curriculum vitae to: **Margaret Paternek, PhD, Deputy Director, UCSF Center for AIDS Prevention Studies, 50 Beale Street, 13th floor, San Francisco, CA 94105.**

UCSF seeks candidates whose experience, teaching, research, or community service has prepared them to contribute to our commitment to diversity and excellence. UCSF is an Equal Opportunity/Affirmative Action Employer. The University undertakes affirmative action to assure equal employment opportunity for underutilized minorities and women, for persons with disabilities, and for covered veterans. All qualified applicants are to apply, including minorities and women.

Assistant/Associate/Full Professor Pharmaceutical Sciences Auburn University

The Department of Pharmacal Sciences at Auburn University's Harrison School of Pharmacy invites applications for several 12-month tenure-track faculty positions in Pharmacology, Toxicology, Pharmaceutics and related disciplines. These positions offer the opportunity to join an expanding enterprise in pharmaceutical science research. The School has recently received new funding and opportunities for research enhancement. Successful candidates are expected to actively participate in the teaching mission of the Harrison School of Pharmacy at the graduate (Ph.D.) and professional (Pharm.D.) levels; develop and/or maintain an independent extramurally funded research program; be involved in collaborative research programs; demonstrate a high level of scholarly activity as evidenced by quality publications in peer-reviewed scientific journals and active participation in professional societies and contribute to Department, School and University service activities.

Applicants must have a demonstrated interest in education of health professionals and graduate students. They must have a Ph.D. or equivalent degree, postdoctoral training and demonstrated research abilities. A professional degree in pharmacy is desirable but not essential. The successful candidate must meet eligibility requirements to work in the U.S. at the time the appointment is scheduled to begin and continue to work legally for the proposed term of employment. They must also be able to communicate effectively in English. Review of applications will begin December 1, 2007 and will continue until the positions are filled. The positions are available January, 2008. Candidates should submit a letter of application, curriculum vitae, statements of research and teaching interests as well as the names and addresses (include e-mail address and phone number) of 3-5 references to: **Chair, Pharmacal Sciences, Search Committee, Harrison School of Pharmacy, 4306 Walker Building, Auburn University, Alabama 36849-5503; Telephone (334) 844-4037; Fax (334) 844-8331.** Applications can also be submitted electronically to **Ms. Kandi Dawson, DAWSOKP@auburn.edu.**

Auburn University is an Equal Opportunity/Affirmative Action Employer. Women and Minorities are encouraged to apply.

Center for AIDS Prevention Studies University of California, San Francisco

Faculty Search-Rank Open: Social Behavioral HIV Prevention Research

The mission of the Center for AIDS Prevention Studies (CAPS) is to conduct domestic and international research to prevent the acquisition of HIV and to optimize health outcomes among HIV-infected individuals. CAPS, based in the Department of Medicine, Division of Prevention Science, at the University of California, San Francisco (UCSF), is recruiting one or more faculty members in the area of HIV/AIDS or social behavioral research applied to prevention science and the development of effective HIV prevention interventions.

UCSF seeks candidates whose experience, teaching, research, or community service has prepared them to contribute to our mission. Strong NIH funding track record and experience directing federally funded research studies required. Research expertise in the following areas sought: social psychology, sociology, epidemiology, clinical psychology, anthropology, community psychology, medical sociology, and statistics. Populations and areas of special interest include: ethnic minority populations, men who have sex with men, women, adolescents, substance users, incarcerated populations and their families, optimizing health outcomes, and biomedical approaches to prevention.

Interested candidates should submit a detailed cover letter describing their interests and experience, as well as curriculum vitae to: **Margaret Paternek, PhD, Deputy Director, UCSF Center for AIDS Prevention Studies, 50 Beale Street, 13th floor, San Francisco, CA 94105.**

UCSF seeks candidates whose experience, teaching, research, or community service has prepared them to contribute to our commitment to diversity and excellence. UCSF is an Equal Opportunity/Affirmative Action Employer. The University undertakes affirmative action to assure equal employment opportunity for underutilized minorities and women, for persons with disabilities, and for covered veterans. All qualified applicants are to apply, including minorities and women.

POSITIONS OPEN

SENIOR (TENURED) FACULTY POSITION
Biology
Illinois Institute of Technology

The Biology Division of the Illinois Institute of Technology (IIT) invites applications for a senior level faculty position sponsored by the IIT Research Institute. This is a tenured position at the **ASSOCIATE or FULL PROFESSOR** level and is intended to take advantage of rapidly expanding research programs in the Biology Division as well as at IITRI. While applications are encouraged from candidates with vigorous research programs in any field of biology, scientists with expertise in endocrinology, pharmacology/drug metabolism, immunology, infectious disease, or physiology are particularly encouraged to apply. Substantial NIH or other extramural funding is essential for this position; a record of continuing research productivity is required for candidates desiring appointment at the Full Professor level. The Biology Division of IIT's Department of Biological, Chemical, and Physical Sciences provides a vibrant, highly interdisciplinary environment with particular strengths in molecular biology and biophysics. The successful candidate will contribute to the education of undergraduate and graduate students, and will establish an active research program in new, state-of-the-art laboratory space. Joint appointment at IIT Research Institute is possible, depending on field of research. Attractive compensation and startup funding will be provided.

To apply, send curriculum vitae with publication list along with statements on research and teaching interests to **e-mail: biology_search@bcps.iit.edu.** For full consideration, application packages should arrive by December 15, 2007. *IIT is an Equal Opportunity, Affirmative Action Employer; women and minorities are strongly encouraged to apply.*

FACULTY POSITION in NUTRIENT/GENE INTERACTIONS and HEALTHY AGING
Linus Pauling Institute, Oregon State University

The Linus Pauling Institute at Oregon State University invites applications for a tenure-track or tenured, full-time faculty position in its newly created Healthy Aging Program. The successful candidate will be expected to establish or maintain a competitive research program focused on studying the role of diet or micronutrients in influencing cellular, genetic, and physiological function during aging. Of particular interest is research on the interactive effects of nutritional factors on genetic or epigenetic imprinting that ultimately influence healthy aging. Though this position has a primary research focus, the successful candidate is also expected to contribute to undergraduate or graduate teaching and academic service appropriate with faculty rank. See the full position announcement and application instructions at **website: http://jobs.oregonstate.edu.** For additional information, please contact: **Barbara McVicar, e-mail: barbara.mcvicar@oregonstate.edu, Linus Pauling Institute, Oregon State University, 571 Weniger Hall, Corvallis, OR 97331.** *OSU is an Affirmative Action/Equal Opportunity Employer.*

DEAN
College of Science, Engineering, and Technology

Murray State University seeks nominations and applications for Dean of the College of Science, Engineering, and Technology. The successful candidate must have an earned Doctorate related to one or more of the Departments in the College: Biological Sciences, Chemistry, Geosciences, Industrial and Engineering Technology, Mathematics and Statistics, and Engineering and Physics. The position will be available July 1, 2008. Application deadline is January 4, 2008. Please see our full posting at **website: http://www.murraystate.edu/provost** for complete list of required qualifications, position responsibilities, and a description of how to apply. *Murray State University is an Equal Education and Employment Opportunity, Minorities/Females/Persons with Disabilities, Affirmative Action Employer. Women and minorities are encouraged to apply.*

POSITIONS OPEN

ASSISTANT PROFESSOR

The Department of Cellular and Structural Biology at the University of Texas Health Science Center at San Antonio invites applications for a tenure-track Assistant Professor position that will involve teaching in human anatomical science courses for students in the health professions schools and establishing an extramurally funded research program. Applicants with teaching experience or formal education in gross anatomy and microscopic anatomy (histology) are preferred. Research endeavors compatible with existing themes in the Department are invited. Areas of ongoing research within the Department include aging, cancer biology, signal transduction and gene expression, DNA damage and repair, diabetes and obesity, reproductive and developmental biology, and molecular immunology. Candidates should have a Ph.D., M.D., D.D.S., or D.V.M. Potential applicants are invited to visit our **website: http://www.uthscsa.edu/csb/.**

The University of Texas Health Science Center at San Antonio provides training for scientists, physicians, dentists, nurses, and other health care professionals. The campus is located in the northwest hills of San Antonio. The health care industry is one of the city's three largest employers. San Antonio experiences over 300 days of sunshine annually. The city and surrounding region has an abundance of recreational and cultural activities.

To apply, please forward curriculum vitae, a statement of teaching philosophy, and a statement of research interests, along with contact information for three references electronically to **e-mail: facsearchcsb@uthscsa.edu.** Alternatively, applications may be mailed to: **Faculty Search Committee, Department of Cellular and Structural Biology, The University of Texas Health Science Center at San Antonio, 7703 Floyd Curl Drive, San Antonio, TX 78229-3900.** Initial review of applications will begin immediately and will remain open until the position is filled.

All faculty appointments are designated as security-sensitive positions. The University of Texas Health Science Center at San Antonio is an Equal Employment Opportunity/Affirmative Action Employer.

REMOTE SENSING FACULTY POSITION

The Rochester Institute of Technology is seeking applicants for a tenure-track faculty position at the rank of **ASSOCIATE PROFESSOR or FULL PROFESSOR** in the Chester F. Carlson Center for Imaging Science (CIS) in the area of remote sensing systems and applications. CIS is a highly interdisciplinary university research and education center, dedicated to pushing the frontiers of imaging in all its forms and uses. Major research thrusts include: astronomy, biomedical imaging, color science, remote sensing, and vision. CIS offers B.S., M.S., and Ph.D. degrees in imaging science with an emphasis on the physics of image formulation, the mathematics and systems engineering of image processing, analysis and information extraction, and the development of sensor systems and imaging instrumentation.

The person recruited for this position will be expected to work closely with other faculty and staff in the Laboratory for Imaging Algorithms and Systems and the Digital Imaging and Remote Sensing Laboratory, and make a substantial contribution to the generation and leadership of research projects, supervision of graduate research, and the development and teaching of related courses. He or she will be a key person in the growth of CIS as a world leader in the science and applications of remote sensing. RIT welcomes applications from individuals interested in contributing to a community committed to diversity.

Additional information and application instructions can be found online at **website: http://www.cis.rit.edu/facultysearch.** Specific questions can be directed to **Search Committee Chair** at **e-mail: facultysearch@cis.rit.edu.**

Interested parties are encouraged to submit their materials by February 1, 2008, to assure optimal consideration.

POSITIONS OPEN

POSTDOCTORAL RESEARCH ASSOCIATE
Cardiovascular Genomics

A Postdoctoral Research Associate position is available to study molecular basis of hypertension and heart diseases. Our research team stands in the forefront of hypertension research. This position has great potential for advancement and promotion based on accomplishments of first two years. Competitive salary and health insurance coverage for family. Ph.D. or/and M.D. Prior experience with at least two of the following is preferred: cardiovascular genomics, gene therapy, signal transduction, aging, receptor biology, protein chemistry, or proteomics. Send detailed curriculum vitae and three references to: **Dr. Zhongjie Sun, Department of Physiology, University of Oklahoma Health Science Center, U.S.A. E-mail: zhongjie-sun@ouhsc.edu.**

POSTDOCTORAL POSITION
Biological Mass Spectrometry

NIH-funded project to study antagonist and agonist interactions with HIV co-receptors CCR5 and CXCR4, using cross-linking, with excellent organic synthesis support. Experience with peptide electrospray ionization, liquid chromatography/mass spectrometry required. Exceptionally qualified candidates will be considered for **RESEARCH ASSISTANT PROFESSOR** rank. **Dr. Edward Dratz, Department of Chemistry and Biochemistry, Montana State University, Bozeman, MT 59717; e-mail: dratz@chemistry.montana.edu.** Complete job announcement and application at **website: http://www.montana.edu/level2/jobs.html.** *ADA/Equal Opportunity/Affirmative Action/Veterans Preference.*

MARKETPLACE

Unmatched resolution in digital specimen radiography.

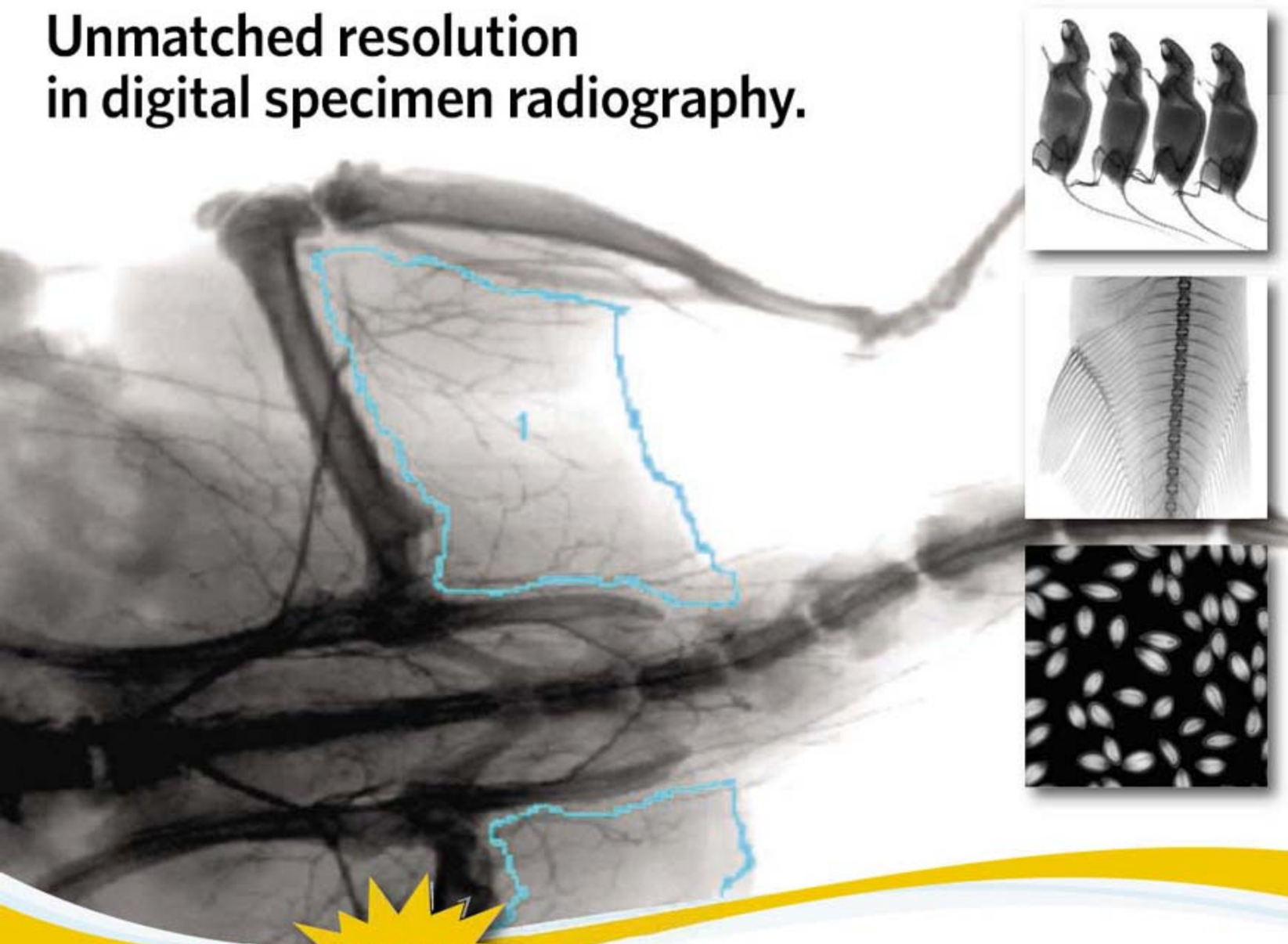

NEW!

Introducing Kodak Digital X-Ray Specimen Systems

KODAK Digital X-ray Specimen 4000 and 4000 Pro Systems deliver greater than 25 line pairs per millimeter with no geometric magnification, providing the best digital resolution available in cabinet x-ray systems.

- Cooled 4 megapixel KODAK CCD camera combined with proprietary phosphor screen technology and a 10X zoom lens.
- True 16-bit imaging — more than 65,000 levels of grayscale resolution for accurate x-ray density measurement.
- Integrated analysis software enables quantification, annotation & databasing of images.
- Upgradeable to optical molecular imaging capabilities, including multi-wavelength fluorescence, radioisotopic, and luminescent imaging.

Find out more. Call **1-877-747-4357**, exp. code 7. Outside the U.S. call **+1-203-786-5657**.

While KODAK Digital X-ray Specimen Products can be used for in vivo and in vitro molecular imaging of materials, researchers should be aware that the methods of preparing and viewing the materials for molecular imaging may be subject to various patent rights. All images were captured using KODAK Molecular Imaging Products.

Kodak
Licensed Product

Carestream Molecular Imaging

A division of Carestream Health

The Innovation Powering KODAK Molecular Imaging Products

Carestream Health, Inc.
150 Verona Street • Rochester, NY 14608

mi.carestreamhealth.com